OPTIMAL DESIGN OF ACTUATION SYSTEMS FOR AN ENHANCIVE ROBOTIC EXOSKELETON

Sina Firouzy

Submitted in accordance with the requirements for the degree of
Doctor of Philosophy

The University of Leeds
Institute of Design, Robotics, and Optimisation
School of Mechanical Engineering

October 2017

The candidate confirms that the work submitted is his own, except where it has been clearly pointed out that other team members have also been involved.

This copy has been supplied on the understanding that it is copyright material and that no quotation from the thesis may be published without proper acknowledgment.

The right of Mr. Sina Firouzy to be identified as Author of this work has been asserted by him in accordance with the Copyright, Designs and Patents Act 1988.

Acknowledgements

Abstract

Enhancing the physical abilities of the human body is desirable for a number of reasons. These reasons include, but are not limited to, avoiding injury of workers who have to handle heavy loads in situations and environments where it is not possible to use conventional machinery (e.g. forklifts). A potential solution to this problem is the use of robotic exoskeletons to augment the strength and endurance of the human body for load-handling tasks.

This study is part of a larger, industry-funded group-research project, done with the aim of developing an enhancive exoskeleton. The needs and target requirements of the final prototype have been determined based on the market-oriented goals of the group project. An energetically autonomous exoskeleton with an acceptably high load-carrying capacity is to be developed, and the key to accomplishing this is the optimal design of the actuation system. The ideal actuation system needs to be strong, but also power-efficient, so that it can be powered by a light-weight, portable power supply. The actuators should also be lightweight, so that the total weight of the exoskeleton is low enough to be safe for the human user. Therefore, this study was done with the aim of developing an optimal design for the actuators to achieve high load-carrying capacity, and low weight and power consumption. To be more specific, the aims of this research included the identification of the degrees of freedom (DOFs) to be actuated, obtaining the torque and power requirements for each actuator, and to design the actuators using the optimal motor size and optimal power transmission mechanism.

Since initial investigations suggested the use of electric motors to achieve an untethered design, the baulk of the work done in this study is focused on actuator design using electric motors. Furthermore, the scope of this research is limited to the lower-body DOFs (namely the ankle, knee and hip joints) in the sagittal plane.

To address the above-mentioned design problem, dynamic modelling and simulation of the exoskeleton movements were performed to obtain the torque and power requirements at the joint. These requirements, in addition to being used later in a novel optimisation algorithm, were also used as guidelines for a market search on electric motors, which resulted in a list which represents the current state of the art of electric motors. The list of motors was saved as

a spreadsheet, in the form of a table containing the technical data which characterise each motor. Similar tables were also created for a number of different types of power transmission mechanisms considered in this study, namely strain gears, chain-and-sprocket mechanisms, and ballscrews. These lists have been used by the optimisation algorithm, which was developed to combine the mathematical models of a motor and a transmission mechanism from the lists, assess the performance of the combination, and repeat this procedure for each and every motor and transmission mechanism in these lists. Thus, through an exhaustive search, the optimum choices for the motors and power transmissions system can be determined for each actuator. Based on the results of the developed optimisation algorithm, a single-joint test prototype was designed, built and used to perform experiments in order to test and validate the reliability of simulations used in the optimisation algorithm. The test results were also used to modify the assumed values of an efficiency parameter within the simulation program. The optimisation algorithm was then refined with the modified parameter value, and the optimal designs of the actuators were obtained for the knee, hip and ankle joints in the sagittal plane. It was also discovered that the most power-efficient motors also yielded the upper bound of the required load-carrying capacity, which is 60 kg. In addition, energy harvesting aspect of such robotic exoskeletons have also been explored.

Table of Contents

List of Tables

List of figures

List of Abbreviations

Abbreviation	Meaning
SEA	Series Elastic Actuator
PEA	Parallel elastic actuator
LCC	Load-Carrying Capacity
ADC	Analogue to digital converter
DOF	Degree of freedom
DC	Direct current
AC	Alternative current
PCB	Printed circuit board
NI	National Instruments™
PWS	Power supply
C-S	Current sensor
I/O	Input/output

The Title of the Prepared Paper

A paper has been written based on the work done in this project, as follows:

Sina Firouzy, Abbas Dehghani, Robert Richardson, *A novel actuation system for an intelligent assistive robotic system*, Journal of Advanced Robotics, under preparation.

The submission of the paper will be subject to the agreement of the industrial sponsor of this project, due to an existing confidentiality agreement.

Chapter 1
Introduction

1.1 Background

The Augmentation of the physical abilities of the human body has always been desirable. One of the solutions to achieve this goal is the utilisation of robotics engineering; that is, robots can be designed in a way that they will share the burden of physical activities with their human users, thus enhancing the strength and endurance of the users. Such an assistive/enhancive device would be favourable in many cases and for many applications; for instance, individuals with impaired physical capabilities could benefit from using such a technology in order to perform at the same level as able-bodied individuals. These technologies are generally referred to as *assistive* ones. On the other hand, healthy users of such a device could handle physical tasks beyond the abilities of a normal individual via increased strength or endurance. Applications of such devices, known as *enhancive* devices, could include use by heavy-duty workers in the industry, such as those who need to handle heavy objects or workers who need to spend extended periods of time working in uncomfortable postures. Another example is the personnel involved in search and rescue operations, firefighters, etc. Other, non-civil, applications include carrying loads over long distances and/or on rough terrain or mountains, which require more strength and endurance than that which is expected from normal individuals.

A robotic device that could be *worn* by its user (i.e. a wearable robot) is referred to as an exoskeleton. A number of enhancive exoskeletons currently exist, which will be illustrated with details in the literature review section, Chapter 2. Each of these devices, like any other engineering product, have their own shortcomings.

The purpose of this study is to tackle the technical challenges involved in the development of exoskeletons and investigate solutions to overcome the defects of existing designs and push the limits of technology and engineering science in the field of robotic exoskeletons. This study focuses on *enhancive* exoskeletons only.

1.2　Motivations

1.2.1　A special note

The project reflected in this report (hereafter referred to as "this project") is an individual project which is part of a larger project. The large project (hereafter referred to as the "team project") has been broken into subprojects (including this project), each of which is to be done by one of the team members. This project focuses on the development of the actuation system of the exoskeleton. The motivations of the team project are mentioned in Section 1.2.2, while section 1.2.3 includes the motivations of this project.

1.2.2　Motivations of the team project

This study has partially been sponsored by an industrial partner with the purpose of developing an enhancive exoskeleton as a marketable product. Therefore, the target requirements of the final product have been chosen to surpass those of the existing exoskeletons. The two key requirements crucial to the competitiveness of the final product are the load-carrying capacity and power efficiency, as will be explained in detail in section 3.3.4 of Chapter 3.

1.2.3　Motivations for this project and the research questions

The motivations behind the commencement of the team project have been pointed out in the previous section, and this section illustrates the motivations for studying the specific research aspects concerned in this project, as well as the research questions to be answered.

As mentioned earlier, the main purpose of the team project is to develop a marketable exoskeleton, which will have some leverage over its competitors. Therefore, the target specifications of the product are quite progressive and unmatched by the specifications of any currently existing exoskeleton. From the point of view of actuation, the design challenge is to develop an energetically autonomous (i.e. untethered) device, with increased strength (in terms of load carrying capacity) compared to its counterparts. In order to achieve this goal, it is necessary to reduce the power consumption while increasing the mechanical output power; in other words, maximisation of the power efficiency of the system is essential to this project. Many design factors

contribute to the power-efficiency of the actuation design, explained in the following paragraph.

As will be explained in section 3.8.1 of Chapter 3 (p67), it has been decided (after investigating different options) that the scope of this study should be limited to rotary electric motors as the active element of the actuators. Also, because the required output torques are large, a power-transmission (or gearing) mechanism is needed. The required transmission ratio depends on the torque capacity of the motor; larger motors require smaller ratios and vice versa. Therefore, varying the transmission ratio allows the usage of motors in a variety of sizes and weights. Finding the right motor requires the investigation of the relation between the motor specifications and the performance characteristics of the actuation system. As will be explained in the modelling section in Chapter 4, Increasing the motor size (and hence, motor maximum torque) decreases the power loss in the motor windings, but it also increases the mass of the system, which in turn increases mechanical power required during different exoskeleton manoeuvres, and decreases the maximum load-carrying capacity (i.e. more effort would be needed to carry the motor itself, for a larger motor). Therefore, an optimum solution should be found to achieve the best trade-off between the power efficiency and the mass of the motor. Although some research has been done in this area, the author could not find any studies in the literature that completely addresses this optimisation problem. Therefore, it is necessary to conduct research in this area to present a method for choosing the optimal motor size and transmission ratio.

Another important aspect of the actuation system is the type of power transmission system. Different transmission mechanisms can be used in the actuation system, including (but not limited to) harmonic drives, gear trains, planetary gears, chain and sprockets, cable and pulleys, and ball-screws. Though some qualitative comparison results have been mentioned in published studies, no detailed, quantitative comparative studies were found that would show the trade-offs between using different transmission system types, or any clear selection criteria. The results of such a study could be used in developing the optimal design concept.

The locations of the actuators also affect the inertial characteristics of the system and therefore the power consumption of the exoskeleton during different manoeuvres. Therefore, an investigation of the actuation system must take into account the mass of the actuators and their locations on the

exoskeleton frame. To the best of the author's knowledge, no studies on the design of exoskeleton actuators have taken this factor into account.

Finally, it is desirable to harvest the energy generated by the exoskeleton joints when the power consumption is negative (i.e. when an actuator is performing as a brake). Storing and reusing the regenerated energy could reduce the total energy consumption of the system, which is desired in an untethered system. A review of the literature done by the author did not reveal any information on this topic.

Based on the above-mentioned issues, a number of research questions have been chosen for this project, as mentioned in the following list. It should be noted that when "optimal" solutions are referred to in the research questions, the optimisation parameters are power consumption, load-carrying capacity, and the total mass of the system.

1. Considering existing off-the-shelf actuators and power transmission mechanisms, what are the optimal choices for each joint's actuator? And how can the answer be found?
2. Considering the answer to the previous research question, what would be the most suitable design of the actuators for an exoskeleton?

1.3 Aims and objectives

1.3.1 Aims of the team project

The aims of the team project are as follows:

I. To carry out fundamental research towards developing a full-body enhancive robotic exoskeleton.

II. To design and develop a prototype of an enhancive full-body exoskeleton.

III. To complete the project from a commercial standpoint, while giving consideration to manufacturing possibilities.

1.3.2 Objectives of the team project

The objectives of the team project are as follows:

(a) An investigation into the establishment of the full requirements and the engineering specifications for a full-body enhancive robotic exoskeleton.

(b) Mechanical design and development of a full-body enhancive robotic exoskeleton.

(c) An investigation into and selection of suitable actuators for the exoskeleton to cover the provision of a range of motions and forces for the exoskeleton joints.

(d) An investigation into and selection of suitable sensors for the full-body exoskeleton to provide full sensory feedback.

The sensors required by the exoskeleton to perform and function in response to the user commands. This would include movement, balance, ground sensing, etc.

(e) Design and development of a suitable controller for the full-body exoskeleton. This will include an investigation into a range of conventional controller strategies as well as into artificial intelligent control based on Neural Networks, Fuzzy Logic or Neuro-Fuzzy based controllers.

(f) An investigation into the required electronics, wireless communication and efficient power systems for the whole robotic exoskeleton.

(g) System integration, testing, and verification of the functionalities of the full system.

1.3.3   Aims of this project

The aims of this project are as follows:

I.   To carry out fundamental research on the actuation system of a lower-body enhancive robotic exoskeleton.

II.   To design and develop the actuation system for a prototype of a lower-body enhancive robotic exoskeleton.

1.3.4   Objectives of this project

In the context of the team project, i.e. the development of a full-body enhancive robotic exoskeleton, the objectives of this project are as follows:

a)   To perform dynamic simulations to assess the torque and power requirements at the exoskeleton joints.

b)   To investigate and characterise the commercially available electric actuators.

5

c)   To design actuation mechanisms for the joints to be actuated.

d)   To find the optimal motor size and transmission ratio for the actuators, with the consideration of the load-carrying capacity, power consumption, and the total mass of the system.

e)   To build a test prototype and perform experiments to validate the simulation and the optimisation process.

f)   To investigate the possibility of energy harvesting when the power consumption at the exoskeleton joints is negative.

1.4   The scope of this research

In this study, the decision on which joints to be actively actuated has been made after considering the torque requirements based on the intended manoeuvres and load carrying capability of the exoskeleton.

Only electrical actuators (including linear and rotary ones) have been considered in this study. This limitation of actuator type has been done because of considerations which have been fully explained in section 3.8.1 Furthermore, only the actuators of the lower-body joints in the sagittal plane have been investigated in this project, due to the limited time available.

1.5   The contributions of this study

As mentioned earlier, this study focuses on the actuators of the lower body joints (i.e. the ankle, knee, and hip joint) acting in the sagittal plane. The contributions of this research are therefore as follows:

- A thorough study was done and revealed that to develop an untethered exoskeleton with an acceptable load-carrying capacity, electric actuators must be used.
- An optimisation algorithm has been developed that uses a large search-space of available motors and power transmission systems. This algorithm can be used as a tool to determine the optimal actuation system for the joints of a robotic exoskeleton.
- It has been found that a ballscrew in a slider-crank mechanism is the best transmission system for the knee and ankle actuators. For the hip actuator, strain gears have been found to be more suitable.

- The most power-efficient motor sizes and actuation system characteristics (transmission ratio, pitch size, and mechanism dimensions) have been found using the developed optimisation algorithm.
- The detailed design of the ankle and knee actuators have been developed, based on the optimisation results.

1.6 Outline of this thesis

Chapter 1 of this thesis represents an introduction to the problem, as well as the aims and objectives of this research, its scope, and its contributions. Chapter 2 contains a literature review, focussing on the existing exoskeletons and ongoing research projects. Active orthotic devices are also covered. Furthermore, the biomechanics of human walking is also briefly demonstrated in section 2.9 of Chapter 2. Chapter 3 covers design considerations on the system level, which include the development of the needs and requirements of the prototype, as well as actuation system requirements. The chapter also covers a preliminary investigation of the different actuation system type that could potentially be used, and the choice that has been made. Chapter 4 covers the optimisation method used in this project, whereas the optimisation results are presented in Chapter 5. Furthermore, the detail design of the three actuators is presented in Chapter 5. The single-joint test prototype and the experiments done with it are covered in Chapter 6, as well as the validation of the method used. Chapter 7 summarises this report and presents the conclusions and the plan for the rest of the project.

Chapter 2
A Literature Review on Exoskeletons and Active Orthoses

2.1 Introduction

In this chapter, a review of the existing devices and ongoing research in the area of exoskeletons and active orthoses will be presented. This literature review covers the important studies and projects done, as well as recent works. Furthermore, section 2.9 of this chapter briefly presents an introduction to the human gait biomechanics. This is because it is necessary to possess a basic understanding of the human gait and its terminology in order to be able to comprehend the dynamic modelling of the exoskeleton motion, which is part of the optimisation method used in this study.

Some of the research projects done in the area of exoskeletons are either outdated or less important and have not been covered in this chapter. Reference [1] presents a good review of these studies, among which is the Hardiman project done in the 1960s, and the set of studies done in the 1960s and 1970s at the Mihailo Pupin Institute. Although these studies investigated some aspects of exoskeleton design and control problem, they also revealed that the state of the technology of those times was not advanced enough for the development of a practical prototype. It was only in more recent years that exoskeletons appeared as working prototypes and even commercialised products. These prototypes and research projects are the main subjects of this chapter, for the purpose of identifying the state of the art, as well as the knowledge gaps in this subject area, and the shortfalls of the existing products and prototypes. Orthotic devices have also been covered in this literature review, because of their similarities to exoskeletons.

2.2 Exoskeletons developed during the EHPA program

The Defence Advanced Research Projects Agency (DARPA), sponsored a program in 2001 called Exoskeletons for Human Performance Augmentation (EHPA) [1]. Prior to that date, other studies had been done in this area, and some prototypes had already been developed. However, the EHPA program is covered in the beginning of this chapter to emphasise its importance, since it resulted in some of the most capable existing exoskeleton prototypes to date, as will be mentioned later in this section. Furthermore, some of the studies done under the EHPA program yielded a number of published works

that have greatly contributed to the existing knowledge of the subject area, as will be mentioned later in this section.

The goal of the program was to "increase the capabilities of ground soldiers beyond that of a human". Three exoskeleton prototypes were developed by different institutions during this program, namely the BLEEX, XOS and MIT exoskeletons, which will be covered in the following sections.

2.2.1 The Berkeley Exoskeleton (BLEEX)

The Berkeley Exoskeleton (BLEEX), shown in **Figure 2-1**, was developed at the University of California Berkeley. Whilst technical data are not available for many of the existing exoskeletons (probably for commercial reasons), several papers have been published on BLEEX [2-7].

Revealed in 2004 for the first time at UC Berkeley, BLEEX allows its user to squat, bend, swing from side to side, walk on a horizontal or inclined ground, and step over and under obstructions while carrying its load.

Figure 2-1. The BLEEX exoskeleton [8]

It has been mentioned that BLEEX can carry 75 kg while being able to walk at 1.3 m/s; any excess load will be carried by the user. The 75 kg weight includes the weight of the exoskeleton itself as well as that of the load it carries [6]. Since the weight of the maximum payload of BLEEX is reported to be 34 kg [3], it could be concluded that the weight of the BLEEX exoskeleton is 41 kg. The weight of the load is transferred to the ground through the frame of the exoskeleton, not through the skeletal structure of the user.

BLEEX has a pseudo-anthropomorphic design, i.e. from a kinematic point of view, its architecture closely matches that of the human body, with some differences. For instance, the hip rotation axis does not pass through the rotation axis of the user's hip joint. Furthermore, the knee joint of BLEEX is a simple rotary joint, whereas the knee joint in human subjects is a combination of rotation and sliding.

Each leg has three DOFs at the hip, namely the flexion/extension (actively actuated), the abduction/adduction (actively actuated and spring loaded), and the rotation (free). The knee joint is a rotary one and actively actuated. The two legs share a sprung rotation joint located in the middle. The motion range of the ankle flexion/extension joint of BLEEX had to be extended to compensate for the lack of the small DOFs existing in the human foot, mainly at the toes.

The actuation system of BLEEX consists of hydraulic actuators, with an internal combustion engine as the power unit (hence, it is an untethered, energetically autonomous exoskeleton). The design team decided to rule out the use of rotary hydraulic actuators because of their internal leakage or large friction. Pneumatic actuators were not used either because of efficiency and controllability issues involved in their application. Hydraulic actuators were chosen because of their weight-power ratio advantage over electric ones [5].

Because the masses and inertial loads and the motion of BLEEX is similar to human lower limbs, Clinical Gate Analysis (CGA) data was used to approximate the joint torques and powers required to move BLEEX.

The application of electric actuators for BLEEX has also been studied by Zoss and Kazerooni [5], who introduced a method used for analysing and predicting the performance of electric actuators. This method is the basis of the optimisation method used in this study, which is explained in Chapter 4. A pancake style (i.e. thin with a rather large diameter) DC motor was used in conjunction with a harmonic drive. The final design of the electric actuator was

almost twice as heavy as the hydraulic actuator used in BLEEX, while being almost twice as power efficient. The study suggests the utilisation of electric actuators while moving the actuator up towards the torso and transferring the motion to the joint, especially for the ankle joint. Nevertheless, the BLEEX project was not carried out with electric actuators and no such version of the product has been built.

2.2.2 The XOS exoskeleton

The XOS exoskeleton (**Figure 2-2**) was developed by the Sarcos Research Corporation, which was later purchased by Raytheon, a huge American defence contractor [9].

Figure 2-2. The XOS exoskeleton [10]

XOS is a full body wearable robot, which is hydraulically actuated. Although the final aim is to develop an energetically autonomous system, XOS2, the latest generation of the device is still a tethered exoskeleton, with an off-board

power unit which is a specially developed internal combustion engine. The servo valves used to control the flow of the hydraulic liquid into the actuators have been custom-designed [7].

The XOS 2 consumes 50% less power than XOS 1, although it is still tethered. The user can "easily lift 200 pounds several hundred times without tiring and repeatedly punch through three inches of wood". The device is also agile enough for its user to be able to kick a football ball, punch a speed bag or climb stairs and ramps with ease [11]. The XOS exoskeleton weighs 68 kg, and can carry 91 kg [12].

2.2.3 The MIT Exoskeleton

Under the DARPA EHPA program, a quasi-passive exoskeleton was developed, named the MIT-Exoskeleton (**Figure 2-3**), at the Massachusetts Institute of Technology [13]. This device utilises passive mechanical components including springs and controllable dampers to produce negative power during passive phases of the motion of each joint in a walking cycle [14].

An interesting aspect of this design is the addition of a cam mechanism at the hip abduction/adduction joint [15]; this was done due to the fact that the centre of rotation of the exoskeleton leg in the coronal plane is not the same as that of the human thigh (i.e. the axis of the exoskeleton abduction/adduction joint does not pass through the user's hip joint). This, in turn, causes a relative change of the distance between the human leg and the exoskeleton leg if a simple rotary joint is used, which is the reason behind the inclusion of a cam mechanism in this joint.

The exoskeleton was tested while worn by a user with a 36 kg load in a backpack attached to the exoskeleton. Experimental tests showed that an average of 80% of the load was transferred to the ground by the exoskeleton. However, the exoskeleton increased the walking metabolic cost by 10% as compared to a 36 kg load carried on a backpack without the exoskeleton [16]. On the other hand, further tests showed that the exoskeleton, equipped with its springs and dampers, reduced the metabolic cost of walking by 12%, compared to the same exoskeleton but without the dampers and springs (i.e. with zero impedance). The research team concluded that the addition of passive elements does help to decrease the metabolic cost of walking, but not enough to compensate for the increase in the user effort in walking caused by other factors. These factors are the mass of the exoskeleton and the kinematic

restrictions that the exoskeleton imposes on the user, causing changes to the natural gait.

The addition of an active actuator at the hip joint to provide positive power was also tested on the MIT exoskeleton [17], but no further publications could be found to indicate that the metabolic cost of walking decreased as a result of this modification.

Figure 2-3. The MIT Exoskeleton [18]

2.3   Other Research Projects and Devices

2.3.1 The ExoHiker™ ExoClimber™ and HULC™ Series

Berkeley ExoWorks, a company formed by members of the Berkeley Robotics and Human Engineering Laboratory at UC Berkeley, was founded in 2005, and renamed as the Berkeley Bionics in 2007; the company was

renamed Ekso Bionics in 2011 [19]. The company (under different names at different times) has developed a number of exoskeletons. Among these products, there are (so far) three generations of enhancive exoskeletons designed for carrying loads. This section explains these three exoskeletons. All three variations are untethered and battery operated.

ExoHiker™

The ExoHiker™, completed in 2005, was the first generation of this family of exoskeletons. The ExoHiker™ is actuated by hydraulic actuators [19]. While there is little technical data available about its design, it can be seen in the available pictures and videos that only the knee joint is actuated. Each actuator seems to be connected to a separate pump that appears to run by an electric motor. The power supply of the system is a battery [8], and the device is reported to be able to walk for 42 miles with a 1 pound battery, although a solar panel option is also available that makes the operation duration unlimited. It is reported that the device runs for 21 hours with an 80 Watt-hour battery; this means that the power consumption of the device is 3.8 Watts. ExoHiker is reported to weigh around 14 kgf (31lbf) [8]. It can carry a load of around 68 kg while the wearer does not feel the load, and the noise of its actuation system is claimed to be "virtually imperceptible". The appearance of the ExoHiker™ is similar to that of the ExoClimber, shown in **Figure 2-4**.

ExoClimber™

The ExoClimber™, introduced in 2005, is also a load-carrying exoskeleton like the ExoHiker, with the difference that it allows rapid ascent of stairs and slopes [8]. It is battery-powered, while a small fuel cell is available as an alternative power source. The device can carry the same amount of load as the ExoHiker (68 kg) and weighs nearly 23 kgf (50 lbf). It is reported to be "as quiet as an office printer". **Figure 2-4** shows the ExoClimber™.

HULC™

The Human Universal Load Carrier (HULC™) is the third generation exoskeleton of this group, which has a similar appearance to that of its previous generations. HULC also uses hydraulic actuators and has two new characteristics that distinguish it from the last two generations. Firstly, it can carry up to nearly 91 kg (200 lb) of load without impeding the user. Second, it lowers the metabolic cost of the user [8]. In other words, it is not only a strength-augmenting exoskeleton but is also the first endurance-augmenting device of its kind. Users wearing the exoskeleton showed a 5%-12% reduction

in oxygen consumption while walking without a payload. When the test users were carrying a load of 37 kg (81 lb) and walking at a speed of 0.9 m/s (2MPH), their oxygen consumption was decreased by around 15%.

Figure 2-4. The ExoClimber exoskeleton [8]

2.3.2 Hybrid Assistive Limb (HAL™)

Hybrid Assistive Limb (HAL) was developed at the University of Tsukuba, Japan by Professor Yoshikuyi Sankai and his team. HAL is available in two forms as an exoskeleton, namely HAL-3 and HAL-5 (**Figure 2-5**). Furthermore, a single joint version of HAL is also available as a knee orthosis, which is explained in section 2.5.2

HAL-3 is a lower limb exoskeleton providing walking assistance to individuals suffering from Gait disorder [20]. It has three joints, each with one DOF, located at the hip knee and ankle. The ankle joint is not actuated whereas the knee and hip flexion/extension joints are powered using DC-motors and harmonic drives placed directly on the joints. HAL is untethered and battery powered, and its frame is made of aluminium alloy for lightness.

Electromyographic (EMG) signals have been used to identify the required torques for each joint [21, 22]. According to the manufacturers of the exoskeleton, it takes two months to calibrate a device for each individual user [23].

HAL-5, the fifth generation of the series, consists of a lower limb and an upper body exoskeleton. While the lower limb exoskeleton (HAL-3) has assistive and rehabilitative applications, the upper body exoskeleton which is part of the HAL-5 could be used to enhance the load-carrying capacity of the user, e.g. in care industry where nurses need to carry the elderly [23]. HAL-5 weighs 21 kg, but it is reported to support its own weight. The lower body of HAL is 15 kg approximately [24].

Figure 2-5. The HAL exoskeletons: (a) HAL-3, (b) HAL-5 [23]

There are no publications on the details of the HAL series design, but from the pictures and videos available online it can be seen that the exoskeleton legs are strapped to the user's thighs and shanks and that the knee joint appears to be a rotary joint, unlike the human knee joint which is a complex joint. This

will cause the motion of the exoskeleton and the user not to be exactly the same (as explained in 2.2.1). Therefore, the strapped connections at the shanks and thighs have to be flexible.

2.3.3 PERCRO's Body Extender

The Body Extender exoskeleton, shown in **Figure 2-6**, was developed at the PerCro (PERceptual RObotics) lab of the Sant'Anna School of Advanced Studies, in Pisa, Italy [25]. The project started in 2004 [26], with the aim of designing an enhancive exoskeleton for the purpose of load-handling. The electrically actuated exoskeleton weighs 160 kg [26] and is reported to be able to carry 50 kg per hand [27]. An external power supply is connected to the system by a tether.

Figure 2-6. The Body Extender exoskeleton [28]

The design of the actuators consists of an electric motor and a ball-screw, as depicted in **Figure 2-7**. The ballscrew converts the rotary motion of the electric motor into linear motion and is connected to a *tendon* made with two wire-

17

ropes in parallel. The tendon, together with a pulley, transfer the motion to the joint of the exoskeleton. Because wire ropes can pull but not push, a linkage mechanism is used to enable movement in both directions.
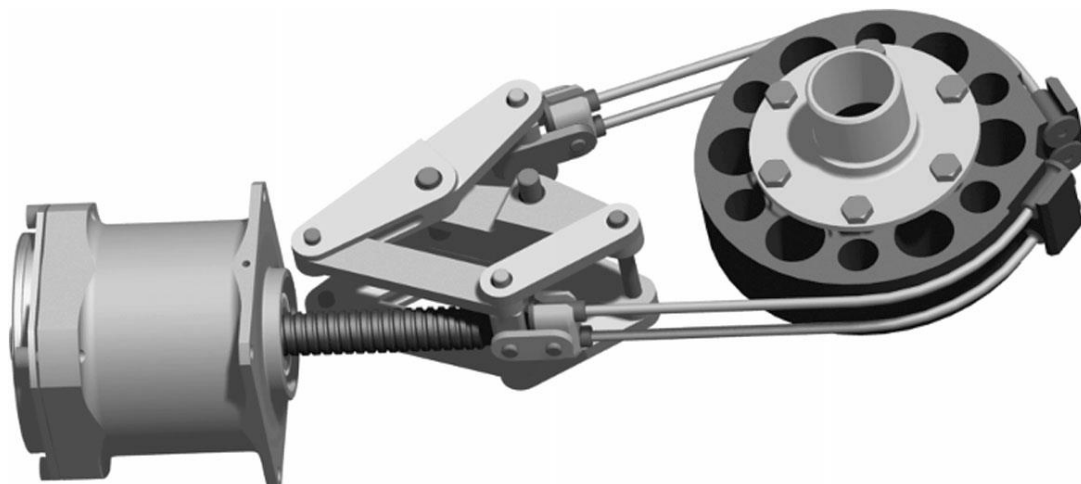
Figure 2-7. The CAD model of the actuators of Body Extender [28]

Despite the innovative actuator design of the Body Extender, the exoskeleton still suffers from two drawbacks, namely the heavy mass of the system, and the high power consumption which necessitates a large external power supply, and prevents the development of an untethered system.

2.3.4 Austin exoskeleton

The Austin exoskeleton (**Figure 2-8**) was developed at UC Berkley in 2011 as a low cost, widely available exoskeleton that provides assistance for walking to paraplegic people and those with mobility disorders [8]. The device was named after its first user, Austin Whitney, a paraplegic student at UC Berkley who walked in the exoskeleton across the stage on his graduation ceremony in 2011 [29]. The device has a stripped down design to minimise the price. The knee joint and the hip flexion/extension joint are coupled together and powered by a single motor for each leg, to lower the price further [30]. The gait follows a predefined pattern, and the legs of the exoskeleton step forward with a command from the user, sent by pressing buttons on the crutches that the user needs to hold. The device is battery powered and therefore untethered.

Figure 2-8. The Austin Exoskeleton [8]

2.3.5 ExoLight™

ExoLight™ is another exoskeleton developed at UC Berkeley for people suffering mobility disorders [31]. The weight of the device is nearly 10 kg (22 pounds) with 1.8 kg (4 pounds) of batteries [8]. There is little technical data available on the details of the device, but it looks to be based on a concept similar to that of the Austin exoskeleton described in section 2.3.3.

2.3.6 eLEGS™ and Ekso™

The Ekso Bionics company (already mentioned in section 2.3.1), debuted the eLEGS™ (**Figure 2-9**) exoskeleton in 2010, a device intended for assisting wheelchair users to walk [19].

Figure 2-9. The eLegs exoskeleton [8]

In 2012, Ekso™, "the first commercialized robotic exoskeleton for use in rehabilitative and medical facilities" was shipped to Craig Hospital. Although little technical data is available on the design of this product family, Ekso™ seems to be the final product developed based on the concept of eLEGS™. Unlike the Austin exoskeleton that receives signals from buttons on the crutches that the user carries, these devices can detect the movement of the user, so that when the user places one of the crutches in front of his/her body, the device initiates a step. Electric motors actuate the device, powered by an onboard battery.

2.3.7 ReWalk™

ReWalk™, developed by Argo Medical Technologies in 2008 [32], is an assistive/rehabilitative exoskeleton suitable for adult individuals with lower limb mobility impairments [33].

Figure 2-10. The ReWalk exoskeleton [34]

The device is actuated by DC motors on the knee and hip flexion/extension joints [34], while the ankle flexion/extension joint is not actuated with spring assisted dorsiflexion [35]. The power supply of the device is an onboard battery. **Figure 2-10** shows the ReWalk exoskeleton. Argo Medical Technologies acquired clearance from the U.S. Food and Drug Administration (FDA) for the ReWalk™ exoskeleton to be used at homes and in the community in June 2014 [33]. The company claims that ReWalk™ is the first exoskeleton available for personal ownership (in some markets).

2.3.8   Vanderbilt Exoskeleton (Indego)

The Vanderbilt Exoskeleton, marketed as Indego, is another device designed to assist individuals with spinal cord injuries to stand up and walk [36]. Tests on the device started in 2010 at Vanderbilt University [36]. The exoskeleton weighs 12 kg (27 pounds) and has been tested on users up to 90 kg (200 pounds) [37]. It is driven by electric motors that actuate the hip flexion\extension and knee joints [36]. **Figure 2-11** shows the Vanderbilt exoskeleton. The device is untethered with a battery as its power supply.

Figure 2-11. The Vanderbilt exoskeleton [37]

2.3.9 Rex Bionics exoskeleton

REX® is an exoskeleton developed by REX Bionics Plc, in New Zealand. The research project that led to the development of the device took nine years, beginning in 2003 [32]. It is actuated by electric motors and is an untethered device. **Figure 2-12** depicts the REX exoskeleton.

Figure 2-12. The Rex Bionics exoskeleton [38]

REX® is available in two varieties, namely REX Rehab™, designed to be used in rehabilitation centres and hospitals, and REX Personal™ which is an assistive device [39]. The operation of the exoskeleton is controlled by the user via a pair of joysticks.

One unique feature of REX® is that the user can walk in it without using crutches, as it keeps its balance while the user is inside it. It is also available to walk up and down stairs and slopes. On the other hand, it could be seen in the videos that the walking speed is quite slow compared to other devices like the Ekso™ that require the use of crutches.

It was reported in 2011 that the exoskeleton was available for 150,000 USD [38].

2.3.10   MINDWALKER

 The MINDWALKER exoskeleton (**Figure 2-13**), developed during a joint European project, is an assistive lower limb exoskeleton developed for people with lower limb disabilities [40].

(a)   (b)
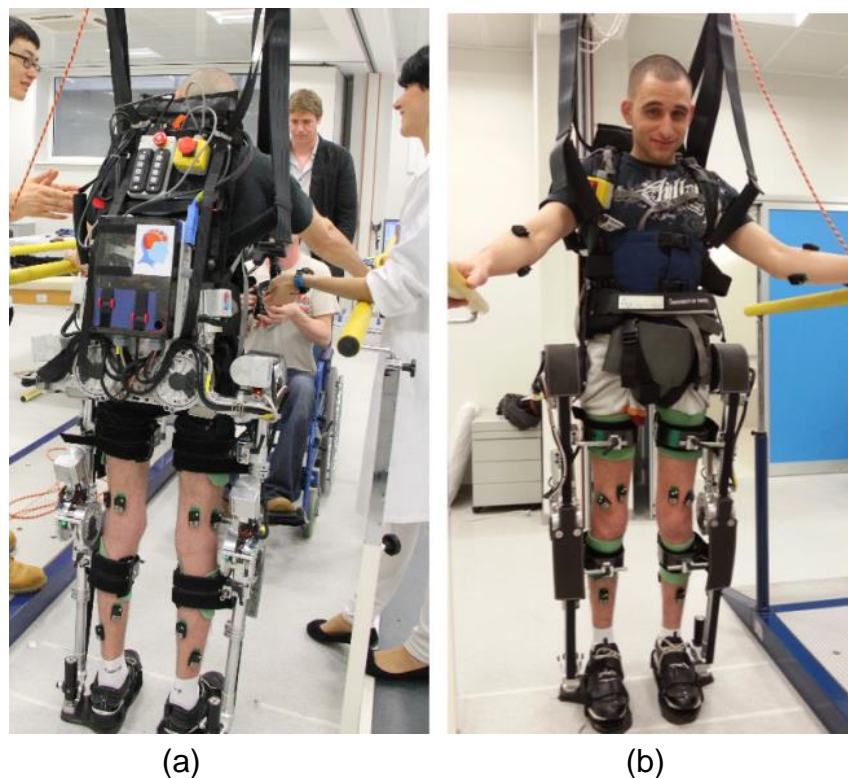
Figure 2-13. The MINDWALKER exoskeleton [41], the front (a) and back (b) views

A prominent aspect of the project is the use of Brain Neural Computer Interfaces (BNCI) technologies for controlling the exoskeleton. MINDWALKER is currently an ongoing project and the exoskeleton is not commercially available yet.

A custom-made series elastic actuator using a DC motor has been developed for the MINDWALKER, which will be explained in more detail in section 3.6.1. The MINDWALKER (excluding the power pack) weighs 24 kg [42].

2.3.11   Mina exoskeleton

The Mina exoskeleton, shown in **Figure 2-14**, is another lower limb exoskeleton developed at the Institute of Human and Machine Cognition (IHMC) to provide assistance to people who suffer from paraplegia.

Figure 2-14. The Mina exoskeleton [43]

The first publication on this exoskeleton was available in 2009 [44]. The exoskeleton has active actuators for the flexion/extension of the hip and knee joints, using identical actuators [43]. Each actuator consists of a DC brushless motor (Moog BN34-25EU-02) and a 160:1 harmonic drive (SHD-20 from HD Systems), combined with springs that form a Series Elastic Actuators (SEA). This provides accurate force feedback and low impedance, although it has the disadvantage of lowering the force-control bandwidth to 10 Hz at torques higher than 15 Nm, and 30 Hz at lower torques [44]. Since the device has

compliant actuators and hence can switch from rigid position control to a more compliant control, it may be more suitable for paraplegic users [43]. The device is attached to its power source via a tether, although the goal is to achieve an untethered commercial exoskeleton.

2.3.12   The Exoskeleton of the University of Tokyo

An assistive exoskeleton has been developed at the University of Tokyo of Agriculture and Technology to assist farmers with low physical abilities in demanding tasks involved in farming [34]. The exoskeleton was reported to be 25 kg, although the plan was to develop the commercial version of the device with half of the weight of the first prototype.

Figure 2-15. The exoskeleton developed at the University of Tokyo [34]

The actuation system of the exoskeleton uses artificial muscles that inflate via air pressure, (and could hence be considered a type of pneumatic actuator) [45]. The device is currently tethered and connected to an off-board air compressor.

2.4   Ankle-Foot Orthoses (AFOs): devices and research projects

2.4.1   A passive device to reduce the metabolic cost of walking

A study published in 2011 reports the results of a research conducted jointly by North Carolina State University and Carnegie Mellon University, on

developing a passive device to reduce the metabolic cost of walking [46]. The device, shown in **Figure 2-16**, only affects the plantar-/dorsiflexion of the ankle joint and comprises a spring and a smart clutch. The clutch disengages the spring during the swing phase of the gait cycle to allow free rotation, while it locks the spring during the stance phase to store energy during dorsiflexion and releases energy during plantar-flexion. The system works purely with mechanical feedback and does not have any motors or electronics. Their study showed that it takes some time for the users to adapt to the exoskeleton [47]; the test subjects used the exoskeleton for walking for 30 minutes per day, and on the fourth day an average of 10% reduction of metabolic cost was observed. It should be mentioned though, that this reduction is with reference to the case "with the added mass" of the device; this implies that no significant reduction was observed as compared to normal walking without the device (similar to the case of the MIT exoskeleton, explained in section 2.2.3). This means that although the energy storage-and-reuse mechanism reduces the metabolic cost of walking, this reduction is still not large enough to compensate for the increase in metabolic cost due to wearing the device.

(a) (b)
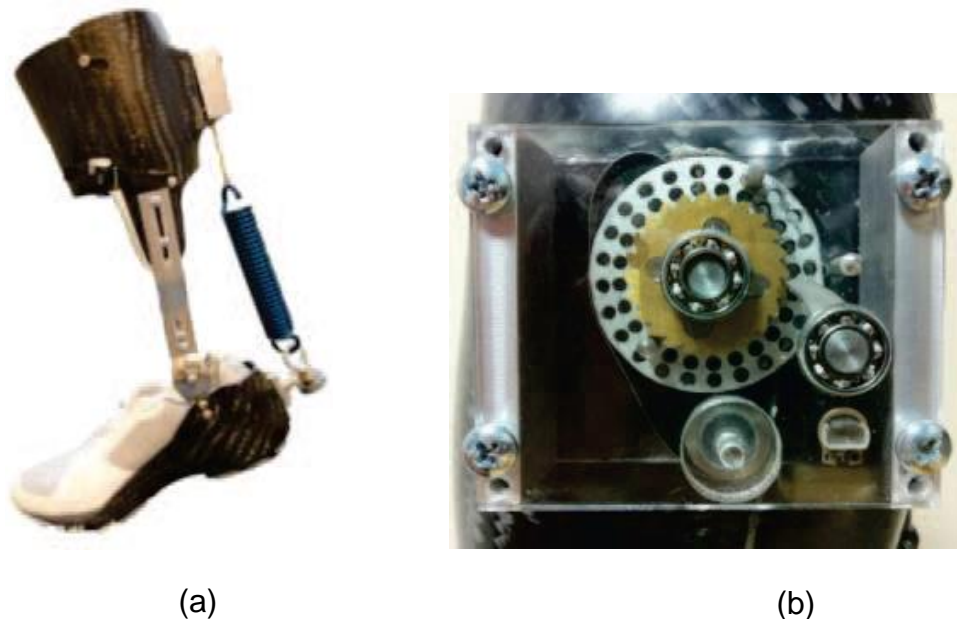
Figure 2-16. Passive ankle exoskeleton to reduce walking metabolic cost, (a) overview of the device, (b) the mechanical mechanism [46]

2.4.2 The MIT active ankle-foot orthosis

The MIT active ankle-foot orthosis, shown in **Figure 2-17**, has been developed by the MIT Biomechatronics group as an active orthotic device to treat drop-

foot gait [48]. The drop-foot gait is a condition which could be created by a stroke, multiple sclerosis, cerebral palsy, and/or other causes. The device uses an SEA (Series Elastic Actuator, explained in section 3.6.1). A linear spring-damper is connected in series with a rotary DC motor and a ball-screw transmission system, to form the SEA. The main purpose of using an SEA is to vary the impedance of the ankle joint in flexion/extension.
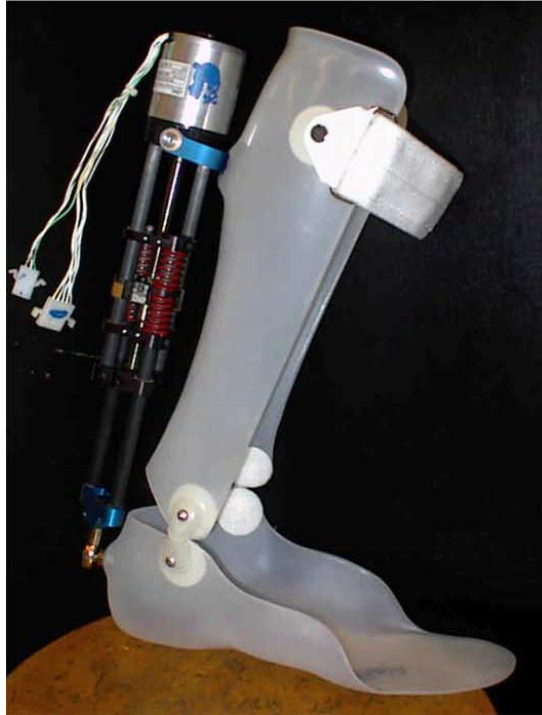
Figure 2-17. The MIT AFO [48]

2.4.3 Other studies on Ankle-Foot Orthoses

A number of research projects have been done on the development of active orthotic devices at the University of Michigan [1, 49]. The focus of the projects is on developing orthotic rehabilitative devices to be worn during therapy; therefore, the devices are not designed to be fully portable and are mainly actuated using pneumatic actuators connected via a tether to a stationary compressor. The actuators used are artificial muscles (depicted in **Figure 2-18**), a type of pneumatic actuator built using carbon fibre and polypropylene, which makes them lightweight. The actuators also have low mechanical impedance, which is an advantage from a safety viewpoint. The evaluation of the mechanical performance of the actuators used was studied [50]. The results showed that the torque production of the actuators was limited by force-length properties and especially by limited bandwidth (2.47 Hz). As a

result, and also because of the dependence of pneumatic actuators on (usually bulky) compressors, the research team concluded that the developed orthoses were not suitable for portable devices, although it could be valuable for gait rehabilitation research on the biomechanics of human walking.

Figure 2-18. University of Michigan AFO [49]

2.5 Knee Orthoses: devices and research projects

2.5.1 RoboKnee

The RoboKnee project was carried out in an attempt to develop a simple device to add power while climbing stairs and squatting while carrying loads. The device, shown in **Figure 2-19**, is based on an off-the-shelf knee brace [51], and a custom-designed Series Elastic Actuator (SEA, refer to section 3.6.1) to actuate the knee joint.
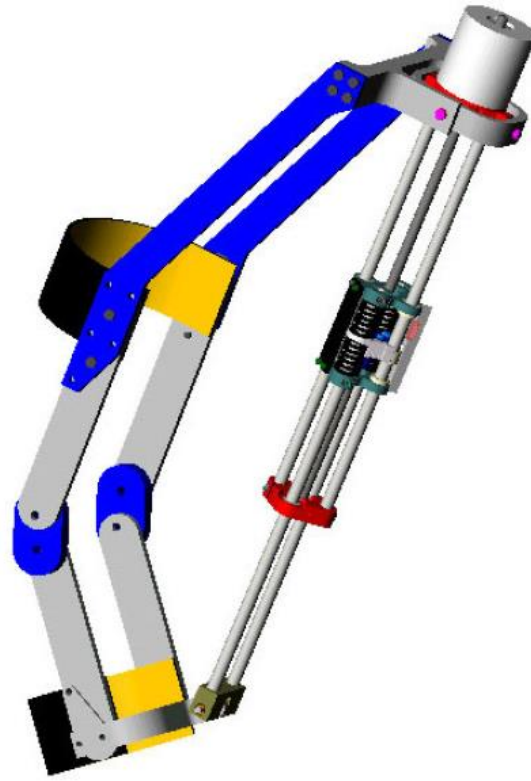
(a)
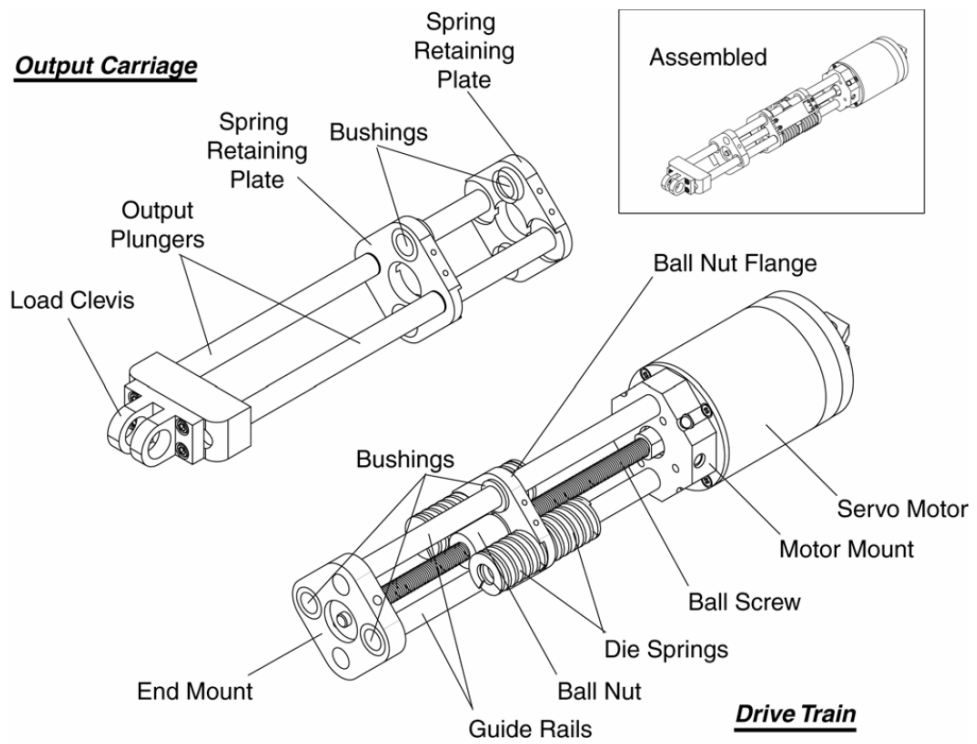
(b)

Figure 2-19. The RoboKnee orthosis (a), and the SEA used for actuation (b) [51]

2.5.2 Single-Joint HAL

A single-joint variation of the HAL exoskeleton (section 2.3.2) has been developed as a knee orthosis [23, 52]. The device, depicted in **Figure 2-20**, seems to use the same type of actuation mechanism as the HAL3 and HAL5 exoskeletons, i.e. electric DC motors and harmonic drives.

Figure 2-20. Single joint HAL [52]

2.5.3 Other studies on knee orthoses

A study was published in 2013 on a prototype of a knee orthosis, mainly on the control aspects [53]. The device, shown in **Figure 2-21**, is actuated via a mechanism comprised of a brushless DC motor, a ball-screw, and a belt drive.
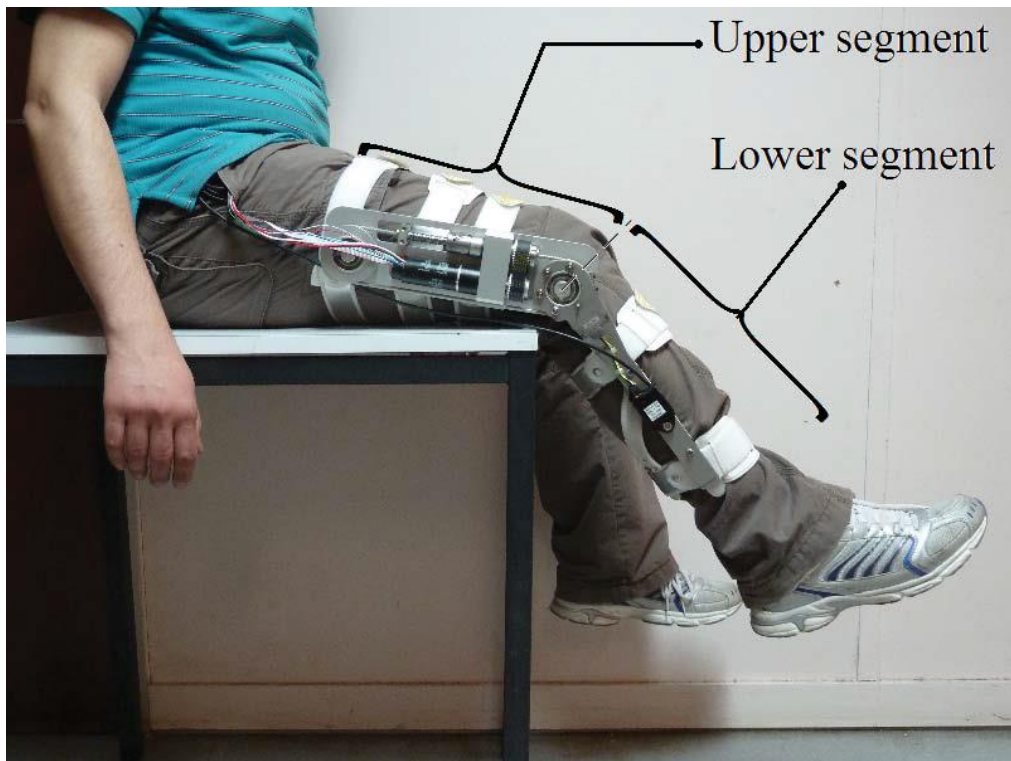
(a)
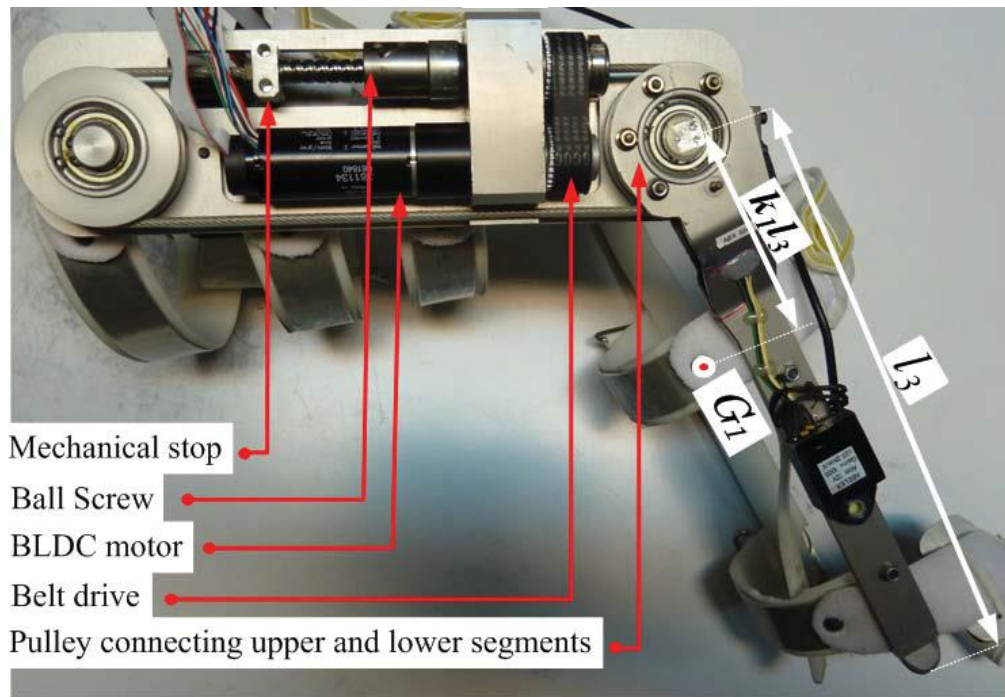
(b)

Figure 2-21. A Knee orthosis prototype (a), and the design details (b) [53]

2.6   Knee and Ankle-Foot Orthoses (KAFOs): devices and research projects

2.6.1   University of Michigan KAFO

Following the projects done on developing an ankle-foot orthosis (AFO) at the University of Michigan (explained in section 2.4.3), the existing AFO design was extended to build a KAFO [54].

(a)   (b)
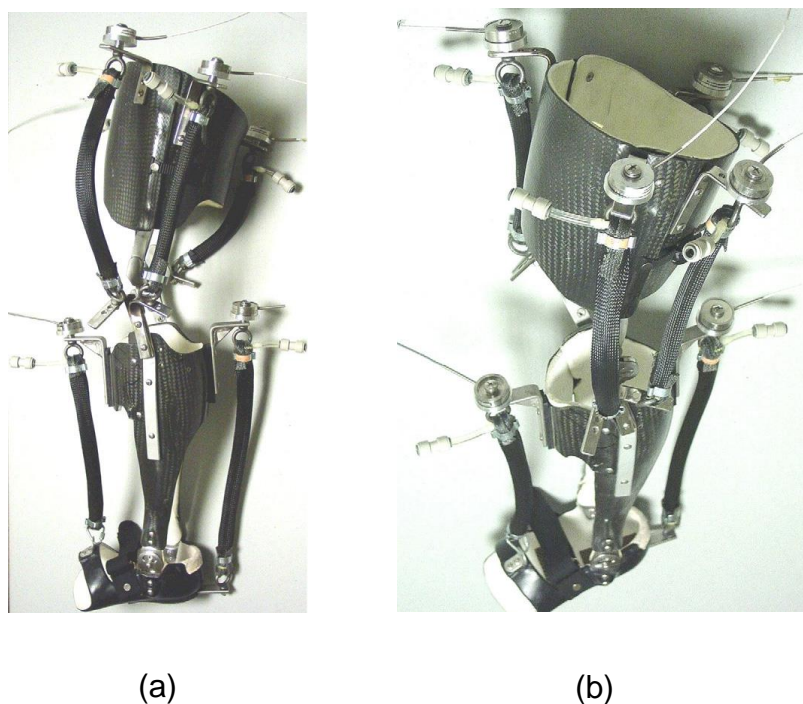
Figure 2-22. University of Michigan KAFO [54], view from the side (a) and the above (b)

Like the AFO, the KAFO (**Figure 2-22**) also uses artificial muscles, which are categorised as pneumatic actuators. The studies revealed that using artificial muscles is not the best option for joints intended to perform negative work (like the knee joint). The reason for this, according to the authors, is most likely the force-length relationship of artificial pneumatic muscles, which results in a steep linear increase in force as an artificial muscle lengthens, which in turn "makes it difficult to perform extended negative work against inertial loads like human body mass".

2.6.2   A power-assist, lower-limb orthosis with pneumatic muscles

Another prototype of a KAFO actuated by artificial muscles was the subject of a study published in 2010, focusing on the control of the pneumatic

actuators used in the prototype [55]. The device, depicted in **Figure 2-23**, is actuated by a tension-only pneumatic muscle, which is attached to a zigzag-shaped steep wire acting as a spring to pre-stretch the pneumatic muscle.

Figure 2-23. A portable pneumatic KAFO [55]

One interesting aspect of this device is that, instead of an air compressor, a compressed carbon-dioxide (CO_2) tank and a gas accumulator power the pneumatic actuator. However, this power supply takes up most of a bulky, 4 kg backpack that the user needs to carry. Therefore, the usability of pneumatic artificial muscles in a portable device remains dependent on developing compact, lightweight power sources for the compressed gas used in the actuators.

2.6.3 Other studies on KAFOs

A study published in 2012 focuses on the design and control of a KAFO, actuated by pneumatic actuators [56]. The frame of the device is a standard metal-frame KAFO, as shown in **Figure 2-24**.
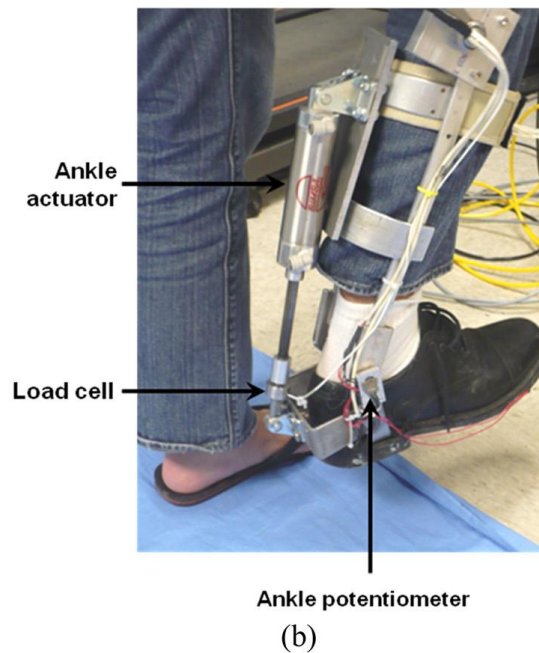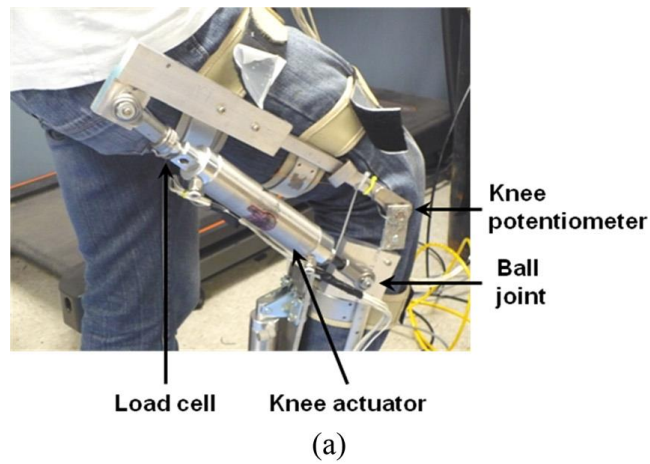
Figure 2-24. A pneumatic KAFO [56], with actuators for the knee (a) and ankle (b)

Unlike the KAFOs previously mentioned (sections 2.6.1 and 2.6.2), this device is actuated by standard, piston-cylinder pneumatic actuators, rather than artificial muscles.

2.7 Hand Orthoses: devices and research projects

2.7.1 ExoHand

The ExoHand (shown in **Figure 2-25**) is a hand exoskeleton developed by Festo [57]. It can be worn like a glove, with the pneumatic actuators amplifying the strength of the fingers.
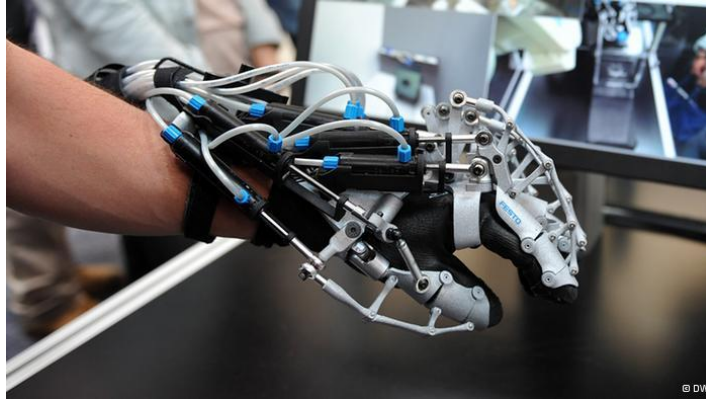
Figure 2-25. ExoHand [57]

2.7.2 Other hand orthosis projects

HyunKi In et al. built a glove-like hand orthosis [58]. The fingers are moved using tendons attached to a motor and gearhead on the palmer side, and two springs on the dorsal side, as shown in **Figure 2-26**. the study focuses on analysing the friction characteristics inside the system, for control purposes.
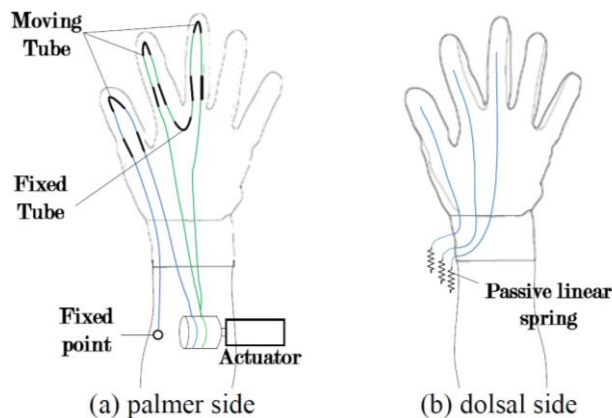
Figure 2-26. A Hand Orthosis with tendons, (a) palmer side, (b) dorsal side [58]

2.8 Arm Orthoses: devices and research projects

2.8.1 Wilmington Robotic Exoskeleton

Although this device is named the Wilmington *Robotic Exoskeleton*, it is actually a passive arm orthosis, as shown in **Figure 2-27**. A very interesting idea, which is used in this design, is the utilisation of passive elements (elastic bands) to assist movements against gravity. The elastic bands partially cancel out the gravity force acting on the arm, making it easier for a user with underdeveloped muscles to lift and move their arm. A version of this device,

made for children, is made from ABS plastic by 3D printing and is very
lightweight [59, 60].

Figure 2-27. The Wilmington Orthosis [60]

2.8.2 The Myomo and MyoPro orthoses

Myomo (**Figure 2-28**) is a rehabilitative device intended to be used by
"individuals affected by brain injury such as stroke, spinal cord injury (SCI),
multiple sclerosis (MS), cerebral palsy (CP), muscular dystrophy (MD) and
traumatic brain injury (TBI)" [61]. The Myomo technology has been developed
at the MIT and is now provided by the Myomo Inc. Commercially known as
mPower 1000, it is an arm brace with sleeve-like parts that is worn by the user.
Myoelectric sensors attached to the users' skin pick EMG signals, and the
electric motor at the elbow joint assists the user in performing arm
movements. The device can be used during rehabilitation in Repetitive Task
Practice and is for use in clinical settings. Research confirms the effectiveness
of therapy with Myomo [62].

A variation of the device is the MyoPro, with a brace that encompasses the
hand as well as the forearm [63], although only the joint at the elbow is actively
actuated.

Figure 2-28. Myomo [61]

2.8.3 Other arm orthosis projects

Herrnstadt and Menon developed a lightweight portable orthosis for suppression of tremor at the elbow [64]. The device, depicted in **Figure 2-29**, is not actively actuated, instead, an electromagnetic brake (EB) with an on-off actuation scheme suppresses the tremor. Their study showed that the device can reduce tremors by over 88%.

2.9 Human movement biomechanics from the actuation point of view

2.9.1 Introduction

This section explains the relevant topics of the human anatomy and the biomechanics of human movements. Because this project starts with the analysis and design of the lower body part of the exoskeleton, this section also focuses on the lower limbs of the human body and the gait cycle.

Figure 2-30a (a) shows the anatomical planes concerned in human gait analysis. The transverse plane is parallel to the ground (horizontal), whereas the coronal and sagittal planes are perpendicular to the ground and to each other. The coronal plane is the plane in which the human front view is depicted, while the profile view lies in the sagittal plane. The motions involved in human walking are mainly (but not entirely) in the sagittal plane. The joint motions are explained in the following section, and more details can be found in [65].
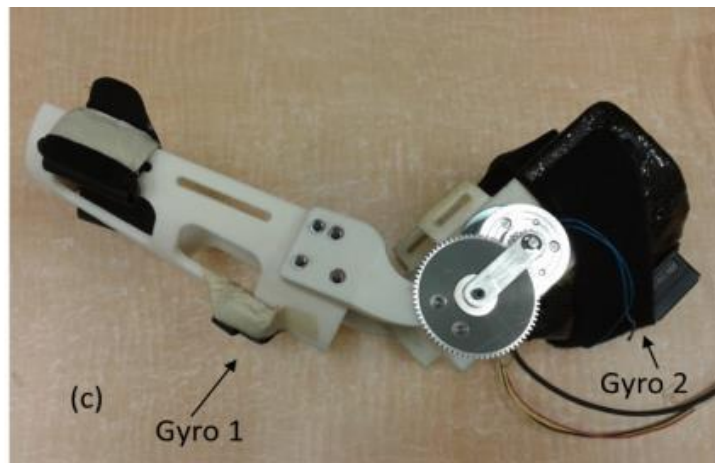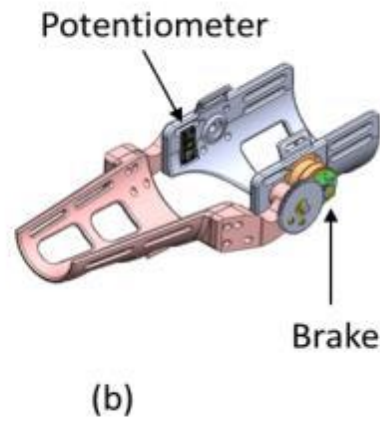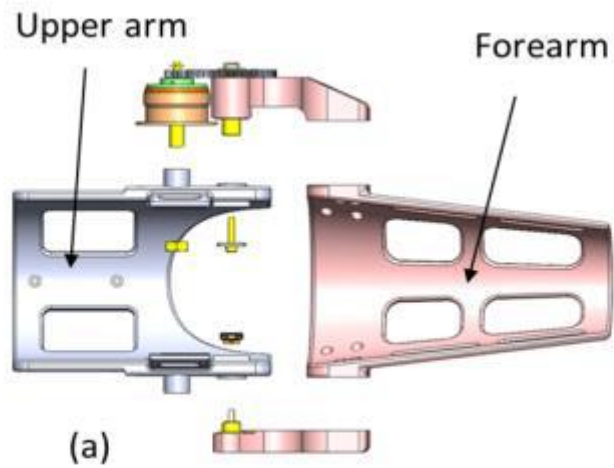
Figure 2-29. An arm orthosis for tremor suppression, (a) frame components, (b) brake and potentiometer, (c) the whole system [64]

The human hip joint can be considered to have three rotational DOFs. The knee is a complex joint with rotation and sliding motions in the sagittal plane, and other small DOFs in other planes; the knee motion in these small DOFs are less important in human gait analysis, as has been explained in reference [1]. Therefore, these DOFs have been neglected in this study, and the knee motion is considered to be a pure rotation. The ankle can be considered to have three rotation DOFs in the three planes. In this report, the terminology used in [1] has been adopted: the motion of the hip, knee and ankle joints in the sagittal plane are referred to as flexion (positive direction) and extension (negative direction), as shown in **Figure 2-30** (b). The motion of the hip in the coronal plane is named abduction (away from the body) and adduction (towards the body). Ankle motion in the coronal plane is referred to as eversion (away from the centre of the body) and inversion (towards the centre of the body). The other motions of these three joints are referred to as rotation throughout this text.
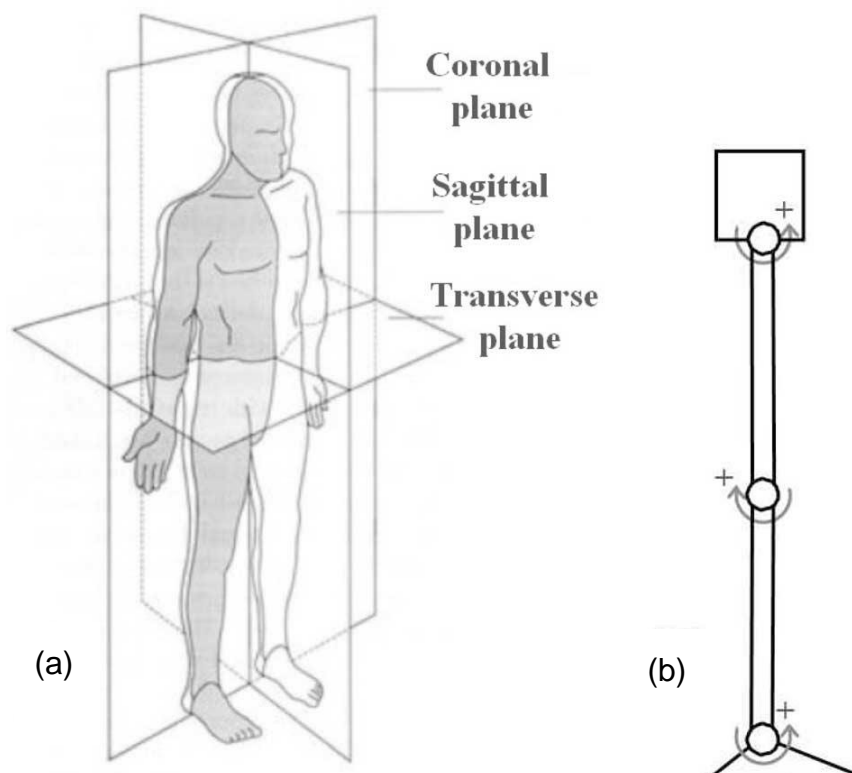
Figure 2-30. (a) Anatomical Planes. (b) a simplified diagram of the leg with all angles at zero degree, and the positive direction of all angles [1]

2.9.2 Human gait cycle

The human gait cycle is divided into a number of stages, as shown in **Figure 2-31**. It starts with the foot strike on one side and ends with the foot strike on the same side (right leg in the figure). The phase during which the foot is on the ground is referred to as "stance", and the one during which the foot is not touching the ground is the "swing" phase.

The joint angles, moments and powers for a normal healthy individual during one gait cycle are shown in **Figure 2-32**, [66]. Note that only the motion in the sagittal plane is considered, and also that these values are approximate and vary amongst different individuals [65, 67].

2.10 Energy harvesting in a robotic exoskeleton

As could be seen in **Figure 2-32** (c), for all three joints, there are sections of the gait cycle where the power consumption is negative. Negative power consumption means that the joint is generating power rather than using it. This means that, in theory, some of the generated energy can be harvested and stored. If energy harvesting can be done, then the total energy consumption of the exoskeleton can be reduced; this is highly desirable for an untethered design since the required energy capacity of the power supply will be reduced.

Although the idea of energy harvesting in exoskeletons was introduced as early as 1973 [1], no further mention of it was found in the literature review done by the author.

2.11 Summary

This chapter presents a review of the existing robotic exoskeletons and active/quasi-active orthotic devices, as well as some other related research projects previously done. The strengths and weaknesses of the devices have been pointed out, as well as interesting features from the design and/or control point of view. This review of the existing exoskeletons and orthotic devices has revealed some gaps in the literature, as will be explained in the following paragraph. It must be noted that the focus here is on enhancive exoskeletons, although assistive devices have also investigated. Furthermore, lower-body and full-body exoskeletons have been considered separately, because of the

difference in their design requirements, as will be mentioned later in this section.
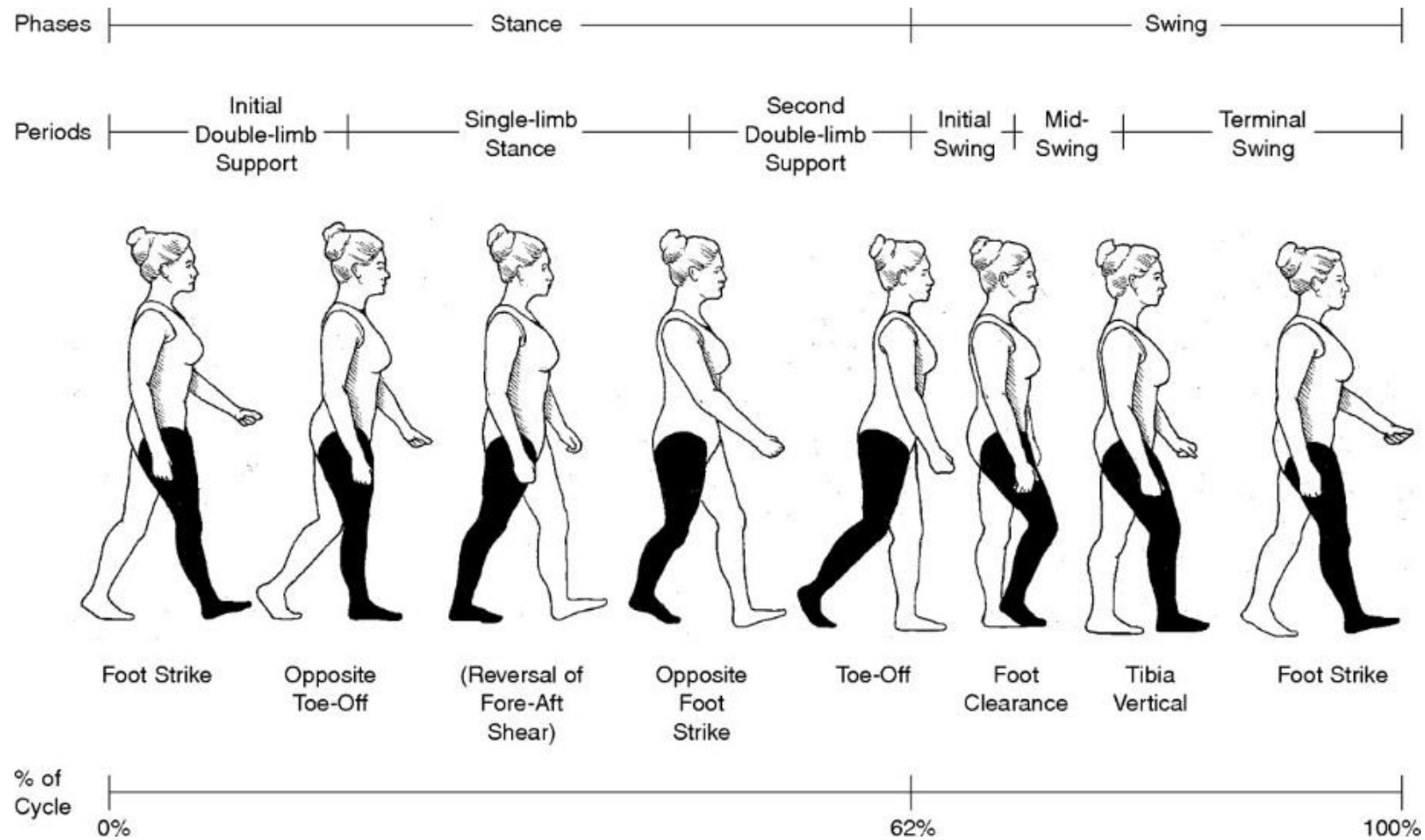
Figure 2-31. The Human Gait Cycle [68]

42
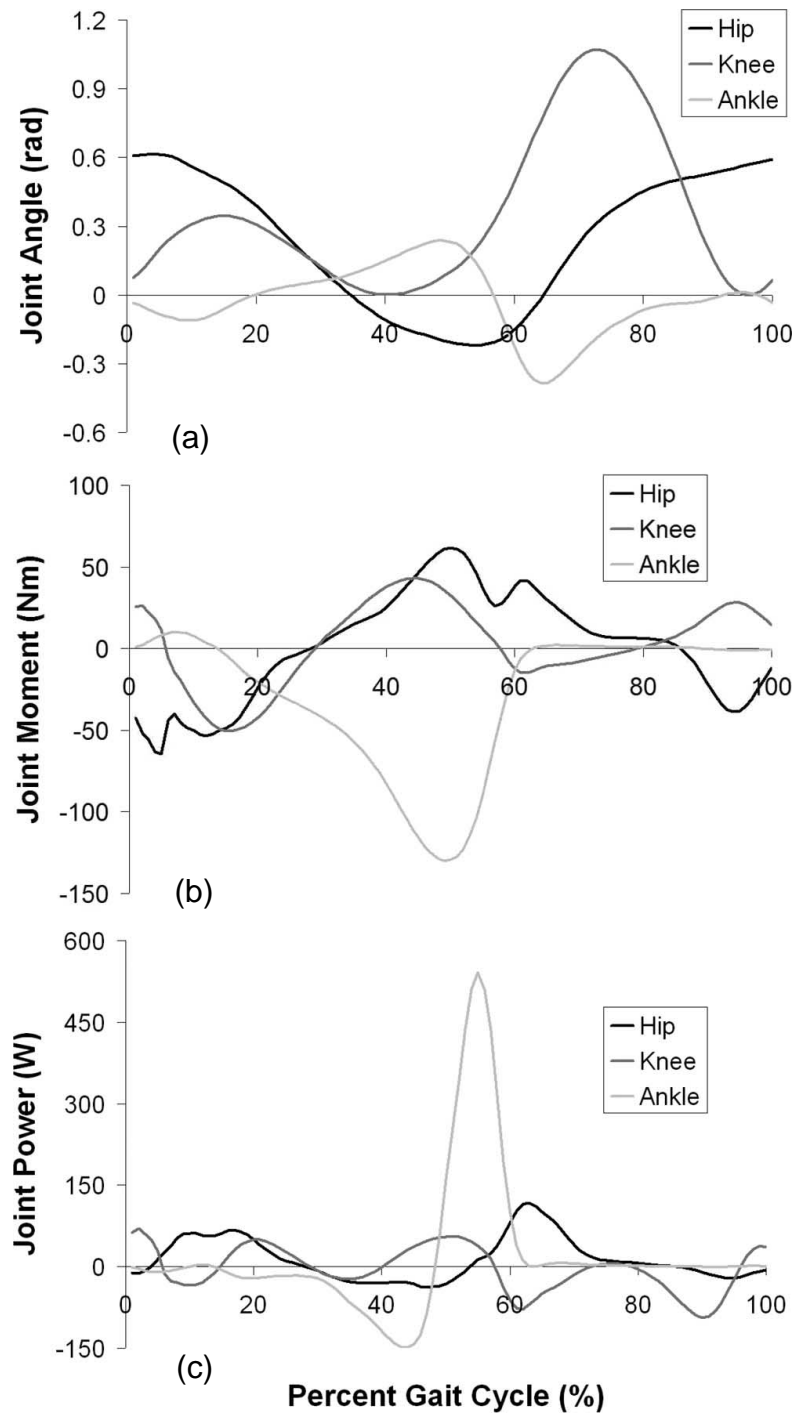
Figure 2-32. Typical values of the flexion/extension motion of human joints during one gait cycle: the angles (a), moments (b) and power (c) [66]

As mentioned earlier in this chapter, a significant amount of research has been carried out on lower-body exoskeletons, some of which has led to the development of operational and even commercially available lower-body

exoskeletons. The commercialised assistive models found in this research are the HAL-3, eKso™, ReWalk™, and Indego™, and the Rex Bionic exoskeletons. However, this study only revealed the existence of one commercialised enhancive lower-body exoskeleton, which is HULC™. Nevertheless, the availability of HULC™ in the market shows that a suitable design solution has been found for the actuators of enhancive lower-body exoskeletons (with acceptably high load-carrying capacity and operation duration). However, this is not the case when it comes to the design of the *lower-body actuators* for a *full-body exoskeleton*, as will be explained in the following paragraph.

Lower-body enhancive exoskeletons consist only of the lower-body section of the device, plus a frame on the back for carrying a backpack and also supporting the other components of the exoskeleton (e.g. the power-supply and electronics). In contrast, a full-body exoskeleton also has an upper-body section, which makes the whole system heavier than a lower-body exoskeleton. This also means that the lower-body frame of a full-body exoskeleton needs to be stronger (and therefore heavier) than a lower-body exoskeleton frame. For these reasons, the *lower-body* actuators of a *full-body* enhancive[1] exoskeleton need to be stronger than the actuators of an enhancive exoskeleton without an upper-body section. Also, stronger actuators are also likely to be heavier, and this increases the weight of the device even further.

Full-body exoskeletons not only need stronger actuators but also more actuators than lower-body exoskeletons. The reason for this is as follows: since lower-body exoskeletons are comparatively light-weight[2], it is not necessary to actively activate all of the DOFs; instead, some of the DOFs could be spring-loaded and/or actuated by the user's effort. An example is the HULC™ exoskeleton, which has active actuators only on the knee joints. On the other hand, most of the DOFs of a full-body exoskeleton need active actuators, because of the excessive weight of the device. Examples are the

---

[1] As mentioned in the beginning of this section, the focus in this literature review, and in this research project, is on enhancive exoskeletons.

[2] The HULC™ exoskeleton without its battery weighs 24kg, which is much ligter than the XOS (68 kg) and the Body Extender (160 kg).

44

XOS and the Body Extender exoskeletons, each with actuators at the ankle, the knee and the hip joints.

The need for more actuators, as well as stronger ones, also means that the power consumption of a full-body exoskeleton would be more than a lower-body exoskeleton with a similar load-carrying capacity. Large power consumption makes it challenging to develop a portable power supply, which is why the Body Extender and XOS exoskeletons are both tethered to their non-portable power sources. In fact, the HAL-5 is the only full-body enhancive exoskeleton developed so far, which can only carry 40 kg of load. To this date, no untethered full-body exoskeleton with a load-carrying capacity larger than 40kg exists. Developing such an exoskeleton would require more weight-efficient power supplies (so that they could be portable), and/or more power-efficient actuators; among these two design improvements, the latter is the aim of this study, which focuses on actuation system design.

Although the concept of energy harvesting in exoskeletons has been suggested in the literature, no reported studies were found on its practicality and the technical challenges involved. Therefore, it cannot be determined from the information found in the literature if energy harvesting in exoskeletons is possible, and if so, how it could be done.

Chapter 3
System Design Considerations

3.1 Introduction

This chapter covers the design considerations of a robotic exoskeleton on the system level. These considerations have been taken into account in order to narrow down the actuation system type for the prototype to be developed. The design method used has been introduced in section 3.2.

Sections 3.3 and 3.4 represent the needs and requirements of the exoskeleton and the actuation system, respectively. Based on these requirements, a decision on the type of the actuation system has been made, which is covered in subsequent sections.

The scope of this research is limited to the use and combination of off-the-shelf components (e.g. hydraulic cylinders, electric motors, and gearing mechanisms), in order to design the actuation system. This means that, for instance, this study has not addressed the design problem of a bespoke electric motor to meet the design requirements; instead, only off-the-shelf electric motors have been considered. Therefore, the investigation presented in this chapter only covers the actuators types already available in the market.

Although actuators exist in different types, not all of them are suitable for a robotic exoskeleton. For instance, to the best of the author's knowledge, Piezoelectric actuators have not yet been successfully used in applications involving macro-scale displacements. Another example is the Magnetorheological systems, which are still under research and have not yet been used in applications similar to the problem at hand. This chapter only covers three types of actuators which are suitable for robotic exoskeletons, namely pneumatic, hydraulic and electric actuators. An investigation of these three actuator types is presented in section 3.5, including the strengths and limitations of each type.

The literature review done in this study revealed a considerable number of research projects on the incorporation of elastic components within the actuators of exoskeletons and orthotic devices. This topic seems to be worth attention and has been covered in section 3.6. Section 3.7 focuses on the location of the actuators, and its effect on system performance. Finally, the comparison between the actuator types and the final selection is covered in section 3.8.

3.2 Methodology

As the first step to understanding and approaching the problem, a literature review has been done on the state of the art powered exoskeletons and the design challenges involved.

In the next stage, the needs and target requirements of the final product have been identified, through consideration of the industry–motivated goals of the project, the need for marketability of the final product, and the shortfalls of the existing exoskeletons. A standard product-development approach towards the identification of the needs and requirements has been taken, elaborated in the following section. **Figure 3-1** shows the product development approach adopted from [69]. A similar approach with slight differences has also been recommended in [70]. Note that the final stage, referred to as production ramp-up, is outside of the scope of this project. It should also be noted that this procedure is iterative rather than linear, and new findings at each stage might necessitate the revisiting of previous stages.
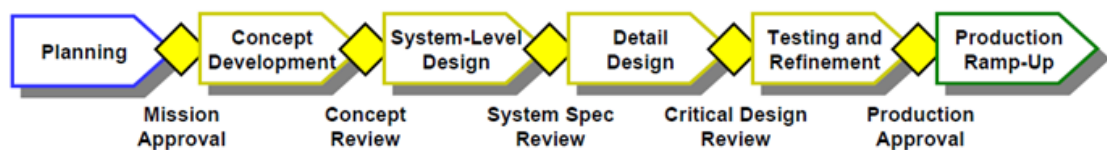
Figure 3-1. The Product development procedure, [69]

The concept development stage involves a procedure illustrated in **Figure 3-2**. It starts with the identification of the product needs, followed by the establishment of the specifications (referred to as "requirements" hereafter in order not to be confused by technical specifications of the product). These two stages and the methodology used are illustrated in the subsequent chapters of this report.

The system level design involves the cooperation of all team members, as each of them (including the author) has been working on a separate sub-system. This report mainly reflects the contribution of the author to the project, which has been on the actuation system, although relevant topics of the design and specification of other subsystems will be mentioned where necessary.

Initial analytical calculations and simulations have been performed on the static and dynamic behaviour of the system to identify the torque requirements and the power consumption of the actuators to perform the required tasks. Based on these results, a market search has been done to identify the most appropriate off-the-shelf electric motors, and transmission systems. The search criteria will be explained in detail in Chapter 4.

Dynamic simulations have been used to assess the performance of the joint actuators with each of the available elements of the actuators, i.e. the motors and transmission systems. The decision for choosing the optimal actuator elements was made with the help of a decision table, based on the load carrying capacity, power consumption, and the total mass of the exoskeleton.

The results of the optimisation procedure included the motors to be used, and the power transmission system (including the transmission ratio/pitch size and other dimensions). Based on these results, a prototype of a single-joint exoskeleton actuator was designed and built. This prototype was used to measure the electric power consumption, which was compared to the value predicted by the simulations. The results of the comparison were used to verify the simulation results, and also to modify the estimated value of the controller efficiency, which is used by the optimisation program. Using the modified value, the optimisation procedure was repeated to obtain a final result that indicates the best options for the motors and transmission mechanisms of the actuators.

It is worth mentioning that during the concept design and detail design stages, many technical problems were encountered which needed to be solved. The author found the *Theory of Inventive Problem Solving* (*TRIZ*) very helpful in finding solutions to these problems [71, 72].

3.3 The Needs and Requirements of the Exoskeleton System

3.3.1 Introduction

The design process followed in this project involves the development of the design concepts for the exoskeleton as a system, which starts with identifying the needs and requirements of the device. The needs and requirements serve as guidelines throughout the design process.
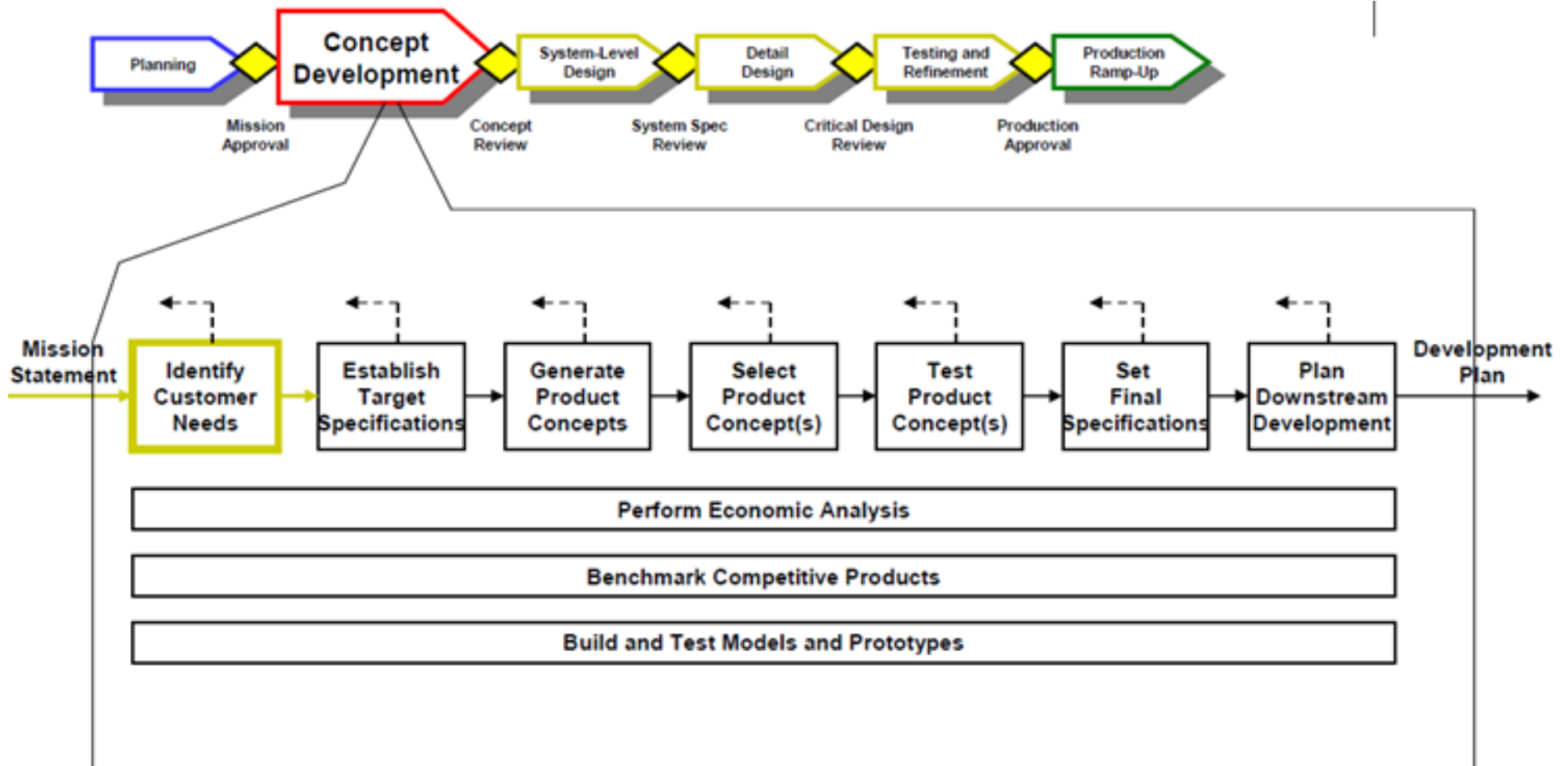
Figure 3-2. Stages of concept development, [69]

The method used in this project, which can be found in [69], has been illustrated in **Figure 3-2** (p49), and involves the following stages: once the needs are identified, the target requirements (sometimes referred to as specifications) should be established. After that, different concepts need to be generated, selected and tested against the requirements. This is an iterative procedure and also involves the modification of the requirement. This process yields a modified, realistic set of requirements and a design concept that can satisfy the requirements. Finally, the rest of the project (in this case, detailed design and testing) need to be planned in details.

The set of product needs specifies what the product is expected to do, regardless of the type of design used. Because this project is partially funded by the industry, the expectations of the industrial partner are crucial to the identification of the needs. On the other hand, inputs from the PhD students of the team and the supervisors have proved to be useful in modifying the product needs to keep them realistic while still aiming for a progressive design. The team had several meetings and all team members contributed to finalising the needs documents.

After completing the list of product needs, the list of product requirements was developed. The requirements are the translation of the needs into technical terms and are more technical and precise than the needs. They specify *what* the device is expected to do (the problem), and not *how* it will do the job (the solution) [69]. Nevertheless, unlike needs that are independent of the solution concepts, the requirements are closely related to the concepts used in the design. This is because the requirements are technical and quantitative. Because of the close relationship between the requirements and the chosen concepts, the requirements cannot be finalised at the initial stages of the project. Instead, after the needs have been identified, a set of *target* requirements should be specified and then modified at a later stage, during concept generation. Finally, after the concept choice is finalised, the list of final requirements will be produced. The process of establishing target requirements is depicted in **Figure 3-3**.

Each requirement is made of a metric and its values. Once the list of metrics has been produced, benchmarking information is gathered based on competitor products. After that, each metric is assigned a marginally acceptable value and an ideal value. In the final stage, the effect of the assigned values on the design and the process (including the manufacturing process) is considered, and any necessary modifications are made.
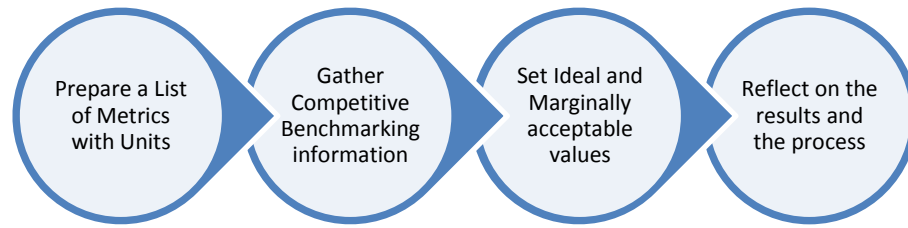
Figure 3-3. The stages of creating target requirements [69]

Through several meetings, as well as individual work done by the team members, the team produced the target requirements list using the above-mentioned approach, and with the aid of the benchmarking information acquired from the literature.

3.3.2 List of needs

The list of the required manoeuvres of the exoskeleton and the complete list of needs are presented in Appendix A and Appendix B. Some of the needs do not concern the actuation system, whereas others should be kept in mind throughout this project. The needs relevant to this project are listed in Table 3-1.

The needs listed in Table 3-1 influence the decisions involved in the actuator design; for instance, need #6 specifies that the device should be untethered. This imposes limitations in the power consumption of the actuators and also intensifies the importance of design optimisation for power-efficiency (stated separately in need #14), which in turn affects the operation duration (need #15). Need #7 steers the design process towards achieving the maximum possible load-carrying capacity. Need #13 points out the importance of lightness of the actuation system, which in turn affects the safety, power consumption and the load-carrying capacity (since a lighter design will require less effort to be spent on moving the exoskeleton itself). Need #24, together with the list of desired manoeuvres (Appendix A), specifies the capabilities of the actuation system. Need #26 mainly influences the power supply and expresses the preference for power source types that do not produce unclean

waste products, such as fumes. This, in turn, affects the choice of actuator type.

Table 3-1. The Needs relevant to the actuation system design

No.	Need	Priority
6	The primary product shall be untethered, i.e. energetically independent.	1
7	The load carrying capacity shall be the maximum achievable amount, considering safety.	1
11	The device shall be safe.	1
12	The device shall be reliable.	1
13	The device shall be weight efficient.	1
14	The power consumption of the device shall be efficient.	1
15	The operation (as explained in Appendix A) duration time shall be long.	1
16	The system shall be cost-effective.	1
17	The appearance of the device shall be acceptable.	1
18	The user shall not be burdened with any extra effort to carry the exoskeleton (while not carrying any payload).	1
19	The device shall comply with the University of Leeds standards.	1
23	The device should decrease the metabolic cost of the load carrying task.	2
24	The actuators of the device should be dynamically strong enough to perform activities specified in Appendix A except for running.	2
26	The device may be clean.	3
28	The noise produced by the primary product may be socially acceptable.	3

3.3.3 Target Requirements

The full list of target requirements are presented in Appendix C. Those requirements that are relevant to the actuation system are presented in Table 3-2. As mentioned earlier, the values of the metrics have been specified with the aim of benchmarking information acquired through literature review. Notice that a smaller priority number means a higher priority.

As mentioned earlier, design concepts should be produced with the aim of satisfying the target requirements. For instance, actuators should be designed to enable carrying an additional load of between 45 (marginally acceptable)

and 60 (ideal) kilograms. On the other hand, the choice of actuators affects weight, size, price, and power consumption. These requirements sometimes contradict each other, and the purpose of the design procedure is to achieve an optimal compromise between the requirements. Through an iterative process, a concept should be developed that could satisfy a modified list of final requirements.

The requirements indicate that the device should be safe for humans; therefore, the supplied voltage in the system should be constrained to a maximum of 60 VDC, to be inherently safe to human users [73].

3.3.4 Main requirements

This section illustrates the identification of the needs and target requirements, which will be used as guidelines for the design process during this project. The requirements presented here are *target* requirements; this means that final requirements will be determined after the investigation and identification of the most appropriate solution concepts.

The list of target requirements defines what the design project is aiming to achieve. In brief, the most important target requirements to be satisfied are the following:

1. The exoskeleton load carrying capacity should be 45-60 kg.
2. It is desired that the exoskeleton should be untethered.
3. The total weight of the exoskeleton should be 21-68 kg.
4. The size of each dimension of the system must be at most 25%-100% larger than the corresponding dimension of the average human.
5. The electric voltage in the system must not exceed 60 VDC.

3.4 Actuation System Requirements

The requirements of the actuation system stem from the requirements of the exoskeleton system, and are as follows:

I. The actuation system of the exoskeleton must be strong enough for a load carrying capacity of 45-60 kg.
II. It must be possible to power the actuators with a portable power-supply so that the exoskeleton could be untethered.
III. The actuators must be light-weight enough to keep the total weight of the exoskeleton within the range of 21-68 kg.

Table 3-2. The requirements relevant to the actuation system

Related Need(s)	Metric	Unit	Priority	Marginally acceptable Value	Ideal Value
28	Noise	subj.	3	Safe for humans	Socially acceptable
26	Cleanliness	subj.	3	No fume	No by-products
6	Untethered	-	1	Tethered	Untethered
7	Load carrying capacity	kg	1	45	60
11	Maximum joint speeds	rad/s	1	Safe	Safe
11	Maximum allowable angular acceleration	rad/s^2	1	Safe	Safe
13	Weight	kg	1	68	21
14	Power consumption	W	1	Lowest possible	Lowest possible
16	Price	$	1	$30K	$10K
17	Appearance	subj.	1	Not a concern	Socially acceptable
32	actively assisted joints	list	3	None	Each joint
18	Decrease of metabolic cost without load.	%	1	0	12%
23	The decrease of metabolic cost with maximum load.	%	2	15	50
21	Maintenance scheme feasibility	subj.	1	Technician-maintained	User-Maintained
11	Vibration	subj.	1	Human safe	Imperceptible
11	Safety	subj.	1	Sade for humans	Sade for humans
12	Reliability	subj.	1	Reliable	Reliable
19	University of Leeds standards compliance	subj.	1	compliant	compliant
22	Life-cycle	year	1	2 years	10 years
2	Size of the longest dimension increase	%	1	100% of average human	25% of average human

IV.   The actuators must be compact enough so that the size of each dimension of the system will remain at most 25%-100% larger than the corresponding dimension of the average human.

V.   If the actuators are electrically powered, then the electric voltage provided to the actuators must not exceed 60 VDC.

VI.   In order to reduce vibrations, and make the system safe and reliable, the actuators must be backlash-free, so that *chatter* is avoided.

With the design requirements determined, an analysis and decision-making on the actuation system type could be performed, as will be stated in the following sections.

3.5   Analysis of the Actuation System Types

3.5.1   Pneumatic Actuators

Pneumatic actuators (including artificial muscles) in general, have a significantly higher power density than DC motors [56]. Additionally, they are inherently compliant due to the compressibility of the air (or other gases used), which is advantageous over hydraulic actuators in applications involving mechanical interaction between humans and machinery. However, pneumatic actuators suffer from controllability and efficiency problems, including bandwidth limitations [50, 74, 75].

Furthermore, the power supplies for pneumatic actuators are generally compressors driven by a source of mechanical power, e.g. an electric motor. Compressors are mainly bulky and heavy, making them unsuitable for untethered devices. For instance, the exoskeleton developed at the University of Tokyo (section 2.3.12) is actuated by pneumatic actuators, which in turn are powered by an off-board compressor [45], resulting in a tethered device. To the best of the author's knowledge, there are currently no untethered pneumatic exoskeletons or active orthoses powered by compressors. Nevertheless, another type of power source for pneumatic actuators has been proposed [76], using gaseous products of chemical reactions. This power supply has been used in a prototype of an untethered Knee Ankle-Foot orthosis (KAFO) (section 2.6.2), but the power supply is heavy and bulky. Considering that an exoskeleton will have far more actuators and a much higher power requirement than a KAFO, the suitability of this type of power source for exoskeletons depends on potential future technological progress.

3.5.2 Hydraulic Actuators

Hydraulic actuators are faster than their pneumatic counterparts as a result of using fluids with very small and negligible compressibility. Furthermore, the torque to mass and power to mass ratios in hydraulic actuators are typically much larger than that of electric actuators [5, 75]; however, it should be noted that using hydraulic actuators for an untethered exoskeleton will incur the addition of the mass of the pumps and motors (as is the case for the HULC™ exoskeleton, mentioned in section 2.3.1of Chapter 2) or an internal combustion engines (as in the design of BLEEX, mentioned in section 2.2.1of Chapter 2). Therefore, the whole mass of an exoskeleton will not necessarily reduce as a result of choosing hydraulic rather than electric actuators. To analyse this further, two possible designs should be considered, as explained in the following paragraphs.

In the first design, used in BLEEX [6], a pump generates pressure for all actuators, and the pressure at each actuator is controlled via a servo-valve. The advantage of this design is that there are only a pump and a motor, which are placed behind the torso, while a lightweight hydraulic actuator is located on the exoskeleton limb. The disadvantage of this design is the high energy dissipation in the servo-valves [2], reducing the energy-efficiency of the whole system. One study done on BLEEX showed that the efficiency of hydraulic actuators used is half of that of an electric actuator design for the same purpose [5]. This will, in turn, necessitates the use of a powerful source of mechanical power to drive the pump, e.g. an internal combustion engine or a high power electric motor, especially if a full body exoskeleton with numerous actuators is considered. Such a large power supply will be too heavy to be placed on the exoskeleton with the currently available technology. One example is the XOS exoskeleton (section 2.2.2) which is tethered to its hydraulic power supply. Currently, there are no full-body hydraulic exoskeletons that are energetically autonomous (i.e. untethered).

The second design is the one used for the HULC family of exoskeletons (section 2.3.1), where each actuator has a separate pump. This allows control of the pressure of the hydraulic fluid at each actuator directly, by using variable-displacement pumps [75], eliminating the power loss associated with the servo-valves. This design is appropriate if the number of actuators is small, like in the HULC exoskeleton where only the knee joints are actuated. Also, in this design, the pumps and motors could be placed behind the torso to reduce the energetic cost of carrying them [77, 78]. On the other hand, for each

actuated joint, there needs to be a hydraulic actuator, a pump and an electric motor (in contrast to electric actuation where only an electric motor and a gearing system is needed). This will result in a heavy and bulky design if there are numerous actuators. To the best of the author's knowledge, this design has not been used in any full-body exoskeletons with numerous actuators.

Based on the above analysis, it could be concluded that for a full-body exoskeleton with numerous actuators, either of the above-mentioned designs would result in either a tethered or a heavy device.

3.5.3 Electric actuators

Introduction

Electric actuators can be divided into linear and rotary actuators. Rotary actuators are discussed in detail in this section. Literature and market research was done in this study on linear electric actuators with macro displacement ranges (i.e. excluding actuators such as piezoelectric ones with micro displacement ranges). The research revealed two categories of linear electric actuators, namely voice coil actuators and actuators that are made of a rotary electric motor and a transmission system such as worm gear to transform rotary motion into linear motion; the former is explained and analysed here, whereas the latter is basically a rotary motor and is discussed later in this section.

Voice coil actuators

Voice coil actuators (VCAs) are linear electromagnetic actuators. They are the force source for audio speakers and are also used in disc drive read heads. The utilization of VCAs in robotics has been studied by McBean et al. [79]. The motivation behind this study was that VCAs are desirable for human-robot interaction (HRI) applications because of their low noise and low mechanical impedance (i.e. back-drivability), as well as smooth and backlash-free motion and high controllability. Another advantage of VCAs is that they are linear, mainly narrow shaped actuators, making them geometrically suitable to be mounted along the links of robotic arms. They are also tolerant of shock loads and have high bandwidths and power densities (i.e. power divided by actuator weight). On the other hand, VCAs have low force densities (i.e. force divided by actuator weight). Therefore, especially where direct-drive systems are

concerned (which is usually the case with any linear actuator), using VCAs results in heavier actuators when compared to other actuators (e.g. rotary electric motors).

Rotary electric motors

Rotary electric motors are available in many different types. For an energetically independent exoskeleton, DC electric motors are more suitable than AC ones, because portable electric power supplies (e.g. batteries and fuel cells) mostly provide DC current. Therefore, this section is restricted to the consideration of DC electric motors.

Actuation with electric motors could be achieved with either a direct drive design or via a reduction system (e.g. gear trains, chain and sprocket mechanisms, etc.) to increase torque at the expense of speed. The former method has the advantage of eliminating the weight of gear chains etc., although it requires higher-torque motors which are heavier than lower-torque motors. Furthermore, larger (i.e. higher torque) motors mainly dissipate less energy in terms of heat loss in the windings [5], making them more energy-efficient. A study on the design of electric actuators for the MINDWALKER exoskeleton (described in section 2.3.10) also showed that motors with higher motor constants (K_M) lead to lighter designs for the actuation mechanism [80]. The study also showed that out-runner motors (i.e. motor in which the rotor is located outside of the stator) have relatively higher efficiency and torque density than in-runners (motors with the rotor inside the stator). It also suggests that the higher inertia of the rotor in larger motors do not necessarily cost more energy.

3.6 Incorporation of elasticity in the actuation mechanism

3.6.1 Series and Parallel Elastic Actuators

The inherent elasticity of human muscles, tendons and ligaments have inspired research on developing elastic actuation systems for exoskeletons, including Series Elastic Actuators (SEA) and Parallel Elastic Actuators (PEA). In an SEA, the motor and the spring are in series, whereas in a PEA, the two are in parallel, as shown in **Figure 3-4** (a) and (b). One example of using SEAs is the RoboKnee, described in section 2.5.1

The XPED project, a collaboration between the University of Twente and the Delft University of Technology [81], focuses on developing an exoskeleton to store the braking energy during walking and reuse it to make walking more energy-efficient. An attempt to achieve this led to the development of a passive exoskeleton with artificial tendons, which used elastic cables spanning multiple joints [82]. Although simulation results predicted a 40% decrease in the metabolic cost of walking, experimental tests showed a negligible reduction of metabolic cost.

(a)   (b)
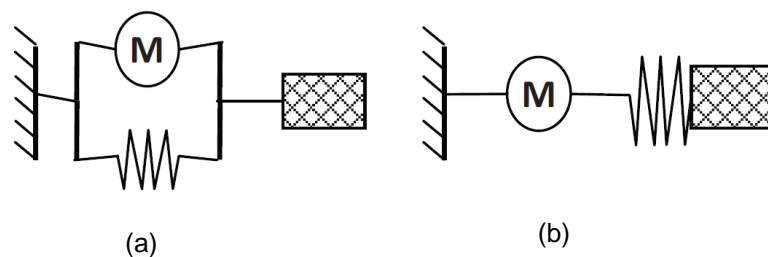
Figure 3-4. The schematic design of parallel (a) and series (b) elastic actuators [83]

Hollander et al. developed an SEA to assist the ankle joint during walking [84, 85]. Their calculation for an ideal case predicted that an SEA can reduce the peak power of the motor by 69%, and the energy consumption in one gait cycle by 42%. Decreased power requirements mean that smaller motors could be used. A prototype built in this study was capable of providing 100% of the required power while being seven times less heavy than an equivalent motor-gearbox actuator (with no elasticity).

In another study [83], series elastic actuators (SEA) and parallel elastic actuators (PEA) have been investigated as an attempt to reduce the power and torque requirements of electric motors in exoskeletons. Utilising SEAs could decrease the power consumption of actuators, by storing energy when the actuator is performing negative work (i.e. breaking) and releasing energy when the actuator is doing positive work. Nevertheless, SEAs cannot reduce torque requirements. On the other hand, PEAs can decrease the maximum torque required from the active component of the actuators, allowing for smaller motors to be used, which in turn reduces input current and copper loss in the motor windings (proportional to current), which means reduced power consumption. Linear springs were considered in the study and optimisation

was done on the values of spring constants (and, in some cases, spring engagement angles). The results for the SEAs are as follows:

Calculations for the ankle actuator showed a decrease of 79% in the peak power and 78% in the RMS power. No obvious reduction was found for the knee and hip flexion-extension (i.e. rotation in the sagittal plane). In the coronal plane, the hip rotation could benefit from a reduction of 60% in peak power and 49% in RMS power [83]. Furthermore, the results for PEAs are as follows:

In the Hip joint, the PEA decreased the peak motor torque by 66% and 53%, and the RMS by 50% and 45%, in the sagittal plane and coronal plane, respectively. For the knee joint, no power reduction was achieved by adding parallel elasticity. For the ankle, a unidirectional spring was proposed, which could reduce the peak power by 48% and the RMS torque by 61%. The study is purely based on calculations and no experimental results were provided. The study suggests using no spring for the knee and concludes that PEAs are more favourable than SEAs for the ankle and the hip (in both the sagittal and the coronal planes), as PEAs can reduce torque (unlike SEA) as well as power. The addition of a SEA to a joint with a PEA was also investigated, but no considerable reduction in power was recorded. Furthermore, although the study found that PEAs are more suitable than SEAs, it does mention that SEAs can still be useful because they reduce the output mechanical impedance of the system and improve force control [83].

It should be noted that the above-mentioned study only considers power and torque reduction in the "gait" cycle; therefore, if an exoskeleton is not primarily designed for walking, the power reduction during the operation of the device (which will be a combination of walking and other manoeuvres) might not be enough to justify the added weight and complexity induced by incorporating elastic components. It should also be considered that the stiffness of the springs have been optimised for a certain user's weight and walking speed. The sensitivity of the optimal stiffness to the speed of walking was found to be small (6.8%); hence, it was suggested that the spring stiffness be optimised for a range of walking speeds. Although the design of a mechanism to regulate the spring stiffness online and automatically is possible in theory, it was not considered in the study as it was anticipated that such a mechanism would be complex and therefore heavy. Therefore, it was suggested that the spring stiffness should be regulated offline (manually) for different user weights [83].

It should be noted that when the design of an enhancive exoskeleton is considered, the optimum value of the spring stiffness will depend on the weight of the load being carried, which could vary continuously during operation. Therefore, the offline regulation of the spring stiffness is not a suitable approach for such a case, while online stiffness regulation could be challenging from the design point of view. To the best of the author's knowledge, no studies are available on developing an enhancive exoskeleton with PEAs.

(a)

(b)

© Delft University of Technology
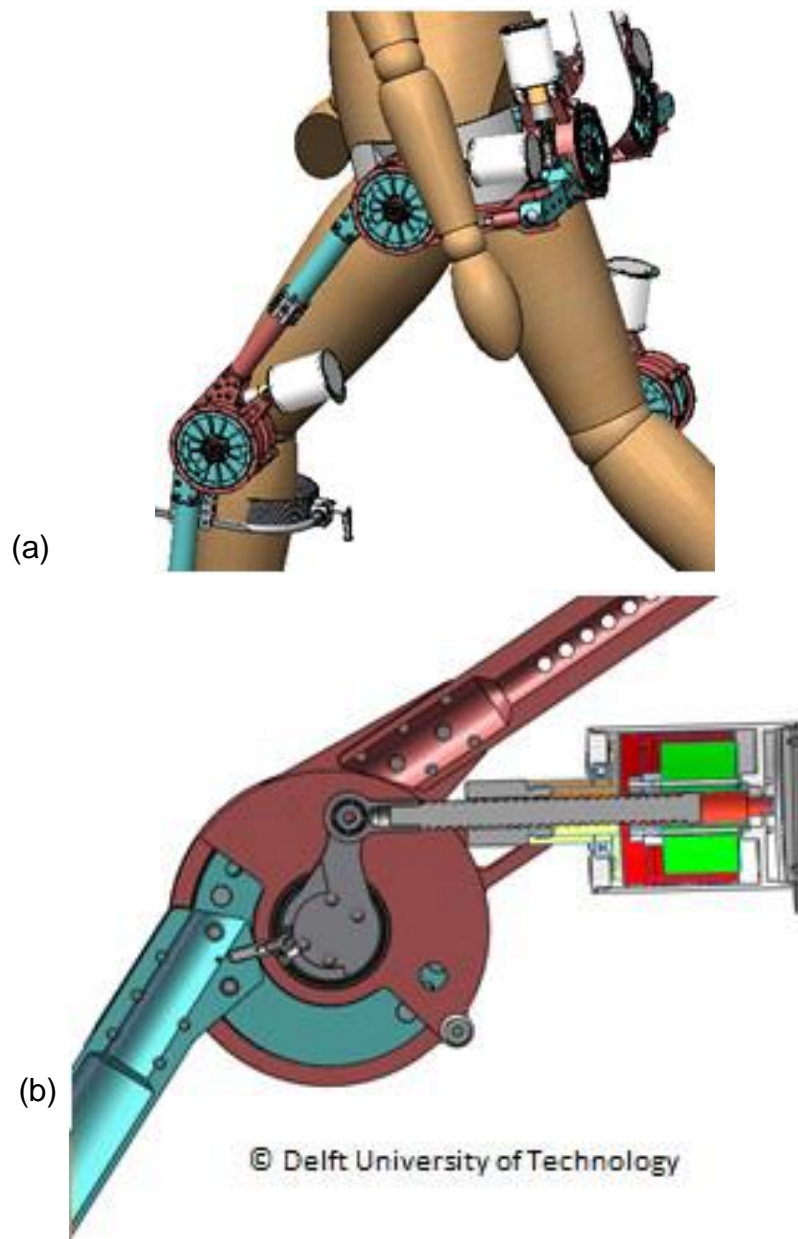
Figure 3-5. the MINDWALKER exoskeleton (a) and the SEA designed for the actuators (b) [80]

The usefulness of SEAs in improving force control and decreasing the impedance of the system is also reported in another study [44], although it has also been pointed out that SEAs yield relatively low bandwidth at high forces, causing a delay in the response of a closed-loop force control system. Nevertheless, Lagoda et al. designed and manufactured an SEA with a bandwidth of 6.9 Hz at 100 Nm, and a total actuator mass of 3.175 kg [84]. In addition, the bandwidth of SEAs can be improved by combining an SEA with a parallel spring [86, 87]. The principle behind this technique is that, because using a parallel spring can reduce the torque requirement of the SEA, the bandwidth will be improved (since the bandwidth of SEAs decreases with an increase in output torque).

Another practical example of incorporating SEAs in exoskeleton actuators is the MINDWALKER exoskeleton (explained in section 2.3.10). The SEA actuator (**Figure 3-5**) was designed and optimised to achieve a light-weight, energy efficient design. It consists of a rotary DC motor with a ball screw and a custom-made spiral spring with a stiffness of 820 Nm/rad. No evaluation results have been published on the performance of the actuator.

Another example of the design and manufacturing of an SEA is reported in [88]. The design is made of a flat brushless DC motor, a Harmonic Drive gear, and a custom-designed torsion spring, as shown in **Figure 3-6**. The actuator, together with a velocity-source type torque control algorithm, is reported to produce a torque of 10 Nm with a bandwidth of 5 Hz. The paper does not mention any comparison or evaluation of the performance of the actuator.

A further example of adding elasticity to the joints is provided in some interesting research, reported in [77], which focuses on designing a quasi-passive lower limb exoskeleton to assist human running, as the assistive significance of springs would be more prominent for running than for walking. A controllable friction-lock clutch engages a spring during the stance phase to store and release energy and disengages it during the swing phase. The clutch is controlled by a controller which recognises a change in the direction of knee joint angular velocity to identify the transition between gait phases. The locking mechanism was moved to the back of the exoskeleton (behind the torso) so that carrying it would incur the least additional metabolic cost. The design is shown in **Figure 3-7**. Experiments showed that the stiffness of the system was sufficient during the stance phase, but "suffered from significant resistance at the beginning of the swing phase due to inertial effects and a kinematic singularity in the exoskeleton".

The MIT AFO is also actuated by an SEA, as described in section 2.4.2.

(a)

(b)
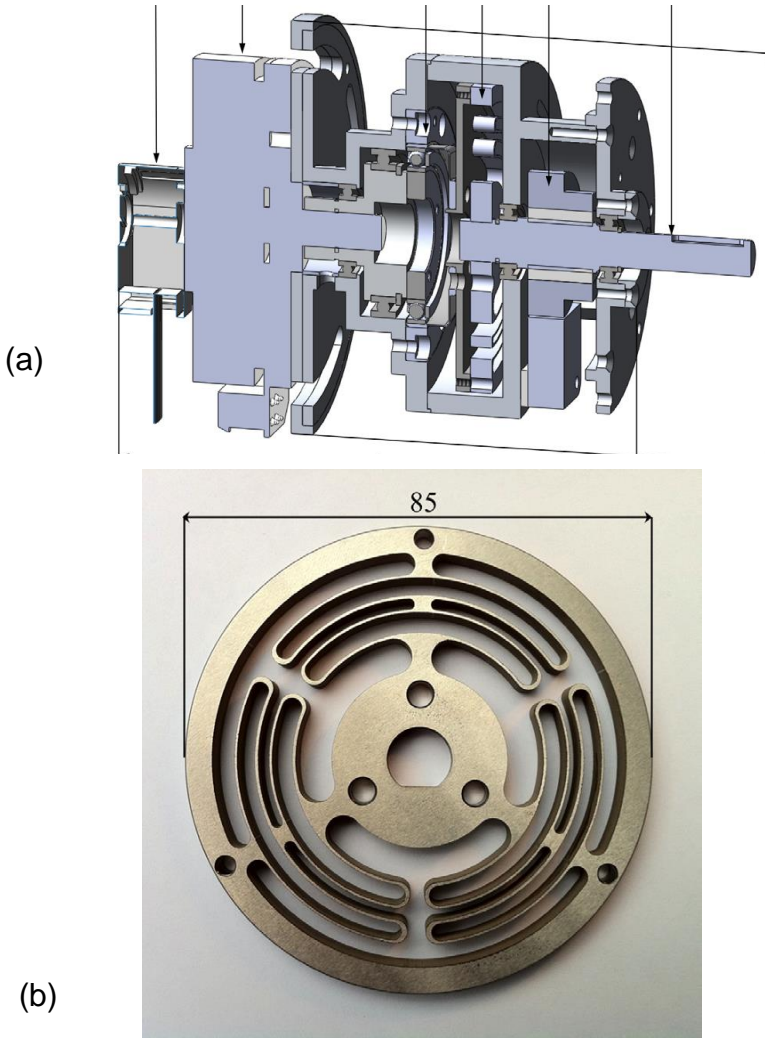
Figure 3-6. The design of an SEA (a) with a torsional spring (b) [88]
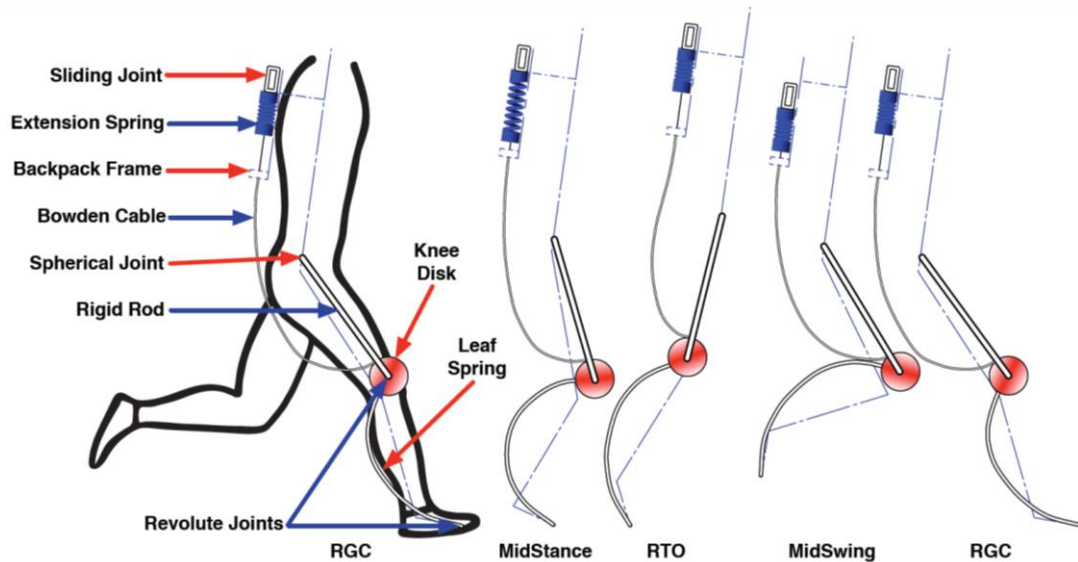
Figure 3-7. Using springs for human running [77]

3.6.2 Gravity balancing using springs

Banala et al. developed a passive orthotic device (**Figure 3-8**) for walking assistance via gravity balancing of the lower limb [89]. The device utilises a combination of linkage mechanisms and springs. The linkage locates the centre of gravity of the lower limb and the orthosis, while the springs compensate the gravitational force; this is done in order to reduce the required effort for lifting the legs during walking. EMG signals were used to verify the effectiveness of the device. Testing of the device on healthy subjects showed that, during walking, the device reduced the required torque at the hip joint, but not at the knee joint. However, the range of motion was improved in both knee and hip joints for a post-stroke patient. The device only compensates for gravity, and not for other forces such as the ones created by limb dynamics; therefore, the device is believed by the authors to be most effective for individuals with slow gait and weakness in their leg muscles. As shown in Figure 3-5, one of the weaknesses of this design is its bulky shape.
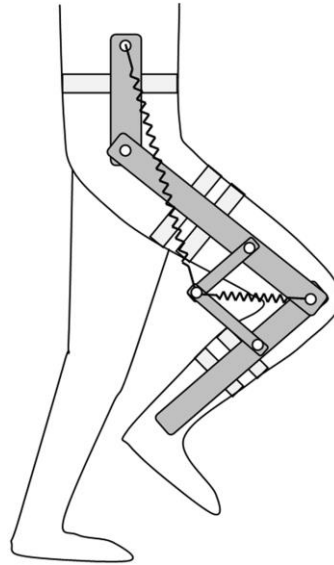
Figure 3-8. Schematic design for gravity balancing with springs [89]

3.7   The importance of the mass and location of the actuators

In human walking, carrying a certain amount of load on different parts of the body requires different amounts of effort, as Browning et.al showed in 2007 in a publication on the correlation between the location of added mass to a human body and the energetics and biomechanics of walking [78]. Their study shows that, for an added mass of 8 kg, carrying the mass on the thigh and the foot increases the metabolic cost by 14% and 48%, respectively, as shown in **Figure 3-9**.
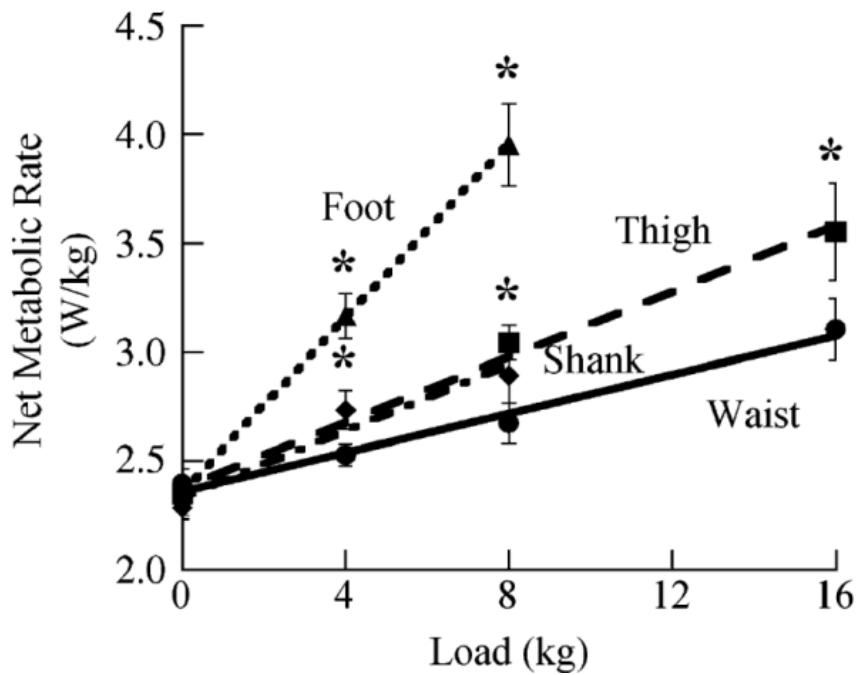
Figure 3-9. The effect of carrying mass on different locations of the body on metabolic cost [78]

The findings of the abovementioned study were considered in the design of a quasi-passive exoskeleton for human running (explained in section 3.6.1). In that design, a spring and clutch system was used to assist the movement of the knee joint. In order to minimise the energetic cost of carrying their weight, the spring and clutch were placed behind the torso, while the spring was attached to the knee joint via a cable.

A study carried out on developing electric actuators for the BLEEX exoskeleton (explained in section 2.2.1) showed that the weight of the actuator was 4.1 kg. The study suggested that the electric actuators should be moved up on the exoskeleton leg to reduce power consumption [5].

The above-mentioned research results show that the mass of the actuators has a considerable effect on the system power consumption, which must not be neglected. For example, using a heavier but more power-efficient *actuator* might not result in a more power-efficient *exoskeleton* compared to a lighter but less power-efficient *actuator*, because of the excessive power requirement of the exoskeleton incurred by the heavier parts. Therefore, the analysis, selection, and design of the actuation system must take into account the mass and location of each actuator.

3.8 Selection of the actuation system type

3.8.1 Actuator types and locations

It should be noted that the choice of actuator type in a system is related to the type of power supply to be used. If an exoskeleton is designed and manufactured with the intention of being used in the community (e.g. at homes, hospitals, workshops etc.), low noise is a requirement of the system. Therefore, internal combustion engines should be ruled out, and an electric power supply (most probably a battery) should be developed. This decision affects the choice of actuator type, especially in regard to hydraulic actuators.

The conclusions obtained from the following discussions are the basis of the decision in the actuator type selection in this project.

As discussed in section 3.2, pneumatic actuators suffer from controllability and performance problems. Furthermore, the current stage of the technology of pneumatic power supplies (e.g. air compressors) does not allow for an untethered full-body exoskeleton. For these reasons, pneumatic actuators were ruled out.

The analysis mentioned in section 3.5.2 shows that a full-body exoskeleton with numerous hydraulic actuators will either be tethered (especially because internal combustion engines are not going to be considered for this project as the power supply) or heavier than one with electric actuators.

As for electric actuators, using voice coil actuators (VCAs, section 3.5.3) would yield a heavier actuation system than rotary electric motors. Therefore, it was decided that rotary electric motors should be used. Because the power supply is going to be a battery, only DC motors have been considered[1].

The masses and locations of the actuators must be taken into account in the optimal design of the actuator system, as will be explained in Chapter 4.

3.8.2 Usage of SEAs and PEAs

The studies carried out on the incorporation of elastic elements in the exoskeleton actuators, (explained in detail in section 3.6.1) have shown

---

[1] It must be noted that many of the DC motors which have been considered in this study, are inherently AC motors with controllers that are fed with DC voltage.

promising results. The main motivation behind using such elements is the desire to minimise the weight and energy consumption of the exoskeleton (without having to sacrifice the load carrying capacity), which could be achieved by reducing the maximum required torque of the motors (using PEAs) and/or reducing the power consumption of the motors (using PEAs and/or SEAs). Due to the low bandwidth of SEAs, PEAs may seem more feasible at a first glance. However, the main challenge in using PEAs is adjusting the spring stiffness online according to the weight of the load being carried by the exoskeleton. This could add to the size and mass of the system, which will, in turn, increase the power consumption and decrease the load carrying capacity. For these reasons, further research is required in order to find out whether to use SEAs or PEAs or even neither; furthermore, considering the promising results of previous studies, it seems that conducting more research in this area seems worthwhile.

The application of springs to enhance human running was not planned to be considered in this project, as the exoskeleton of this project is not primarily designed for running (as stated in need #24, mentioned in section 3.3.2). Also, it was decided that gravity balancing with springs should be left out because previous research suggests that the resulting design would be bulky, and also because this technique could only be beneficial in slow gait (as mentioned in section 3.6.2).

3.8.3 A note on Control

Since this study includes the design and construction of a prototype and performing test experiments, the development and implementation of a control method are required. The control method also needs to be suitable for an electric motor, which is the chosen actuator type. PID control is widely used for electric motors, and therefore has been chosen for this project.

3.9 Summary

This chapter covers the concept design for the exoskeleton as a system, including the decision on the actuator system type. The design method used has been explained and was followed by the needs and requirements presented (both for the exoskeleton as a system and for the actuation system as a sub-system). The investigation done on the available actuator types has been presented, as well as the decisions made. The requirement for having

an untethered system plays a crucial role in the selection of the actuation system type.

Pneumatic, hydraulic and electric actuation systems have been investigated in this study. Among these, pneumatic actuators were ruled out because of controllability and performance issues, as well as the lack of availability of portable pneumatic power supplies at the present. Furthermore, the analysis revealed that a lightweight hydraulic exoskeleton will have to be tethered to an external power supply and that an untethered hydraulic design will be heavier than an electric one. Therefore, it was decided that electric actuators would be used in this project.

It was also found that the incorporation of elasticity (in the form of SEAs and PEAs) might yield good results, and is worth investigating. However, gravity balancing with springs was decided to be left out of this study, in order to keep the design compact.

Finally, it was revealed that the mass and locations of the actuators are likely to influence the system power consumption, and hence have to be taken into account in the design procedure.

Chapter 4
Optimal Design of the Actuation System

4.1 Introduction

In the previous chapter, it was explained that electric actuators are the most appropriate choice for the design problem at hand. Furthermore, the set of design requirements of the actuation system was developed. This chapter explains the method used to optimally design the actuators of the lower-body exoskeleton in the sagittal plane.

As mentioned in the previous chapter, the design requirements include a load-carrying capacity of no less than 45kg, and ideally 60 kg. The requirements also state that the weight of the exoskeleton should not exceed 68 kg. Furthermore, it is desired that the exoskeleton should be untethered, i.e. energetically autonomous. Considering the limitations of portable batteries, and in order to maximise the possibility of satisfying the energetic autonomy requirement, the power consumption of the exoskeleton needs to be minimised, while keeping the load carrying capacity and the exoskeleton weight within the acceptable ranges. Therefore, a multi-factor optimisation problem is to be solved here.

A part of the optimisation method used in this project involves the assessment of different actuator design candidate. Such an assessment is necessary in order to verify whether a given design candidate would satisfy the design requirements, and also to rank different designs and choose the optimal one. This performance assessment entails obtaining knowledge of the torque and velocity requirements at the exoskeleton joints, which can be obtained from the dynamic modelling and simulations of the exoskeleton manoeuvres, as explained in section 4.2.

Once the torque and velocity requirements at the exoskeleton joints have been obtained, a model of a design candidate can be used to convert the joint torque and velocity into the required torque and velocity of the electric motor, so that the performance of the given electric motor candidate can be assessed. In order to map the torque-velocity graph of the joints onto the torque-velocity plane of the electric motor, a model of the power transmission system -hereafter referred to as *the transmission*- is needed. The analysis, type selection and modelling of the selected transmission types have therefore been done in this project, and are explained in sections 4.3 and 4.4. Using the

model of the transmission system, the torque and velocity requirements of the electric motor can be obtained, and used together with the model of the electric motor (explained in section 4.5) to assess the performance of a the given electric motor (and hence, the performance of the given candidate for the actuator design). The assessment method has been explained in section 4.7.

Using the assessment technique explained above, each design candidate can be given a score, and a search method could be used to find the design candidate that scores highest. This search method needs a list of candidate electric motors, which has been developed via an extensive market search, explained in section 4.6. This list and the above-mentioned search method have been used in an iterative optimisation method, which has been explained in section 4.8.

The optimisation algorithm has been implemented using a computer program. Section 4.9 covers the development of the optimisation software.

4.2 Dynamic Modelling of the Manoeuvres of the Exoskeleton

4.2.1 Introduction

The first step in the actuation system design is to acquire the requirements on the torque and angular velocity (and hence, the mechanical power) at each joint of the exoskeleton. Once these requirements are known, they could be used to predict the performance characteristics of different actuator design candidates. The design candidates can then be assessed against the system requirements (explained in section 3.3.4 of Chapter 3), and also against one another. In this study, the values of the required joint torques and angular velocities have been acquired using dynamic simulations of the exoskeleton motion.

The three-dimensional motion of the human and exoskeleton limbs can be divided into motions in three planes, mainly the sagittal, Coronal and Transverse planes, as demonstrated in **Figure 4-1**.

The motions involved in human walking are mainly in the sagittal plane [1]. Previous studies have shown that modelling the exoskeleton movements only in the sagittal plane (i.e. two-dimensional modelling) is sufficient for the analysis of the actuators that act in the sagittal plane [3]. Therefore, although

71

the exoskeleton model is three dimensional, the dynamic modelling and the simulations performed in this study are two dimensional.
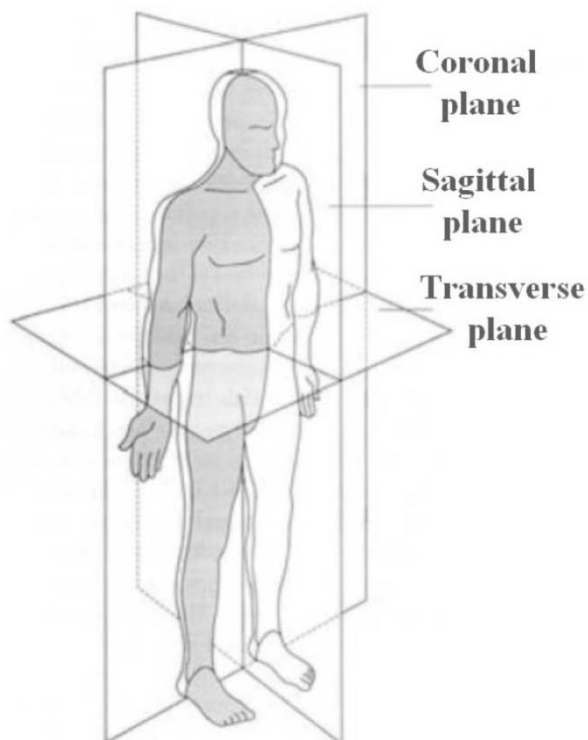
Figure 4-1. The three planes of human locomotion [1]

4.2.2 Modelling and Simulation Method

The optimisation algorithm (which will be explained in detail later in this chapter) requires the execution of dynamic simulations of the exoskeleton manoeuvres. These simulations need to be repeated numerous times within the algorithm and therefore have to be embedded inside the computer program that implements the optimisation algorithm. For this purpose, a parametric mathematical model of the system was developed, in which the values of the parameters (e.g. the mass and inertia of the actuators) could be changed automatically in the program according to the optimisation algorithm. The dynamic model was obtained using the Newton–Euler method by analysing the free body diagram of each link separately and combining all of the equations at the end. The entire optimisation program, including the dynamic simulation section, was written in a MATLAB® code.

Two manoeuvres have been simulated by the dynamic model, namely gait and squat. These manoeuvres were chosen because they represent the working conditions involved in load-handling.

The kinematic inputs of the simulations are the data acquired from motion capture. The motion capture measurements involved the following steps: a human subject performed the intended motions, while a number of cameras were recording the location of markers placed on certain points on the subject's body. The markers were located on the lower back and the foot of the user, which are the points where there would be a connection between the user and the exoskeleton. The motion of the exoskeleton and the user at these connection points would be identical; therefore, the kinematic data of the motion of these points could be used as inputs to the dynamic model of the exoskeleton.

The raw data acquired from motion capture consists of sampled positions of the markers, paired with the time at which each sample was taken. By numerical differentiation, the linear velocity and acceleration of each marker were acquired. It should be mentioned that the raw data was first filtered to eliminate noise, which could cause some unrealistically large values to be generated by numerical differentiation. The cut-off frequency of the low-pass filter was chosen to be 10 Hz. This frequency is high enough not to eliminate any of the frequency components of the motion, as studies suggest that the position bandwidth of human movements is around 5 Hz for "internally generated or learned trajectories" [90].

Once the timed vectors of position, velocity, and acceleration were obtained for the markers, they were fed into the kinematic model of the exoskeleton, to obtain the joint angles, angular velocities and angular accelerations. These values are used by the kinetic model to obtain the joint torques. Figure 4-2 shows the block diagram of the dynamic simulation process.

It could be seen in Figure 4-2 that two additional sets of inputs are also required, namely the dimensions of the exoskeleton (the lengths of its links[2]), and the exoskeleton's inertial parameters (the mass, moment of inertia and the location of the centre of mass for each link). The inertial parameters of the exoskeleton frame were estimated using a simple model. However, the masses of the actuators also contribute to the inertial parameters of the links. Since different actuator design candidates differ in mass, the program has been developed in a way so that it automatically modifies the exoskeleton

---

[2] The length of the links were chosen to match the limbs of the test subject of the Motion Capture measurements.

inertial parameters according to the design candidate being investigated, as will be mentioned in section 4.8.2. The method used to calculate the inertial parameters is explained in detail in Appendix G. **Figure 4-3** is an example of the simulation results and shows the torque and power requirement of the knee joint in the squat manoeuvre with a load of 45 kg. The results for the hip and ankle joints are presented in **Figure 4-4**.
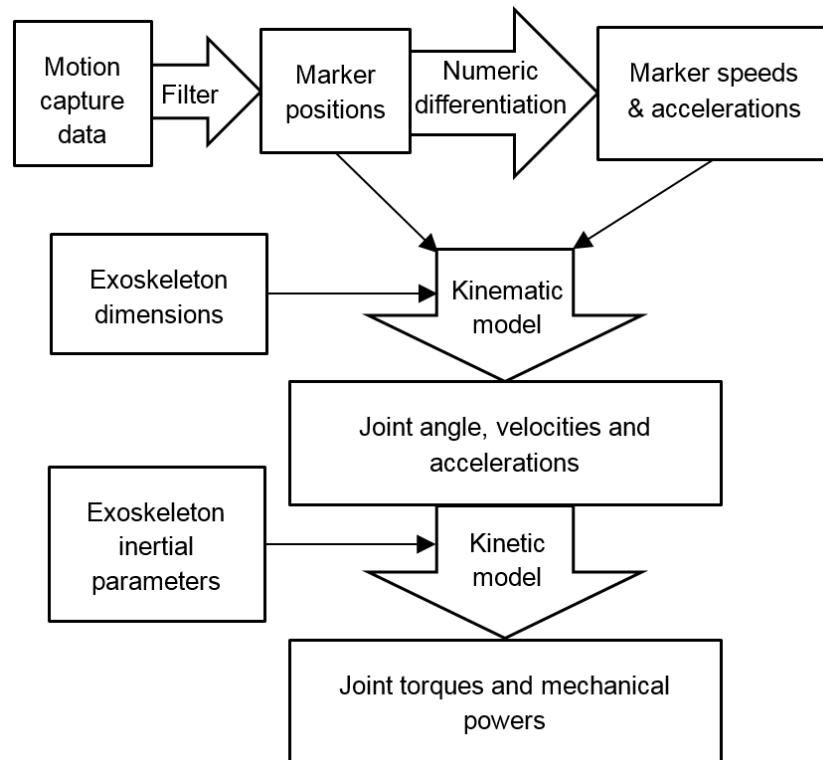
Figure 4-2 The block diagram of the dynamic simulation process

In order to verify the validity of the above-mentioned simulation model, the exoskeleton was also modelled using the SolidWorks Motion Analysis®. The model, depicted in **Figure 4-5**, consists of two legs, and a hip part. Each leg has a shank, a thigh and foot part. This model was used to simulate both the gait and squat manoeuvres, and to obtain the torque and power requirements at the joint. The results were similar and quite close to those obtained from the previously mentioned parametric model (as demonstrated in **Figure 4-6**), and this confirms the integrity of the parametric model used for dynamic simulations in the optimisation algorithm.
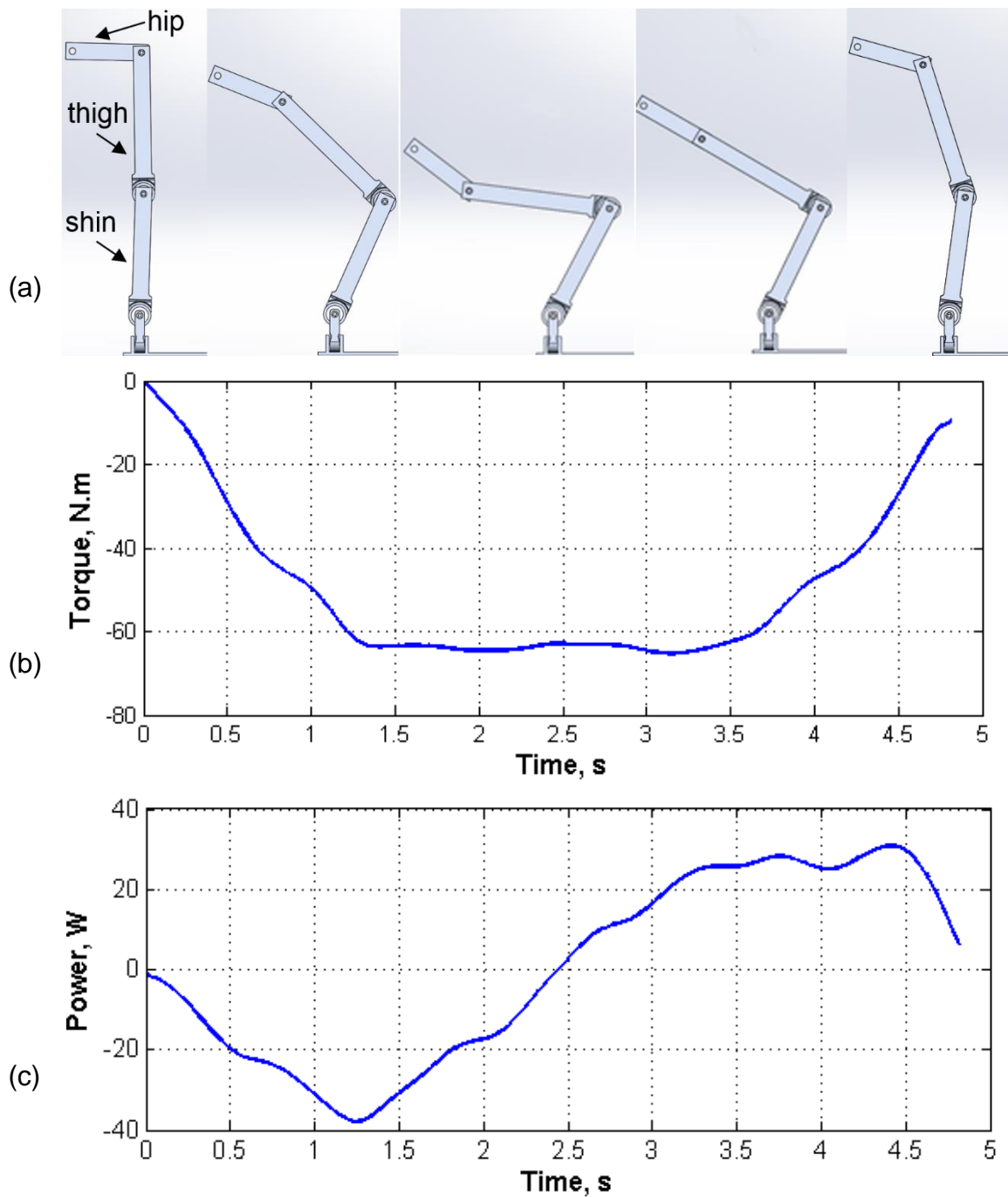
Figure 4-3. Screenshots of the simulation animation of the squat manoeuvre with no payload load (a), and the simulation results for the knee joint: the required torque (b) and power (c). The exoskeleton model is depicted in Figure 4-5 **(p 77).**

After obtaining the angular velocity and torque of the exoskeleton joints, the effect of the power transmission system must be taken into account, in order to find the velocity and torque of the electric motor. This is explained in section 4.3.
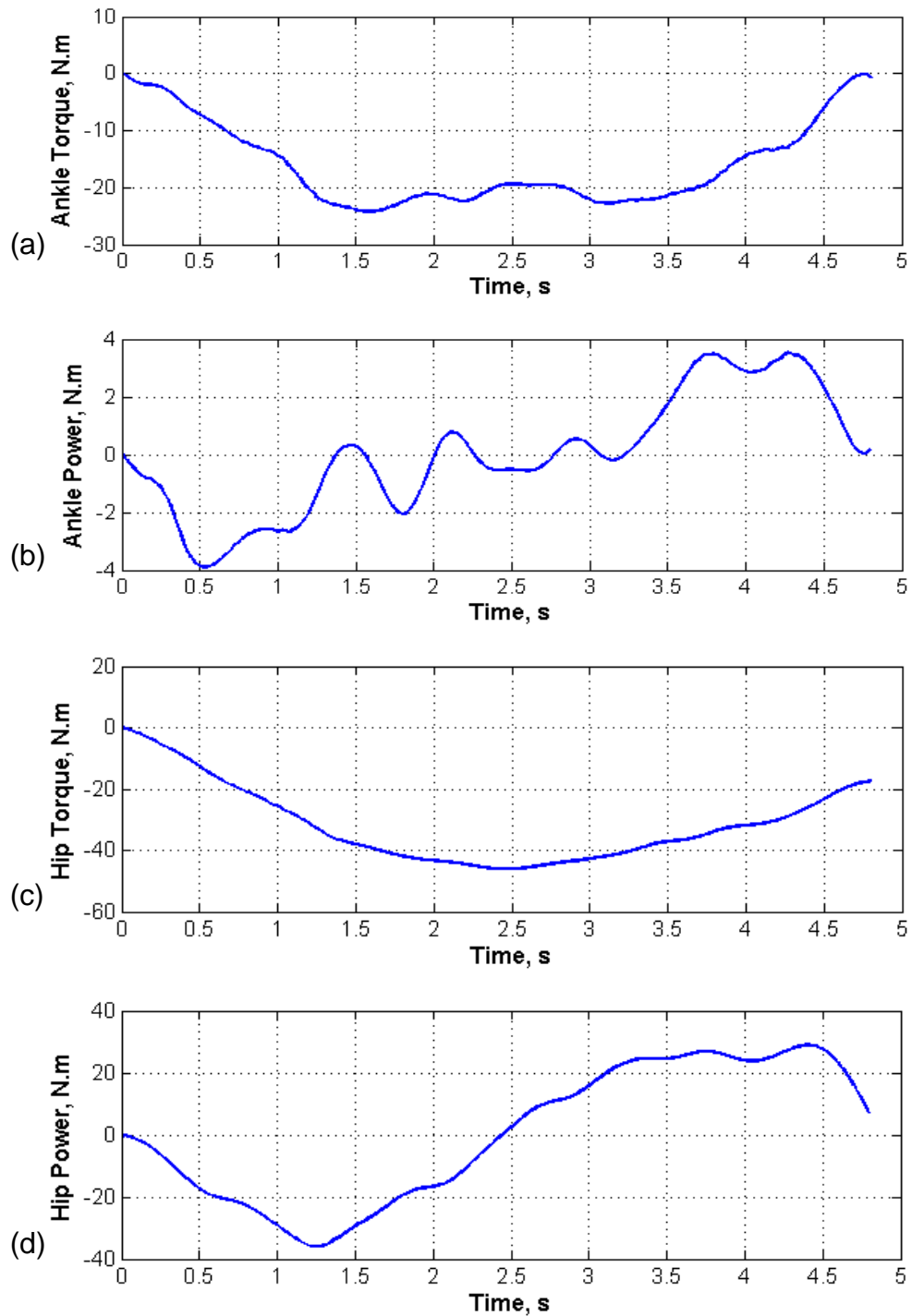
Figure 4-4 The simulation results of the ankle and hip joints for the squat manoeuvre illustrated in Figure 4-4 **(a): ankle torque (a), ankle power (b), hip torque (c) and hip power (d). The kinematic inputs of the simulations have been obtained by Motion Capture measurements of a human subject's motion. The small peaks in the curves are due to the fact that the natural motion of the human subject is not smooth.**
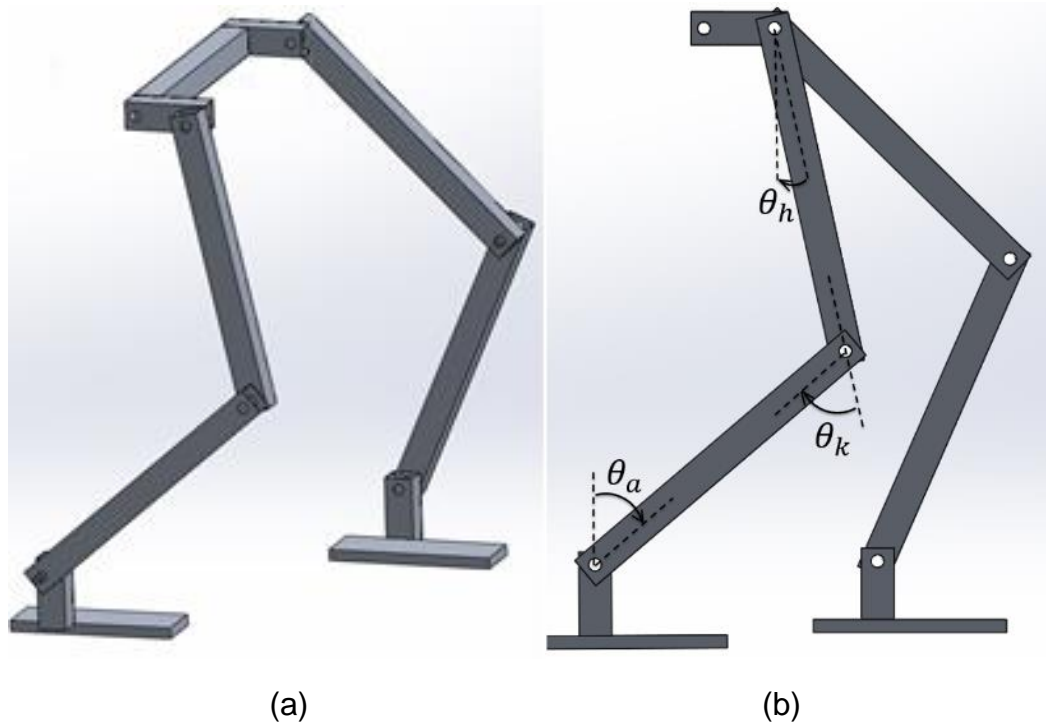
Figure 4-5. The exoskeleton model created in the SolidWorks® Motion Analysis environment; dimetric view (a) and side view (b). The joint angles (shown for the for the rear leg) are θ_a (ankle joint angle), θ_k (knee joint angle), and θ_h (hip joint angle).

Figure 4-6 demonstrates a comparison between the simulation results obtained from the SolidWorks Motion Analysis® software and the MATLBA program developed in this project. The results correspond to the squat and gait manoeuvres with a payload of 45 kg, and are therefore different form the ones in **Figure 4-3** and **Figure 4-4**, which belong to the manoeuvres without any payload. It could be seen that the results are close, although not identical. Furthermore, some fluctuations exist in the results from SolidWorks, which is due to the fact that SolidWorks performs a forward kinetic calculation (unlike the MATLAB program which only performs a backward kinetic solution). The fluctuations depend on the solver used, and decrease in size with a decrease in the simulation time-step. However, these fluctuations are small compared to the size of the required torque. Therefore, it could be concluded that the amount of torques predicted by the MATLAB program are sufficiently close to the SolidWorks results, and hence reliable.
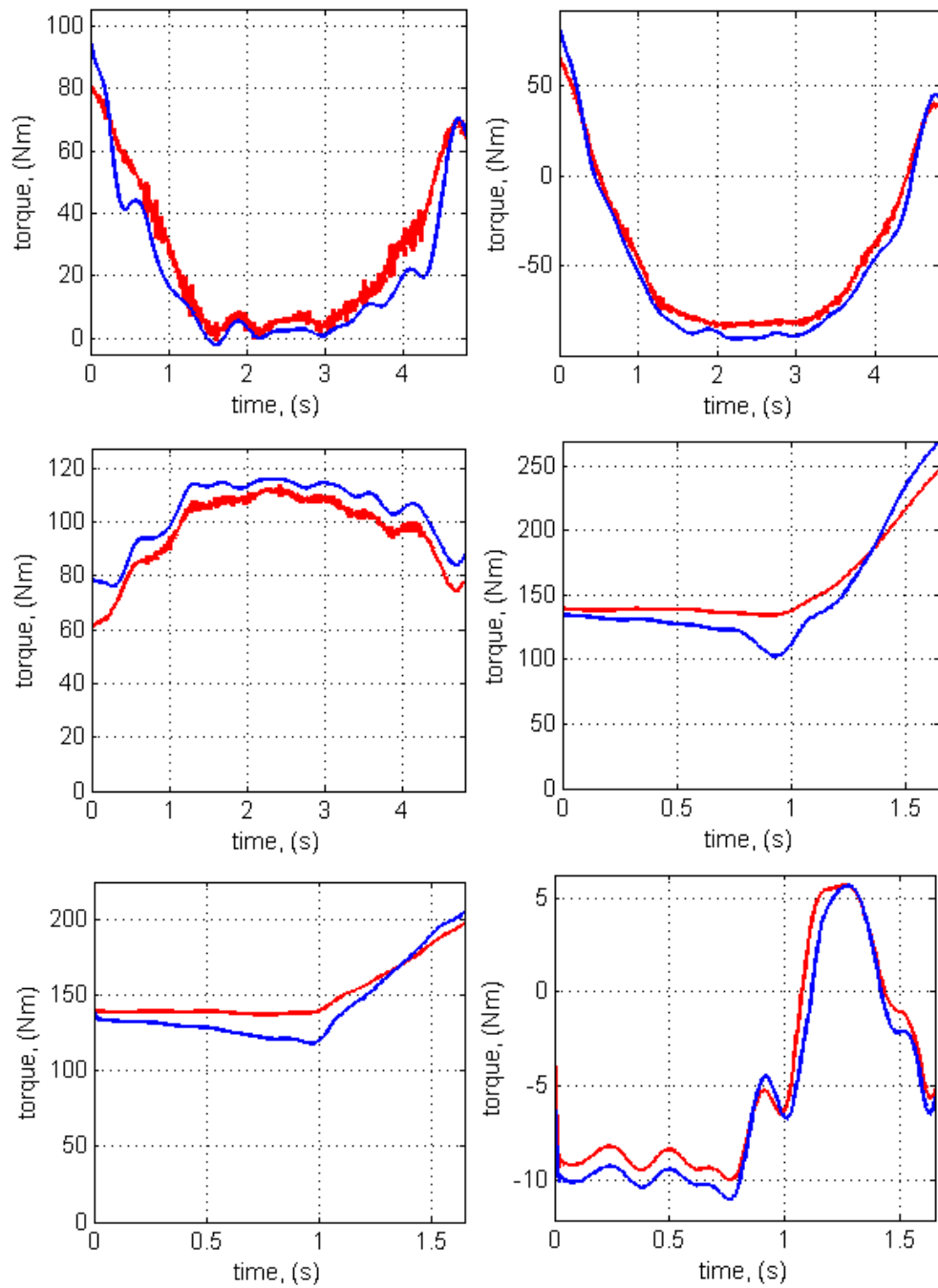
Figure 4-6 comparison between the simulation results in SolidWroks (in red) and MATLAB (in blue), with a payload of 45kg for squat at the ankle (a), knee (b), and hip (c) and for the gait at the ankle (d), knee (e), and hip (f) joint on the stance leg.

4.2.3 Two Alternative Exoskeleton Gait Types

The exoskeleton can walk in two different ways, which are explained in this section. In the first gait type, the knee joints of the exoskeleton are bent during the gait manoeuvre. An example of this can be seen in Figure 4-7 which shows the Body Extender Exoskeleton. It could be seen in the picture that the knees of the exoskeleton are bent while in standing position, while the knees of the human user are straight. This is because the limbs of the exoskeleton are longer than those of the user, and hence have to be bent.

The bent-knee design, explained above, has the advantage that the exoskeleton can fit users with a variety of heights, without needing for size adjustments and simply by changing the angles of the knee, ankle, and hip joints. However, having the lower limb joints constantly bent means that the knee actuators will have to continuously apply some torque even in standing position. Furthermore, as will be explained in Chapter 5, the torques required for walking become much larger than those with the other design (explained later in this section), which will require larger and heavier actuators, which in turn increases the power consumption. Heavier actuators also could cause safety issues due to the heavy mass of the exoskeleton. For example, as mentioned in section 2.3.3, the Body Extender exoskeleton weighs 160 kg; if the exoskeleton stumbles or if the actuation/control systems fail for some reason, then the user may get seriously injured due to the immensity of the exoskeleton. Furthermore, the body Extender is powered by an off-board power supply, which implies that its power requirement is too large for a battery. Although the bent-knee design was originally considered for the exoskeleton to be developed in this project, it was abandoned due to the above-mentioned problems which were revealed after simulations (explained in Chapter 5). Instead, a different design and gait type were considered, as follows.

Figure 4-7. The Body Extender exoskeleton

The second gait cycle is an anthropomorphic one, in which the knee joint remains unbent during standing and in the stance phase of the gait cycle. One example is the HAL exoskeleton, shown in **Figure 4-8**. The main advantage of this design is reduced torque and power requirements (as will be explained in Chapter 5). However, size adjustability would be required for the limbs of the exoskeleton in order for it to fit different users.

Figure 4-8 The HAL exoskeleton walks with unbent knee joints [91]

4.3 Selection of the Power Transmission Systems for Further Analysis

An electric actuator is made of electric motors and a power transmission system[3]. Before proceeding with the modelling of the actuation system, the appropriate types of transmission system need to be identified. This is explained in this section.

For the sake of ease of control, it is desirable that the power transmission system be backlash-free, so that *chatter* is avoided. Other requirements include acceptable size and weight, and sufficient transmission ratio.

In theory, any backlash-free transmission system can be used in an exoskeleton, but practical limitations could rule out some transmission mechanisms. For instance, strain gears (aka Harmonic Drives) are not

---

[3] The exception is the direct-drive design, where the transmission system is eliminated, and the transmission ratio is *unity*. However, the results of the optimisation method used in this study have shown that the required transmission ratios for all actuators are larger than *unity*; this means that the direct-drive system is unsuitable in this case, and a power transmission mechanism is needed.

normally available in ratios smaller than 50:1. Therefore, if a smaller ratio is required, strain gears cannot be used alone. The investigations carried out in this study showed that the selection of a proper transmission system is a challenging design problem, when considering the demanding requirements of exoskeletons.

In the beginning stages of this study, a number of transmission systems were disqualified after a preliminary analysis, including spur and bevel gears. Furthermore, rack-and-pinions are available in anti-backlash configurations, but they either suffer from low torque capacities or are too large and heavy to be suitable for an exoskeleton. Pulleys and timing belts were ruled out because of insufficient torque capacity (for an acceptable pulley size)[4]. The remaining types of transmission systems which were investigated in detail were strain gears (aka Harmonic Drives), chain and sprockets, ballscrews, linkage mechanisms, and rope drives. The modelling of these transmission mechanisms is explained in the next section.

4.4 Modelling of the Power Transmission System

4.4.1 Introduction

As explained in section 4.1, a model of the power transmission system is needed for the optimisation method used in this study, in order to convert the required torque and velocity at the joints to those of the electric motor in an actuator. This section includes the modelling method of the transmission system types selected and mentioned in the previous section, namely strain gears, chain-and-sprockets, and ballscrews.

4.4.2 Strain Gears

Strain gears -sometimes referred to as Harmonic Drives- have been used in the design of the actuators for the HAL family exoskeletons [20] as shown in Figure 2-5 in section 2.3.2 of Chapter 2. Strain gears can provide high transmission ratios in a compact and lightweight design, as shown in **Figure 4-9**. The analysis and design of an exoskeleton actuator with strain gears and

---

[4] However, as will be explained in the next chapter, belt and pulleys can be used in combination with strain gears. This way, the torque transmitted by the belt and pulleys is reduced to safe values.

electromotors have been investigated in details by Zoss et al [5], whose method is the basis of the modelling method presented in this chapter and has been expanded to find an optimal design in this study (as will be explained in section 4.8).

For an actuator with a strain gear, the relationship between the torques and angular velocities of the exoskeleton joint and the motor are as follows [5]:

$$\begin{cases} (\tau_m)_{out} = \dfrac{\tau_j}{\eta.N}, & P > 0 \\ (\tau_m)_{out} = \dfrac{\eta.\tau_j}{N}, & P < 0 \end{cases} \qquad \text{4-1}$$

$$\begin{cases} \omega_m = N.\omega_j \\ \alpha_m = N.\alpha_j \end{cases} \qquad \text{4-2}$$

where τ_j, ω_j and α_j represent the torque, angular velocity and angular acceleration of the joint, while $(\tau_m)_{req}$, ω_m and α_m denote those of the motor. Notice that the subscript "*out*" in $(\tau_m)_{out}$ indicates that this is the required output torque of the motor, which is not equal to the torque created inside the motor between the stator and the rotor; this will be explained in detail later. *N* is the transmission ratio, and η is the gear efficiency. The joint power, *P*, is equal to the product of the torque and angular velocity of the joint.

In addition to the efficiency, other considerations involved here are the no-load torques, namely the no-load starting torque, no-load back-driving torque and the no-load running torque. The value of $(\tau_m)_{out}$ is equal to the smallest value between the result of equation 4-1 and the no-load torque (or the no-load starting torque, at the beginning of the motion). Furthermore, in back-driving, if τ_j is smaller than the no-load back-driving torque of the gear, then τ_j must be replaced by the no-load back-driving torque in equation 4-1 to obtain the value of $(\tau_m)_{out}$. These considerations have been taken into account in the computer program that converts the joint torque to the motor output torque.
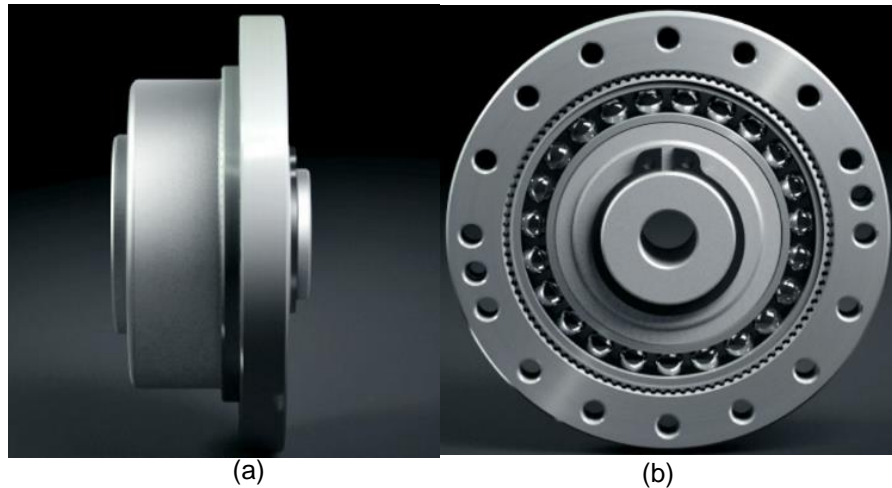
Figure 4-9. A Strain Gear, the side view (a) and front view (b) (courtesy of Harmonic Drive AG5)

The values of the efficiency and no-load torques of strain gears depend on the torque, angular velocity and temperature [92]. However, a fixed average value can be used to estimate the efficiency of a strain gears, as has been done in other studies [5, 93]. In this study, however, the graphs provided by the manufacturers have been used to interpolate the efficiency and no-load torques for each point of the discretized trajectory of the exoskeleton joint. These graphs and the interpolation method used have been presented in Appendix D.

There are a few companies that manufacture strain gears, but only one of them provides detailed data on the efficiency of the gears [92], the products of which were chosen in this study. When selecting the gears to be included in the list, their torque capacities were compared to the required torques predicted by simulations. The final list contains 57 gears, with gear ratios ranging from 50:1 to 16:1, in different sizes (and hence, different torque capacities). The lightest gear is 0.055kg and the heaviest is 0.89kg.

Section E.1 of Appendix E contains the Table of the specification of all of the strain gears considered in this study.

---

[5] http://harmonicdrive.de/en/company/corporate-development/

4.4.3 Chain and Sprockets

Chain and sprockets could be used as the gearing mechanism for the actuator either in a single-stage design for small transmission ratios or as a multi-stage reduction train for larger ratios. Furthermore, they can be used in a *speed-up* configuration in conjunction with a strain gear to achieve a smaller transmission ratio than the smallest available with strain gears (generally 50:1). Equations 4-1 and 4-2 used for strain gears, also apply to a chain and sprocket mechanism; the difference here is that the efficiency can be considered constant, and can be assumed to be at least 98% under ideal conditions [94].

Chains and sprockets are widely available for different transmission ratios and torque capacities. Values of the mass and movement of inertia can be calculated from the density of the material used (in this case, steel) and the dimensions provided by the manufacturer [95]. Estimated inertial values were developed and used for the initial iterations of analysis and size optimisation. The inertia of the chain was also converted into an *equivalent* moment of inertia and added to that of the sprockets; to do this, it needs to be noted that the chain moves with a linear velocity equal to the radius of the sprocket multiplied by the angular velocity of the sprocket. Therefore, the equivalent rotary inertia term is equal to the total mass of the chain, multiplied by the radius of the sprocket.

By combining different sizes of the driving sprocket and the driven one, it is possible to achieve different transmission ratios. Furthermore, a double-stage reduction mechanism (i.e. two sets of chains and sprockets in series) allows for larger reduction ratios. The original list of transmission ratios was made by discretizing the available range of reduction ratios into a number of ratios. This list was used for initial iterations of optimisation, to obtain the desired transmission ratio. After that, the closest ratio available by combining different sprockets would be used for further analysis.

It must be noted that chains and sprockets are available in three designs, namely Simplex, Duplex and Triplex designs, demonstrated in **Figure 4-10**. Among these, Triplex and Simplex sprockets have the largest and smallest torque capacities [95].
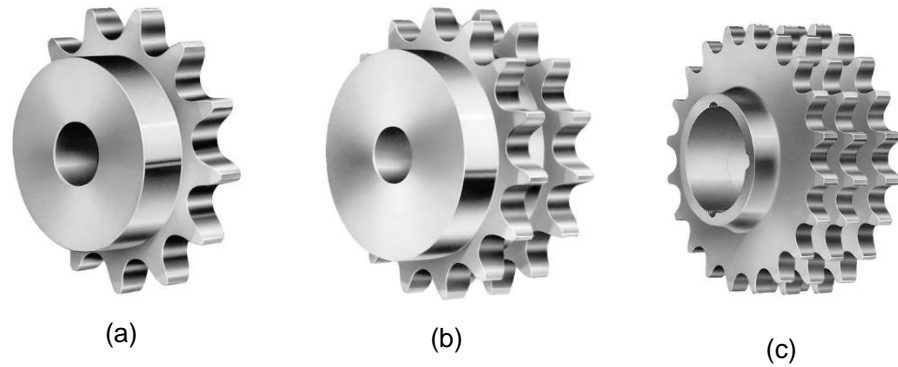
Figure 4-10 different type of sprockets: Simplex (a), Duplex (b) and Triplex (c)[6]

4.4.4 Ballscrews

Ballscrews can provide virtually zero backlash motion with an efficiency of at least 90% in forward-driving [96] and around 80% in back-driving [97], with large transmission ratios. The term *transmission ratio* has a different meaning here because a ballscrew converts the rotary motion of an electromotor to linear motion. In order to convert the output linear motion back into the rotary motion of the exoskeleton joint, two solutions have been considered here, namely rope and pulley drives and slider-crank linkage mechanisms, which will be explained further in the following sections.

The design variables to be selected in ballscrews are the pitch size and the diameter of the screw. The pitch size affects the transmission ratio, whereas the diameter affects the load/torque capacity as well as the total mass of the actuator. After comparing the available products from different manufacturers, the products of one of the manufacturers with an extensive range of pitch and diameter sizes were considered for the optimisation procedure [98]. Initial investigations ruled out some of the available sizes due to insufficient torque and/or excessively large screw diameter (that would make it impossible for the screw to pass through the hollow shaft of the electromotor). A total of 11 ballscrews were investigated with pitch sizes ranging from 2 mm to 25 mm, and diameters of 10 mm to 25 mm[7]. The selection of the pitch size affects the

---

[6] https://simplybearings.co.uk/

[7] The pitch sizes are 2, 4, 5, 10, 12.7, 16, 20 and 25 mm. The diameters are 10, 12, 12.7, 14, 16, 20 and 25 mm.

ratio and dimensions of the transmission mechanism, whereas the selection of the diameter affects the strength of the mechanism. The inertial characteristics of the nut and screw were calculated from the dimensions and material (steel) density.

Ballscrew Combined with Pulley and Rope

The rope drive mechanism consists of a pulley and a tendon rigidly connected to the pulley. Two different designs have been used for developing exoskeleton actuators with a wire-rope mechanism combined with a ballscrew [28, 99], as shown in **Figure 4-11**.
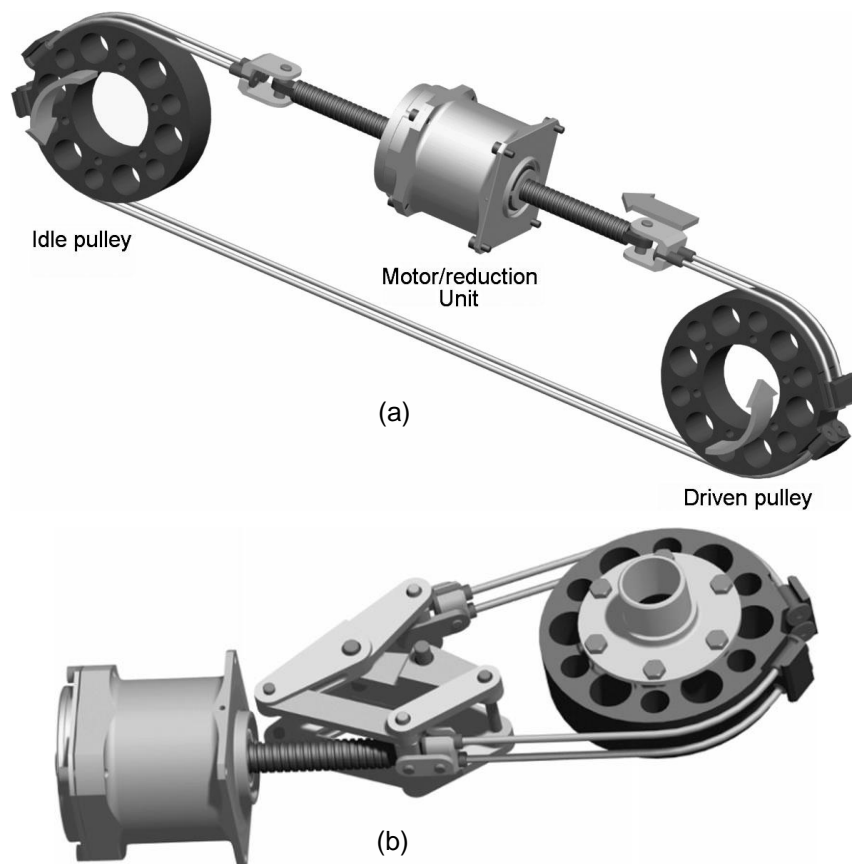
Figure 4-11. The actuator design with a driven pulley and an idle one (a), and the actuator design for the PERCRO body extender (b), where the idler pulley has been replaced by a linkage mechanism [28].

As shown in **Figure 4-11** (a), an additional (idler) pulley is required in the first design. In the second design, shown in **Figure 4-11** (b), a linkage mechanism replaces the idler pulley to achieve a more compact design. The latter is the design used in the PERCRO Body Extender exoskeleton.

For both designs, the equations 4-1 and 4-2 apply, and the transmission ratio N can be obtained from the following relation:

$$N_{rope-drive} = \frac{2\pi.r_{pulley}}{p} \qquad \text{4-3}$$

where p is the pitch size of the ballscrew, and r_{pulley} is the pulley radius.

Ballscrew in a Slider-Crank Mechanism

A slider-Crank mechanism could be used to convert the linear motion of the ballscrew to rotary motion at the joint. A variation of the slider crank mechanism (named the inverted slider-crank mechanism) has been developed in this project, which is the simplest variation of the mechanism for the design problem at hand. A schematic diagram of the actuator design is depicted in **Figure 4-12**.

The motor and the end of the screw are connected to the proximal and distal links at points P_p and P_d, respectively, via pivoted joints. The nut of the ballscrew is rigidly connected to and rotates with the rotor of the motor, and the screw moves linearly. This design requires a motor with a hollow shaft so that the screw can pass through the motor, as shown in the figure. The following nomenclature is used:

$$\begin{cases} r_p = \overline{OP_p} \\ r_d = \overline{OP_d} \\ L_s = \overline{P_pP_d} \end{cases} \qquad \text{4-4}$$
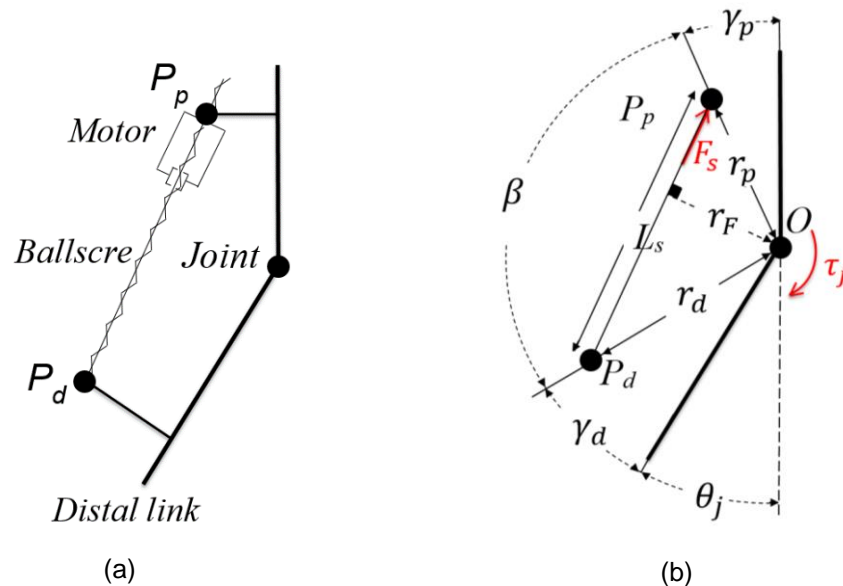
Figure 4-12. The schematic diagram of the actuator design (a), and the nomenclature of the parameters (b)

Four design parameters determine the dimensions of the linkage mechanism, namely r_p, r_d, γ_d and γ_d (shown in **Figure 4-11** (b)). The normal distance between the joint (point O) and the screw, r_p, is the lever arm length of the axial force in the ballscrew. So, the amount of torque created around point O depends on the screw force F_s, and r_p, as shown in the following relations:

$$F_s = \frac{2\pi}{p}\eta(\tau_m)_{out} \tag{4-5}$$

$$\beta = \pi - \theta_j - \gamma_p - \gamma_d \tag{4-6}$$

$$L_s = \sqrt{\left(r_p^2 + r_d^2 - 2r_p r_d \cos\beta\right)^2} \tag{4-7}$$

$$r_F = \frac{r_p r_d \sin\beta}{L_s} \tag{4-8}$$

$$\tau_j = F_s r_F = \frac{2\pi}{p}\eta r_F(\tau_m)_{out} \tag{4-9}$$

$$\omega_m = \frac{2\pi}{p}r_F \omega_j \tag{4-10}$$

Equations 4-9 and 4-10 show that the transmission ratio is not a fixed number, but a non-linear function of the joint angle and the design parameters. Further differentiation of equation 4-10 with respect to time yields the formula for the angular acceleration:

$$\dot{\omega}_m = \frac{2\pi}{p}\left(r_F \alpha_j + \dot{r}_F \omega_j\right) \tag{4-11}$$

where $\dot{r}_F$ can be obtained from:

$$\dot{r}_F = \frac{d}{dt}\left(\frac{r_d r_p \sin\beta}{L_s}\right) = r_d r_p \left(\frac{\omega_j \cos\beta}{L_s} - \sin\beta \frac{\dot{L}_s}{L_s^2}\right) \tag{4-12}$$

and

$$\dot{L}_s = \frac{p}{2\pi}\omega_m \tag{4-13}$$

The non-linear relations mentioned above have been used in the simulation program to convert the values of torque, angular velocity and angular acceleration of the joint to those of the motor.

To create the list of potential transmission mechanisms based on the above-mentioned mechanism, the five design parameters are varied, namely the ballscrew pitch size and the slider-crank mechanism dimensions which are r_p, r_d, γ_d and γ_d. The pitch size is limited to the values available from the

manufacturer. As for the mechanism dimensions, each of them are limited by design constraints, e.g. the acceptable size of the actuator, space limitation due to the existence of the exoskeleton frame parts, and avoiding singular positions of the mechanism. The computer program initially creates a list of mechanisms by varying the four dimensions within their allowable range; this means that the four dimensional search space of the possible mechanism dimensions is discretized. Then the above mentioned constraints are applied by the program to eliminate the unacceptable mechanisms. Finally, the program checks the axial load applied to the ballscrew (obtained from the dynamic simulation of the exoskeleton manoeuvres and the model of the transmission system), and eliminates any mechanisms that cannot withstand the load. The output of this program is a list of transmission systems with their dimensions and mass (which is obtained from the length and diameter of the ballscrew and its material density). Section E.2 of Appendix E contains the list of the mechanisms developed by the program.

4.4.5 Selection of the power transmission ratio

The transmission ratio (hereafter referred to as ratio) is the ratio of the angular velocity of the motor shaft divided by that of the actuated joint of the exoskeleton. It should be noted that the ratio is constant in some transmission systems (e.g. gear trains), whereas it is a function of the exoskeleton joint angle in other mechanisms (e.g. ball-screws combined with linkage mechanisms). The problem of ratio selection for the latter type changes into the selection of the dimensions of the mechanism.

For each electric motor, the performance of the actuator depends on the choice of the ratio. Therefore, a part of the optimisation problem involves choosing the optimal ratio, which has been done using a search-and-assessment method, explained in section 4.8.1

4.5 Modelling of the Electric Motor of the Actuator

After obtaining the required joint torques and velocities from the dynamic simulation of the exoskeleton manoeuvres, the model of a given candidate transmission system can be used to obtain the motor torque-versus-velocity graphs. Using these torque and velocity requirements, the motor model can

then be used to check if the motor is capable of performing the required task, as explained in this section. The model used here has been explained in detail in previously published works on the investigation of electric actuators [5, 93].

The sum of the torques applied to the rotor of the motor equals the rotor acceleration multiplied by its moment of inertia. Therefore, the relation between the output torque of the motor τ_{out} and the torque created between the stator and rotor is as follows:

$$\tau_m = \tau_{out} + I\alpha_m + D\omega_m \qquad \text{4-14}$$

In equation 4-14, I is the total moment of inertia of the rotor, the shaft and the nut of the ballscrew and any connecting parts, while D is the viscous damping of the motor.

The instantaneous maximum torque $(\tau_m)_{max}$ that an electromotor can provide, is a function of the angular velocity of the rotor. This is illustrated in **Figure 4-13**, which shows the typical torque vs velocity graph for electric motors. The grey area in the figure represents the available instantaneous torque area. If the graph representing the torque versus angular velocity falls within this area (for a given required motion), then the motor can perform the required motion. The available instantaneous torque decreases with an increase in the angular velocity; this effect is shown by the *Winding Line* in the diagram, which is defined by the following equation:

$$(\tau_{max})_{winding} = \frac{K_T}{R}V_{max} - K_M^2\omega_m \qquad \text{4-15}$$

where K_T, K_M and R are the torque constant, motor constant, and winding resistance of the motor, respectively. V_{max} is the maximum allowable voltage, limited by the characteristics of the power supply and controller, as well as safety considerations. As stated in section 3.3.3 of Chapter 3, the product requirements state that maximum allowed voltage is 60 VDC, for safety reasons.

In addition to the winding line, the available instantaneous torque is also limited by the maximum current that the power supply and the controller can provide, as depicted in the figure by the *Current Line*, which is simply defined by the maximum current that the power supply and the controller can provide, I_{max}:

$$(\tau_{max})_{current} = K_T I_{max} \qquad \text{4-16}$$

The maximum allowed instantaneous current (I_{max}) depends on the limitations of the power supply and the motor controller. At the beginning, the power supply model to be used was known. However, the motor controller to be used would depend on the selected motor, which would only be known after the optimisation was finished. Therefore, initially, the maximum instantaneous current was assumed to be equal to the maximum available current from the power supply, which is 50A. After performing the optimisation and selecting the motor and the controller (which was recommended by the motor manufacturer), it was found that the maximum allowable current of the selected controller is 30A. This new value however did not change the optimisation results, and was used in the consequent iterations of the optimisation procedure.
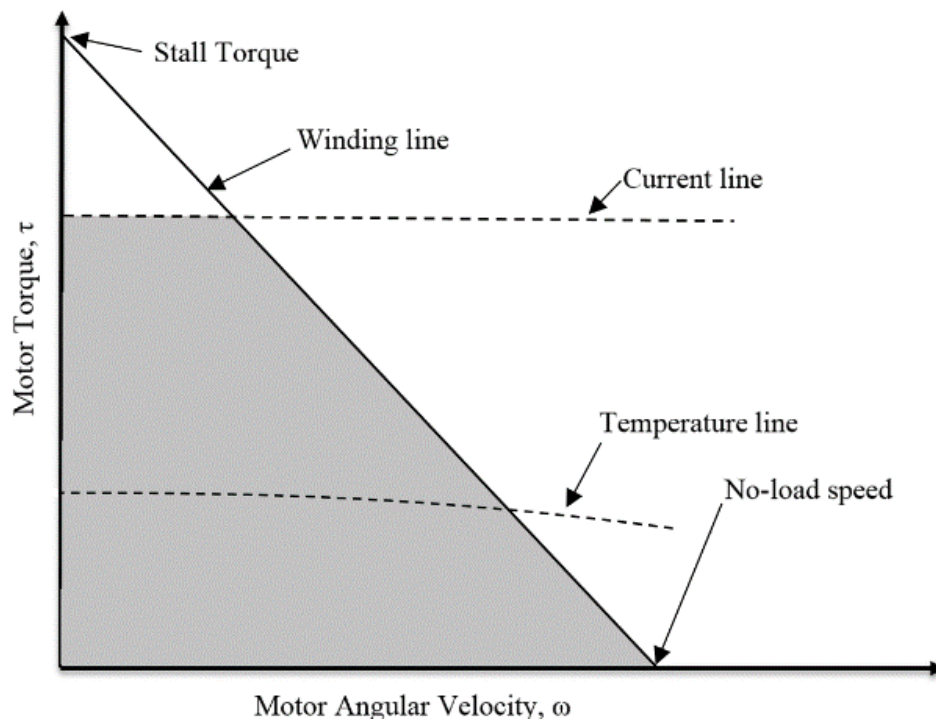
Figure 4-13. A typical diagram of the torque limit lines of an electromotor [5]. The motor torque graph for the desired manoeuvre must be limited to the shaded area, and the average torque versus average velocity point must lie underneath the temperature line.

The above equations determine the maximum instantaneous torque. However, in order to avoid the overheating of the motor winding, the point marking the average torque versus average velocity of the motor (during a

given desired motion) must lie underneath the *Temperature Line*, defined by the following equation:

$$\tau_{temp} = K_M \sqrt{\frac{\Delta T_{max}}{TPR} - D\omega^2} \qquad \text{4-17}$$

In equation 4-17, ΔT_{max} is the maximum temperature-rise that the motor can withstand, and TPR is the thermal resistance of the motor.

The power consumption of the actuator can be obtained from the following equation:

$$P = \begin{cases} \dfrac{\tau_m^2}{K_M^2 \gamma} + \tau_m \omega_m & , if \ P \geq 0 \qquad (a) \\[4mm] \dfrac{\tau_m^2 \gamma}{K_M^2} + \tau_m \omega_m & , if \ P < 0 \qquad (b) \end{cases} \qquad \text{4-18}$$

where γ is the efficiency of the amplifier and other electric components in the motor controller. In a previously published study on electric actuators [5], reported values of amplifier power loss imply an average efficiency of approximately 76%. However, it was decided to use a smaller value (50%) in the initial simulations in this study to represent other modelled losses, although the experimental test results suggested an even lower value, as will be explained in Chapter 6.

The values of the parameters that define the equations of the motor model can be found in data sheets of motor manufacturers. For some motors, the values related to the temperature line are explicitly mentioned, while in other cases the values need to be extracted from graphs provided by the manufacturers. In this study, an extensive market search was done on electric motors, and the required parameters of each motor were obtained from their datasheets and enlisted in a single spreadsheet. This spreadsheet was then used by the optimisation program for finding the motors that would perform best for each of the considered joint actuators, as will be explained in detail in the next sections.

4.6 The Extensive Market Search on Electric Motors

As explained earlier in section 4.1, the optimisation method used in this study involves a search method on a list of candidate electric motors. This list has been obtained via an extensive market search, explained in this section. Since the power supply for an energetically autonomous exoskeleton would most

probably be a battery, the search was limited to motors that could be powered with DC voltage[8], including brushed and brushless ones. Appendix F contains a report on the market search, including the search engines and websites used, the search keywords, and the number of pages of search results for each keyword that has been studied. The report also includes the full list of motors found, with all of the parameter values.

A total of 151 motors were chosen, and the values of their parameters were extracted from their data sheets and recorded onto a spreadsheet. The chosen motors come in different designs, including frameless motors that allow the designer to fit the motor in the actuator design with a bespoke frame design. There are also pancake-type (disc-shaped) motors with large nominal torques, but also large moments of inertia. In contrast, some of the motors are slim, with small values of the rotor moment of inertia (and hence, improved agility), but also small nominal torques.

In order to ensure that the optimal motor size would be within the size range chosen, it was decided to investigate motors in a size range that is larger than the expected range of motors that would be suitable for the job. The average required power was originally estimated by the simulations to be between 140W and 250W, for the ankle and knee joints. Therefore, motors within a nominal power range of 40W to 4,750W were chosen for the list, which is a range that spans from 30% to 1900% of the minimum and maximum power required. Since this range is much larger than the required power range, it could be expected that the optimal motor choice will not be overlooked. The mass of the motors in the list range from 0.32 kg (which was found after simulations to be incapable of performing the task) to 16.8 kg (which was later found to be suboptimal because it was too heavy).

Although the motor list is not comprehensive, it is a good representative of state of the art, containing 151 motors in a vast variety of designs and a large range of sizes, nominal torques and nominal powers. **Table 4-1** contains an excerpt of the full table of motors found, which is presented in section F.4 of Appendix F.

Initial iterations of analysis were done with the full list of the motors and revealed which ones were capable of performing the required tasks. These

---

[8] Notice that some of the motors found are internally AC motors, with controllers that convert DC voltage into AC.

motors were then chosen to form a smaller list for further iterations. This way, the run-time length of the optimisation code was greatly reduced.

Table 4-1. An excerpt of the table of the results of the motor market search carried out in this work

Nominal power (W)	Rated torque (N.m)	Weight (kg)	Type	Model number	Manufacturer
323.00	0.77	1.50	brushless	BM130	Aerotech
322.00	0.76	2.20	brushless	BG 75 50 SI	M Rutty & CO
320.00	0.85	0.20	brushed	MS31	Dynetic Systems
320.00	1.02	2.40	brushed	GN12T	PML MOTORS
300.00	0.96	2.30	brushed	U 16 FS	Printed Motors
295.00	0.86	1.14	brushless	BLDC 65S53A	NMB
276.00	0.16	0.55	brushed	H5067-009	Igarashi Motor
275.00	0.92	3.10	brushed	U12D-A	KOLLMORGEN
260.00	1.26	1.90	brushed	SL 120-2NFB	HEINZMANN
250.00	1.20	2.30	brushless	80ZW3S	3X MOTION
250.00	0.70	1.85	brushless	ASB87S048030	Nanotech
250.00	0.81	3.10	brushed	U12DT-A	KOLLMORGEN
245.00	0.85	3.30	brushless	DC083B-2	Haydon Kerk
232.00	tbc	1.12	brushless	MF0150010	Allied Motion
226.00	0.11	0.40	brushless	Series 3863...C	FAULHABER
220.00	0.70	1.85	brushless	EL86BLS71	Elmeq Group

4.7 The Performance Assessment of Actuator Design Candidates

As mentioned in the introduction section, the optimisation method used in this project involves an assessment of each actuator design candidate against the

design requirements, and against other candidates. The performance assessment method is described in this section.

Each design candidate consists of a motor and a transmission system, with known values of the parameters related to their technical specifications (e.g. the transmission ratio of a strain gear, and the torque constant of the motor, etc.). These values, together with the models explained in sections 4.4 and 4.5, are used in to assess the performance of the design candidates, as explained in sections 4.7.1 and 4.7.2.

4.7.1 Calculation of the Load-Carrying Capacity

Part of the performance assessment procedure involves the calculation of the load-carrying capacity of the exoskeleton for a design candidate. This process is done separately for different joints, and different manoeuvres (i.e. gait and squat).

The algorithm involves the implementation of dynamic simulations to obtain the values of torque, velocity, and acceleration for the manoeuvres being investigated. After that, the models of the transmission system and the motor are used to map the torque-vs-velocity graph of the joint onto the torque-vs-velocity plane of the motor (shown in **Figure 4-13**). If the graph lies within the allowable area, and the average torque also lies underneath the temperature line, then the given motor-transmission combination is capable of performing the required task, and vice versa. This criterion is the core of the algorithm explained here.

Three parameters are used in the algorithm, as follows:

1. *Starting value*: At the beginning of the algorithm, the mass of the payload is assumed to be equal to a large starting value. This value must be equal to the maximum expected load-carrying capacity of the actuator design candidate[9]. In this study, the starting value is 60kg, which is the upper bound of the required load-carrying capacity

---

[9] If the load-carrying capacity is found by the algorithm to be equal to the *starting value* in the first iteration, then there will be a chance that the starting value was not large enough and the design candidate can carry even larger loads.

according to the product requirements (section 3.3.4 of Chapter 3, p53).

2. The *upper bound* and the *lower bound* are variables that specify the maximum and minimum possible value of the load-carrying capacity. These variables change during the execution of the algorithm. The initial value of the upper bound is equal to the initial assumed value of the load (mentioned above), while the lower bound is initially assigned zero (0 kg).

3. The *search resolution* specifies the precision of the answer found by the algorithm. In this study, the value assigned to the search resolution was 0.5 kg.

For a given joint, and a given manoeuvre, the iterative procedure has been illustrated in Figure 4-14. The algorithm finds the load carrying capacity by moving the upper bound and lower bound closer to each other until the difference between them becomes equal to or smaller than the *search resolution*.

The above-mentioned algorithm is used as part of the performance assessment for each design candidate, which is explained in the next section.

4.7.2 The Performance Assessment Method

When a given motor and a given transmission system (e.g. a strain gear with known transmission ratio, efficiency, and inertial properties) are considered together as a design candidate for the actuator of a given joint, the performance of the actuators can be assessed according to the following procedure, which has been used in this study:

1. First, the total mass of the motor and transmission system are included in the dynamic model of the exoskeleton. In addition, the estimated mass of the additional parts (e.g. connectors, housings, etc.) are also taken into account. To simplify the modelling process in this study, the added masses are incorporated in the model as mass points (particles) attached to the exoskeleton links (**Figure 7-7** in Appendix G). Furthermore, the sum of the estimated mass of the exoskeleton upper body section and that of the load being carried by the exoskeleton are also included in the model as a mass point fixed to the hip part of the exoskeleton. Then the masses and moments of inertia of the links are recalculated, and the equations of the dynamic model of the system are rebuilt.
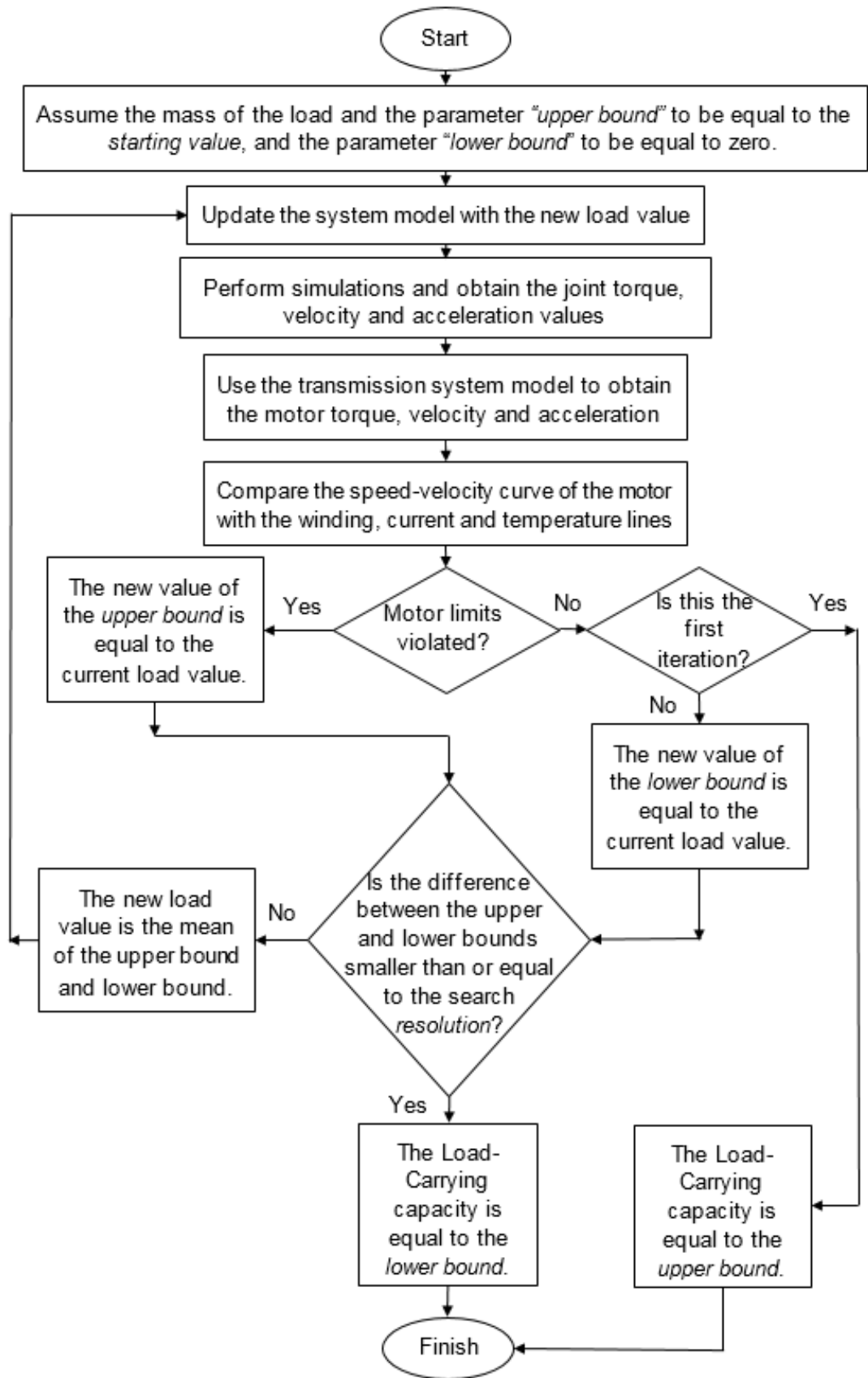
Figure 4-14 the flowchart of the algorithm for finding the load-carrying capacity for an actuator design candidate at a given joint

2. Using the system model, dynamic simulations are performed to obtain the joint torques for a set of manoeuvres. This set of manoeuvres represents the operation conditions of typical load-handling tasks, where a payload is to be picked up from the floor at its original location, carried to its destination, and put back on the floor at the destination. This is then followed by the exoskeleton walking back to the original location, potentially to carry more load. To model all of the above-mentioned tasks, the program performs simulations of the following movements:

   a. Sitting down into a squat position in 2 seconds, without any load. This is the stage in which the exoskeleton is reaching down to pick up the load from the ground.

   b. Performing a squat manoeuvre with a payload of 45 kg (the minimum acceptable value) in 2 seconds. This is the stage in which the exoskeleton is lifting the load up from the ground surface, and into a standing position.

   c. Walking for 10 seconds while carrying the load. In this stage, the exoskeleton is carrying the load to its destination.

   d. Sitting down into a squat position in 2 seconds, with the load, in order to put the load down on the floor at the destination.

   e. Performing a squat manoeuvre without any load, in 2 seconds, this is the standing up stage before walking back to the original position.

   f. Walking without load for 10 seconds, back to the original position.

The calculated power consumption of the exoskeleton for this set of manoeuvres is one of the factors involved in the optimisation process, as will be mentioned later.

3. The method explained in section 4.7.1 is used to find out the load-carrying capacity (LCC) of the exoskeleton with the given actuator design candidate.

4. The power consumption of the actuator is also calculated for the set of manoeuvres mentioned in step 2, using equation 4-18.

5. Finally, the estimated total weight of the exoskeleton with the given motor and transmission system is also recorded, as it is one of the factors that contribute to the value function used in the optimisation algorithm, as explained later.

It should be noted that the above method should be used while taking into account all of the actuators, for three reasons. The first reason is that the LCC of the exoskeleton is determined by the actuator with the smallest LCC, i.e. the *bottleneck* of the system. Therefore, the actuators selected for all three joints need to be known in order to calculate the LCC. Secondly, the total mass of the exoskeleton, also one of the design optimisation factors, depends on the masses of all actuators. Finally, it is the total power consumption of all of the actuators which is desired to be as low as possible. On the other hand, preliminary simulations performed in this study showed that the mass of each joint's actuator affects the mechanical power required at that joint, as well as other joints. The results of these preliminary analyses suggested that, although the selection of larger motor for a given joint may lower the power consumption of the joint, it may as well increase the total power consumption of all joints together. In other words, a large and heavy actuator may have a large energy density, but it may as well be suboptimal from the point of view of the *total* power consumption of the system. In order to investigate this, dynamic simulations were carried out while factoring in the mass of the actuators at all joints and recording the individual and total power consumptions of the joints. The results are demonstrated in Figure 4-15. This diagram only shows the effect of changing the size of the knee actuator (mainly by varying the motor size); the size of hip and ankle actuators have been fixed in the simulation model in this case. It could be seen that the smallest power consumption of the knee actuator *alone* is obtained with the selection of an actuator that weighs over 8 kg. However, it could also be seen that, when the sum of the power consumption of all actuators (i.e. the knee, hip and ankle actuators) is taken into account, the optimal actuator weighs nearly 4 kg. Hence, this optimisation problem can only be solved by considering the performance of all actuators. It should be noted that the masses of the actuators shown in Figure 4-15 have been obtained by summing up the motor and transmission mass, as well as the estimated weights of the other components (e.g. housings designed for frameless motors). The detail design of the actuator prototype proved that the mass of the extra parts had originally been underestimated. Modified values have been used in the re-optimisation process after the investigation of the experimental test results, as will be explained later.
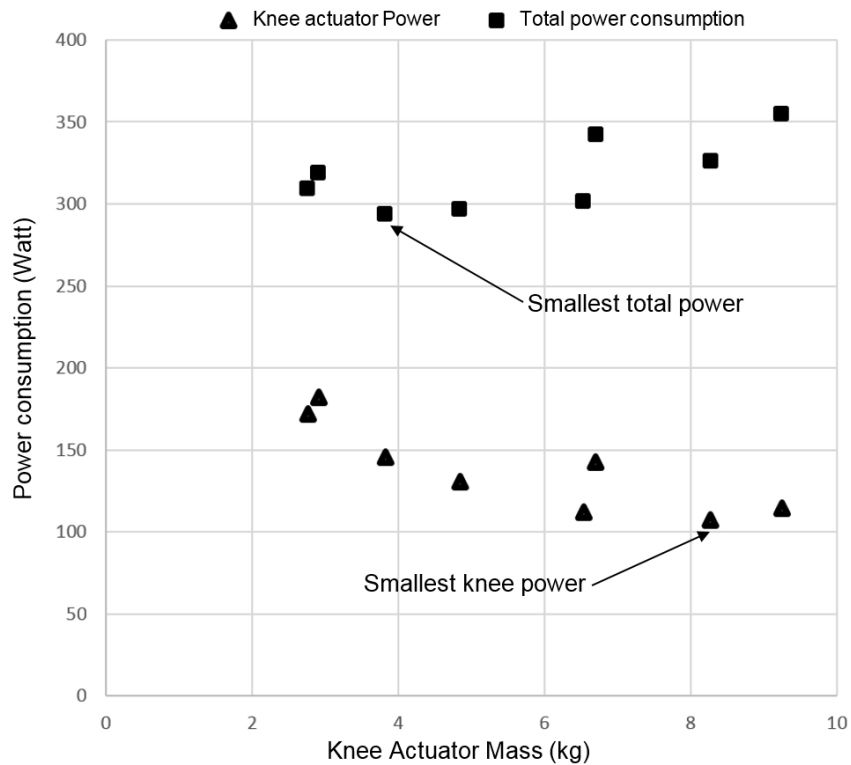
Figure 4-15. Simulation results of the power consumption of the knee actuator for different actuator sizes.

4.8   The Optimisation Algorithm

As mentioned in the previous section, it has been found from the investigations carried out in this research that the optimisation problem at hand needs to be solved by considering all three joint actuators together. However, since each joint's actuator consists of two components (a motor and a transmission system), the search space is 6 dimensional. It was originally intended to perform an exhaustive search in this 6-dimensional space and choose the optimal combinations of motors and transmissions for all three joints; however, simple calculations showed that the run-time of the optimisation code would be unfeasibly long. To demonstrate this, let us assume that there are 20 motor options and 10 transmission system options for each joint. This means that, for the three joints, there is a discrete search space of $(20 \times 10)^3 = 8 \times 10^6$ points. On average, the optimisation program takes 0.53s to assess the performance of one actuator. This means that the total search space can be covered in nearly 50 days. Therefore, an alternative algorithm was devised which is consisted of a single-joint optimisation

algorithm, repeated inside a triple-joint algorithm, as explained in the following sections.

For convenience, the optimisation process was done separately for different types of transmission mechanisms.

4.8.1 Single-Joint Optimisation

The single-joint optimisation algorithm used in this study is based on assigning a *value function* to each design candidate and then choosing the candidate with the maximum value function. The value function is a numeric score, which quantitatively shows the suitability of the design candidates in comparison to one another. The method for calculating the value function will be explained further in this section.

In this algorithm, only one of the three joints is considered, and it is assumed that the actuators of the other two joints have been selected. The single-joint optimisation algorithm consists of the following stages, aimed to maximise the value function:

- I.   Select the first motor in the list.
- II.   Select the first transmission in the list.
- III. The combination of the selected motor and transmission system yields the actuator design candidate to be assessed, as follows:
    - a. Replace the numeric values of the motor and transmission parameters in the equations that describe the actuator model, as explained in sections 4.4 and 4.5.
    - b. Assess the actuator candidate design as explained in section 4.7. Record the load-carrying capacity (LCC), power consumption, and the total mass of the exoskeleton (which depends on the motor and transmission chosen)[10]. These values will be used to form the value function, as explained later.
- IV.   Select the next transmission system in the list.
- V.   Repeat steps III and IV until all of the transmission systems in the list have been examined.

---

[10] The values of other variables, e.g. the maximum current drawn, are recorded to check the design feasibility. However, they do not contribute to the formation of the value function, and hence are not used for comparing different motor-transmission options.

VI.   Select the next motor in the list.

VII.   Repeat steps II to V until all of the motors in the list have been examined.

The result of the algorithm is a list of different design candidates (i.e. motor-transmission combinations) with the variables that characterise their performance, namely the load-carrying capacity (LCC), power consumption, and the total mass of the exoskeleton. At this stage, there is a problem of multi-factor decision making; hence, a normalised weighted decision table must be developed to choose between the possible combinations [70] as explained briefly here. First, the three variables are normalised by dividing their value by their range. These normalised values are then multiplied by weighting (i.e. importance) factors. The values of the weighting factors depend on the design intent; in this study, equally large weighting factors were assigned to maximum allowable load and power consumption, since these parameters are equally important. A smaller value was assigned to the weighting factor of the total mass of the exoskeleton, as shown in Table 4-2. Notice that the weighting factors for the power consumption and exoskeleton mass are negative because these are parameters that are desired to be reduced. Finally, the value function is formed by summing the weighted normalised values. The motor-transmission combinations are then ranked and sorted in the spreadsheet according to the values of the value function. The motor-transmission combination with the largest score is chosen as the optimal solution at this stage.

Table 4-2. The weighting factors of the variables used in the value function

Variable	Weighting factor
Load-Carrying Capacity	0.3
Power consumption	-0.3
Exoskeleton mass	-0.1

The above-mentioned algorithm has been illustrated in Figure 4-16. It must be noted that the solution obtained at this stage is not the final answer, as explained in the following section.
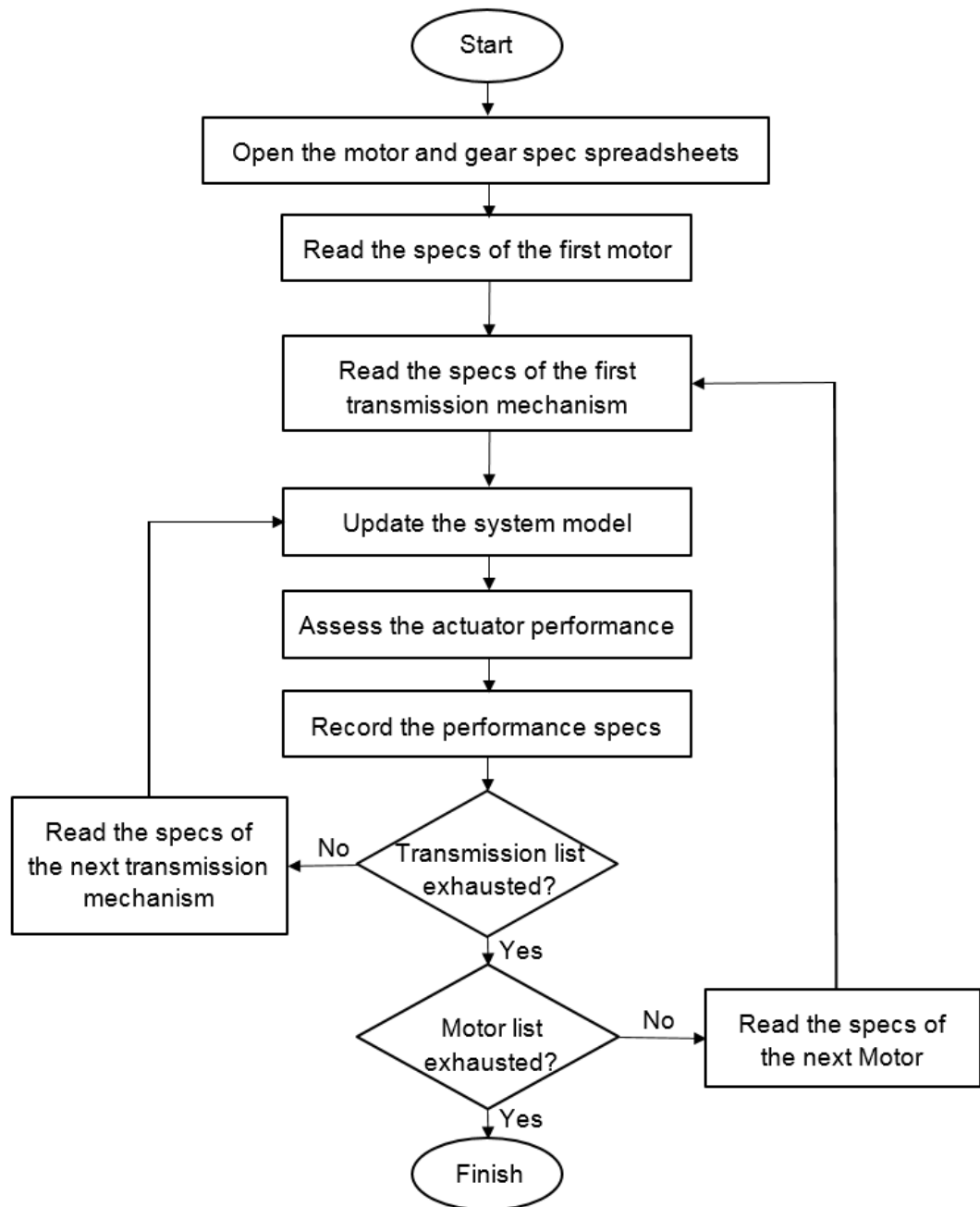
Figure 4-16. The flowchart of the single-joint assessment algorithm

4.8.2 Triple-Joint Optimisation

The triple-joint algorithm explained in this section has been devised so that the optimisation problem could be solved for all three joint actuators. This is done while taking into account the effect of each joint's actuator mass on the power consumption of the other joints' actuators. The algorithm is made of the following steps:

1. It is initially assumed that the most lightweight motors and transmission mechanisms in the lists are allocated to the ankle and hip actuators[11].
2. The single-joint optimisation algorithm is performed for the knee joint. The result is assumed to be the knee actuator for the next step.
3. Step 2 is repeated for the ankle joint. The result is assumed to be the ankle actuator for the next step.
4. Step 2 is repeated for the hip joint. The output is assumed to be the hip actuator for the next step.
5. Steps 2 to 4 are repeated until the answers yielded by the program for each joint's actuators stop changing in each iteration. At this stage, the final solution has been found.

The algorithm is shown in the flowchart in Figure 4-17. The algorithm starts with the assumption that the most lightweight motors are located at the hip and ankle joints before the first optimisation iteration for the knee joint is performed. The reason for this is as follows: It is known from the simulation results that the assumption of the most lightweight possible actuators at the hip and ankle joints would lead to an underestimated power requirement of the knee actuator in the first iteration. This means that, in the very first iteration, the knee actuator will be optimised for a power requirement lower than that of the real case. Therefore, since larger motors are more power efficient, it is expected (and confirmed by the results, as explained later in the results section), that the selected knee motor in the first iteration would be smaller or the same size as that in the final iteration. Furthermore, each iteration of the algorithm provides the input for the next iterations. Thus, in each subsequent iteration, the motors assumed for the actuators are the results of previous iterations. This means that, in each subsequent iteration, more realistic power requirements are assumed for the optimisation process. As expected, the motors chosen by the algorithm were larger than the lightweight motors initially selected (this will be explained in the results sections). The iterative algorithm continues until the optimisation results do not change for any of the actuators compared to the previous iteration. At this stage, the final solution has been found.

---

[11] For the very first iteration only, the efficiency values of the hip and ankle actuators are replaced by estimated values obtained from single-joint simulations.
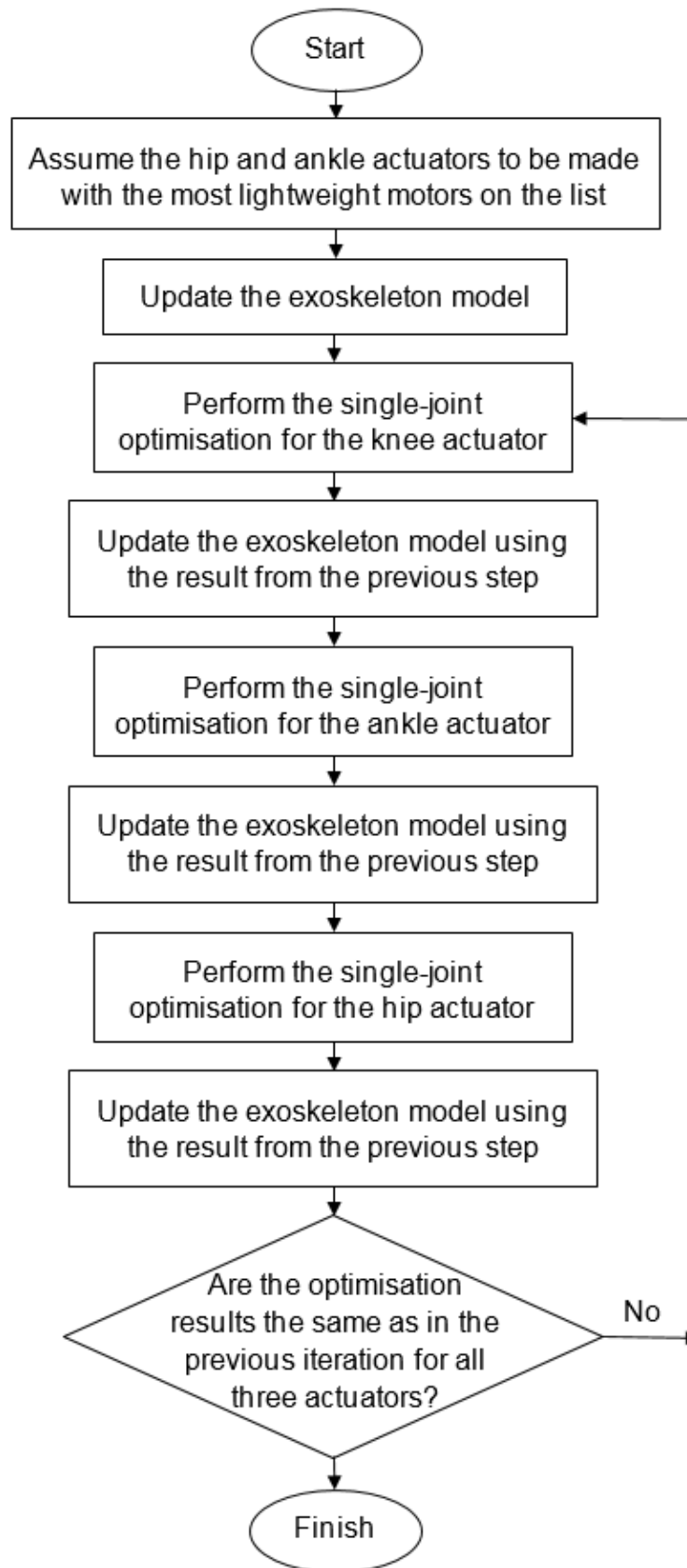
Figure 4-17. The flowchart of the triple-joint optimisation algorithm

4.9   The optimisation software development

4.9.1   Introduction

As mentioned earlier, the optimisation procedure done in this study has been performed using a program written in MATLAB™. This section briefly covers the software development procedure.

4.9.2   Software requirements

The single-joint optimisation program should perform the following tasks:

1. Take the dimensions and inertial parameters of the exoskeleton frame (including estimated mass values for the computer and power supply).
2. Read the kinematic inputs of the exoskeleton motion for the squat and gait manoeuvres, which are the angles, angular velocities and angular accelerations of the joints.
3. Open the spreadsheets of the motors and transmission systems, and read the numeric values of the parameters.
4. For each motor and each transmission system, read the mass values and place corresponding mass-points (particles) in the corresponding locations in the exoskeleton model, and reconstruct the model accordingly.
5. Perform dynamic simulations, and calculate the load-carrying capacity and power consumption of the system, for all of the motor-transmission combinations.
6. Save the results in a spreadsheet.

The single-joint optimisation process (section 4.8.1) is implemented by running the program and saving the results in a spreadsheet. The normalised weighted decision matrix is then manually created inside MS Excel™ (using a template created for this purpose), and the optimal choice is then found.

The triple-joint optimisation is performed by repeating the above-mentioned procedure, according to the algorithm explained in section 4.8.2.

4.9.3   The structure of the software

The software consists of one main program which calls a number of subroutines to perform different tasks involved in the optimisation algorithm, e.g. opening and spreadsheets, constructing the system model, and running

simulations. A simplified model of the software is demonstrated in the block diagram shown in Figure 4-18.
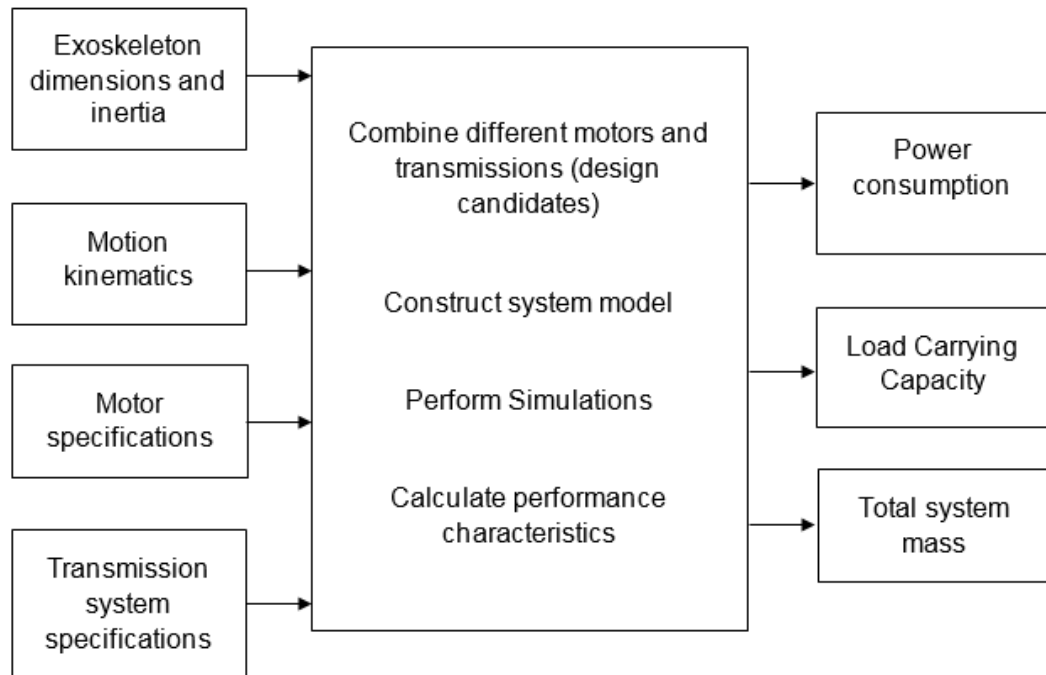
Figure 4-18. The block diagram of the assessment program

4.10 Summary

This chapter presents the method used in this project for the optimal design of the actuators of an enhancive robotic exoskeleton. The design optimisation method is done with the consideration of the design requirements and constraints explained in section 3.3 of Chapter 3. Furthermore, as stated in section 1.4 of Chapter 1, the scope of this research covers only the lower-body actuators in the sagittal plane, at the ankle, knee and hip joints.

Section 4.2 explains the dynamic modelling and simulation of the exoskeleton manoeuvres. The results from these simulations are the joint angle, velocity and acceleration values, as well as the required torque at each joint (which should be provided by the actuators). These results are used as inputs for the simulation model of the power transmission system, explained in the following paragraph.

A preliminary analysis (explained in section 4.3) has been carried out to rule out unsuitable power transmission systems, which determined that three types of transmission mechanisms could potentially be appropriate for this

design problem. These mechanisms (which are strain gears, chain-and-sprockets, and ballscrews) have been modelled and investigated using the optimisations procedure. The modelling of these mechanisms has been covered in section 4.4. The results of the joints motions and torques, acquired from the simulation of the exoskeleton motion, are fed into the model of the transmission mechanism, to obtain the required values of the torques, velocities, and accelerations of the motors at each joint. These values, in turn, are used as inputs to the simulation model of the electric motors, explained in section 4.5.

Since the optimisation algorithm used in this study is based on an exhaustive search method, the search space needs to encompass all of the motor candidates. Developing a list of all of the existing motors in the market is not practical. However, an extensive market search, covered in section 4.6, has been carried out in this project which results in a large list of motors which represent the state of the art. The list contains 151 motors, in a large variety of sizes, designs, nominal torques, and nominal powers. This list has been used by the optimisation program to find the best candidate for each of the joint actuators.

The optimisation procedure consists of three stages, each being executed by the program. The first stage is the assessment of each actuator candidate, comprised of a transmission system and a motor from the list. This assessment procedure yields the power consumption and load-carrying capacity of the exoskeleton if the given actuator candidate is used. This assessment process is explained in section 4.7.

A single-joint optimisation procedure, explained in section 4.8.1, is performed by the optimisation program to select the best candidates for the motor and transmission system for the actuator of a given joint. This procedure is then repeatedly executed within the triple-joint optimisation algorithm, as explained in section 4.8.2. After numerous iterations, the algorithm converges to the final result for the motors and transmission mechanisms of the actuators at all three joints.

The results of the optimisation algorithm for the selected types of the transmission system are presented in Chapter 5.

Chapter 5
Optimisation Results and Actuation System Design

5.1 Introduction

In this chapter, the results of the optimisation algorithm explained in the previous chapter are presented for the selected types of transmission systems. Analysis and optimisation was first done on the knee actuator, and then the ankle and hip actuators. The final solutions and the parameters for the design of the three actuators are also presented in this chapter.

As explained in section 4.2.3 of Chapter 4, two different designs can be used for the exoskeleton with two different types of gait cycle. Originally, a design with long limbs and bent knees was considered (hereafter referred to as the *bent-knee design*), which requires large values of torque and power at the joints. For this design, most design concepts proved to be incapable of performing the required motion. Therefore, a different design was chosen, in which the limbs are the same length of the user's limbs[12], and the knee joint remains unbent while standing and in the stance phase of walking. This design, hereafter referred to as the *straight-knee design*, has relatively smaller torque and power requirements compared to the bent-knee design, and was therefore chosen for the exoskeleton. The analysis results for both designs are mentioned in this chapter.

As explained later, the final design concept chosen for the exoskeleton consists of ballscrews on the knee and ankle joints, and strain gears on the hip joints. The optimisation results for this design concept, mentioned in section 5.3 of this chapter, are presented with more details compared to the other concepts which have been ruled out due to unsatisfactory analysis results.

The optimisation results yield the parametric design for the actuators, which include the motors to be used, and the specifications of the transmission systems. Once these parameters are known, detail design can be done for the actuators, which is covered in section 5.4.

---

[12] This requires length-adjustable links, so that different users would fit.

5.2 Results for the bent-knee design

5.2.1 Results on Chain and Sprockets for the Knee and Ankle Actuators, for the bent-knee design

The reduction ratio achievable by chain and sprockets is limited by factors including the minimum allowable number of teeth on the small (driving) sprocket, the largest acceptable diameter of the large (driven) sprocket, and the required torque capacity (which places a lower bound on the pitch size and therefore on the sprockets diameter). A double-stage reduction system was used in the design concept to expand the available range of reduction ratio to 81:1 with a triplex chain and sprocket system.

The results of the optimisation program show that a double-stage reduction system can perform the required task, with triplex chain and sprockets and a ratio of 36:1 for the knee and 25:1 for the ankle. The most severe drawback of this design concept is that the actuators would be heavy; the reasons is that four sprockets are needed for a double-stage chain system, which make the transmission system heavy, especially when Triplex chain and sprockets are used. The estimated weight of each actuator is over 12 kg. Furthermore, having to use a two stage system also means that the actuator will become bulky. For these reasons, this design concept was relinquished.

5.2.2 Results on Strain Gears for the Knee and Ankle Actuators, for the bent-knee design

The results for the knee joint showed that many motor-gear combinations could perform the task during the squat manoeuvre. Also, a lot of them were suitable for the stance-side knee joint. However, none of the combinations could provide the required torque at the knee joint of the stance leg. Further investigations of the problem showed that the smallest available gear ratio for the strain gears (50:1) is still too large, as explained in the following paragraphs.

Figure 5-1 shows the simulation result for one of the motors, with a payload of 45kg, and two different gear ratios, 50:1 and 80:1. The graphs showing the required torque-vs-angular velocity of the motor have been shown in blue, and the motor limiting lines (explained in section 4.5 of Chapter 4) are shown in red.

It could be seen in **Figure 5-1** that in both cases, the maximum required angular velocity is so high that parts the blue graphs lie outsides of the allowed area. Since the motor velocity is equal to the joint velocity multiplied by the gear ratio, reducing the gear ratio will reduce the required motor velocity. This could be seen by comparing the two graphs, which shows that a gear ratio of 50:1 will bring the blue graph closer to the allowed limits, though not enough. Since strain gears are not available in ratios below 50:1, this design concept is not suitable.
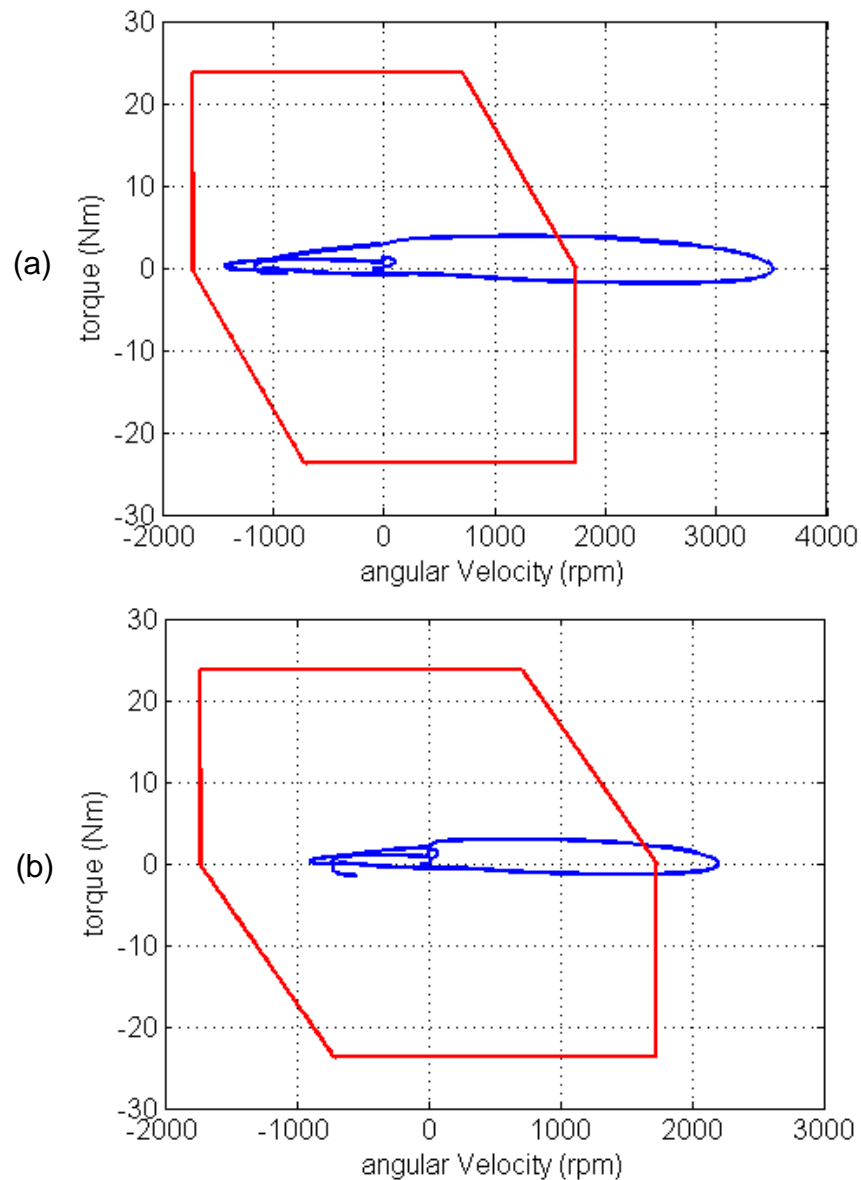
Figure 5-1 The torque versus velocity during the swing stage of gait: the required motor torque curves (in blue) and the motor torque limits for one of the motors (in red), with a gear ratio of 80 (a) and 50 (b), for a payload of 45 kg.

In the case demonstrated in **Figure 5-1**, the knee joint of the swinging leg is being investigated, where a rather small amount of torque is required (nearly 4 N-m with a ratio of 50:1). However, the required angular velocity is quite large (3500 rpm for a ratio of 80:1, and 2200 rpm for a ratio of 50:1). The maximum required motor speed exceeds its no-load speed, even with a gear ratio of 50:1 which is the smallest available ratio. A smaller ratio is therefore desired, and a solution for achieving this will be explained in the next section.

An interesting point that could be seen from **Figure 5-1** is that a gear ratio (80:1) not only increases the required motor velocity, but also the required torque. At a first glance, this may seem counterintuitive if the motor torque is assumed to be equal to the joint torque divided by the gear ratio. However, part of the required motor torque is needed to overcome the rotor inertia. Let us review equation 4-14:

$$\tau_m = (\tau_m)_{out} + I\alpha_m + D\omega_m$$

where τ_m is the required motor torque, and $(\tau_m)_{out}$ is the joint torque divided by the gear ratio, after taking into account the efficiency, as explained in equation 4-1, which is repeated here:

$$\begin{cases} (\tau_m)_{out} = \dfrac{\tau_j}{\eta.N}, & P > 0 \\ (\tau_m)_{out} = \dfrac{\eta.\tau_j}{N}, & P < 0 \end{cases}$$

However, the frictional and inertial terms, $D\omega_m$ and $I\alpha_m$, depend on the motor angular velocity and acceleration, which in turn depend on the gear ratio, as was mentioned in equation 4-2:

$$\begin{cases} \omega_m = N.\omega_j \\ \alpha_m = N.\alpha_j \end{cases}$$

So it can be seen that, while an increase in the gear ratio N would reduce the size of the term $(\tau_m)_{out}$, it will increase the size of $D\omega_m$ and $I\alpha_m$. Thus with an increase in N, if the velocity and acceleration are large enough, their increasing effect may overcome the decreasing effect related to the term $(\tau_m)_{out}$, as is the case here. This effect has been illustrated in **Figure 5-2**.
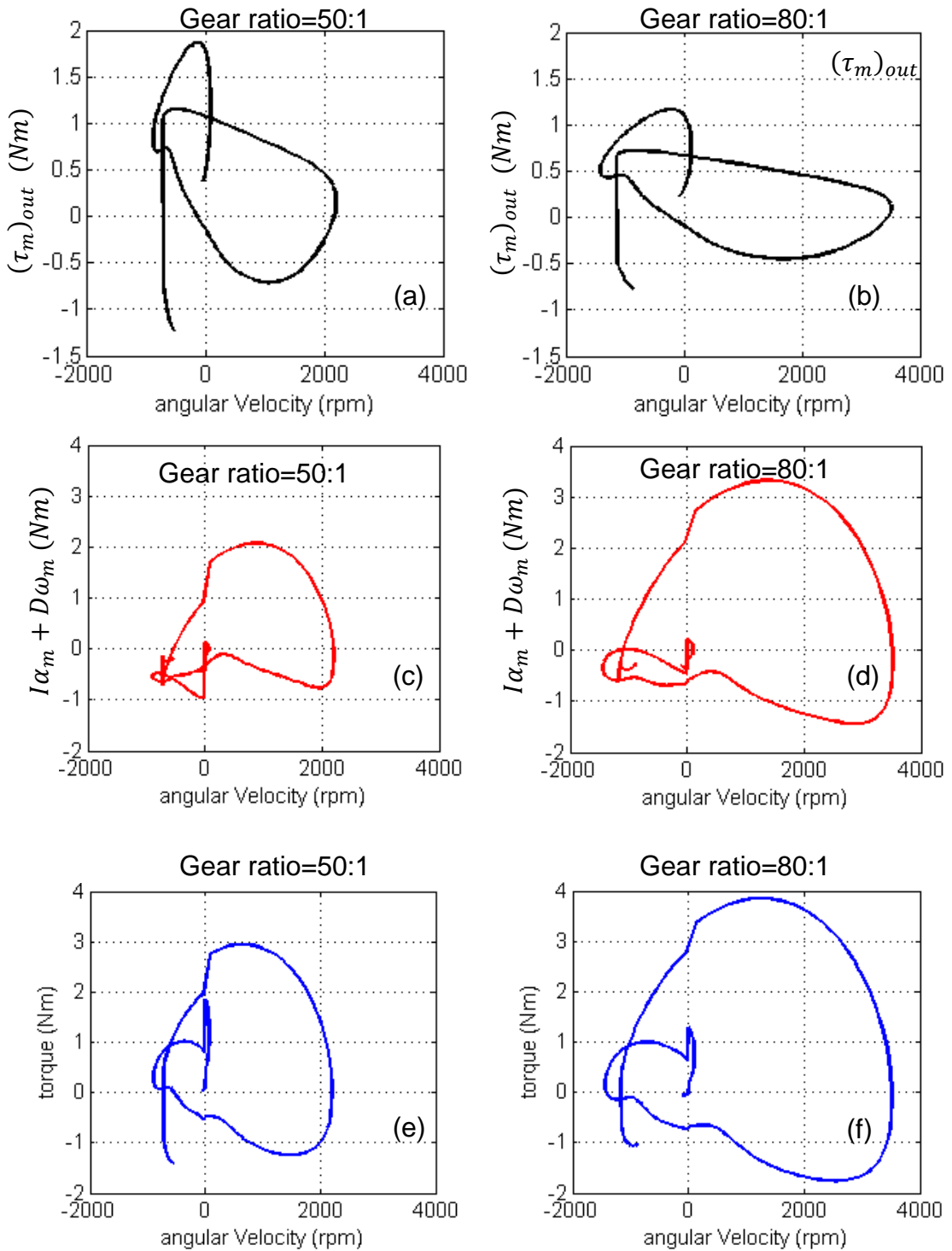
Figure 5-2 The different components of the torque versus velocity: the term $(\tau_m)_{out}$ (a and b), the inertial and frictional torque (c and d), and the total required motor torque (e and f) for gear ratios of 50:1 and 80:1.

It could be seen in **Figure 5-2** that, for a gear ratio of 80:1, although $(\tau_m)_{out}$ is smaller (a and b), the frictional and inertial torques are lager (c and d), and hence the total torque is larger (e and f).

In order to find the optimal gear ratio (even if it is not available for strain gears), a modified version of the optimisation program was run that could assume the gear ratio to be smaller than 50:1. The results showed that the required ratio is 37:1 for the knee and 25:1 for the ankle, both below the minimum available for strain gears. However, the optimal gear ratio for the hip actuator is approximately 80:1, which is available on strain gears. Therefore, this design concept can be used for the hip joint, but not for the ankle and knee joints.

Figure 5-3 shows the simulation results for the knee and ankle joints, with gear ratios of 37:1 and 25:1, respectively. It can be seen that the required torque graphs are within the allowed region (enclosed by the red lines). However, as mentioned earlier, the optimal gear ratio for both the ankle and knee actuators are below the minimum value available for strain gears. To achieve these transmission ratio values, another design concept was investigated, as explained in the next section.

(a)
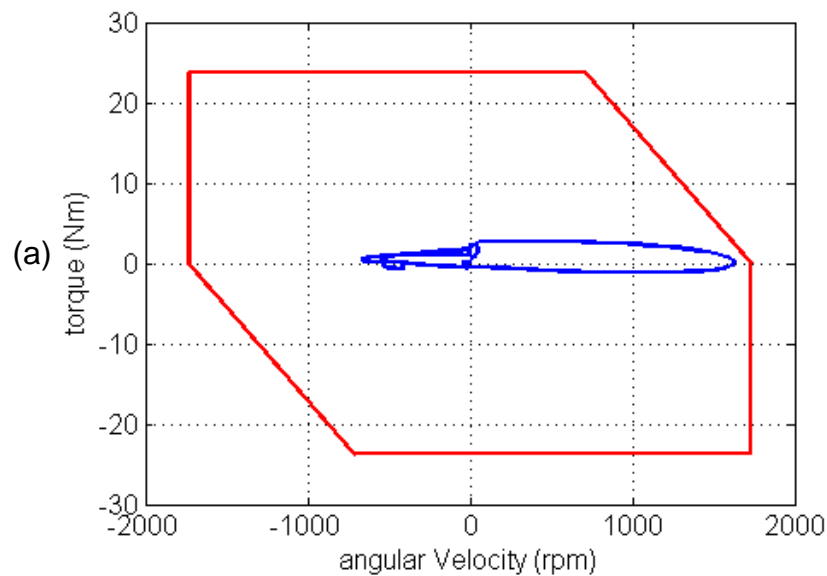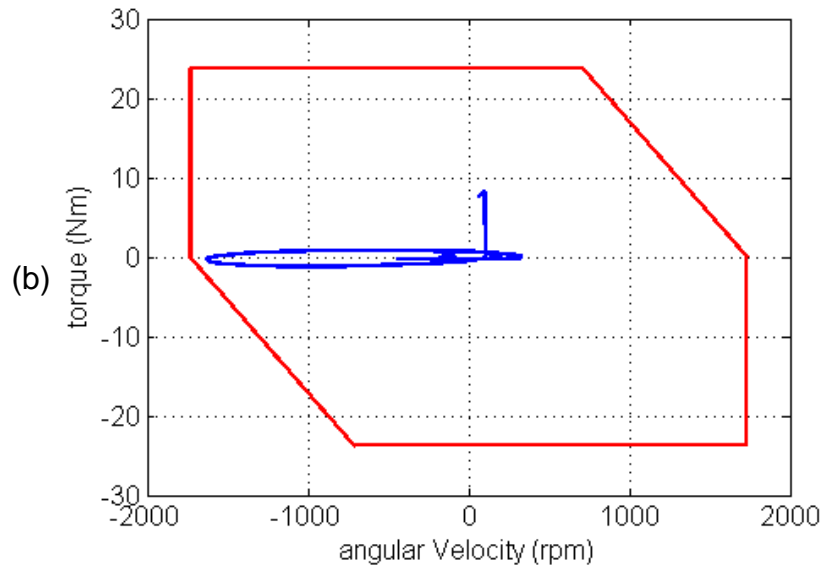
Figure 5-3 The torque versus velocity: the required motor torque (in blue) for the knee (a) and ankle (b) actuators, and the motor limiting lines (in red)

5.2.3 Results on Strain Gears combined with Chain and Sprockets for the Knee and Ankle Actuators, for the bent-knee design

To reduce the total transmission ratio, a strain gear can be used in combination with a speed-up chain and sprocket mechanism. A chain and sprocket system with a ratio of 10:13, combined with a strain gear with a ratio of 50:1, yields a total ratio of 38.5:1, which is close to the target value of 37:1 mentioned in the previous section. Although the results of the optimisation program (mentioned in the previous section) predict that this design could do the job, the actuator would be rather large and heavy (approximately 6.5 kg), and hence suboptimal compared to the design with a ballscrew and slider-crank, which will be explained later.

5.2.4 Results on Ballscrews with Cable and Pulleys for the Knee and Ankle Actuators, for the bent-knee design

Analysis and design of the actuator

For the cable and pulleys design concept, as with the previous concept (section 5.2.3), the optimisation program suggested the transmission ratios of 37 and 25 for the knee and ankle, respectively. This design concept,

116

demonstrated in **Figure 4-11** (a) of Chapter 4 (87), theoretically allows for any desired transmission ratio with the right choice of pitch length and the pulley diameter, as shown in equation 4-3 (p88). However, there are a number of design limitations. First of all, the available ballscrew pitch sizes are limited. Furthermore, the maximum pulley diameter is constrained by the acceptable size limit according to the design requirements, as mentioned in requirement number 36, Appendix C, which states that in each dimension, the size of the system should not be larger than 100% of the size of an average human. In order to avoid the joints from becoming too large, it was decided to set the maximum allowed pulley diameter to 130mm, which is also the pulley diameter of the actuators of the Body Extender exoskeleton [28], covered in section 2.3.3 of Chapter 2.

There is also a lower bound for the pulley diameter. The minimum allowed pulley diameter is linearly related to the thickness of the wire ropes used, with the proportion depending on the rope design [100]. If the pulley diameter is smaller than the minimum allowed value, the portion of the wire rope that is bent onto the pulley will acquire a plastic deformation. This also means that the maximum allowed rope thickness is limited by the maximum allowed pulley diameter. Therefore, the rope thickness cannot be increased without limit if an increase of the strength should be required; instead, a stronger *tendon* can be made by using a number of ropes in parallel, as shown in **Figure 4-11** in Chapter 4 (p87) where the tendon consists of two ropes.

Due to the low reliability of rope drive mechanisms, large safety factors are normally used, which could be as large as nearly 12 for critical cases [101]. The smallest suggested safety factor is 3.2. The design investigation was carried out with the assumption of a safety factor of 5, the most common value used. For a given peak torque at the pulley, the choice of a larger pulley diameter would reduce the axial force in the tendon; this may reduce the required number of wires in parallel, and hence lead to a slimmer design.

To achieve the desired transmission ratio of 37, a ballscrew with a pitch size of 10mm can be used together with a pulley of 118 mm diameter, which is close to the largest acceptable diameter[13].

---

[13] The next available larger pitch size for the ballscrew is 12.67 mm, which would require the pulley diameter to exceed the maximum acceptable value.

According to the dynamic simulations, the peak torque at the knee joints is 416 Nm. This means that, for a pulley diameter of 118mm, the force in the tendon will be equal to 7.05 KN. This must be multiplied by a load factor of 2 in order to account for modelled shock loads. Also, a safety factor of 5 has been used, as mentioned before. Therefore, the tendon must bear a tensile force equal to 70.5 KN.

To design the tendon, different wire rope designs were investigated, all manufactured by the Carl Stahl GmbH, which also provides a detailed technical design guide [100]. The ropes come in different designs, distinguished by the way that the wires have been weaved to form the ropes, as depicted in **Figure 5-4**.

The relation between the minimum pulley diameter and rope thickness is different for different designs, and is presented in Table 5-1.

Furthermore, available thickness ranges are not the same for all of the rope designs, as shown in Table 5-2.
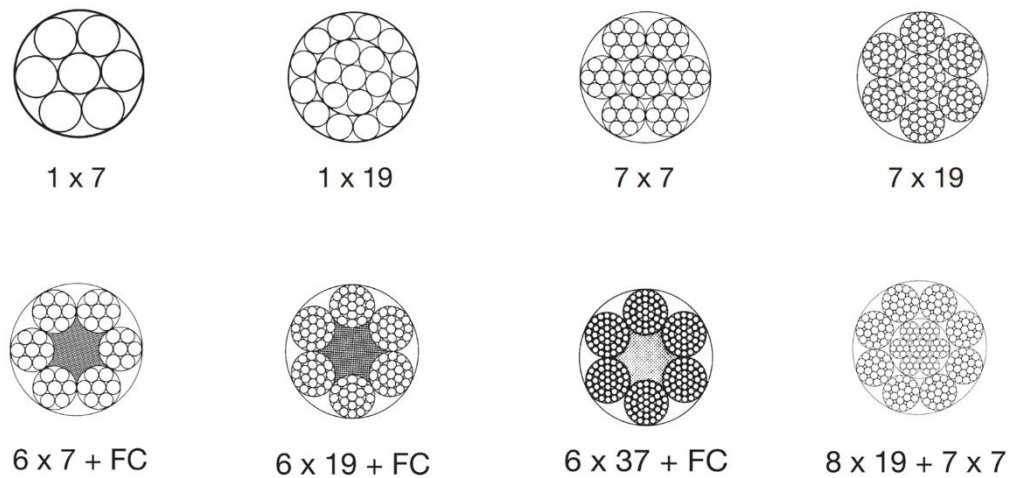
Figure 5-4 Different rope designs [102]

Table 5-1 The minimum pulley diameter for different rope designs [102]

Rope design	Minimum pulley diameter
7×7 and 6×7+FC	42 × Rope diameter
7×19 and 6×19+FC	25 × Rope diameter
8×19+7×7	16 × Rope diameter

Table 5-2 Available thickness range for different rope designs

Rope design	Rope thickness range (mm)
7×7	0.12 – 6.00
6×7+FC	1.50 – 5.00
6×19+FC	3.00 – 8.00
7×19	0.45 – 8.00
8×19+7×7	0.57 – 4.00

The ropes are designed to be connected to other components with the swaged terminals at the end of the ropes (shown in **Figure 5-5**). The terminals are thicker than the ropes; therefore, the thickness of a tendon will be equal to the thickness of the terminal, multiplied by the number of ropes in parallel within the tendon. The *ball* type terminal **Figure 5-5** (b) is shorter and thinner than the *shank* type; however, the ball terminal is only available for wires with a thickness of 4mm or less. Hence, for ropes which are 5mm or thicker, the shank type terminal has to be used. This means that the calculation of the tendon thickness is different for different designs, depending on the available terminal type. It must be noted that other terminal types are also available, but are either larger than the two types shown in **Figure 5-5**, or too weak to bear the required load, or unavailable for the types of ropes used. Therefore, only the two types shown in the figure below have been considered in this study.

(a)   (b)
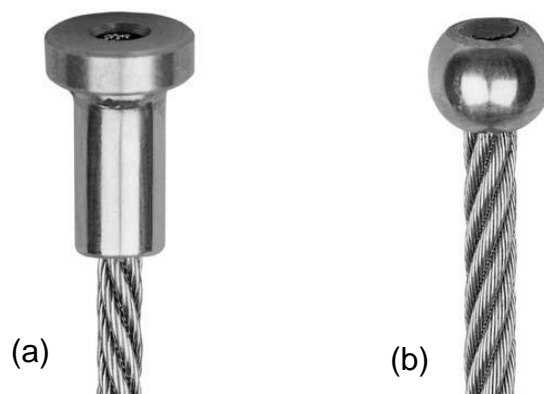
Figure 5-5 Swaged terminal types of the rope, shank (a) and ball (b).

Using the data presented in Table 5-1 and Table 5-2, an investigation was done to find the rope design that would yield the slimmest tendon, for the given

strength requirement. To calculate the required number of parallel ropes, we can use the following equation:

$$Number\ of\ ropes = \frac{2 \times N \times 7.05}{F_{break}}$$

<div align="right">5-1</div>

where F_{break} is the breaking load of the rope in KN (which depends on the rope design and thickness) and N is the safety factor (5). A shock load factor of 2 has been multiplied in the required force, which is 7.05 KN, as stated earlier in this section. Furthermore, the safety factor can be calculated as follows:

$$N = \frac{F_{break} \times Number\ of\ ropes}{2 \times 7.05}$$

<div align="right">5-2</div>

Several tendon designs have been considered, and presented in Table 5-3. It could be seen that only the designs of the first three rows offer an acceptable safety factor (at least 5). Among these, the first row shows the slimmest design, which has been chosen.

Table 5-3 Design candidates for the tendon

Rope type	Rope nominal thickness (mm)	F_{break} (KN)	# of Ropes in parallel num_r	Swaged terminal thickness, D_t (mm)	Tendon Width $num_r \times D_t$ (mm)	Min Pulley diameter (mm)	Safety factor $\frac{F_{break} \times num_r}{2 \times 7.05}$
8×19 +7×7	4	9.1	8	10	80	16×4=64	5.16
6×19 +FC	3	4.90	14	8	112	25×3=75	5.56
7×7	3	5.06	14	8	112	42×3=126	5.02
6×19 +FC	5	13.60	5	16	80	25×5=125	4.82
7×19	5	13.00	5	16	80	25×5=125	4.6
7×19	4	8.34	8	10	80	25×4=100	4.73
6×19 +FC	4	8.70	8	10	80	25×4=100	4.93

8×19 +7×7	3	5.35	13	8	104	16×3=48	4.93
6×7+ FC	3	5.29	13	8	104	42×3=126	4.88
7×19	3	4.69	15	8	120	25×3=75	4.99

In addition to the main pulley, a linear guide rail would also be required to bear any load components that are perpendicular to the axis of the ballscrew. Furthermore, an idler pulley is also needed. An attempt was made to develop a detailed design based on this concept, which revealed that the total width of the design would be nearly 120mm. The total weight of the actuator, including the motor and housing, the ropes, and the main and idler pulleys, was estimated to be approximately 19 kg.
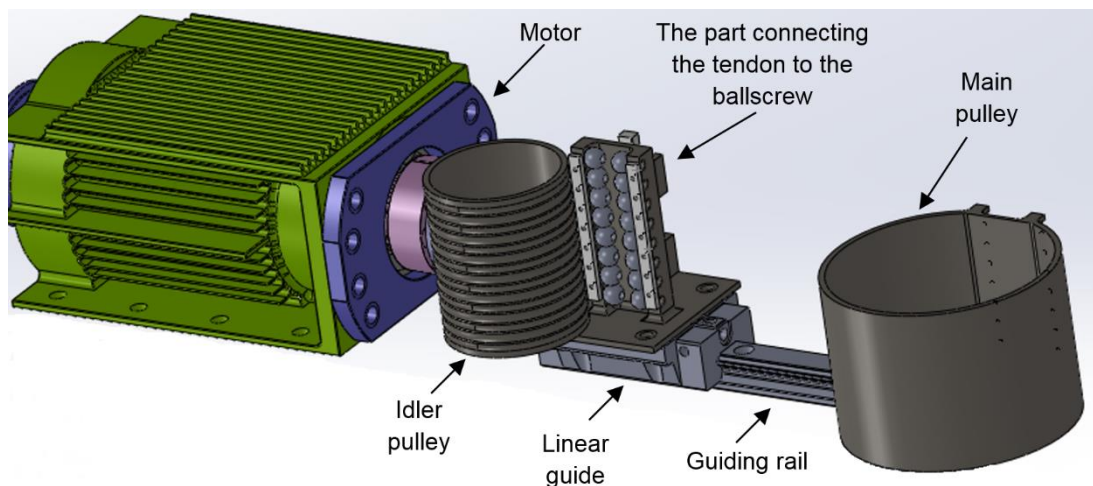
Figure 5-6 The CAD model of the actuator design with ropes-and-pulleys, based on the design concept shown in Figure 4-11 **(a) on page 87. The ballscrew and the ropes are not shown.**

Because this concept seemed to lead to the design of a bulky actuator, it was decided to consider another, simpler concept, as explained in section 5.2.5. However, before moving to the next design concept, a critical analysis of the actuator design of the Body Extender (section 2.3.3, p17), will be presented, since the design concept is the same as the one covered in this section.

A critical analysis on the design of the actuators of the Body Extender

The actuators of the Body Extender are reported to have been designed to apply a peak torque of 600 Nm [28]. The pulley diameter is 130 mm, which means that the maximum tensile force at the tendon is equal to

$$F_{tendon} = \frac{600}{0.130/2} = 9,230N \qquad \text{5-3}$$

The tendon is made of two wire ropes, each of which have a diameter of 4 mm. Therefore, the force in each rope, F_{rope}, is half of F_{tendon}.

$$F_{rope} = \frac{9,230}{2} = 4,615N \qquad \text{5-4}$$

Like the ropes analysed in this project, the Body Extender tendons are also made of ropes made by CarlStahl GmbH. Although the rope design has not been specified, three designs could potentially be used, which are presented in Table 5-4.

Table 5-4 Different possible tendon designs for the Body Extender

Rope type	Rope nominal thickness (mm)	F_{break} (KN)	# of Ropes in parallel num_r	F_{tendon} (KN)	$F_{rope} = \frac{F_{tendon}}{num_r}$ (KN)	Safety factor $\frac{F_{break}}{F_{rope}}$
8×19 +7×7	4	9.1	2	9.23	4.615	1.97
7×19	4	8.34	2	9.23	4.615	1.81
6×19 +FC	4	8.70	2	9.23	4.615	1.89

It can be seen that the largest safety factor that can be achieved is 1.97, which is not only way below the safety factor of 5 considered in this design, but also less than the smallest safety factor use for rope and pulley mechanisms, which is 3.8 [101]. Therefore, it could be concluded that the actuators of the Body Extender are unsafe.

5.2.5   Results on Ballscrews with inverted Slider Crank for the Knee and Ankle Actuators, for the bent-knee design

The simulation results for the knee and ankle actuators showed that this design concept would be able to perform the required task. However, at this stage it had been clear that the bent-knee design requires large values of torque and power at the joints, and it was decided that the design should be changed to one with shorter limbs which could walk with straight knee joints, as mentioned in section 4.2.3 of Chapter 4. Therefore, before continuing with further optimisation and detail design, the design was changed and the simulations redone. The results are presented in the next sections.

5.3 Results for the straight-knee design

5.3.1 Modelling considerations and transmission system type selection

In this design, as mentioned in section 4.2.3 of Chapter 4, the limbs of the exoskeleton are assumed in the dynamic model to be the same length as those of the user. The exoskeleton, however, still needs to follow the motion of the user at the connection points[14] between the user and the exoskeleton (as explained in the dynamic modelling of the exoskeleton manoeuvres in Appendix G). Therefore, the modelling method and the inputs of the dynamic simulations are the same as before; the only difference is that the length of the shank and thigh links in the exoskeleton model needed to be changed to be the same length as those of the user[15], and the same simulation programs would perform the simulations.

The previous simulation results (mentioned in section 5.2) helped to narrow down the list of design concepts to be considered. The chain and sprocket design had already proved to work, even for the bent-knee design; however, this concept would also lead to a bulky actuator design, as mentioned in section 5.2.1. Therefore, it was left as a last solution in case no other design concept would work. However, as will be explained in the following sections, other design concepts showed satisfactory results in the simulations, and therefore this design concept was relinquished. The same applies to the cable

---

[14] The exoskeleton and the user are assumed to be connected at the lower back and the feet. Therefore, the exoskeleton should follow the motion of the user at those points.

[15] In this case, the limb lengths were chosen to be the same as those of the test subject who performed the Motion Capture experiments.

and pulleys design concept, due to its inherent unreliability and the necessity of using a large safety factor, as mentioned in section 5.2.4. The remaining concepts are strain gears (alone or combined with chain and sprockets) and the inverted slider-crank mechanism with a ballscrew (hereafter simply mentioned as the ballscrew design concept). The results will be covered in the following sections.

5.3.2 Results on Ballscrews on the Knee and Ankle with strain gears on the hip, for the straight-knee design

As mentioned earlier, the triple-joint optimisation method requires the optimisation of the three joints in an iterative manner. In each iteration, one of the joint actuators will be optimised according to the single-joint optimisation method (section 4.8.1 of Chapter 4). However, the optimisation of each joint involves the calculation of the power consumption of all joints, as mentioned in section 4.7 of Chapter 4. Therefore, to run the optimisation program, the design concepts for all three joints need to be known and the simulation models must have been developed first.

In the analysis covered in this section, the actuators for the ankle and knee have been assumed to consist of ballscrews combined with slider-crank mechanisms. However, this design concept cannot be used for the hip actuator. The first reason for this is that, due to the excessively large range of motion of the hip actuator (nearly 180 degrees), using the slider crank mechanism is likely to be problematic, as the mechanism could get too close to a singular position. Furthermore, it could be seen from the knee and hip actuator designs (illustrated in Chapter 6) that such a design would be too large for the hip actuator. Therefore, the design chosen for the hip actuator consists of a strain gear, combined with a chain and sprockets if necessary.

For the ankle and the knee actuators, ballscrews with different pitch sizes were investigated, and the optimal result for each pitch size was obtained, as will be explained later. Theoretically, any pitch length can be used if the dimensions of the slider-crank mechanism could also be scaled accordingly. However, a larger pitch requires a larger mechanism as well, which could make the actuator too large to be acceptable. On the other hand, if the pitch is too small, then the required dimensions of the slider-crank mechanism will become so small that the mechanical components of the mechanism would interfere, rendering the mechanism physically unbuildable. After several trials with different pitch lengths, it was found that the smallest manufacturable

actuator size would be achieved with a pitch length of 16 mm. The diameter of the selected ballscrew is 10 mm. A smaller diameter would lack the required strength, and a larger one would make the actuator unnecessarily heavy. **Figure 5-7** shows the selected ballscrew model.

Figure 5-7 The ballscrew model selected for the knee and ankle actuators [98]

The results of the iterations of triple-joint optimisation are shown in Table 5-5. As explained earlier, the triple-joint optimisation algorithm starts with the assumption that the most light-weight motors in the list have been used in the ankle and hip actuators. This can be seen in the first row of the table, corresponding to iteration 0 (i.e. before starting the algorithm). In the first iteration[16], the knee actuator is optimised with the above-mentioned assumption about the ankle and hip motors. As shown in the second row of the table, the motor chosen by the algorithm (with its frame) weighs 4.14 kg. In the second iteration, the optimal motor option for the ankle is found, while assuming that the knee motor is the one found in iteration 1 and the hip motor is the one assumed in iteration 0. The motor chosen for the ankle by the algorithm happens to be the same model as that of the knee. The hip actuator is then optimised in iteration 3, while assuming that the ankle and knee motors are the ones found in iterations 1 and 2, respectively. The algorithm has chosen a motor for the hip actuator that weighs 3.03 kg with its frame. **Figure 5-8** shows pictures of the two motor models used. The motor chosen for the hip is shorter, but has a larger diameter.

---

[16] More detail will be presented later in this section to explain how the optimal motor-transmission combination is chosen in each iteration.

Table 5-5. The results of the iterations of triple-joint optimisation, with ballscrews on the ankle and knee joints and strain gears on the hip joints

Iteration	Actuator being optimised	Framed Knee motor mass (kg)	Framed Ankle motor mass (kg)	Framed Hip motor mass (kg)
0	-	-	0.99 (assumed)	0.99 (assumed)
1	knee	**4.14**	0.99 (assumed)	0.99 (assumed)
2	ankle	4.14	**4.14**	0.99 (assumed)
3	hip	2.76	4.14	**3.03**
4	knee	**4.14**	4.14	3.03
5	ankle	4.14	**4.14**	3.03
6	hip	4.14	4.14	**3.03**

The optimal transmission ratio for the hip was found to be very close to 80, which is a ratio available with strain gears. This means that it is not necessary to use a chain and sprockets mechanism in combination with the strain gear[17]. After the third iteration, the three consequent iterations show no change in the result of the optimisation for none of the joints, and the algorithm ends in iteration 6.

The final selection of the actuators enable the exoskeleton to carry 60 kg, and the total power consumption of the exoskeleton is estimated by the simulations to be 54W.

---

[17] As mentioned in section 5.2.3, a chain and sprockets mechanism can be used to adjust the total gear ratio of the transmission system, if the desired transmission ratio is too far from any of the ratios available for strain gears.

(a)   (b)
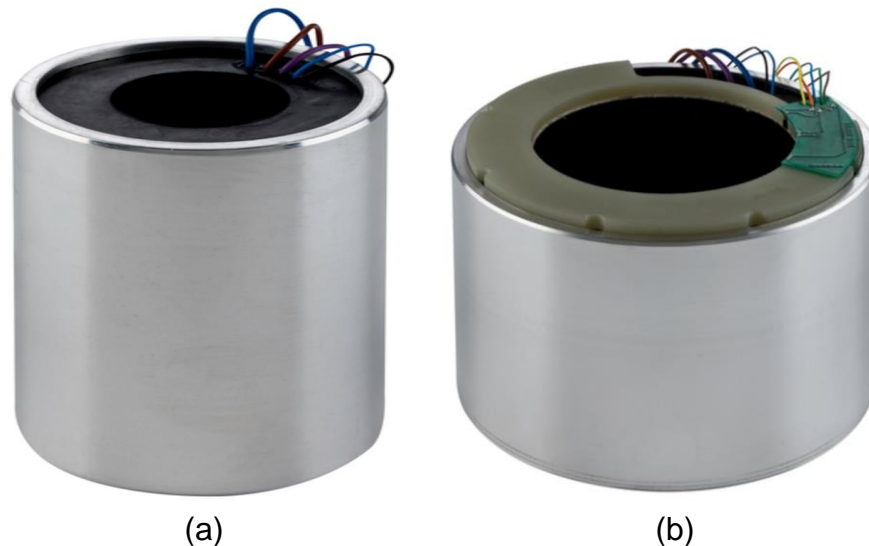
Figure 5-8 The selected motors: KBM17X03D (a), selected for the ankle and the knee actuators, and the KBM25X01C model (b), selected for the hip actuator[18]

In each of the iterations of the triple-joint optimisation algorithm, the single-joint optimisation method (explained in section 4.8.1of Chapter 4) is performed on one of the joint actuators (specified in the second column of Table 5-5 for each iteration). In order to further explain the single-joint optimisation method, the results of the third iteration are going to be presented. The third iteration has been chosen for demonstration because the optimisation results do not change after the third iteration, as could be seen in Table 5-5. Notice that the abridged table which will be presented is an excerpt from the complete table, which has over one thousand rows[19].

---

[18] http://www.kollmorgen.com/en-gb/products/motors/direct-drive/kbm-series-frameless/

[19] There are nearly 151 motors in the list, and for each motor there are numerous options for power transmission. The total number of combinations is equal to the number of motors multiplied by the number of transmission systems.

(a)   (b)
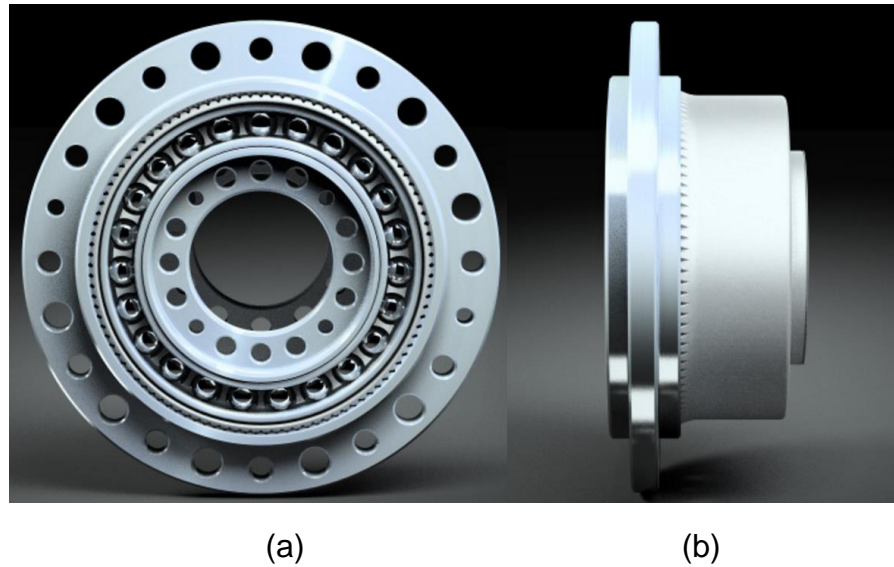
Figure 5-9 The strain gear chosen for the hip actuator, model CPL-2A-32, front view (a) and side view (b) [92]

The abridged table contains the results for all of motors that could perform the required task (i.e. carry at least 45 kg of load, which is the minimum acceptable value according to the design requirements, as mentioned in section 3.3.4 of Chapter 3). For each motor, only the results for the best transmission option[20] has been included in the abridged table, to keep the size of the table presentable. The abridged table has 88 rows, and is presented in Appendix H. The rows of the table have been sorted in the descending order of the value function (described in step 6 of the single-joint optimisation algorithm, explained in section 4.8.1 of Chapter 4); therefore, the upper rows of the table contain the more desirable solutions. Table 5-6 shows the top rows of the abridged decision table, and all of the motors shown can carry 60 kg of load (the full table of Appendix H contains motors that could carry less than 60 kg). However, choosing the best motor is still a multi-factor decision making process. For example, the motor in the first row would consume less power than the one in the second row, but would also make the exoskeleton heavier. If the weighting factors of the value function (presented in Table 4-2 of section 4.8.1 in Chapter 4) have been chosen properly to quantify the design intentions and preferences, then the top rows of the table will show the more desirable design candidates. However, this does not mean that the very top

---

[20] The best transmission option for each motor was determined based on the cost function, as will be explained further in this section.

row has to be selected, as the performance factors[21] of the different solutions are quite close. In this case, the motor represented in the first row has been selected.

It must be noted that some of the motors considered in the analysis are frameless, and data on their mass is presented by the manufacturers without taking into account the mass of the housing that needs to be built for them. To make a reliable comparison between the mass of framed and frameless motors, it was originally assumed that the addition of a frame (with a shaft, connectors and bearings) would increase the total motor mass by 30% of the frameless motors mass. However, this percentage was found to be almost 50% after doing the detailed design of the single-joint actuator (Chapter 6). The optimisation iterations were then performed again with the new correction factor for the additional mass of motor frames. All of the tables presented here are based on the modified estimates of the mass of the framed motors.

5.3.3 Results on Strain Gears (combined with Chain and Sprockets if necessary) for all the Actuators, for the straight-knee design

As mentioned in sections 5.2.2, strain gears proved to be unsuitable for the bent-knees design, because the smallest available gear ratio is 50:1 for strain gears[22]. To solve that issue, a new design concept was considered that consists of a strain gear in series with a speed-up chain and sprockets mechanism, so that the total transmission ratio can be adjusted. This concept was investigated for the bent-knee design in section 5.2.3. Here, the simulation optimisation results for this concept are presented for the straight-knee design; however, the simulation program was slightly modified to model both of the above-mentioned designs, which are strain gears with and without chain and sprockets.

Table 5-6. The top rows of the decision table for the optimisation of the hip actuator, in the third iteration of the triple-joint optimisation algorithm

---

[21] In this case, since the load carrying capacity is 60kg for all rows, the performance factors to be compared are the power consumption and total exoskeleton weight.

[22] Smaller gears are available with a ratio of 30:1, but their torque capacities are insufficient for the application at hand.

Motor weight with frame (kg)	Gear ratio	exoskeleton weight (kg)	Maximum Load (kg)	Power consumption (W)	value function
3.03	81	73	60	54	4,366
2.24	105	72	60	59	4,358
2.90	97	73	60	56	4,350
2.45	105	72	60	60	4,331
4.14	81	76	60	53	4,308
3.32	97	74	60	57	4,308
3.63	89	75	60	56	4,301
2.81	73	73	60	64	4,260
3.20	89	74	60	63	4,253
1.89	129	71	60	71	4,239
5.58	73	78	60	53	4,216
5.25	34	78	60	56	4,207
3.3	97	74	60	68	4,181
1.5	153	70	60	80	4,152
3.20	97	74	60	71	4,151
1.64	129	71	60	80	4,151

As shown in Table 5-7, the simulation results for the actuators show that the optimal motor sizes for the knee and ankle are the same as in the result with the ballscrew design (explained in section 5.3.2).

As mentioned in the previous section, the hip transmission system has to be a strain gear as ballscrews cannot be used on the hip. On the other hand, on the ankle and knee actuators, both ballscrews and strain gears can be used. Therefore, a comparison is required. Both designs can carry a load of 60 kg, however, the power consumption varies in these designs, as will be explained in the following.

Table 5-7. The results of the iterations of triple-joint optimisation, with strain gears on all joints

Iteration	Joint actuator being optimised in this iteration	Frameless Knee motor mass (kg)	Frameless Ankle motor mass (kg)	Frameless Hip motor mass (kg)
0	-	-	0.99 (assumed)	0.99 (assumed)
1	knee	**4.14**	0.99 (assumed)	0.99 (assumed)
2	ankle	4.14	**4.14**	0.99 (assumed)
3	hip	2.76	4.14	**3.03**

4	knee	**4.14**	4.14	3.03
5	ankle	4.14	**4.14**	3.03
6	hip	2.76	2.76	**3.03**

Table 5-8 shows the optimisation results for the knee actuator with strain gears, while the hip and ankle actuator designs are assumed to be the same as the one mentioned in section 5.3.2, i.e. strain gears at the hips and ballscrews at the ankles.

Table 5-8. Optimisation results for the knee actuator with a strain gear, if the ankle actuator is designed with a ballscrew

Knee motor weight (kg)	Knee gear ratio	total device weight (kg)	Maximum Load (kg)	Power consumption	Value Function
4.14	**54**	**102**	**60**	**61**	1,918
5.58	40	105	60	63	1,909
2.955	45	100	60	69	1,879
3.03	34	100	60	71	1,867
1.74	68	98	60	78	1,834
2.52	68	99	60	78	1,834
5.4	36	105	60	81	1,819
7.95	25	110	60	85	1,794
2.805	50	100	60	89	1,774
3.3	73	101	53	97	1,619
1.5	100	97	20	119	918

As Table 5-8 shows, using strain gears on the knee and hip, while using the ballscrew design on the ankle, would yield an average power consumption of nearly 61W in the best case (the first row of the table). In comparison, as mentioned in section 5.3.2, if ballscrews are used on the ankle and knee joints, the power consumption becomes nearly 54W. This means that using strain gears on the knee joint increases the power consumption by 13% compared to the ballscrew design. Now let us assume that in addition to the knee actuator, the ankle actuator is also designed with a strain gear. The optimisation results for this case are shown in Table 5-9.

As could be seen in Table 5-9, if strain gears are used on both the knee and ankle actuators, then the power consumption becomes 68W, which is 26% larger than the design with ballscrews at the ankle and knee.

Table 5-10 presents a comparison of the power consumption with the two different designs. The design with ballscrew on the knee and ankle joints has been chosen as it results in the lowest power consumption, compared to the other designs.

Table 5-9. Optimisation results for the ankle actuator with strain gear, if the knee actuator is also made with a strain gear

ankle motor weight	Ankle gear ratio	total device weight (kg)	Maximum Load (kg)	Power consumption (W)	Value Function
4.14	**41**	**104**	**60**	**68**	2,330
1.74	87	99	60	75	2,308
2.52	80	101	60	79	2,246
1.89	99	99	60	81	1,996
1.5	99	99	46.875	81	1,855
1.485	100	99	50.625	83	1,824
0.96	99	98	22.5	88	1,573
1.0545	100	98	24.375	90	1,567
1.0545	100	98	25.3125	92	1,551
1.35	99	98	16.875	108	1,354

Table 5-10. The comparison of the power consumption between ballscrew and strain gear for the ankle and knee actuators, while the hip actuator is made with a strain gear

Hip Transmission	Ankle Transmission	Knee Transmission	Power consumption (W)
Strain gear	Ballscrew	Ballscrew	54
Strain gear	Ballscrew	Strain gear	61
Strain gear	Strain gear	Strain gear	68

5.4 Detail design

This section briefly covers the detail design for the three actuators. The designs are based parameters obtained from optimisation algorithm (i.e. the specifications of the motors and transmission systems to be used).

5.4.1 The knee and ankle actuator designs

The knee and ankle actuators are both based on the design concept consisting of an electric motor and a ballscrew, and are therefore covered together.

The knee actuator was built as a single-joint prototype, covered in the next chapter in detail. Therefore, only the ankle actuator design is presented here.

The ankle actuator, illustrated in **Figure 5-10**, has one difference with the knee actuator design (explained in the next chapter), which is the incorporation of an anti-backlash timing belt mechanism. This feature has been added to reduce the length of the actuator, otherwise it would not fit onto the shank link of the exoskeleton which is shorter than the thigh link. The experiments done with the test prototype (covered in the next chapter) revealed that there will be some angular paly. Therefore, a linear guide has also been included in the design.

(a)   (b)   (c)
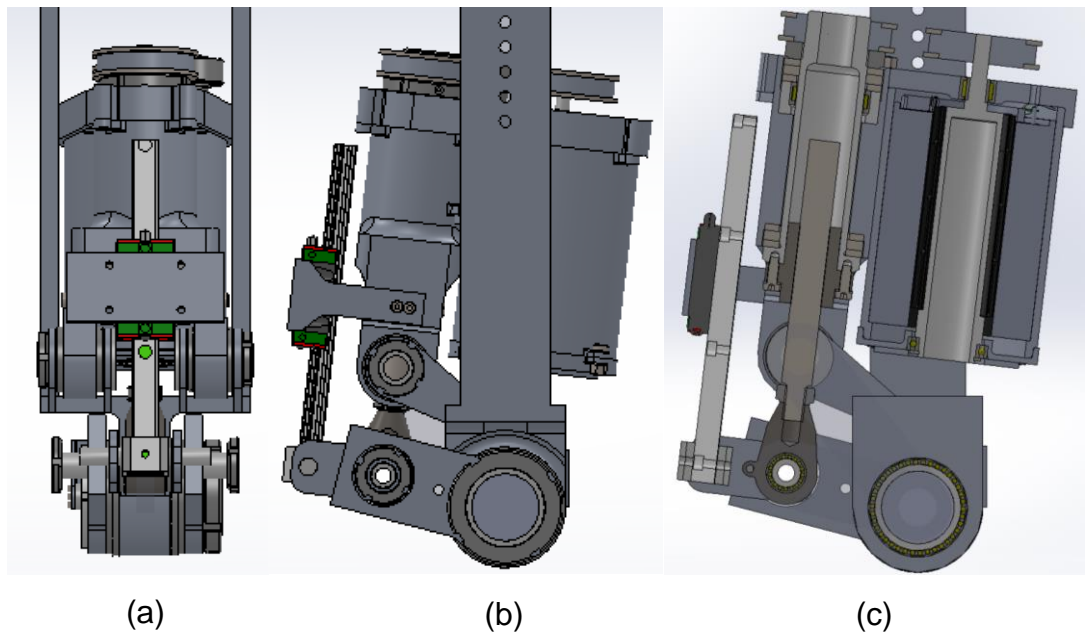
Figure 5-10. The CAD model of the ankle actuator: side view (a), front view (b) and section view (c)

5.4.2 The hip actuator design

The hip actuator consist of a harmonic drive, and an anti-backlash timing belt mechanism, which allows the motor to be place next to the joint and achieve a rather slim design.
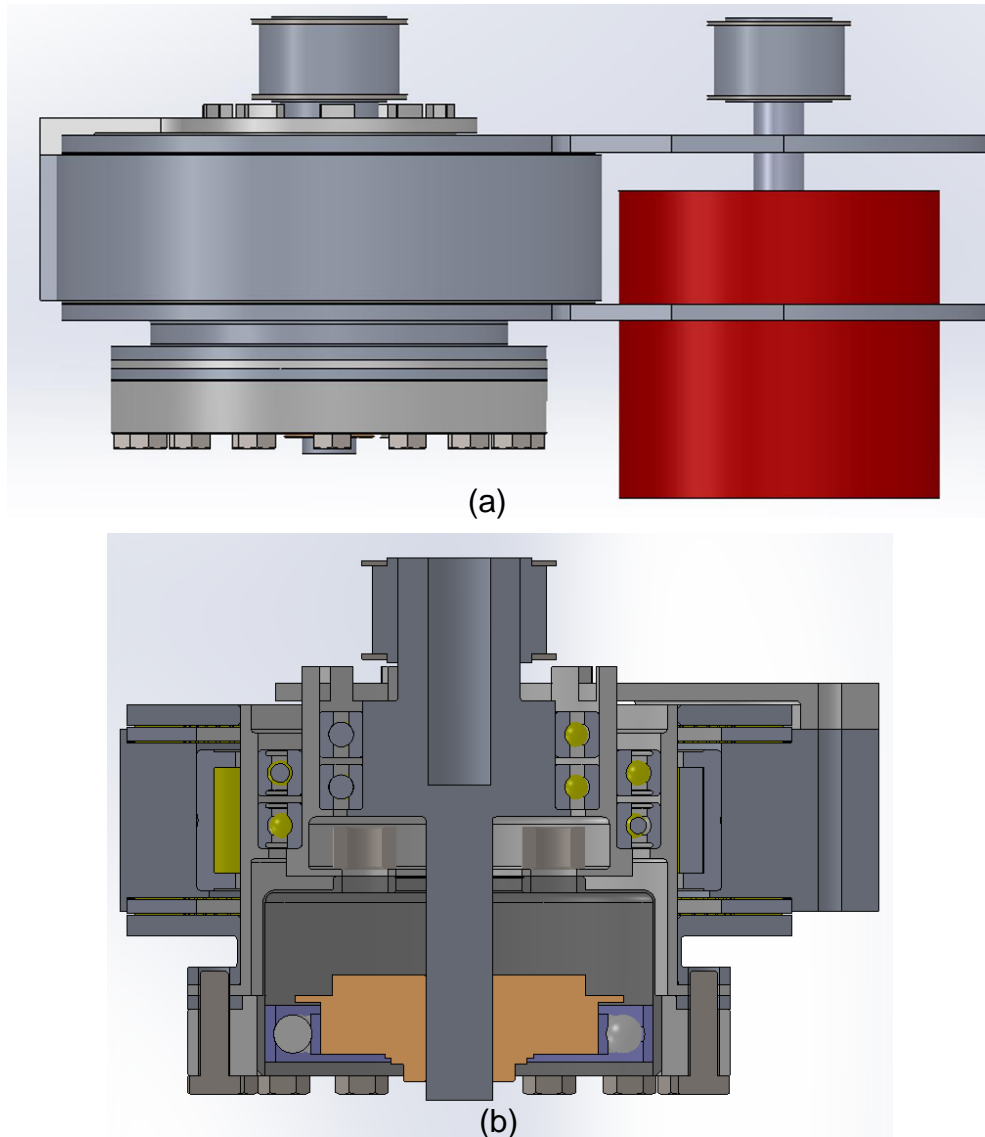
Figure 5-11 CAD model of the hip actuator (a), with a section view of the harmonic drive and the connecting parts (b).

It must be noted that the hip actuator has not been built and tested in this study. This is due to the fact that this design concept has already been investigated in a published research [5].

5.4.3 The leg design with all three actuators

Figure 5-12 shows the three actuators together in leg of the exoskeleton, in standing and squatting positions.
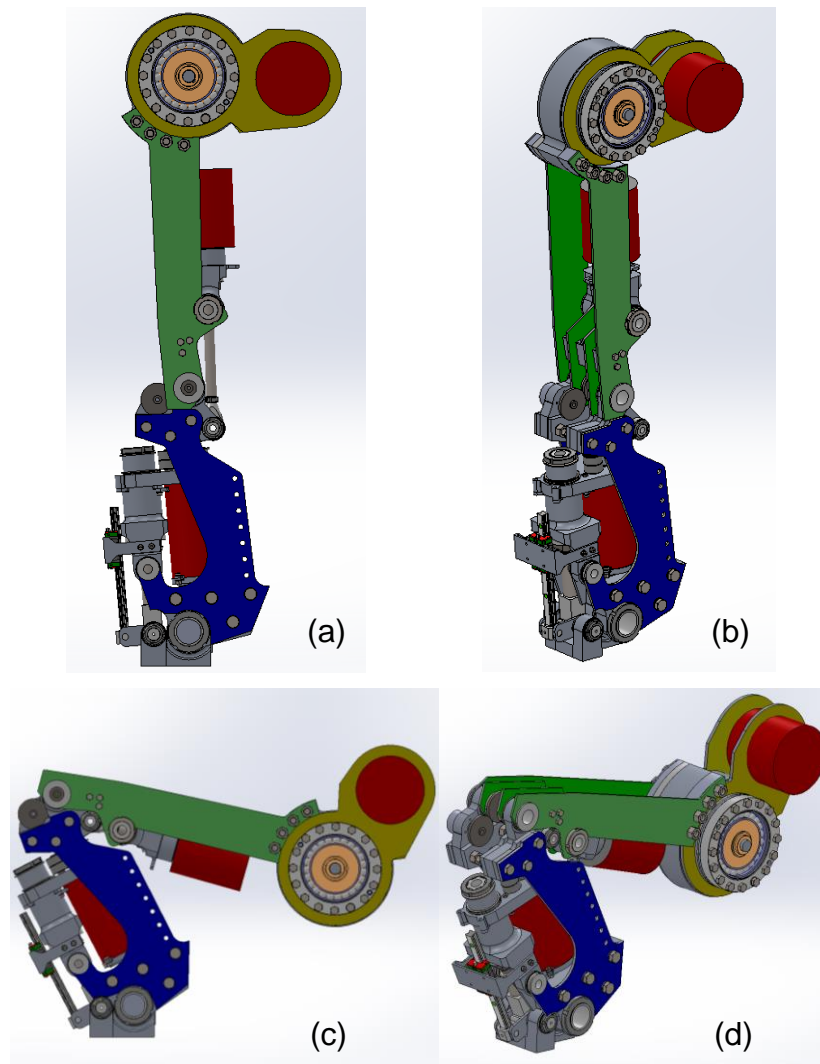
Figure 5-12 The exoskeleton leg: standing position from the side view (a) and dimetric view (b), and the squat position in the side view (c) and dimetric view (d).

5.5 Summary

This chapter covers the results of the of the optimisation procedure for the three joints, and the final selection of the motors and power transmission mechanisms for the ankle, knee and hip joints.

As mentioned in section 4.2.3 of Chapter 4, two alternative exoskeleton designs can be chosen, each of which determines the gait type of the exoskeleton. These designs are referred to in this text as the bent-knee and the straight-knee designs. The optimisation results for these two designs have been presented separately in this chapter.

Section 5.2 covers the optimisation results for the bent-knee design. All of the analysis done on this design were on the knee actuator. Other joints were not considered, since the optimisation results of the knee joint were unsatisfactory and suggested that the bent-knee design should be relinquished. In summary the results indicated that using strain gears, chain and sprockets or cable and pulley mechanisms would all results a heavy actuator design. Ballscrews could be used in an inverted slider-crank mechanism, however, the large torque requirements of the bent-knee design suggested that the straight-knee design should be investigated in an attempt to achieve a lighter design.

The optimisation results for the straight-knee design have been covered in Section 5.3. The chain and sprocket and the cable and pulley mechanisms were excluded from the analysis, since it had been shown (in the analysis of the bent-knee design) that they would produce bulkier designs than the other candidates. Strain gears and ballscrews (in an inverted slider crank mechanism) were investigated, and the results showed that the best results are achievable by using ballscrews at the ankle and the knee joints, and a strain gear at the hip joint.

The optimisation process explained in this chapter has provided an answer for the parametric design problem, i.e. the electric motor models to be used as well as the transmission systems (including the gear ratio of the strain gear, the pitch size of the ballscrews, and the dimensions of the slider –crank mechanisms). However, in order to verify the suitability of these parameters, it was necessary to build an actuator prototype and perform tests. Since the actuator design concept used for the hip joint (with strain gears) has been built and investigated in previously published work [5], it was decided that the first prototype should be based on the design concept of the knee and ankle actuators (with ballscrews). Chapter 6 covers the detail design of a single-joint prototype, its manufacturing and the experiments done with it, and finally the verification of the optimal design carried out in this project.

Chapter 6
The Single-Joint Test Prototype and Design Verification

6.1 Introduction

The optimisation algorithm used in this study is based on the simulation results of the exoskeleton as a system. In order to verify the simulations, and hence the optimisation results, a single-joint test prototype has been designed. The tests done with this test rig provided experimental results, which have been compared to the results predicted by the simulations, as explained later in this chapter. The comparison of the simulation and experimental results have been used to verify the simulations, and also to obtain the value of a modification factor for the efficiency of the controller, as explained later in this chapter.

In addition to the simulation verification and modification, the other goal of the tests is to generally investigate the performance of the actuator, and spot any potential flaws.

Section 6.2 briefly covers the design and development of the test prototype. The hardware setup of the prototype is explained in section 6.3. This is followed by an explanation of the control algorithm and the software developed, presented in section 6.4. The experiment protocol is covered in section 6.5. Section 6.6 contains the experiment results and a discussion, which also covers energy harvesting. Finally, a summary is presented in section 0.

6.2   The development of the prototype

A prototype of the actuator with a ballscrew and an inverted slider-crank mechanism has been designed and manufactured, in order to perform experiments to verify the results of the simulations used in the optimisation process. **Figure 6-1** demonstrates the 3D model of the exoskeleton design.

Although the ballscrew pitch size and the dimensions of the inverted slider crank mechanism were already given by the optimisation program, other details of the design had to be decided on at this stage. The detail design involved creating CAD models of the components (using the SolidWorks™ software), stress analysis (via the FEA method, using SolidWorks Simulation™), and the selection of off-the-shelf components (bearings, bolts,

and nuts). The analysis and design methods used were adopted from an engineering design handbook [94].

(a)   (b)
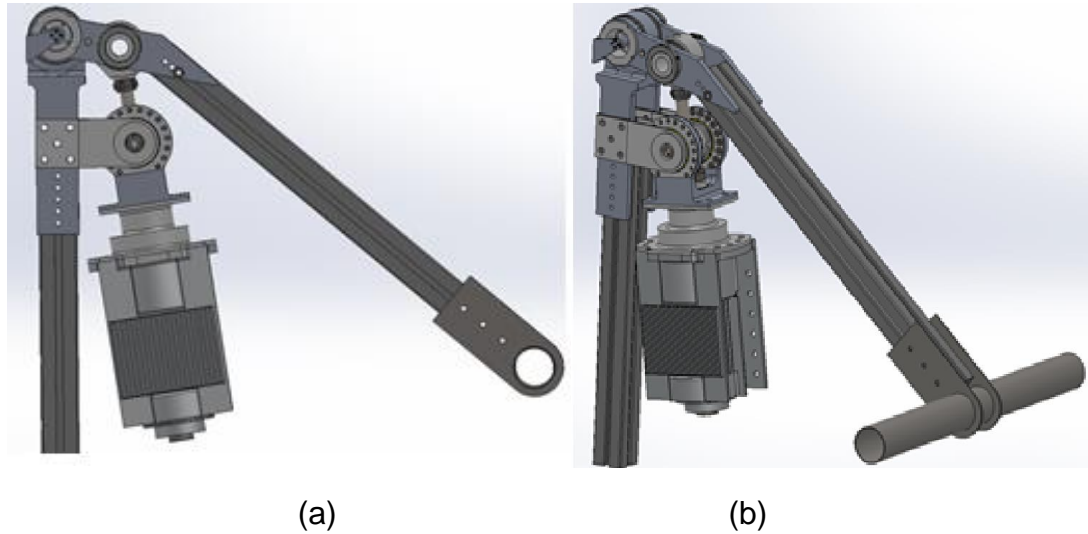
Figure 6-1. The 3D model of the actuator design for the single-joint prototype, side view (a) and dimetric view (b)

After the parts were manufactured or purchased, they were assembled to form the prototype, shown in **Figure 6-2**.

(a)   (b)
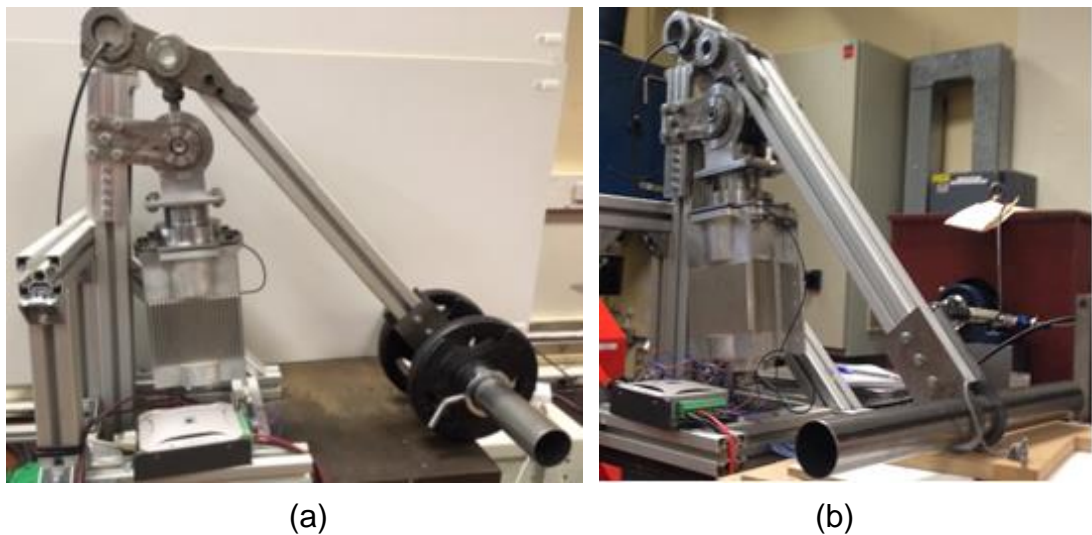
Figure 6-2. The single-joint prototype, side view (a) and dimetric view (b)

6.3 The test set-up

In addition to the single-joint prototype, the test setup also consists of electric and electronic hardware, as explained in this section. A block diagram of the test setup can be seen in Figure 6-3.
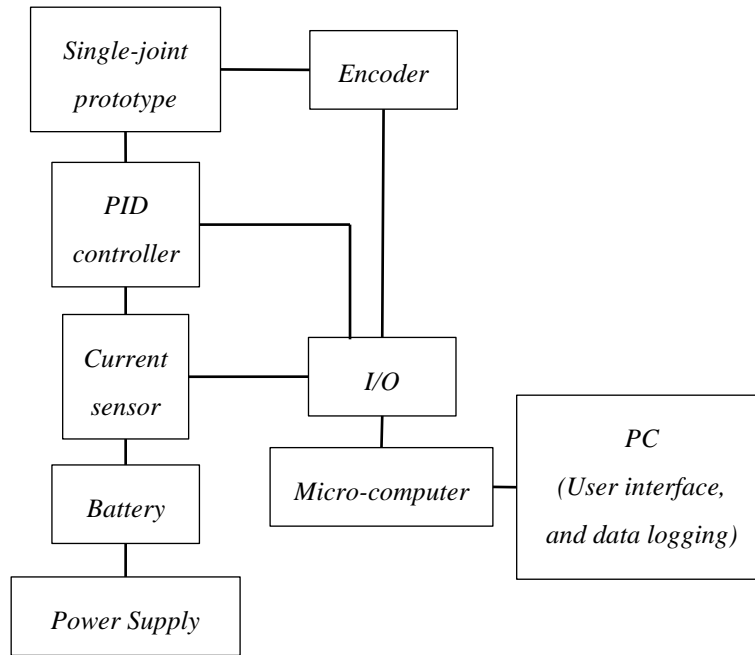
Figure 6-3 The block diagram of the test setup hardware

The joint angle is measured using an absolute encoder. An electronic printed circuit board (PCB), shown in **Figure 6-4** (a), converters the signal from the encoder to a signal recognisable through the digital Input/output (I/O) module, which is made by the National Instrument ™ (NI) company (**Figure 6-4** (b)).

The high-level control algorithm is implemented by the microcomputer, which is an NI CompactRio™ (hereafter referred to as cRIO) and is shown in **Figure 6-4** (a) and (b). The control algorithm has been written by the NI LabVIEW™ programming language, and loaded onto the cRIO. The high-level controller (the cRIO) calculates the values of the desired motor current, and sends it to the low-level controller (explained in the following paragraph). The communication between the high-level and low-level controllers is made using the CAN bus communication protocol. The CAN bus module can be seen in **Figure 6-4** (b).
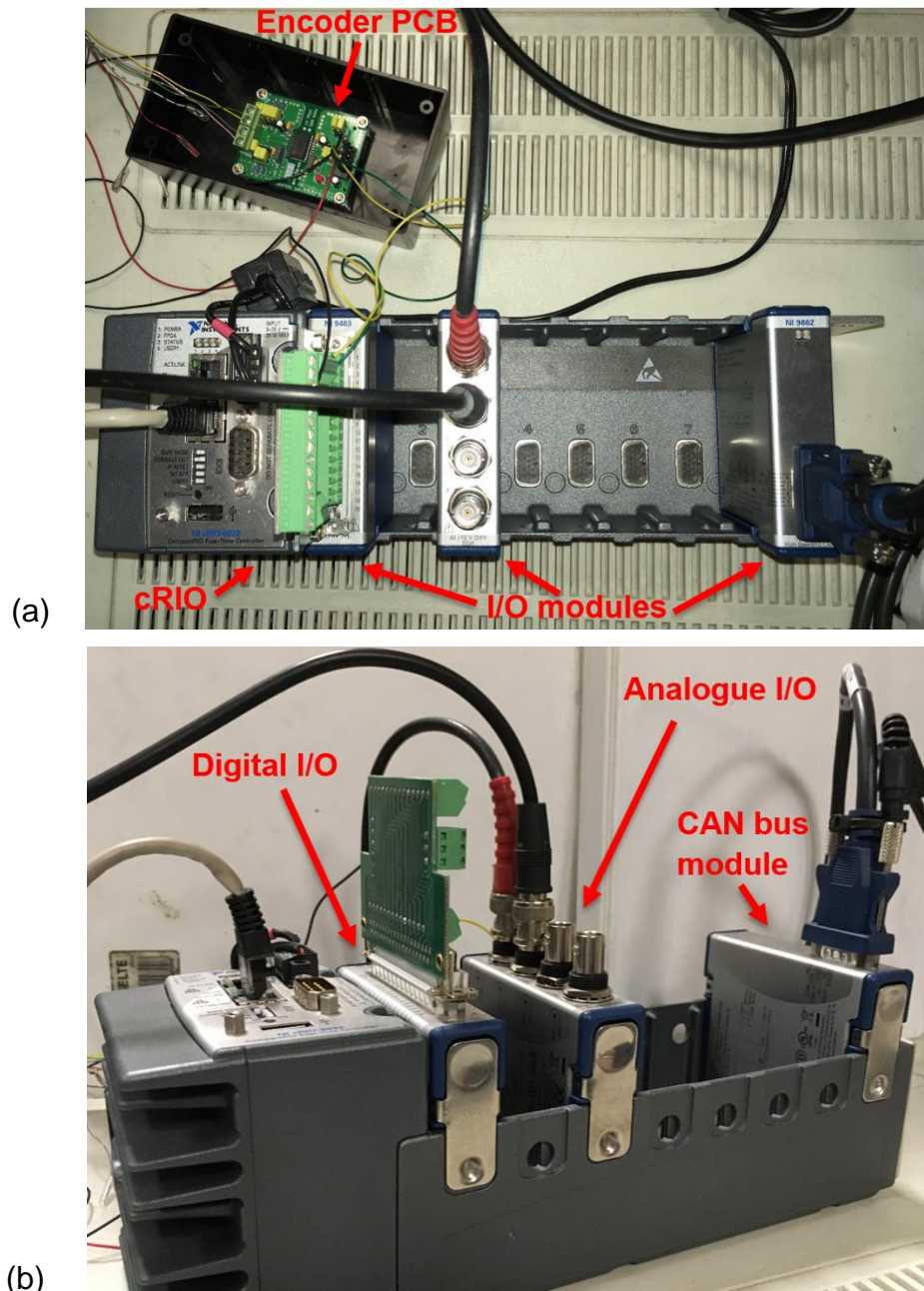
Figure 6-4 The sensing and control hardware: cRIO, I/O modules and the encoder PCB (a). Another view of the cRIO shows the I/O modules which are a digital and an analogue I/O, and a CAN bus module (b).

The low-level controller is an ION 3000 PID motor controller (Figure 6-5), developed by Performance Motion Devices, Inc. The low-level controller receives the value of the desired current from the high-level controller, and then sends a control signal to the motor to track the desired current. The PID coefficients have been tuned using some auto-tuning software provided by the manufacturer. The controller also feeds the current measurement values back to the high-level controller.

Figure 6-5 The PID motor controller

A DC power supply is used to convert the AC mains power into a DC voltage. A battery has also been connected in parallel with the power supply, in order to absorb and store the regenerated power that is sent back by the controller when the actuator is braking, i.e. when the arm of the prototype is moving downwards in a controlled manner. Without the battery, the voltage at the power supply would be raised beyond the safe limit, and cause the controller to automatically shut down. An important implication in regard to this phenomenon is that energy harvesting is possible in exoskeletons, as will be discussed in section 0. The battery and the power supply (PWS1) are shown in Figure 6-6.

Figure 6-6 The power supplies (PWS1 and PWS2), battery and current sensor (C-S)

Another power supply (denoted by PWS2) can be seen in Figure 6-6, which is used to power the current sensor (at 12 VDC), as well as the encoder PCB and the CAN bus module (at 5VDC).

Finally, some custom-made circuity has been built and used to measure the current of the controller, and therefore the power consumed by the actuator. This current sensor is denoted by C-S in Figure 6-6.

6.4 The control software

The model-based high-level control algorithm has been written with NI LabVIEW and implemented on the NI CompactRIO. The control program needs to perform the following tasks:

1. Take the amount of the payload and the desired duration of the motion as inputs.
2. Create a discrete trajectory for the motion of the prototype arm[23].
3. Construct the system model, using the amount of load, as well as the kinematic and kinetic characteristics of the arm.
4. Using the system model and the desired trajectory, calculate the desired torque at the joint for each point of the discrete trajectory.
5. Convert the joint torque to motor torque by using the joint angle feedback (obtained from the absolute encoder) and the model of the actuator.
6. Calculate the desired motor current by using the torque constant of the motor (equation 4-16).
7. Send the desired current value to the low-level controller.

This control method is referred to as the computed torque method, and does not use any feedback of the actual velocity and acceleration of the joint. Therefore, the actual trajectory does not necessary follow the desired one closely, due to modelling errors (e.g. ignored friction and estimation errors in the inertial parameters of the system). However, this algorithm proved to be enough for the sake of the test experiment, since the measurement of the

[23] The motion of the joint involves moving up from the rest position to the upper end position, in which the joint angle is 90°, and then moving back down to the rest position.

power consumption is the main objective here, rather than precise trajectory tracking. **Figure 6-7** shows a block diagram of the control algorithm.
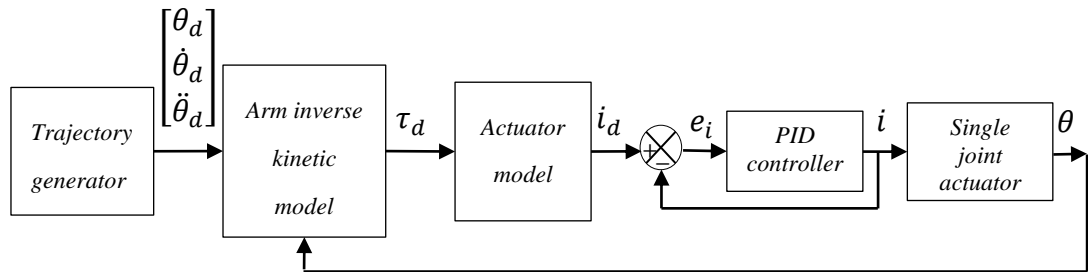
Figure 6-7. The block diagram of the test prototype system.
θ_d, $\dot{\theta}_d$ and $\ddot{\theta}_d$ are the desired values of joint angle, velocity and acceleration, and i_d is the desired motor current. θ is the measured joint angle and i is the actual motor current.

Figure 6-8 shows a screenshot of the graphical user interface (GUI) of the control program developed in LabVIEW.
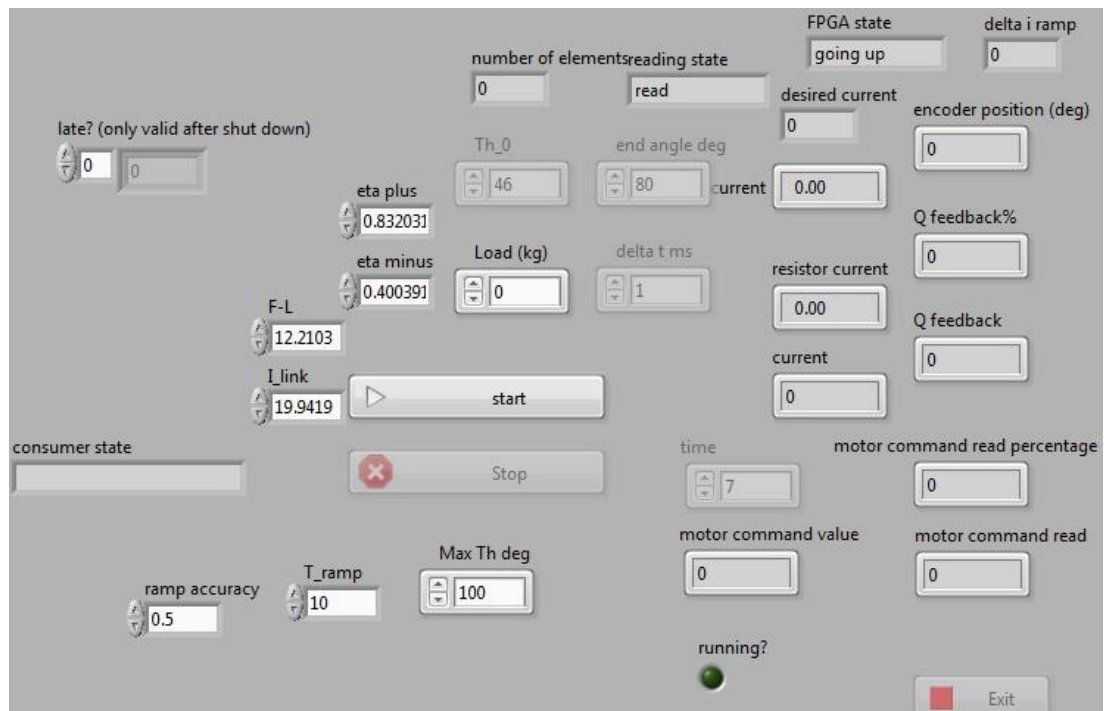
Figure 6-8 The graphical user interface (GUI) of the control program

6.5 The experiment protocol

The stages below were followed in the experiment:

1. A manoeuvre of the prototype was performed in which the free arm moves upward, while carrying some load at the end of the arm.
2. The joint angle of the arm was continuously measured and logged during the motion.
3. The current drawn from the power supply was continuously measured and logged during the experiment.

These stages were repeated for different values of load, and the corresponding data was saved separately. The raw data was then interpreted using the method explained in the next section.

6.6 Test Results and discussions

6.6.1 The method for processing the test data

The main purpose of performing the tests was to compare the value of the measured power consumption to the value predicted by the simulation model. If the predictions yielded by the simulations are accurate, then the model is shown to be accurate. This would then mean that the optimisation results are reliable, since the same model has been used in the optimisation program.

As stated earlier, the two quantities to be compared are the measured and predicted values of the power consumption. The methods used to obtain each are as follows:

Since the voltage of the power supply was constant at 48VDC, the measurement of the power consumption could be conducted by current sensing. The power consumption would then be equal to the fixed voltage multiplied by the measured current.

To obtain the power consumption value predicted by the model, the measured values of the arm joint angle were used together with a model of the system. The values of angular velocity and acceleration were obtained using numeric differentiation (after low-pass filtering to remove noise, with a cut-off frequency of 10HZ, for reasons explained in section 4.2.2 of Chapter 4). Having obtained these values, the actuator model was then used to obtain an estimate for the total power consumption of the system. Figure 6-9 illustrates the method explained in this paragraph.
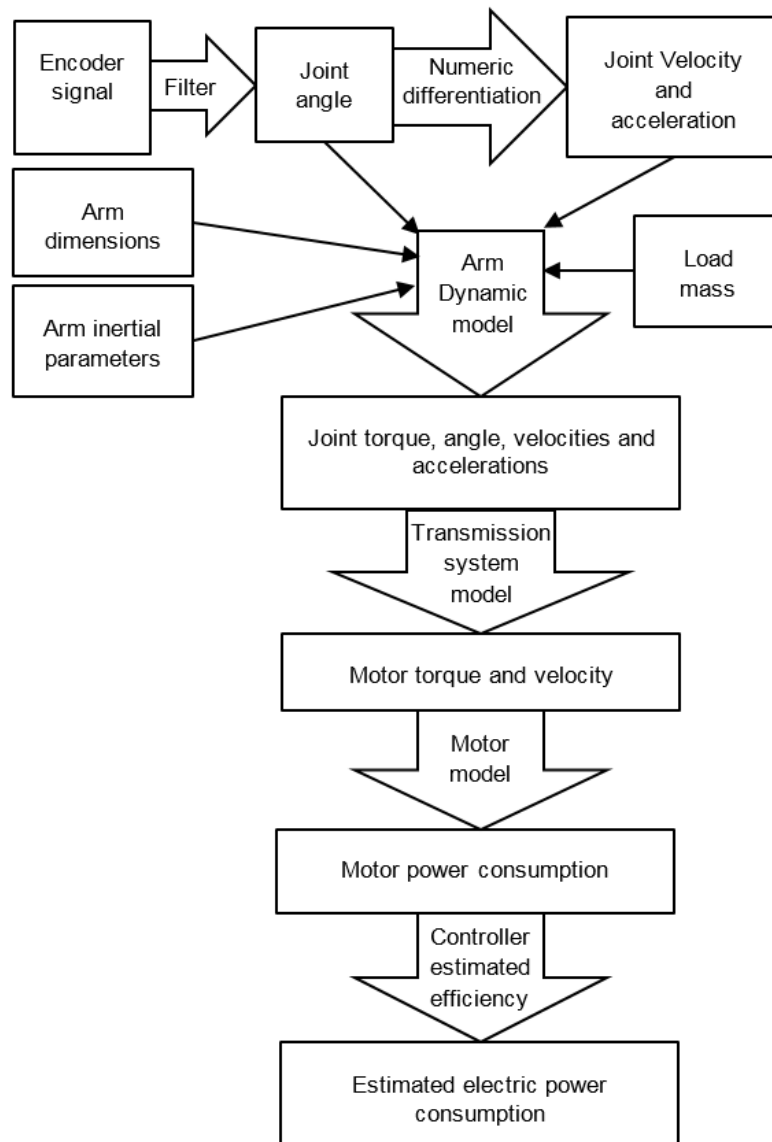
Figure 6-9 A flowchart fo the method used to estimate the power consumption

It could be seen in Figure 6-9 that an estimate for the efficiency of the controller is needed. A previous study suggests an efficiency of 76% [5]; however, to account for other modelled losses, a value of 50% was initially used (knowing that a reliable value would be obtained from the test results, as explained in section 6.6.2). The analysis of the test results suggests a lower value, as presented in the next section.

6.6.2 Analysis of the Results

Figure 6-10 (b) and (c) shows the joint angle of the arm during its motion in one of the experiments, before and after filtering. The joint angle increases in

the first part of the motion in which the arm moves upwards, and decreases in the second part when the arm moves downwards. During the second part of the motion, the power consumption of the actuator is negative, i.e. the actuator is performing a *braking* function. Data relating to this part of the motion will be investigated in section 0, where energy harvesting is discussed. Therefore, this section focuses on the first part of the motion, in which the actuators consume positive power.

The necessity for filtering the raw data could be seen from **Figure 6-11**, which shows the measured current drawn from the power supply for one of the experiments (with 25 kg of payload). It could be seen that the raw data is very noisy, which is why it had to be filtered (with a cut-off frequency of 10HZ, as explained in section 4.2.2 of Chapter 4). However, even the filtered data shows oscillations. This is because of the existence of some looseness and *play* in the bolted joints of the arm, which caused the arm to vibrate during the movements and rendered the system response oscillatory. These oscillations can also be seen in the motion of the arm, as depicted in **Figure 6-12**, showing the joint angle versus time for one of the experiments. As mentioned earlier, the vibrations of the arm are caused by the looseness in the bolted connections. This flaw needs to be removed in the final design of the exoskeleton prototype, since such vibrations can cause stability and controllability problems, and are also destructive to the exoskeleton.

As with any vibratory system, the oscillations of the arm result from a phenomenon in which kinetic energy is alternately stored as potential energy (due to elasticity) and released as kinetic energy (the arm motion). This phenomenon has not been modelled in the simulations, which assume that the arm is rigid.

However, the simulation model is still valid for modelling an exoskeleton, since the exoskeleton frame must be highly rigid and show only a negligible degree of vibrations. On the other hand, to use this rigid model with the raw data from the experiments considered here, it is necessary to use the portions of the data which pertain to rather smooth sections of the motion, where there is less vibration. In the absence of (large) vibrations, the rigid model proved to be able to successfully simulate the system behaviour, as will be shown in the results presented later in this section.
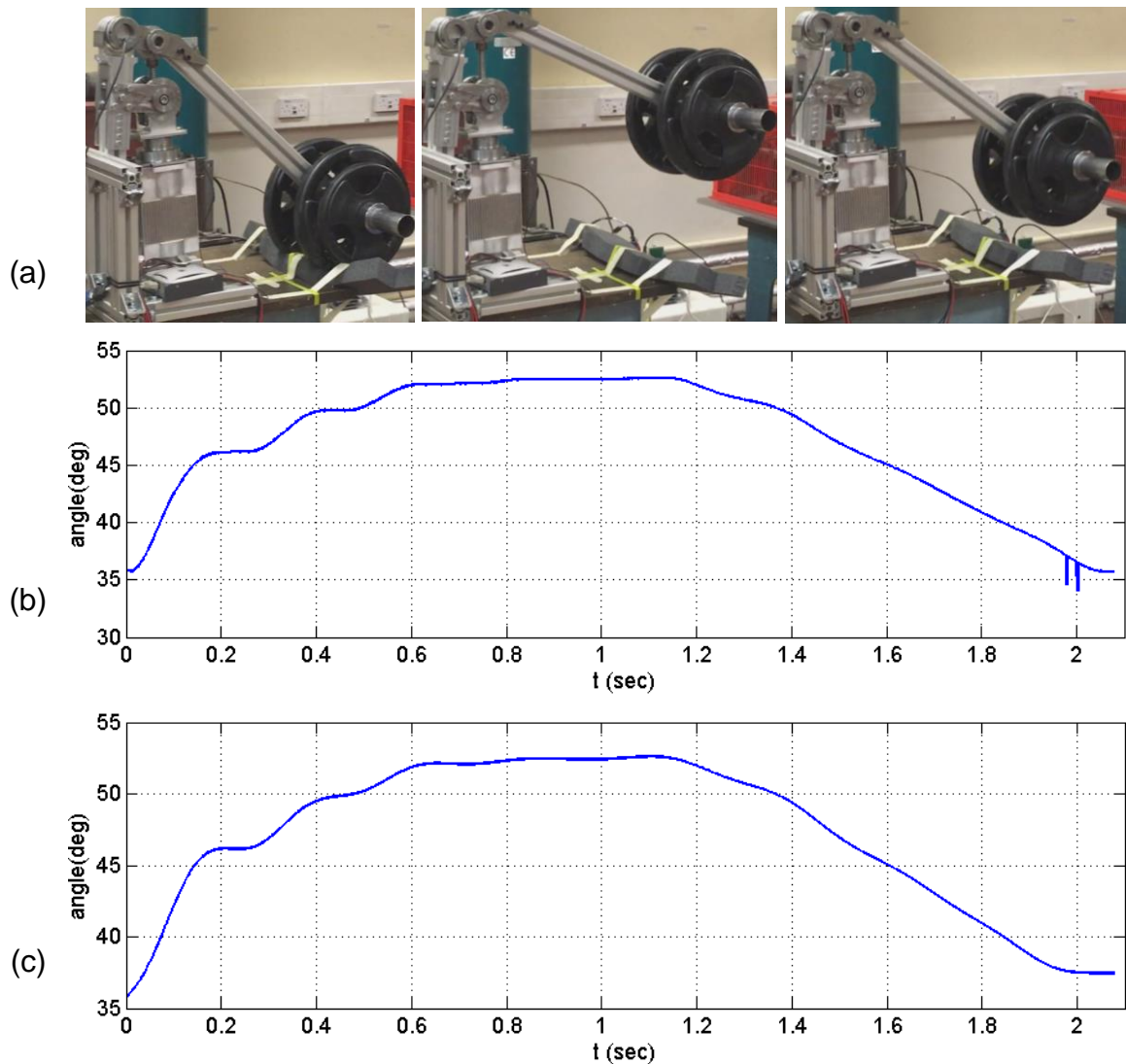
Figure 6-10 The arm movement during the experiments (a), and the unfiltered (b) and filtered (c) joint angle

Another advantage of choosing smooth sections of the arm motion is that numeric differentiation yields more reliable results in the absence of abrupt fluctuation, for the following reason. As explained in section 6.6.1, the existence of noise in the raw data necessitates performing low-pass filtering before numeric differentiation (Figure 6-9). However, if the signal itself is oscillatory, then it might contain high-frequency components, which will be removed in the filtering process. Using a high cut-off frequency for the filter could leave some noise in the signal, whereas a low cut-off frequency might lead to the elimination of part of the original signal. Therefore, numeric differentiation of fluctuating signals could yield unreliable results. This is

another reason for choosing rather smooth portions of the arm motion for the investigations.
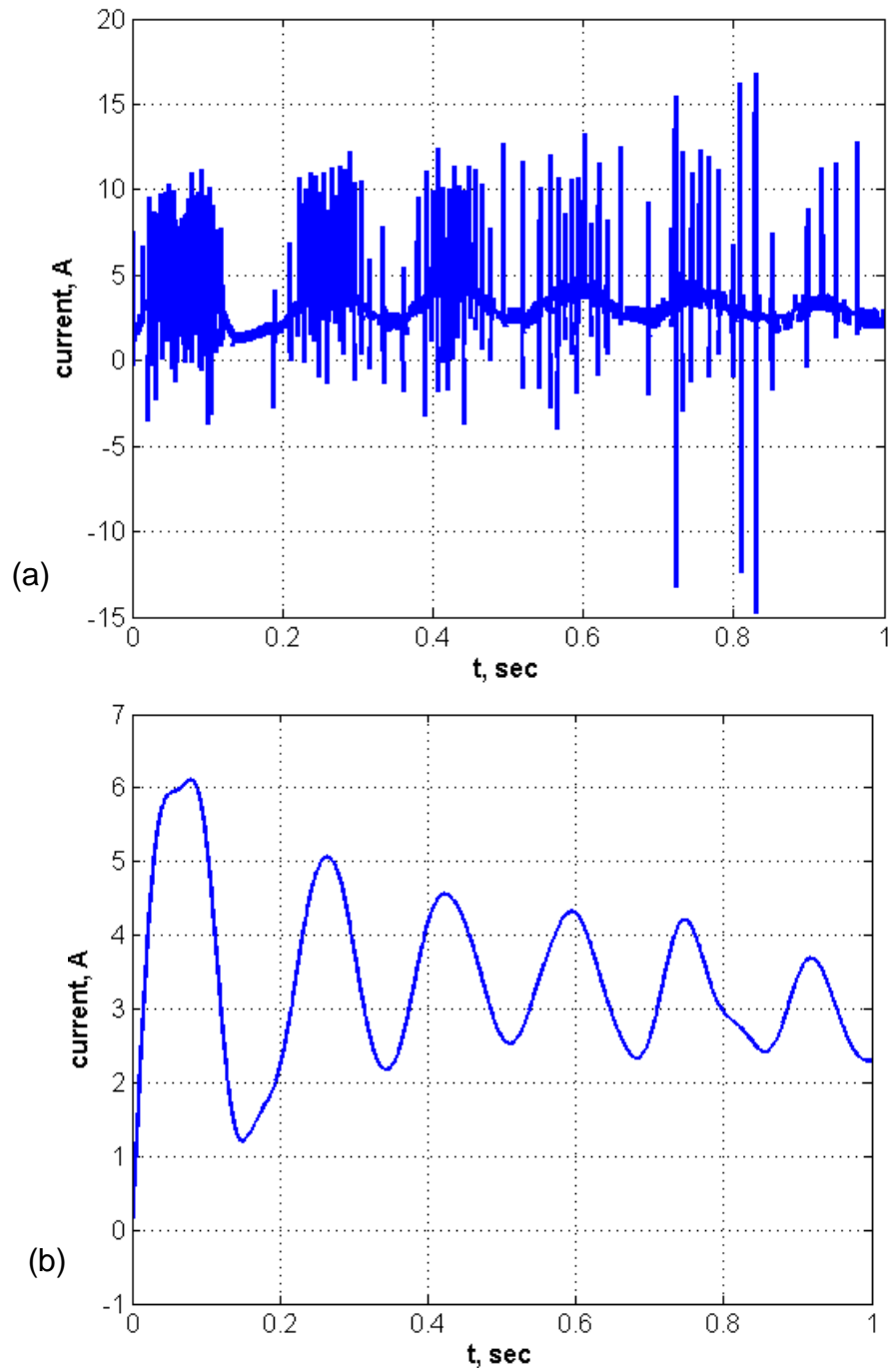
Figure 6-11 The current drawn from the power supply for one of the experiments, unfiltered data (1) and filtered data (2)
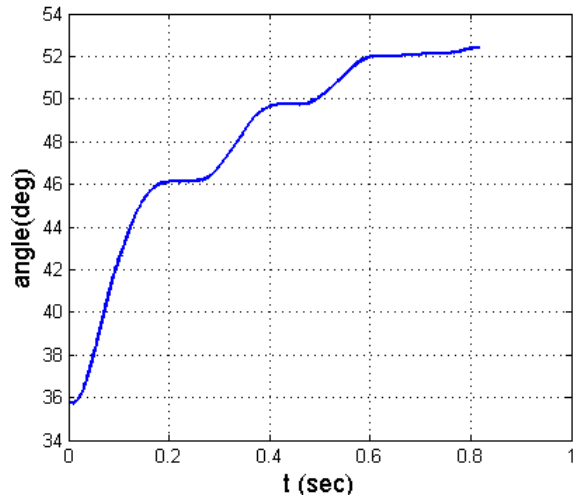
Figure 6-12 The arm joint angle for one of the experiments. Oscillations can be seen in the joint angle.

Figure 6-13 shows the graph of simulated and measured values of the power consumption of the actuation system while lifting up a payload of 5kg.
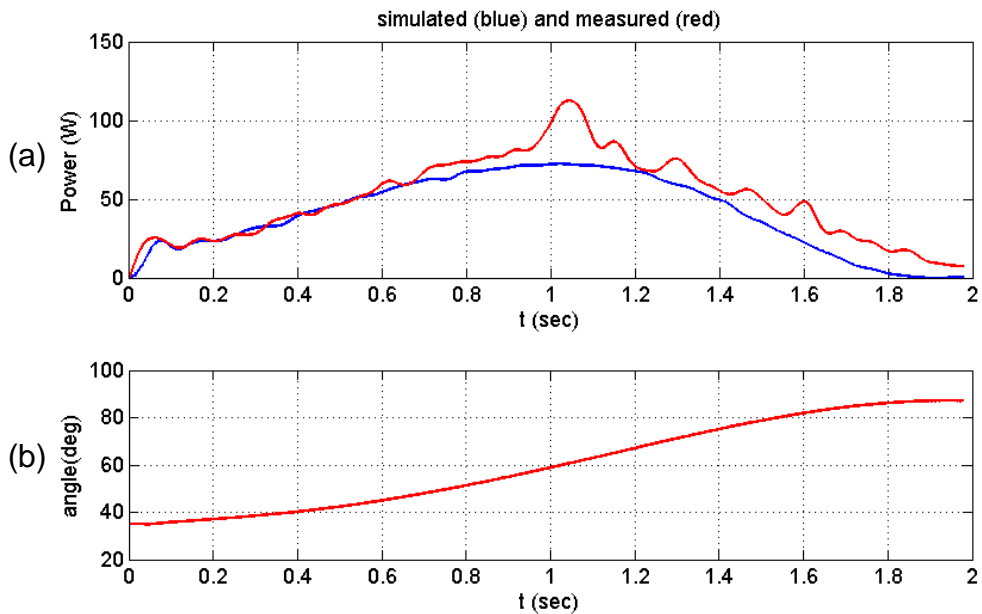
Figure 6-13. The initial estimation results of the power consumption of the actuation system, with 5kg of payload (a), and the joint angle (b). The blue curve shows the simulation predicted power, whereas the red curve shows the measurement results.

149

It could be seen in **Figure 6-13** (b) that the arm movement is rather smooth. This was due to the fact that the payload was small (5 kg). Experiments with higher payloads showed more oscillations in the motion, as will be shown later in this section.

The two graphs in **Figure 6-13** (a) are not identical, due to modelling imperfections which are to be expected. However, they look roughly similar, which shows that the model can predict the power consumption with rather good accuracy. On the other hand, it could be seen that the simulation slightly underestimates the power consumption, and that the prediction precision can be improved, as explained in the following paragraph.
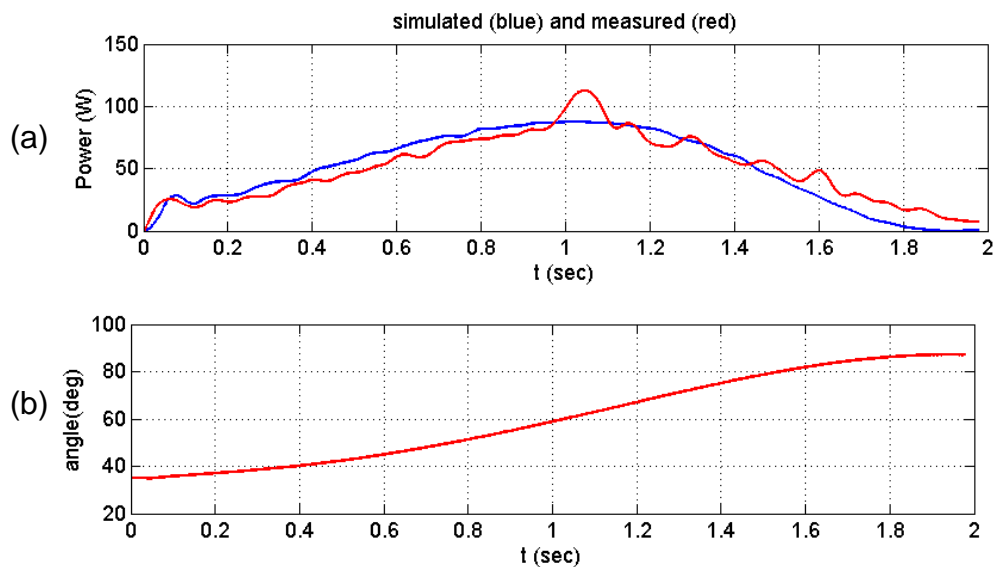
Figure 6-14 Simulation and measurement results for power consumption (a) with the modified value for controller efficiency, for a payload of 5kg, and the joint angle (b).

As mentioned before, a value of 50% was originally assumed and used in the program for the power-efficiency of the controller. Comparisons between the measured and simulated values of the energy consumption (for different payloads up to 30 kg) revealed that the initial simulations underestimated the power loss in the controller and/or other components. It was found that an efficiency value of 41.2% provides a more accurate estimate of the power loss in the controller, as well as other un-modelled or incorrectly modelled losses in other components. More accurate predictions were obtained by using this new value with an error RMS of 8%, as shown in **Figure 6-14** for a payload of 5kg, and in **Figure 6-15** for other payload values.
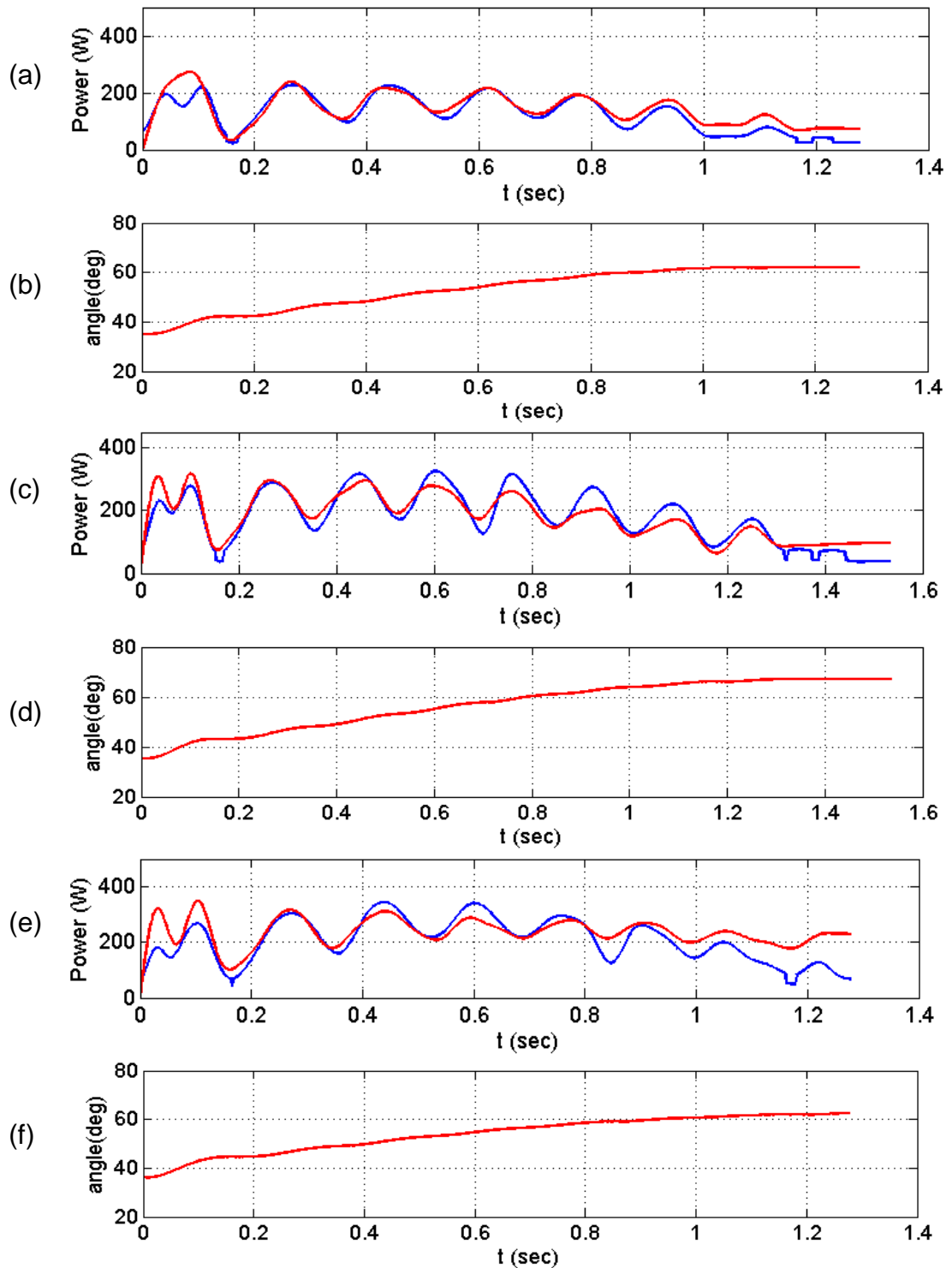
Figure 6-15. Simulation and measurement results with the modified value for controller efficiency, for payloads of 20kg (a), 25kg (c) and 30kg (e), with joint angles (b, d, and f, respectively). The blue curves show the power consumption predicted by the program, and the red curves show the measured values.

After obtaining the new estimate for the controller efficiency (41.2%), the optimisation program was modified and the optimisation process was repeated. However, the optimisation results did not change compared to the previous time. This is expected since the optimisation program compares the power consumption of different actuator design candidates. Hence, while the new value of the controller efficiency increased the estimated power consumption for *all* of the design candidates, it did not alter their ranking based on power consumption.

The total efficiency of the whole actuation system has been calculated by dividing the mechanical energy output of the arm by the consumed electrical energy, as shown in **Figure 6-16**. On average, 27.2% of the consumed electrical energy has been converted into mechanical energy.
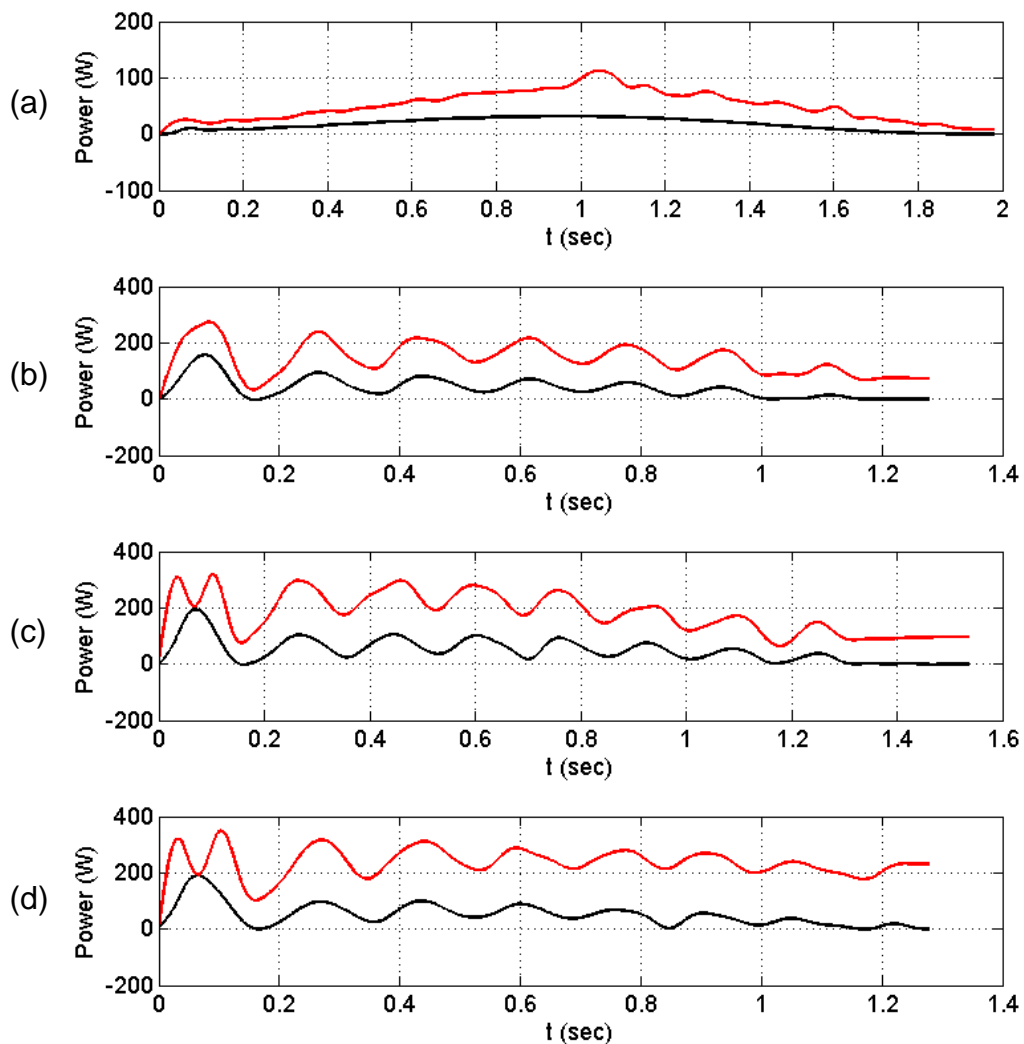
Figure 6-16 The power comparison: output mechanical power of the arm (black) and the consumed electric power (red) for payloads of 5 kg (a), 20kg (b), 25kg (c) and 30kg (d). The average efficiency is 27.2%.

Although the efficiency of the actuation system may not seem very high, comparison with other designs show that this design is quite efficient. A study on electric actuator design for the BLEEX exoskeleton (using harmonic drives) showed that the efficiency of the actuators for the ankle, knee and hip joints are 14.5%, -21.2%[24] and 9.5%, respectively [5]. These values are lower than the efficiency of the actuator designed in this study, which is 27.2%.

An efficiency comparison with the actuators of the Body Extender exoskeleton would also be beneficial. However, the information available on the Body Extender only include the *mechanical efficiency* [28], which has been measured by measuring the motor torque for moving a known amount of load. The mechanical efficiency of the Body Extender actuators is 85%. However, this value does not include the electrical power loss in the motor winding and the controller. In contrast, as explained earlier, the actuator's efficiency in this study has been found by measuring the total electrical power consumed. Therefore, a comparison is not possible.

6.6.3 Findings on energy harvesting

As mentioned earlier in section 6.3, one of the components of the experiment hardware is a battery connected in parallel with the power supply. This component was originally not included in the set-up, and the initial experiments were done without it. However, during the experiments, it was observed that when the power consumption at the joint was negative[25], the motor controller would sometimes shut down. An investigation into the problem revealed that the motor controller used is a regenerative controller which, together with the motor, performs as a generator when the motor is braking. This phenomenon is referred to as regenerative braking [103], during which electric power is fed from the motor back into the power supply. Since the power supply used in this study has not been designed for storing

---

[24] A negative efficiency for the knee joint indicates that although the net mechanical power consumption of the joint is negative during gait, the actuator has to consume a net positive power, due the power loss in the system. The subject of negative power and harvesting energy is covered in detail in the next section.

[25] Negative power consumption refers to the portion of the arm movement when the arm is moving downwards under its gravity. During this motion, the actuator will perform as a brake, resisting against the arm's weight in order to create a slow and smooth motion.

regenerated energy, the voltage across its terminals would quickly rise during this period and, in turn, would trigger an auto-shutdown mechanism inside the controller to protect it against an over-voltage.

In order to solve the above-mentioned problem, a battery was included in the test hardware set-up to store the regenerated energy, as mentioned before. This solution not only solved the problem, but also revealed that energy harvesting in exoskeletons is possible, as long as a power supply is used which can store the regenerated energy, e.g. a battery. Since an untethered exoskeleton will be battery-powered, energy harvesting would be possible.

Figure 6-17 shows the simulation-predicted and the measured values of the regenerated power, with different payloads up to 30 kg. The graphs in **Figure 6-17** have been obtained using a modified value for the controller efficiency, equal to 62.1%. We will refer to this value as the *backward efficiency* of the controller, which seems to be higher than the *forward efficiency* obtained in section 6.6.2 (41.2%). However, this might be because the backward efficiency of other components in the system is higher than their forward efficiency. The whole actuation system seems to be more efficient in back-driving than in forward-driving, as explained in the following paragraph.

To obtain the total efficiency of the whole actuation system in energy harvesting, the calculated mechanical energy of the arm was compared to the electrical energy fed back into the battery, as shown in Figure 6-18. Comparison shows that, on average, 34.9% of the available mechanical energy has been stored as electrical energy. Therefore, the energy harvesting efficiency of the actuation system is more than its forward-driving efficiency, which is 27.2%.

The backward efficiency of the actuator prototype is higher than the corresponding value reported for the electric actuator designed for BLEEX. As mentioned in section 6.6.2, the efficiency of the BLEEX knee joint is reported to be -12.2% for the gait cycle. This means that, although the net mechanical energy at the joint is negative, the actuator still needs to consume a positive net electric energy, because of power inefficiency. In contrast, the prototype built in this study absorbs 34.9% of the mechanical power during braking, and regenerates electric power which can be stored by the power supply.
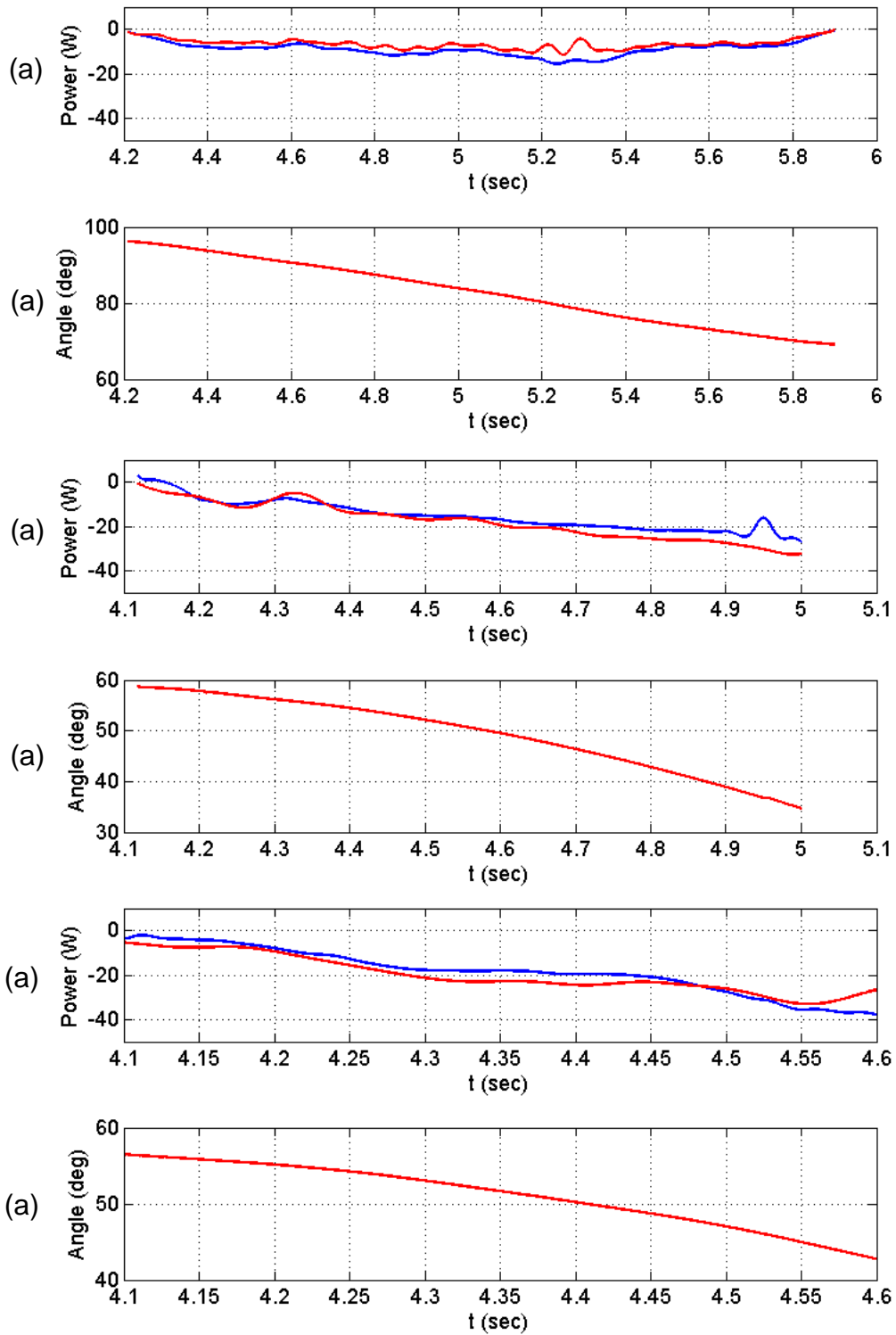
Figure 6-17 Simulation and measurement results of the regenerated power, for payloads of 20kg (a), 25kg (c) and 30kg (e), with joint angles (b, d, and f, respectively). The blue curves show the power consumption predicted by the program, and the red curves show the measured values.

The backward efficiency of the actuator prototype is higher than the corresponding value reported for the electric actuator designed for BLEEX. As mentioned in section 6.6.2, the efficiency of the BLEEX knee joint is reported to be -12.2% for the gait cycle. This means that, although the net mechanical energy at the joint is negative, the actuator still needs to consume a positive net electric energy, because of power inefficiency. In contrast, the prototype built in this study absorbs 34.9% of the mechanical power during braking, and regenerates electric power which can be stored by the power supply.
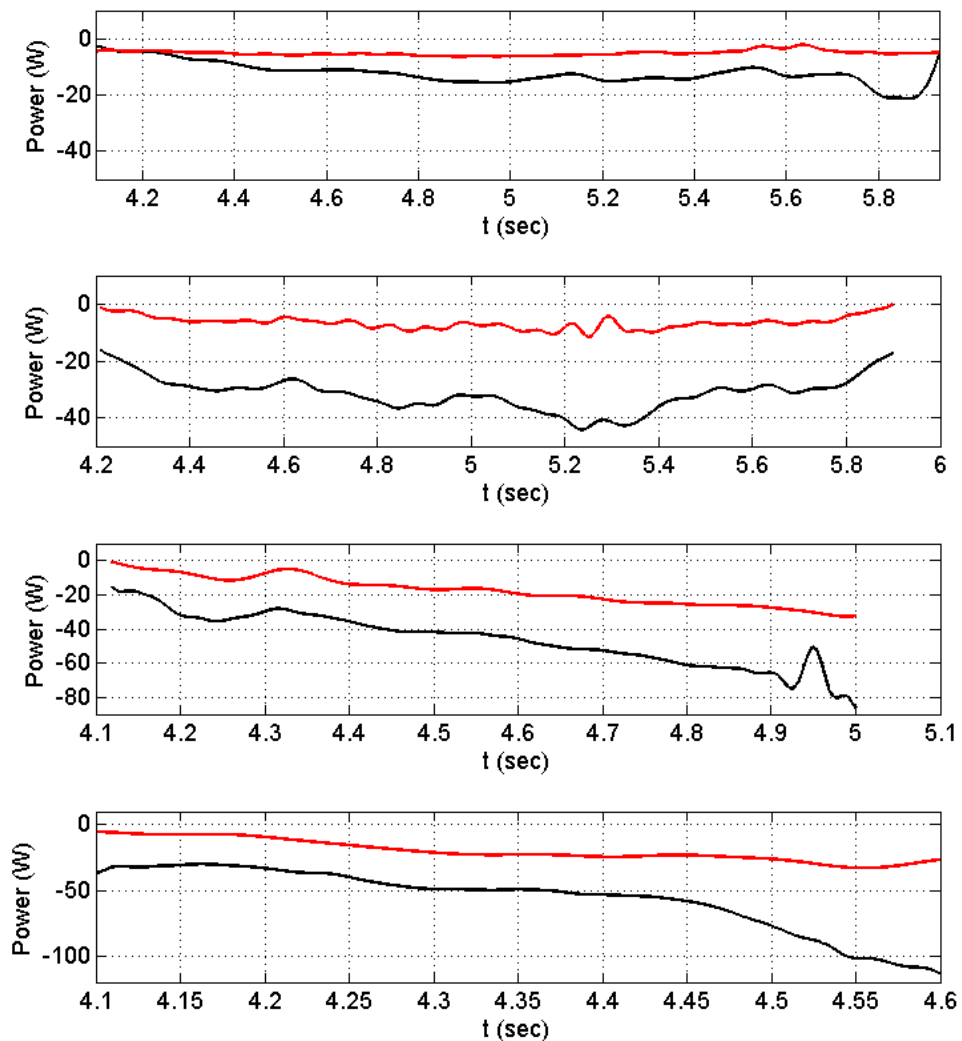
Figure 6-18 Negative power comparison: The Mechanical power of the arm (black) and the harvested electric power (red) for payloads of 5 kg (a), 20kg (b), 25kg (c) and 30kg (d). The average efficiency of energy harvesting is 34.9%.

6.7 Summary

This chapter covers the prototype and the experiments performed on it. The hardware setup and the control software have been explained, as well as the test protocol.

The test results confirmed that the simulation program provides a close approximation of the power consumption of the actuators. However, it was revealed that the actual value of the controller efficiency seems to be lower than the original estimate used in the program. This value was then replaced by the value suggested by the experiment results, and the simulations were performed again. Comparison of the modified simulation results and the experimental results shows a good prediction accuracy, with an estimation RMS error of 8%.

During the experiments done with the test rig, it was found that there is some angular play in the ballscrew, between the screw and nut. This would cause the components to be subject to shock loads, and could be destructive. Therefore, a linear guide has been added to the design of the actuator to eliminate this angular play. This will be explained in the next chapter, in section 7.1.

As stated earlier, a battery needed to be used in parallel to the power supply to absorb and store the regenerated power when the actuator acts as a brake, i.e. when the power consumption of the actuator is negative. This shows that energy harvesting is possible in exoskeletons, as long as the batteries can safely absorb the regenerated current.

Chapter 7
Summary, Conclusion and Future work

7.1 Summary and assessment of the research objectives

This industrially funded research project has been conducted with the aim of developing an enhancive exoskeleton as a marketable product. The key requirements of the product are the load-carrying capacity (between 45 and 60 kg) and energetic autonomy. The latter requirement necessitates the design of a power-efficient system. Furthermore, the size and weight of the system are required to stay within safe limits (for the human users).

This study has focussed on the problem of lower body actuator design in the sagittal plane for an enhancive exoskeleton. The aims were to carry out fundamental research on the actuation system of lower-body enhancive exoskeleton, and to design and build the actuators for a prototype. To achieve these aims, a number of objectives were defined. These objectives, and the assessment of how well they have been accomplished, are covered in this section, as follows.

- To perform dynamic simulations to assess the torque and power requirements at the exoskeleton joints.

As mentioned earlier, the scope of this research is limited to the analysis of the lower-body DOFs in the sagittal plane, and the design of actuators for those DOFs. Furthermore, previous studies have shown that a two dimensional model is sufficient to model the joint motions in the sagittal plane. Therefore, modelling of the exoskeleton motion has been performed with a two-dimensional model in the sagittal plane.

Kinematic and kinetic models of the exoskeleton have been formulated in this study, using the Newton-Euler method. The models have been used to model two manoeuvres, namely gait and squat, which have been used as representatives of the working condition of the exoskeleton in load-handling tasks. The developed formulations were then placed inside a simulation program written in MATLAB™, to perform simulations. The results of these simulations were compared to the simulation results of the exoskeleton motion obtained from the SolidWorks Motion™ software. The comparisons revealed

that some refinements were required in the formulations. After carrying out the necessary modifications, the results from the two methods became identical, which showed that the simulation program was reliable and could be used in the optimisation program explained later in this section.

- To investigate and characterise the commercially available electric actuators.

Extensive market research was conducted in this project to characterise a large number of electric motors available in the market. The result is a list of 151 motors, in a vast variety of designs, and a large range of sizes, nominal powers and nominal torques. The list contains all of the relevant technical specifications for each motor, and can be considered to represent the state of the art. This list was used by the optimisation program to conduct an exhaustive search, as explained later in this section.

- To design actuation mechanisms for the joints to be actuated.

Different power transmission mechanisms (in combination with electric motors) have been considered when generating design concepts for the actuators. Initial studies revealed that of many transmission systems were unsuitable due to backlash, low torque capacity, and excessive size/mass. The remaining transmission mechanisms, considered potentially appropriate for the design problem, were strain gears, ballscrews, and chain and sprockets. The models for each of these mechanisms were formulated, to be used in the optimisation program, as stated in the following paragraphs.

In addition to the transmission system models, a model was also made for electric motors, to assess their performance for given tasks. Both the motor and the transmission system models were used by the optimisation program.

- To find the optimal motor size and transmission ratio for the actuators, with consideration to the load-carrying capacity, power consumption, and the total mass of the system.

An optimisation program, written in MATLA™, has been developed to find the best design for the actuators of each joint. The program opens spread sheets that contain the lists of electric motors and transmission systems, and investigates them one by one by combining each motor with all of the transmission systems in the list, to create *design candidates*. The mass of the motors and transmission systems is then added to the dynamic model of the exoskeleton, and the model parameters are updated. After that, an iterative set of simulations are performed to find out the load-carrying capacity and power consumption in walking and squatting, for the considered motors and transmission mechanism. This procedure is carried out for all of the motors and transmission mechanisms on the lists, to complete an exhaustive search. The results are saved in a spreadsheet.

The result table of the above-mentioned exhaustive search was then used to perform a multi-factor *decision table* to choose the best design candidate. The load-carrying capacity, power consumption, and the estimated mass of the whole exoskeleton were chosen as the factors to be considered in the decision making. These factors were normalised, and given *weighting factors* (i.e. importance factor). The sum of the weighted normalised factors form a *value function*, for each design candidate. By sorting the design candidate according to the value function, the most desirable candidates appear in the top rows of the decision table.

- To build a test prototype and perform experiments to validate the simulation and the optimisation process.

Based on the results of the optimisation procedure, a test prototype has been developed to assess the performance of the designed actuator, and verify the reliability of the modelling and simulation which is the basis of the optimisation procedure. Test experiments have been performed and comparisons were made between experimental and simulation results, to verify and fine-tune the simulations and slightly modify the parameter values used. The simulation program with the modified parameters was then used one more time to find the optimal solution, which was found to be the same as the results previously found.

- To investigate the possibility of energy harvesting when the power consumption at the exoskeleton joints is negative.

While performing the experiments, it was found that the motor controller used was a regenerative controller which turns negative mechanical power into electric power and feeds it back to the power supply. Therefore, energy harvesting is possible ion exoskeletons, as long as the power supply can store the power fed to it by the controller.

7.2   Conclusions

Before mentioning the conclusions, it is useful to present the research questions again:

1. Considering existing off-the-shelf actuators and power transmission mechanisms, what are the optimal choices for each joint's actuator? And how can the answer be found?

Initial investigations revealed that electric actuators would be the most suitable type, if it is desired that the exoskeleton should be untethered. Furthermore, the results of the optimisation procedure ruled out the usage of a direct-drive mechanism. Hence, the actuator design should consist of an electric motor and a power transmission mechanism.

An optimisation program, explained in the previous section, has been developed in this research to find the best design solutions. The optimisation results showed that ballscrews combined with slider-crank mechanisms should be used as the power transmission mechanisms for the knee and ankle joint actuators. The best diameter and pitch size for the ballscrews were found to be 16mm and 10mm, respectively. The dimensions of the slider-crank mechanism have been found for both of the actuators.

The same motor size was found to be suitable for both the knee and ankle, which weighs approximately 4.14 kg with the frame, shaft and bearings.

A strain gear with a ratio of 80 was found to be the best choice for the hip actuators, with a motor that weighs approximately 3.03 kg including the frame, shaft and bearings.

Investigations showed that the usage of ballscrews with rope-and-pulley mechanisms would result in bulky and heavy actuators. This design concept has been used for the actuators of the Body Extender exoskeleton (covered in section 2.3.3 of Chapter 2), which were shown in this study to be unsafe (p122).

2. Considering the answers to the previous research question, what would be the most suitable design of the actuators for an exoskeleton?

The actuators for the ankle and knee have been designed in detail in this study. A test prototype of the knee actuator was built in this study, and the experimental results obtained from the tests confirmed the suitability of the design, as well as the integrity of the optimisation procedure and the reliability of the results.

The ankle and hip actuators has also been designed in this project, although time limitation did not allow for building it. The ankle actuator design is different from the knee actuator design in that it incorporates an anti-backlash timing belt mechanism, in order to reduce the length of the actuator. Also, a linear guide has been added to alleviate angular play which is inherent in ballscrews. The hip actuator consists of a harmonic drive, and a timing belt and pulley mechanism.

7.3 Future work

The next steps that can be taken towards developing an exoskeleton (with the intended requirements) would be to build a single-leg prototype.

Once the single-leg prototype has been built, tests should be performed to assess the performance of the actuators, and to make modifications to the design if necessary. These tests could also provide a more reliable estimate of the power consumption, which could be used to conduct research on the

development of a portable power source (most probably a battery) for the exoskeleton.

After having taken the above-mentioned steps, a lower-body prototype can be developed, with further investigations conducted. More research also need to be done in order to decide which non-sagittal plane joints need to be actuated, and then to find optimal design solutions for the actuators. After developing a fully actuated lower-body prototype, the design of the upper body actuators could be pursued.

List of References

1. Dollar, A.M. and H. Herr, *Lower extremity exoskeletons and active orthoses: Challenges and state-of-the-art.* Ieee Transactions on Robotics, 2008. **24**(1): p. 144-158.
2. Chu, A., et al., *On the biomimetic design of the Berkeley Lower Extremity Exoskeleton (BLEEX)*, in *2005 IEEE International Conference on Robotics and Automation*. 2005. p. 4345-4352.
3. Kazerooni, H. and R. Steger, *The Berkeley Lower Extremity Exoskeleton.* Journal of Dynamic Systems Measurement and Control-Transactions of the Asme, 2006. **128**(1): p. 14-25.
4. Zoss, A.B., H. Kazerooni, and A. Chu, *Biomechanical design of the Berkeley lower extremity exoskeleton (BLEEX).* Ieee-Asme Transactions on Mechatronics, 2006. **11**(2): p. 128-138.
5. Zoss, A. and H. Kazerooni, *Design of an electrically actuated lower extremity exoskeleton.* Advanced Robotics, 2006. **20**(9): p. 967-988.
6. Amundson, K., et al., *Development of hybrid hydraulic-electric power units for field and service robots.* Advanced Robotics, 2006. **20**(9): p. 1015-1034.
7. Guizzo, E. and H. Goldstein, *The rise of the body bots.* Ieee Spectrum, 2005. **42**(10): p. 50-56.
8. *Berkeley Robotics & Human Engineering Laboratory, exoskeletons.* 27/06/2014]; Available from: http://bleex.me.berkeley.edu/research/exoskeleton/.
9. Highfield, R., *Telegraph.*
10. *seattlepi.* 16/07/2014]; Available from: http://www.seattlepi.com/national/article/Next-evolution-in-our-love-of-robots-4371815.php.
11. *Raytheon website.* 27/06/2014]; Available from: http://multivu.prnewswire.com/mnr/raytheon/46273/.
12. ; Available from: https://ipfs.io/ipfs/QmXoypizjW3WknFiJnKLwHCnL72vedxjQkDDP1m XWo6uco/wiki/Sarcos.html.
13. Valiente, A., *Design of a Quasi-Passive Parallel Leg Exoskeleton to Augment Load Carrying for Walking* in *Department of Mechanical Engineering*2005, MASSACHUSETTS INSTITUTE OF TECHNOLOGY.
14. Walsh, C.J., *Biomimetic Design of an Under-Actuated Leg Exoskeleton For Load-Carrying Augmentation* in *Mechanical Engineering*2006, Massachusetts Institute of Technology.
15. Walsh, C.J., et al., *Development of a lightweight, underactuated exoskeleton for load-carrying augmentation*, in *2006 Ieee International Conference on Robotics and Automation*. 2006, Ieee: New York. p. 3485-3491.

16. Walsh, C.J., K. Endo, and H. Herr, *A quasi-passive leg exoskeleton for load-carrying augmentation.* International Journal of Humanoid Robotics, 2007. **4**(3): p. 487-506.

17. Walsh, C.J., K. Pasch, and H. Herr. *An autonomous, underactuated exoskeleton for load-carrying augmentation*. in *Intelligent Robots and Systems, 2006 IEEE/RSJ International Conference on*. 2006.

18. *IEEE Spectrum*. 17/07/2014]; Available from: http://spectrum.ieee.org/automaton/robotics/robotics-software/mit_robotic_exoskeleton_struts.

19. *Exo Bionics official Website*. 27/06/2014]; Available from: http://eksobionics.com/ourstory.

20. Kawamoto, H. and Y. Sankai, *Power Assist System HAL-3 for Gait Disorder Person*, in *Computers Helping People with Special Needs*, K. Miesenberger, J. Klaus, and W. Zagler, Editors. 2002, Springer Berlin Heidelberg. p. 196-203.

21. Kawamoto, H., et al., *Power assist method for HAL-3 using EMG-based feedback controller*, in *2003 Ieee International Conference on Systems, Man and Cybernetics, Vols 1-5, Conference Proceedings*. 2003, Ieee: New York. p. 1648-1653.

22. Hayashi, T., et al., *Control method of robot suit HAL working as operator's muscle using biological and dynamical information*. 2005 IEEE/RSJ International Conference on Intelligent Robots and Systems, Vols 1-4. 2005, New York: Ieee. 3455-3460.

23. *CYBERDYNE official website*. 27/06/2014]; Available from: http://www.cyberdyne.jp/english/.

24. Mohammed, S. and Y. Amirat. *Towards intelligent lower limb wearable robots: Challenges and perspectives - State of the art*. in *Robotics and Biomimetics, 2008. ROBIO 2008. IEEE International Conference on*. 2009.

25. Lucchesi, N., et al. *An approach to the design of fully actuated body extenders for material handling*. in *19th International Symposium in Robot and Human Interactive Communication*. 2010.

26. Marcheschi, S., et al. *Body Extender: Whole body exoskeleton for human power augmentation*. in *2011 IEEE International Conference on Robotics and Automation*. 2011.

27. *Robotic Exoskeleton Lifts 50 Kilos Per Hand*. Available from: http://www.iflscience.com/technology/robotic-exoskeleton-lifts-50-kilos-hand/.

28. Bergamasco, M., et al., *A Novel Actuator for Wearable Robots with Improved Torque Density and Mechanical Efficiency.* Advanced Robotics, 2010. **24**(14): p. 2019-2041.

29. 27/06/2014]; Available from: http://www.sfgate.com/education/article/Exoskeleton-lets-UC-Berkeley-grad-take-a-huge-step-2371372.php#photo-1898726.

30. *ForeFront Magazine*. 27/06/2014]; Available from: http://bleex.me.berkeley.edu/wp-content/uploads/2011/05/ForfrontArticle.pdf.

31. 02/07/2014]; Available from: https://www.youtube.com/watch?v=o7xH5kOXU5k.

32. Viteckova, S., P. Kutilek, and M. Jirina, *Wearable lower limb robotics: A review.* Biocybernetics and Biomedical Engineering, 2013. **33**(2): p. 96-105.

33. *Argo Medical Technologies* 27/06/2014]; Available from: http://www.argomedtec.com/.

34. Bogue, R., *Exoskeletons and robotic prosthetics: a review of recent developments.* Industrial Robot-an International Journal, 2009. **36**(5): p. 421-427.

35. Talaty, M., A. Esquenazi, and J.E. Briceno, *Differentiating ability in users of the ReWalk(TM) powered exoskeleton: an analysis of walking kinematics.* IEEE ... International Conference on Rehabilitation Robotics : [proceedings], 2013. **2013**: p. 6650469-6650469.

36. 03/07/2014]; Available from: http://news.vanderbilt.edu/2012/10/exoskeleton/.

37. *Center of Intelligent Mechatronics, Vanderbilt University*. Available from: http://research.vuse.vanderbilt.edu/cim/research_orthosis.html.

38. *Endgadget.* 03/07/2014]; Available from: http://www.engadget.com/2010/07/15/rex-the-robotic-exoskeleton-aims-to-make-wheelchairs-obsolete/.

39. *Rex Bionics.* 03/07/2014]; Available from: http://www.rexbionics.com/products/.

40. Gancet J., I.M., Cheron G., Ivanenko Y., Van der Kooij H., Van der Helm F., Zanow F., Thorsteinsson F., *MINDWALKER: A BRAIN CONTROLLED LOWER LIMBS EXOSKELETON FOR REHABILITATION. POTENTIAL APPLICATIONS TO SPACE*, 2011: ESA ASTRA Workshop, April 2011 [in press]

41. *The MINDWALKER project website.* 07/07/2014]; Available from: https://mindwalker-project.eu/.

42. Gancet, J., et al., *MINDWALKER: Going One Step Further with Assistive Lower Limbs Exoskeleton for SCI Condition Subjects.* 2012 4th Ieee Ras & Embs International Conference on Biomedical Robotics and Biomechatronics (Biorob), 2012: p. 1794-1800.

43. Neuhaus, P.D., et al. *Design and evaluation of Mina: A robotic orthosis for paraplegics*. in *Rehabilitation Robotics (ICORR), 2011 IEEE International Conference on*. 2011.

44. Hian Kai, K., et al. *Development of the IHMC Mobility Assist Exoskeleton*. in *Robotics and Automation, 2009. ICRA '09. IEEE International Conference on*. 2009.

45. *Tokyo University of Science Robotics on Beyond Tomorrow*. 09/07/2014]; Available from: https://www.youtube.com/watch?v=rg246IFabOc.

46. Wiggin, M.B., G.S. Sawicki, and S.H. Collins. *An exoskeleton using controlled energy storage and release to aid ankle propulsion*. in *Rehabilitation Robotics (ICORR), 2011 IEEE International Conference on*. 2011.

47. *Passive Elastic Exoskeleton Reduces Metabolic Cost of Walking*. 09/07/2014]; Available from: https://www.youtube.com/watch?v=0fgC4qOWcxg.

48. Blaya, J.A. and H. Herr, *Adaptive control of a variable-impedance ankle-foot orthosis to assist drop-foot gait.* Ieee Transactions on Neural Systems and Rehabilitation Engineering, 2004. **12**(1): p. 24-31.
49. Ferris, D.P., J.M. Czerniecki, and B. Hannaford, *An ankle-foot orthosis powered by artificial pneumatic muscles.* Journal of Applied Biomechanics, 2005. **21**(2): p. 189-197.
50. Gordon, K.E., G.S. Sawicki, and D.P. Ferris, *Mechanical performance of artificial pneumatic muscles to power an ankle-foot orthosis.* Journal of Biomechanics, 2006. **39**(10): p. 1832-1841.
51. Pratt, J.E., et al., *The RoboKnee: An exoskeleton for enhancing strength and endurance during walking*, in *2004 Ieee International Conference on Robotics and Automation, Vols 1- 5, Proceedings*. 2004. p. 2430-2435.
52. Shingu, M., et al., *Substitution of motor function of polio survivors who have Permanent Paralysis of Limbs by using Cybernic Voluntary Control.* 2009 Ieee International Conference on Robotics and Biomimetics. 2009. 504-509.
53. Mefoued, S., S. Mohammed, and Y. Amirat, *Toward Movement Restoration of Knee Joint Using Robust Control of Powered Orthosis.* Ieee Transactions on Control Systems Technology, 2013. **21**(6): p. 2156-2168.
54. Sawicki, G.S. and D.P. Ferris, *A pneumatically powered knee-ankle-foot orthosis (KAFO) with myoelectric activation and inhibition.* Journal of Neuroengineering and Rehabilitation, 2009. **6**.
55. Yeh, T.J., et al., *Control of McKibben pneumatic muscles for a power-assist, lower-limb orthosis.* Mechatronics, 2010. **20**(6): p. 686-697.
56. Wu, S.-K., T. Driver, and X. Shen, *Design and Control of a Pneumatically Actuated Lower-Extremity Orthosis.* Journal of Medical Devices-Transactions of the Asme, 2012. **6**(4).
57. *Festo*. 27/06/2014]; Available from: http://www.festo.com/cms/en_corp/12713.htm.
58. In, H., et al., *Investigation of Friction Characteristics of a Tendon Driven Wearable Robotic Hand*. International Conference on Control, Automation and Systems. 2010. 568-573.
59. *JAECO Orthopedics*. 27/06/2014]; Available from: http://jaecoorthopedic.com/products/categories/Mobile-Arm-Supports/WREX-%252d-Wilmington-Robotic-EXoskeleton/.
60. *Stratasys*. 27/06/2014]; Available from: http://www.stratasys.com/resources/case-studies/medical/nemours.
61. *Myomo Inc.* 27/06/2014]; Available from: http://myomo.com/myomo-solutions-technology-for-increasing-mobility-after-brain-injury-stroke/.
62. Page, S.J., et al., *Portable Neurorobotics for the Severely Affected Arm in Chronic Stroke: A Case Study.* Journal of Neurologic Physical Therapy, 2011. **35**(1): p. 41-46.
63. *MyoPro* 27/06/2014]; Available from: http://www.myopro.com/.
64. Gil Herrnstadt, C.M., *On-Off Tremor Suppression Orthosis with Electromagnetic Brake.* International Journal of Mechanical Engineering and Mechatronics, 2013. **Volume 1**(Issue 2).

65.   Whittle, M., *Gait analysis: an introduction*. 2007: Butterworth-Heinemann.

66.   Popovic, M.B., A. Goswami, and H. Herr, *Ground reference points in legged locomotion: Definitions, biological trajectories and control implications.* International Journal of Robotics Research, 2005. **24**(12): p. 1013-1032.

67.   Winter, D.A., *The biomechanics and motor control of human gait: normal, elderly and pathological.* 1991: University of Waterloo Press.

68.   Lim, M.R., et al., *Evaluation of the Elderly Patient With an Abnormal Gait.* Journal of the American Academy of Orthopaedic Surgeons, 2007. **15**(2): p. 107-117.

69.   Ulrich, K.T. and S.D. Eppinger, *Product design and development.* 2012, Maidenhead: McGraw-Hill.

70.   Dieter, G.E., G.E. Dieter, and L.C. Schmidt, *Engineering Design.* 2012: McGraw-Hill Higher Education.

71.   Savransky, S.D., *Engineering of creativity: introduction to TRIZ methodology of inventive problem solving.* 2000, Boca Raton, Fla: CRC Press.

72.   Kalevi Rantanen, E.D., *Simplified TRIZ: new problem solving applications for engineers and manufacturing professionals* 2007, New York: Auerbach Publications.

73.   Standard, B., *Robots and robotic devices — Safety requirements for personal care robots*, in *5.3.1.2. Inherently Safe Design*2014.

74.   Granosik, G. and J. Borenstein. *Minimizing air consumption of pneumatic actuators in mobile robots*. in *Robotics and Automation, 2004. Proceedings. ICRA '04. 2004 IEEE International Conference on*. 2004.

75.   Hollerbach, J.M., I.W. Hunter, and J. Ballantyne, *A comparative analysis of actuator technologies for robotics*, in *The robotics review 2*, K. Oussama, et al., Editors. 1992, MIT Press. p. 299-342.

76.   Goldfarb, M., et al., *Design and energetic characterization of a liquid-propellant-powered actuator for self-powered, robots.* Ieee-Asme Transactions on Mechatronics, 2003. **8**(2): p. 254-262.

77.   Cherry, M.S., et al., *AN ELASTIC EXOSKELETON FOR ASSISTING HUMAN RUNNING*. Proceedings of the Asme International Design Engineering Technical Conferences and Computers and Information in Engineering Conference, Vol 7, Pts a and B. 2010. 727-738.

78.   Browning, R.C., et al., *The effects of adding mass to the legs on the energetics and biomechanics of walking.* Med Sci Sports Exerc, 2007. **39**(3): p. 515-25.

79.   McBean, J. and C. Breazeal. *Voice coil actuators for human-robot interaction - An exploration of the use of electromagnetic voice coils as compliant, forcecontrolled actuators in direct-drive robots for visual and tactile interaction with humans*. 2004.

80.   Wang, S., C. Meijneke, and H. van der Kooij, *Modeling, design, and optimization of Mindwalker series elastic joint.* IEEE ... International Conference on Rehabilitation Robotics : [proceedings], 2013. **2013**: p. 6650381.

81. *Delf University of Technology.* 09/07/2014]; Available from: http://www.3me.tudelft.nl/en/about-the-faculty/departments/biomechanical-engineering/research/dbl-delft-biorobotics-lab/exoskeleton/.

82. van Dijk, W., H. van der Kooij, and E. Hekman. *A passive exoskeleton with artificial tendons: Design and experimental evaluation.* in *Rehabilitation Robotics (ICORR), 2011 IEEE International Conference on.* 2011.

83. Shiqian, W., W. van Dijk, and H. van der Kooij. *Spring uses in exoskeleton actuation design.* in *Rehabilitation Robotics (ICORR), 2011 IEEE International Conference on.* 2011.

84. Hollander, K.W., et al., *An efficient robotic tendon for gait assistance.* Journal of Biomechanical Engineering-Transactions of the Asme, 2006. **128**(5): p. 788-791.

85. Hitt, J., et al., *Dynamically controlled ankle-foot orthosis (DCO) with regenerative kinetics: Incrementally attaining user portability*, in *Proceedings of the 2007 Ieee International Conference on Robotics and Automation, Vols 1-10.* 2007. p. 1541-1546.

86. Au, S.K., et al., *Powered ankle-foot prosthesis for the improvement of amputee ambulation.* Conference proceedings : ... Annual International Conference of the IEEE Engineering in Medicine and Biology Society. IEEE Engineering in Medicine and Biology Society. Conference, 2007. **2007**: p. 3020-6.

87. Au, S.K., J. Weber, and H. Herr, *Powered Ankle-Foot Prosthesis Improves Walking Metabolic Economy.* Ieee Transactions on Robotics, 2009. **25**(1): p. 51-66.

88. Sergi, F., et al., *Design and Characterization of a Compact Rotary Series Elastic Actuator for Knee Assistance During Overground Walking*, in *2012 4th Ieee Ras & Embs International Conference on Biomedical Robotics and Biomechatronics*, J.P. Desai, L.P.S. Jay, and L. Zollo, Editors. 2012. p. 1931-1936.

89. Banala, S.K., et al., *Gravity-Balancing Leg Orthosis and Its Performance Evaluation.* Robotics, IEEE Transactions on, 2006. **22**(6): p. 1228-1239.

90. Brooks, T.L. and Ieee, *TELEROBOTIC RESPONSE REQUIREMENTS.* 1990 Ieee International Conference on Systems, Man, and Cybernetics. 1990. 113-120.

91. *TechCrunch.* Available from: https://techcrunch.com/2007/04/24/rent-the-hal-5-exoskeleton-for-590mo/.

92. *Harmonic Drive AG.* Available from: http://harmonicdrive.de/en/products/component-sets/cobaltline-2a.html.

93. Zoss, A.B., *Actuation Design and Implementation for Lower Extremity Human Exoskeleton*, 2006, University of California, Berkeley

94. Shigley, J.E.M., C.R., *Standard HAndbook of Machine Design.* 2nd ed.

95. *HPC Gears.* Available from: http://www.hpcgears.com/.

96. *Morre International Ltd.*; Available from: http://www.mooreinternational.co.uk/.

97. *Nook Industires*. Available from: http://www.nookindustries.com/LinearLibraryItem/Ballscrew_Torque_Calculations.

98. *Moore International Ltd.* Available from: http://www.mooreinternational.co.uk/.

99. Garrec, P., et al. *A New Force-Feedback, Morphologically Inspired Portable Exoskeleton*. in *Robot and Human Interactive Communication, 2006. ROMAN 2006. The 15th IEEE International Symposium on*. 2006.

100. *CarlStahl TECHNOCABLES Catalog*.

101. Budynas, R. and K. Nisbett, *Shigley's Mechanical Engineering Design*. 2010: McGraw-Hill Education.

102. *Carl Stahl GmbH Catalog*. Available from: http://www.carlstahl-technocables.com/fileadmin/files/katalog-carl-stahl-technocables.pdf.

103. Dixon, J. *Energy storage for electric vehicles*. in *2010 IEEE International Conference on Industrial Technology*. 2010.

Appendix A - List of desired manoeuvres

No.	Activity
1.	Walk on level ground
2.	Walk on rough terrain
3.	Run
4.	Squat
5.	Get up from a fallen position
6.	Walk up the stairs
7.	Walk up the slopes
8.	Walk down the stairs
9.	Walk down the slopes
10.	Go through doorways
11.	Walk on level ground with load
12.	Walk on rough terrain with load
13.	Run with load
14.	Squat with load
15.	Get up from a fallen position with load
16.	Walk up the stairs with load
17.	Walk up the slopes with load
18.	Walk down the stairs with load
19.	Walk down the slopes with load
20.	Go through doorways with load
21.	Deadlift
22.	Overhead shoulder press (with bar)
23.	Vertical jump
24.	Bench press (with bar)
25.	Horizontal push (full body)
26.	Horizontal pull (full body)
27.	Biceps curl (with bar)
28.	Bent over row (with bar)
29.	Pull down

Appendix B - Product Needs

No.	Need	Priority
1.	The device shall be a full body exoskeleton.	1
2.	The kinematic design of the frame shall allow the device to perform activities specified in the Appendix A.	1
3.	The frame shall be adjustable for different user size.	1
4.	The frame shall be modular.	1
5.	The joint and the actuator for each DOF shall be a separable module.	1
6.	The primary product shall be untethered, i.e. energetically independent.	1
7.	The load-carrying capacity shall be the maximum achievable amount, considering the safety.	1
8.	The system shall be able to sense human motion (kinematics and dynamics).	1
9.	The device shall be easy to use.	1
10.	The device shall be easily adaptable to a new user.	1
11.	The device shall be safe.	1
12.	The device shall be reliable.	1
13.	The device shall be weight efficient.	1
14.	The power consumption of the device shall be efficient.	1
15.	The operation duration time shall be long.	1
16.	The system shall be cost-effective.	1
17.	The appearance of the device shall be acceptable.	1
18.	The user shall not be burdened with any extra effort to carry the exoskeleton (while not carrying any payload).	1
19.	The device shall comply with University of Leeds standards.	1
20.	The device shall comply with BS EN ISO 13482:2014.	1
21.	There shall be a feasible maintenance scheme in place.	1
22.	The device shall have an acceptable life-cycle.	1
23.	The device should decrease the metabolic cost of load carrying task.	2
24.	The actuators of the device should be dynamically strong enough to perform activities specified in Appendix A except for running.	2
25.	The device should not impede movements.	2
26.	The device may be clean.	3
27.	The device may be easily put on and off by the user without any assistance.	3

28.	The noise produced by the primary product may be socially acceptable.	3
29.	An assistive variation of the device may be possible to achieve via modular changes (low cost, assistive, with the minimum possible actuators).	3
30.	An enhacive variation of the device, which is only for carrying loads on a backpack, may be possible to achieve via modular changes (lower limb with a backpack frame, enhancive).	3
31.	The full-body variation of the device may be possible to achieve via modular changes (lower limb exoskeleton, hung from a frame or the ceiling, used for rehabilitation).	3
32.	The design should allow for subsystems of the product to be used as orthotic devices.	2

Appendix C - The target requirements

Note: The values of quantitative metrics are expressed in the units specified. As for non-quantitative metrics, the following nomenclature has been used:

"List" means that a list of items specify the value of the metric.

"Subj." means that the metric is a subjective one, and the value will be assessed by the team.

Corresponding Need(s)	Metric	Unit	Priority	Marginally acceptable Value	Ideal Value
7	1. Mechanical Strength (weight of the user and load)	kg	1	45	60
2	2. Possible manoeuvres	-	1	Appendix A	Appendix A
4, 29, 31, 32, 30, 5	3. List of separate modules	list	1	Lower body and upper body	Each actuator, each link, each joint
3	4. Adjusting features	list	1	Limbs length, trunc length	Limbs length, trunc length
28	5. Noise	dB, subj.	3	Safe for humans	Socially acceptable
26	6. Cleanliness	subj.	3	No fume	No by-products of energy consumption
6	7. Untethered	-	1	Tethered	Untethered
7	8. Load-carrying capacity without user effort while walking	kg	1	45	60
11	9. Maximum allowable angular velocity of joints	rad/s	1	Safe	Safe
11	10. Maximum allowable angular acceleration	rad/s^2	1	Safe	Safe
13	11. Weight	kg	1	68	21

174

14	12. Power consumption	W	1	Lowest possible considering other requirements	Lowest possible considering other requirements
15	13. Operation duration	hours	1	1	2h and 40min
16	14. Price	£, $, €	1	$30K	$10K
17	15. Appearance	subj.	1	Not a concern	Socially acceptable
32	16. The joint motions actively assisted by intended orthotic sub-products	list	3	None	Each joint
10	17. Ease of control system adaptation	-	1	1-2 weeks	Wear-and-use
9, 10	18. Time to learn to operate the device	h	2	1 week training	Immediate
8	19. Human motions sensed	list	1	To be confirmed	To be confirmed
9	20. Ease of use	subj.	1	Trained users can use the exoskeleton	Any user can naturally move inside the exoskeleton
27	21. Ease of putting on and off	min., subj.	3	1 person's aid is required to put the device on and off	The user does not require any help to put the device on and off
18	22. Endurance augmentation (decrease of metabolic cost) without load.	%	1	0	12%
23	23. Endurance augmentation (decrease of metabolic cost) with maximum load.	%	2	15	50
21	24. Maintenance scheme feasibility	subj.	1	Maintainable by technicians	Maintainable by the user

11	25. Vibration	subj.	1	Human safe	Imperceptible
11	26. Safety	subj.	1	Sade for humans	Sade for humans
12	27. Reliability	subj.	1	Reliable	Reliable
11, 25, 2	28. Ranges of motion of joints	rad	1	As required by the maneuvers listed in Appendix A	Full range of human motion
19	29. University of Leeds standards compliance	subj.	1	compliant	compliant
20	30. Standard BS EN ISO 13482:2014 compliance	subj.	1	Not-compliant	Compliant
21	31. Maintainability	subj.	1	Maintainable	Maintainable
22	32. Life-cycle	years	1	2 years (guaranteed)	10 years
29	33. Cost of the Type 1 variation	£, $, €	3	To be confirmed	To be confirmed
30	34. An option for a backpack frame	subj.	3	Yes	Yes
31	35. Rehabilitative capabilities	subj.	3	None	Available for each joint
2	36. Size of the longest dimension increase of the system	%	1	100% of average human	25% of average human

Appendix D - The efficiency and no load torque of strain gears

D.1   Introduction

Equation 4-1, mentioned in section 4.4.2of Chapter 4, describes the relations between the motor output torque and the output torque of the strain gear. This equation is repeated here for convenience:

$$\begin{cases} (\tau_m)_{out} = \dfrac{\tau_j}{\eta.N}, & P > 0 \\ (\tau_m)_{out} = \dfrac{\eta.\tau_j}{N}, & P < 0 \end{cases} \qquad \text{7-1}$$

where τ_j is the joint torque (which is the output torque of the strain gear), $(\tau_m)_{out}$ is the output torque of the motor (which is the input torque of the strain gear), η is the strain gear efficiency, and N is the gear ratio. *P* is the output power of the gear, and is positive when the gear output torque and angular velocity are in the same direction, and vice versa.

However, there are other considerations in the calculation of $(\tau_m)_{out}$, which will be explained in this section. When there is no resistance at the output of the strain gear, i.e. $\tau_j = 0$, then $(\tau_m)_{out}$ must be equal to τ_{nl}, the "*no-load torque*" of the strain gear; however, the "*no-load torque*" has a different value at the starting point of motion, τ_{nl_s} , due to the presence of the static friction.

Finally, the "*no-load back-driving torque*", τ_{nl_b}, must be taken into account. When the gear is being back-driven (i.e. *P<0*), if the value of τ_j is larger than or equal to τ_{nl_b}, then the gear will be back driven. In this case, τ_{nl_b} must be first subtracted from τ_j, and then equation 7-1 can be used to calculate $(\tau_m)_{out}$. But if $\tau_j < \tau_{nl\_b}$, then motor must provide a torque equal to $\frac{\tau_{nl\_b}}{\eta.N}$, and in the same direction as the angular velocity of the joint.

The values of the efficiency and no-load torques of strain gears depend on the torque, angular velocity and temperature. However, a fixed average value can be used to estimate the efficiency of a strain gears, as has been done in other studies [5, 93]. In this study however, the graphs provided by the manufacturer [92] have been used to interpolate the efficiency and no-load torques for each point of the discretised trajectory of the exoskeleton joint. These graphs and the interpolation method used have been presented in the next sections. It must be noted that the operation temperature of the exoskeleton is assumed to be 20 degrees in all of the calculations in this section.

D.2 Efficiency

D.2.1 The correction Factor

After finding the efficiency from the graphs as will be mentioned in the next section, a correction factor might need to be used, if the gear is operating at a load below its rated torque. To obtain the correction factor, the torque factor V must first be calculated, as follows:

$$V = \frac{T_{ave}}{T_N}$$

7-2

where T_N is the rated torque of the strain gear, and T_{ave} is the average output torque. However, if the torque is being calculated for each point of the discretized trajectory, then the output torque at that point can be used instead of T_{ave} to obtain a more precise value. Once V has been calculated, then the correction factor η can be found from the graph bellow:
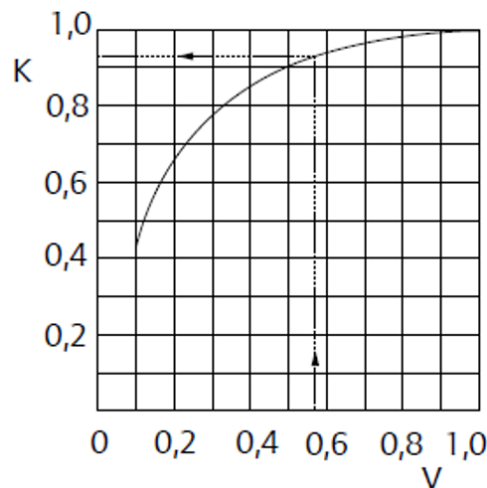
Figure 7-1. The graph for efficiency correction factor versus the torque factor for strain gears [92]

In order to programmatically use the graph in Figure 7-1, the values of K were extracted from the graph for a number of discrete points, presented in Table 7-1. After that, a polynomial needed to be fitted onto the graph so programmatically estimate the value of K for any given value of V. The order of the best fitting curve had to be found by examining the root mean square of the estimation error (RMSE). Therefore, a number of curves were fitted using linear regression, and it was found that increasing the order beyond 6 would

make little change to the RMSE. The sixth degree polynomial of the fitted curve is as follows:

$$K = [V^6\ V^5\ V^4\ V^3\ V^2\ V\ 1] \times P \qquad 7\text{-}3$$

Where the value of the vector of polynomial coefficients *P* is as follows:

$$P = \begin{bmatrix} -9.722222222218084 \\ 37.21153846152321 \\ -58.07158119655891 \\ 47.81133449881820 \\ -22.68509518258902 \\ 6.489668997667889 \\ -0.0339999999992991 \end{bmatrix}$$

Table 7-1 The values of K versus V for 10 point on the graph of Figure 7-1

V	K
0.1	0.43
0.2	0.66
0.3	0.77
0.4	0.85
0.5	0.9
0.6	0.93
0.7	0.96
0.8	0.98
0.9	0.99
1	1

The simulation program uses equation 7-3 to calculate the correction factor if the gear output torque is smaller than the nominal torque of the gear.

D.2.2　　　The Efficiency charts

The efficiency charts of the strain gears considered in this study are shown in Figure 7-2. As can be seen, the graphs are different for gears with different ratios. Therefore, the simulation program needs to use different estimation methods for different gear ratios. Furthermore, the efficiency is dependent on the temperature. Since no information is available on the operation temperature of the exoskeleton, it has been assumed that the temperature would be 20°C, which is the room temperature[26]. At 20°C, for a given gear ratio, the information available from the graphs provide the efficiency at four different output velocities, ranging from 500 to 3500 rpm. In a similar way to what was explained in section D.2.1, the linear regression method has been used to fit polynomials onto the existing points, in order to interpolate the value of efficiency. In the following tables, the extracted values are presented, followed by the values of the fitted polynomials. The polynomials have to be third degree ones, because the efficiency is only provided for four values of velocity. Furthermore, for velocity values outside the range given in the graphs, the program assumes the velocity to be equal to the extremum closest to the actual velocity.

Notice that, although efficiency values for a gear ratio of 30 are also presented in Figure 7-2, this ratio is only available in small gear sizes. The larger gears with torque capacities high enough for our application are only available with a minimum ratio of 50. Therefore, the fitted polynomials have only been calculated for ratios of 50 and above.

---

[26] https://ahdictionary.com/word/search.html?q=room+temperature
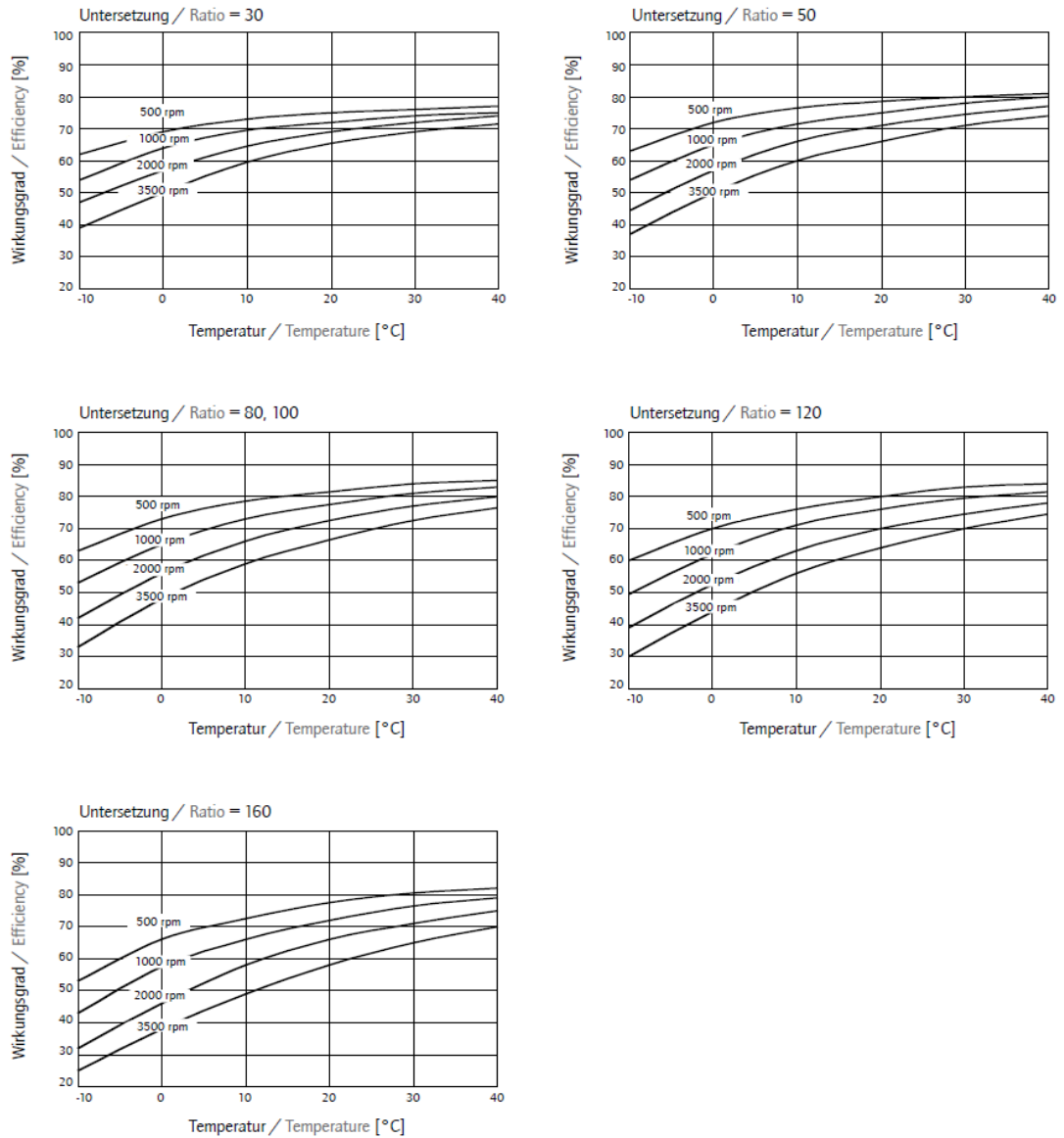
Figure 7-2 The efficiency charts of the strain gears [92]

The fitted polynomial is the following format:

$$\eta = [\ \omega^3\ \omega^2\ \omega\ 1] \times P_\eta \qquad\qquad 7\text{-}4$$

where η is the efficiency and ω is the output angular velocity of the gear. Also, notice that before performing the linear regression, the values of ω were converted from rpm to rad/s.

181

D.2.2.1　　　Ratio 50

Table 7-2 Extracted efficiency values for Ratio 50:1

rpm	Eta
500	0.78
1000	0.75
2000	0.71
3500	0.66

P_e=[-3.340703643936105e-10　　　　　7.890461036076985e-07　　　　　-6.522311350282374e-04

8.117899829298972e-01];

$$P_{\eta\_50} = \begin{bmatrix} -3.340703643936105e-10 \\ 7.890461036076985e-07 \\ -6.522311350282374e-04 \\ 8.117899829298972e-01 \end{bmatrix}$$

D.2.2.2　　　Ratios 80 and 100

Table 7-3 Extracted efficiency values for Ratio 80:1 and 100:1

rpm	Eta
500	0.82
1000	0.77
2000	0.73
3500	0.66

$$P_{\eta\_80,100} = \begin{bmatrix} -4.807887545619474e-10 \\ 1.105420605865836e-06 \\ -8.702238141111563e-04 \\ 8.588358339417646e-01 \end{bmatrix}$$

D.2.2.3   Ratio 120

Table 7-4 Extracted efficiency values for Ratio 120:1

rpm	Eta
500	0.8
1000	0.76
2000	0.7
3500	0.64

$$P_{\eta\_50} = \begin{bmatrix} -5.910705958345415e-10 \\ 1.286927843656137e-06 \\ -9.522242869884818e-04 \\ 8.466750590986378e-01 \end{bmatrix}$$

D.2.2.4   Ratio 160

Table 7-5 Extracted efficiency values for Ratio 160:1

rpm	Eta
500	0.78
1000	0.72
2000	0.66
3500	0.58

$$P_{\eta\_50} = \begin{bmatrix} -7.541947696307964e-10 \\ 1.632046835510191e-06 \\ -1.179313636559307e-03 \\ 8.342724007236504e-01 \end{bmatrix}$$

D.3   The no-load starting torque

The no-load starting torque is presented in Figure 7-3.

Untersetzung Ratio	Baugröße / Size								
	14	17	20	25	32	40	45	50	58
30	6,4	9,3	15	25	54	–	–	–	–
50	4,1	6,1	7,8	15	31	55	77	110	160
80	2,8	4,0	4,9	9,2	19	35	49	66	98
100	2,5	3,4	4,3	8,0	18	31	43	58	88
120	–	3,1	3,8	7,3	15	28	39	52	80
160	–	–	3,3	6,3	14	24	33	45	68

Figure 7-3 The no-load starting torque [92]. The values are in N.cm

D.4   The no-load back-driving torque

The no-load starting torque is presented in Figure 7-4.

Untersetzung Ratio	Baugröße / Size								
	14	17	20	25	32	40	45	50	58
30	2,4	3,8	6,2	11	23	–	–	–	–
50	1,6	3,0	4,7	9,0	18	33	47	62	95
80	1,6	3,0	4,8	9,1	19	33	48	63	96
100	1,8	3,3	5,1	9,8	20	36	51	68	110
120	–	3,5	5,5	11	22	39	55	73	110
160	–	–	6,4	13	26	46	64	85	130

Figure 7-4 The no-load back-driving torque [92]. The values are in N.cm.

D.5   The No-load running torque

The no-load running torque is presented in Figure 7-5.

Baugröße Size	Untersetzung / Ratio				
	30	50	80	120	160
14	2,5	1,1	0,2	–	–
17	3,8	1,6	0,3	-0,2	–
20	5,4	2,3	0,5	-0,3	-0,8
25	8,8	3,8	0,7	-0,5	-1,2
32	16,0	7,1	1,3	-0,9	-2,2
40	–	12	2,1	-1,5	-3,5
45	–	16	2,9	-2,1	-4,9
50	–	21	3,7	-2,6	-6,2
58	–	30	5,3	-3,8	-8,9
65	–	–	8,1	-5,8	-13,7

Figure 7-5 The no-load running torque [92]. The values are in N.cm.

Appendix E - The specifications of the power transmission systems

E.1　　　The specifications of the strain gears

Series	Size	Ratio	Rated Torque (Nm)	Moment of Inertia (*10^-6 kgm^2)	Repeatable Peak torque (Nm)	Average torque (Nm)
CSD-2A	14	50	4	2.1	12	4.8
CSD-2A	14	100	5	2.1	19	7.7
CSD-2A	17	50	11	5.4	23	18.0
CSD-2A	17	100	16	5.4	37	27.0
CSD-2A	20	50	17	9.0	39	34.0
CSD-2A	20	100	28	9.0	57	34.0
CSD-2A	20	160	28	9.0	64	34.0
CSD-2A	25	50	27	28.2	69	38.0
CSD-2A	25	100	47	28.2	110	75.0
CSD-2A	25	160	47	28.2	123	75.0
CSD-2A	32	50	53	109.0	151	75.0
CSD-2A	32	100	96	109.0	233	151.0
CSD-2A	32	160	96	109.0	261	151.0
CSG-2A	14	50	7	3.3	23	9.0
CSG-2A	14	80	10	3.3	30	14.0
CSG-2A	14	100	10	3.3	36	14.0
CSG-2A	17	50	21	7.9	44	34.0
CSG-2A	17	80	29	7.9	56	35.0
CSG-2A	17	100	31	7.9	70	51.0
CSG-2A	17	120	31	7.9	70	51.0
CSG-2A	20	50	33	19.3	73	44.0
CSG-2A	20	80	44	19.3	96	61.0
CSG-2A	20	100	52	19.3	107	64.0
CSG-2A	20	120	52	19.3	113	64.0
CSG-2A	20	160	52	19.3	120	64.0
CSG-2A	25	50	51	41.3	127	72.0
CSG-2A	25	80	82	41.3	178	113.0
CSG-2A	25	100	87	41.3	204	140.0
CSG-2A	25	120	87	41.3	217	140.0
CSG-2A	25	160	87	41.3	229	140.0
CSG-2A	32	50	99	196.0	281	140.0
CSG-2A	32	80	153	196.0	395	217.0
CSG-2A	32	100	178	196.0	433	281.0
CSG-2A	32	120	178	196.0	459	281.0
CSG-2A	32	160	178	196.0	484	281.0

Series	Size	Ratio	Rated Torque (Nm)	moment of Inertia (*10^-6 kgm^2)	Repeatable Peak torque (Nm)	Average torque (Nm)
CPL-2A	14	50	5	2.0	18	6.9
CPL-2A	14	80	8	2.0	23	11.0
CPL-2A	14	100	8	2.0	28	11.0
CPL-2A	17	50	16	4.9	34	26.0
CPL-2A	17	80	22	4.9	43	27.0
CPL-2A	17	100	24	4.9	54	39.0
CPL-2A	17	120	24	4.9	54	39.0
CPL-2A	20	50	25	11.2	56	34.0
CPL-2A	20	80	34	11.2	74	47.0
CPL-2A	20	100	40	11.2	82	49.0
CPL-2A	20	120	40	11.2	87	49.0
CPL-2A	20	160	40	11.2	92	49.0
CPL-2A	25	50	39	26.3	98	55.0
CPL-2A	25	80	63	26.3	137	87.0
CPL-2A	25	100	67	26.3	157	108.0
CPL-2A	25	120	67	26.3	167	108.0
CPL-2A	25	160	67	26.3	176	108.0
CPL-2A	32	50	76	92.4	216	108.0
CPL-2A	32	80	118	92.4	304	167.0
CPL-2A	32	100	137	92.4	333	216.0
CPL-2A	32	120	137	92.4	353	216.0
CPL-2A	32	160	137	92.4	372	216.0

E.2 The specifications of the inverted slider-crank mechanism and ballscrew

The following table contains the specifications of different slider-crank mechanisms that could be combined with a ballscrew with a pitch legato of 10 mm. The parameters r_p, r_d, γ_p and γ_d have been defined in section 4.4.4 of Chapter 4. The moment of inertia has been calculated for the nut of the ballscrew, which is the only part that rotates with the motor shaft (the ballscrew itself only has a linear motion in this design). The parameter h represents the maximum distance of the ballscrew form the centre of the shank link in the motion range of the actuator. This parameter is a representation of the size of the actuator for each mechanism.

This table is only for a pitch length of 10mm. Similar tables were made for other pitch lengths, but for the sake of brevity, they will not be mentioned here.

Pitch (mm)	r_p (mm)	γ_p (rad)	r_d (mm)	γ_d (rad)	Moment of Inertia (*10^5 kg-m^2)	Weight for the max length (kg)	Max axial force (N)	Weight per length (kg/m)	Max h (m)	Max load (kg)
10	100	0	62	1.92	288	0.155	8667	1.578	43	60
10	100	0	62	1.99	288	0.148	8667	1.578	51	60
10	100	0	62	2.06	288	0.141	8667	1.578	58	60
10	100	0	62	2.13	288	0.134	8667	1.578	64	60
10	100	0	62	2.21	288	0.127	8667	1.578	68	60
10	100	0	62	2.28	288	0.120	8667	1.578	71	60
10	100	0	62	2.35	288	0.113	8667	1.578	70	60
10	100	0	62	2.42	288	0.106	8667	1.578	67	60
10	100	0	62	2.49	288	0.100	8667	1.578	64	60
10	100	0	63	1.85	288	0.162	8667	1.578	40	60
10	100	0	63	1.92	288	0.155	8667	1.578	43	60
10	100	0	63	1.99	288	0.148	8667	1.578	51	60
10	100	0	63	2.06	288	0.141	8667	1.578	59	60
10	100	0	63	2.13	288	0.134	8667	1.578	65	60
10	100	0	63	2.21	288	0.127	8667	1.578	69	60
10	100	0	63	2.28	288	0.120	8667	1.578	72	60
10	100	0	63	2.35	288	0.113	8667	1.578	72	60
10	100	0	63	2.42	288	0.106	8667	1.578	69	60
10	100	0	63	2.49	288	0.099	8667	1.578	65	60
10	100	0	64	1.85	288	0.162	8667	1.578	41	60
10	100	0	64	1.92	288	0.155	8667	1.578	43	60
10	100	0	64	1.99	288	0.149	8667	1.578	51	60
10	100	0	64	2.06	288	0.142	8667	1.578	59	60
10	100	0	64	2.13	288	0.134	8667	1.578	65	60
10	100	0	64	2.21	288	0.127	8667	1.578	70	60
10	100	0	64	2.28	288	0.120	8667	1.578	73	60
10	100	0	64	2.35	288	0.113	8667	1.578	73	60

10	100	0	64	2.42	288	0.106	8667	1.578	70	60
10	100	0	64	2.49	288	0.099	8667	1.578	66	60
10	100	0	64	2.56	288	0.092	8667	1.578	63	60
10	100	0	65	1.85	288	0.163	8667	1.578	42	60
10	100	0	65	1.92	288	0.156	8667	1.578	44	60
10	100	0	65	1.99	288	0.149	8667	1.578	51	60
10	100	0	65	2.06	288	0.142	8667	1.578	59	60
10	100	0	65	2.13	288	0.135	8667	1.578	65	60
10	100	0	65	2.21	288	0.127	8667	1.578	71	60
10	100	0	65	2.28	288	0.120	8667	1.578	74	60
10	100	0	65	2.35	288	0.113	8667	1.578	74	60
10	100	0	65	2.42	288	0.106	8667	1.578	72	60
10	100	0	65	2.49	288	0.098	8667	1.578	68	60
10	100	0	65	2.56	288	0.091	8667	1.578	64	60
10	100	0	66	1.85	288	0.163	8667	1.578	43	60
10	100	0	66	1.92	288	0.156	8667	1.578	45	60
10	100	0	66	1.99	288	0.149	8667	1.578	51	60
10	100	0	66	2.06	288	0.142	8667	1.578	59	60
10	100	0	66	2.13	288	0.135	8667	1.578	66	60
10	100	0	66	2.21	288	0.127	8667	1.578	71	60
10	100	0	66	2.28	288	0.120	8667	1.578	74	60
10	100	0	66	2.35	288	0.113	8667	1.578	75	60
10	100	0	66	2.42	288	0.105	8667	1.578	73	60
10	100	0	66	2.49	288	0.098	8667	1.578	69	60
10	100	0	66	2.56	288	0.091	8667	1.578	65	60
10	100	0	67	1.85	288	0.164	8667	1.578	44	60
10	100	0	67	1.92	288	0.157	8667	1.578	46	60
10	100	0	67	1.99	288	0.150	8667	1.578	51	60
10	100	0	67	2.06	288	0.142	8667	1.578	59	60
10	100	0	67	2.13	288	0.135	8667	1.578	66	60
10	100	0	67	2.21	288	0.128	8667	1.578	72	60
10	100	0	67	2.28	288	0.120	8667	1.578	75	60
10	100	0	67	2.35	288	0.113	8667	1.578	76	60
10	100	0	67	2.42	288	0.105	8667	1.578	74	60
10	100	0	67	2.49	288	0.098	8667	1.578	70	60
10	100	0	67	2.56	288	0.090	8667	1.578	66	60
10	100	0	68	1.85	288	0.165	8667	1.578	46	60
10	100	0	68	1.92	288	0.157	8667	1.578	47	60
10	100	0	68	1.99	288	0.150	8667	1.578	51	60
10	100	0	68	2.06	288	0.143	8667	1.578	59	60
10	100	0	68	2.13	288	0.135	8667	1.578	66	60
10	100	0	68	2.21	288	0.128	8667	1.578	72	60
10	100	0	68	2.28	288	0.120	8667	1.578	76	60
10	100	0	68	2.35	288	0.113	8667	1.578	78	60
10	100	0	68	2.42	288	0.105	8667	1.578	76	60
10	100	0	68	2.49	288	0.097	8667	1.578	72	60
10	100	0	68	2.56	288	0.090	8667	1.578	68	60
10	100	0	69	1.85	288	0.165	8667	1.578	47	60
10	100	0	69	1.92	288	0.158	8667	1.578	48	60
10	100	0	69	1.99	288	0.151	8667	1.578	51	60
10	100	0	69	2.06	288	0.143	8667	1.578	59	60

10	100	0	69	2.13	288	0.136	8667	1.578	67	60
10	100	0	69	2.21	288	0.128	8667	1.578	73	60
10	100	0	69	2.28	288	0.120	8667	1.578	77	60
10	100	0	69	2.35	288	0.113	8667	1.578	79	60
10	100	0	69	2.42	288	0.105	8667	1.578	77	60
10	100	0	69	2.49	288	0.097	8667	1.578	73	60
10	100	0	70	1.85	288	0.166	8667	1.578	48	60
10	100	0	70	1.92	288	0.158	8667	1.578	49	60
10	100	0	70	1.99	288	0.151	8667	1.578	51	60
10	100	0	70	2.06	288	0.144	8667	1.578	59	60
10	100	0	70	2.13	288	0.136	8667	1.578	67	60
10	100	0	70	2.21	288	0.128	8667	1.578	73	60
10	100	0	70	2.28	288	0.120	8667	1.578	78	60
10	100	0	70	2.35	288	0.113	8667	1.578	80	60
10	100	0	70	2.42	288	0.105	8667	1.578	79	60
10	100	0	70	2.49	288	0.097	8667	1.578	75	60
10	100	0	71	1.78	288	0.174	8667	1.578	47	60
10	100	0	71	1.85	288	0.166	8667	1.578	49	60
10	100	0	71	1.92	288	0.159	8667	1.578	51	60
10	100	0	71	1.99	288	0.152	8667	1.578	52	60
10	100	0	71	2.06	288	0.144	8667	1.578	59	60
10	100	0	71	2.13	288	0.136	8667	1.578	67	60
10	100	0	71	2.21	288	0.128	8667	1.578	74	60
10	100	0	71	2.28	288	0.120	8667	1.578	78	60
10	100	0	71	2.35	288	0.113	8667	1.578	81	60
10	100	0	71	2.42	288	0.105	8667	1.578	80	60
10	100	0	71	2.49	288	0.097	8667	1.578	76	60
10	100	0	72	1.78	288	0.174	8667	1.578	48	60
10	100	0	72	1.85	288	0.167	8667	1.578	50	60
10	100	0	72	1.92	288	0.160	8667	1.578	52	60
10	100	0	72	1.99	288	0.152	8667	1.578	53	60
10	100	0	72	2.06	288	0.144	8667	1.578	59	60
10	100	0	72	2.13	288	0.136	8667	1.578	67	60
10	100	0	72	2.21	288	0.129	8667	1.578	74	60
10	100	0	72	2.28	288	0.121	8667	1.578	79	60
10	100	0	72	2.35	288	0.113	8667	1.578	82	60
10	100	0	72	2.42	288	0.104	8667	1.578	81	60
10	100	0	72	2.49	288	0.096	8667	1.578	77	60
10	100	0	73	1.78	288	0.175	8667	1.578	49	60
10	100	0	73	1.85	288	0.168	8667	1.578	51	60
10	100	0	73	1.92	288	0.160	8667	1.578	53	60
10	100	0	73	1.99	288	0.153	8667	1.578	55	60
10	100	0	73	2.06	288	0.145	8667	1.578	59	60
10	100	0	73	2.13	288	0.137	8667	1.578	67	60
10	100	0	73	2.21	288	0.129	8667	1.578	74	60
10	100	0	73	2.28	288	0.121	8667	1.578	79	60
10	100	0	73	2.35	288	0.113	8667	1.578	83	60
10	100	0	73	2.42	288	0.104	8667	1.578	82	60
10	100	0	73	2.49	288	0.096	8667	1.578	79	60
10	100	0	74	1.78	288	0.176	8667	1.578	50	60
10	100	0	74	1.85	288	0.168	8667	1.578	52	60

10	100	0	74	1.92	288	0.161	8667	1.578	54	60
10	100	0	74	1.99	288	0.153	8667	1.578	56	60
10	100	0	74	2.06	288	0.145	8667	1.578	59	60
10	100	0	74	2.13	288	0.137	8667	1.578	67	60
10	100	0	74	2.21	288	0.129	8667	1.578	74	60
10	100	0	74	2.28	288	0.121	8667	1.578	80	60
10	100	0	74	2.35	288	0.113	8667	1.578	83	60
10	100	0	74	2.42	288	0.104	8667	1.578	84	60
10	100	0	75	1.78	288	0.176	8667	1.578	50	60
10	100	0	75	1.85	288	0.169	8667	1.578	53	60
10	100	0	75	1.92	288	0.161	8667	1.578	55	60
10	100	0	75	1.99	288	0.154	8667	1.578	57	60
10	100	0	75	2.06	288	0.146	8667	1.578	59	60
10	100	0	75	2.13	288	0.138	8667	1.578	67	60
10	100	0	75	2.21	288	0.129	8667	1.578	75	60
10	100	0	75	2.28	288	0.121	8667	1.578	80	60
10	100	0	75	2.35	288	0.113	8667	1.578	84	60
10	100	0	75	2.42	288	0.104	8667	1.578	85	60
10	100	0	76	1.78	288	0.177	8667	1.578	51	60
10	100	0	76	1.85	288	0.170	8667	1.578	54	60
10	100	0	76	1.92	288	0.162	8667	1.578	56	60
10	100	0	76	1.99	288	0.154	8667	1.578	58	60
10	100	0	76	2.06	288	0.146	8667	1.578	60	60
10	100	0	76	2.13	288	0.138	8667	1.578	67	60
10	100	0	76	2.21	288	0.130	8667	1.578	75	60
10	100	0	76	2.28	288	0.121	8667	1.578	81	60
10	100	0	76	2.35	288	0.113	8667	1.578	85	60
10	100	0	76	2.42	288	0.104	8667	1.578	86	60
10	100	0	77	1.78	288	0.178	8667	1.578	52	60
10	100	0	77	1.85	288	0.170	8667	1.578	55	60
10	100	0	77	1.92	288	0.163	8667	1.578	57	60
10	100	0	77	1.99	288	0.155	8667	1.578	60	60
10	100	0	77	2.06	288	0.147	8667	1.578	61	60
10	100	0	77	2.13	288	0.138	8667	1.578	67	60
10	100	0	77	2.21	288	0.130	8667	1.578	75	60
10	100	0	77	2.28	288	0.122	8667	1.578	81	60
10	100	0	77	2.35	288	0.113	8667	1.578	86	60
10	100	0	77	2.42	288	0.104	8667	1.578	87	60
10	100	0	78	1.78	288	0.179	8667	1.578	53	60
10	100	0	78	1.85	288	0.171	8667	1.578	56	60
10	100	0	78	1.92	288	0.163	8667	1.578	58	60
10	100	0	78	1.99	288	0.155	8667	1.578	61	60
10	100	0	78	2.06	288	0.147	8667	1.578	63	60
10	100	0	78	2.13	288	0.139	8667	1.578	67	60
10	100	0	78	2.21	288	0.130	8667	1.578	75	60
10	100	0	78	2.28	288	0.122	8667	1.578	82	60
10	100	0	78	2.35	288	0.113	8667	1.578	86	60
10	100	0	78	2.42	288	0.104	8667	1.578	88	60
10	100	0	79	1.78	288	0.179	8667	1.578	54	60
10	100	0	79	1.85	288	0.172	8667	1.578	57	60
10	100	0	79	1.92	288	0.164	8667	1.578	60	60

10	100	0	79	1.99	288	0.156	8667	1.578	62	60
10	100	0	79	2.06	288	0.148	8667	1.578	64	60
10	100	0	79	2.13	288	0.139	8667	1.578	67	60
10	100	0	79	2.21	288	0.131	8667	1.578	75	60
10	100	0	79	2.28	288	0.122	8667	1.578	82	60
10	100	0	79	2.35	288	0.113	8667	1.578	87	60
10	100	0	79	2.42	288	0.104	8667	1.578	89	60
10	100	0	80	1.78	288	0.180	8667	1.578	55	60
10	100	0	80	1.85	288	0.172	8667	1.578	58	60
10	100	0	80	1.92	288	0.165	8667	1.578	61	60
10	100	0	80	1.99	288	0.156	8667	1.578	63	60
10	100	0	80	2.06	288	0.148	8667	1.578	65	60
10	100	0	80	2.13	288	0.140	8667	1.578	67	60
10	100	0	80	2.21	288	0.131	8667	1.578	75	60
10	100	0	80	2.28	288	0.122	8667	1.578	82	60
10	100	0	80	2.35	288	0.113	8667	1.578	87	60
10	100	0	80	2.42	288	0.105	8667	1.578	90	60
10	100	0	81	1.71	288	0.189	8667	1.578	53	60
10	100	0	81	1.78	288	0.181	8667	1.578	56	60
10	100	0	81	1.85	288	0.173	8667	1.578	59	60
10	100	0	81	1.92	288	0.165	8667	1.578	62	60
10	100	0	81	1.99	288	0.157	8667	1.578	64	60
10	100	0	81	2.06	288	0.149	8667	1.578	67	60
10	100	0	81	2.13	288	0.140	8667	1.578	68	60
10	100	0	81	2.21	288	0.131	8667	1.578	75	60
10	100	0	81	2.28	288	0.123	8667	1.578	82	60
10	100	0	81	2.35	288	0.114	8667	1.578	88	60
10	100	0	81	2.42	288	0.105	8667	1.578	91	60
10	100	0	81	1.71	288	0.190	8667	1.578	54	60
10	100	0	81	1.78	288	0.182	8667	1.578	57	60
10	100	0	81	1.85	288	0.174	8667	1.578	60	60
10	100	0	81	1.92	288	0.166	8667	1.578	63	60
10	100	0	81	1.99	288	0.158	8667	1.578	65	60
10	100	0	81	2.06	288	0.149	8667	1.578	68	60
10	100	0	81	2.13	288	0.141	8667	1.578	70	60
10	100	0	81	2.21	288	0.132	8667	1.578	75	60
10	100	0	81	2.28	288	0.123	8667	1.578	82	60
10	100	0	81	2.35	288	0.114	8667	1.578	88	60
10	100	0	81	2.42	288	0.105	8667	1.578	92	60
10	100	0	82	1.71	288	0.190	8667	1.578	55	60
10	100	0	82	1.78	288	0.183	8667	1.578	58	60
10	100	0	82	1.85	288	0.175	8667	1.578	61	60
10	100	0	82	1.92	288	0.167	8667	1.578	64	60
10	100	0	82	1.99	288	0.158	8667	1.578	67	60
10	100	0	82	2.06	288	0.150	8667	1.578	69	60
10	100	0	82	2.13	288	0.141	8667	1.578	71	60
10	100	0	82	2.21	288	0.132	8667	1.578	74	60
10	100	0	82	2.28	288	0.123	8667	1.578	82	60
10	100	0	82	2.35	288	0.114	8667	1.578	89	60
10	100	0	82	2.42	288	0.105	8667	1.578	93	60
10	100	0	83	1.71	288	0.191	8667	1.578	56	60

10	100	0	83	1.78	288	0.183	8667	1.578	59	60
10	100	0	83	1.85	288	0.175	8667	1.578	62	60
10	100	0	83	1.92	288	0.167	8667	1.578	65	60
10	100	0	83	1.99	288	0.159	8667	1.578	68	60
10	100	0	83	2.06	288	0.150	8667	1.578	70	60
10	100	0	83	2.13	288	0.142	8667	1.578	73	60
10	100	0	83	2.21	288	0.133	8667	1.578	74	60
10	100	0	83	2.28	288	0.124	8667	1.578	82	60
10	100	0	83	2.35	288	0.114	8667	1.578	89	60
10	100	0	83	2.42	288	0.105	8667	1.578	93	60
10	100	0	84	1.71	288	0.192	8667	1.578	56	60
10	100	0	84	1.78	288	0.184	8667	1.578	60	60
10	100	0	84	1.85	288	0.176	8667	1.578	63	60
10	100	0	84	1.92	288	0.168	8667	1.578	66	60
10	100	0	84	1.99	288	0.160	8667	1.578	69	60
10	100	0	84	2.06	288	0.151	8667	1.578	71	60
10	100	0	84	2.13	288	0.142	8667	1.578	74	60
10	100	0	84	2.21	288	0.133	8667	1.578	76	60
10	100	0	84	2.28	288	0.124	8667	1.578	82	60
10	100	0	84	2.35	288	0.115	8667	1.578	89	60
10	100	0	84	2.42	288	0.105	8667	1.578	94	60
10	100	0	85	1.71	288	0.193	8667	1.578	57	60
10	100	0	85	1.78	288	0.185	8667	1.578	61	60
10	100	0	85	1.85	288	0.177	8667	1.578	64	60
10	100	0	85	1.92	288	0.169	8667	1.578	67	60
10	100	0	85	1.99	288	0.160	8667	1.578	70	60
10	100	0	85	2.06	288	0.151	8667	1.578	73	60
10	100	0	85	2.13	288	0.143	8667	1.578	75	60
10	100	0	85	2.21	288	0.134	8667	1.578	77	60
10	100	0	85	2.28	288	0.124	8667	1.578	82	60
10	100	0	85	2.35	288	0.115	8667	1.578	89	60
10	100	0	85	2.42	288	0.106	8667	1.578	94	60
10	100	0	86	1.71	288	0.194	8667	1.578	58	60
10	100	0	86	1.78	288	0.186	8667	1.578	61	60
10	100	0	86	1.85	288	0.178	8667	1.578	65	60
10	100	0	86	1.92	288	0.169	8667	1.578	68	60
10	100	0	86	1.99	288	0.161	8667	1.578	71	60
10	100	0	86	2.06	288	0.152	8667	1.578	74	60
10	100	0	86	2.13	288	0.143	8667	1.578	76	60
10	100	0	86	2.21	288	0.134	8667	1.578	79	60
10	100	0	86	2.28	288	0.125	8667	1.578	82	60
10	100	0	86	2.35	288	0.115	8667	1.578	89	60
10	100	0	86	2.42	288	0.106	8667	1.578	95	60
10	100	0	87	1.71	288	0.195	8667	1.578	59	60
10	100	0	87	1.78	288	0.187	8667	1.578	62	60
10	100	0	87	1.85	288	0.179	8667	1.578	66	60
10	100	0	87	1.92	288	0.170	8667	1.578	69	60
10	100	0	87	1.99	288	0.162	8667	1.578	72	60
10	100	0	87	2.06	288	0.153	8667	1.578	75	60
10	100	0	87	2.13	288	0.144	8667	1.578	78	60
10	100	0	87	2.21	288	0.135	8667	1.578	80	60

10	100	0	87	2.28	288	0.125	8667	1.578	82	60
10	100	0	87	2.35	288	0.116	8667	1.578	89	60
10	100	0	88	1.71	288	0.196	8667	1.578	60	60
10	100	0	88	1.78	288	0.188	8667	1.578	63	60
10	100	0	88	1.85	288	0.179	8667	1.578	67	60
10	100	0	88	1.92	288	0.171	8667	1.578	70	60
10	100	0	88	1.99	288	0.162	8667	1.578	73	60
10	100	0	88	2.06	288	0.153	8667	1.578	76	60
10	100	0	88	2.13	288	0.144	8667	1.578	79	60
10	100	0	88	2.21	288	0.135	8667	1.578	81	60
10	100	0	88	2.28	288	0.126	8667	1.578	84	60
10	100	0	88	2.35	288	0.116	8667	1.578	89	60
10	100	0	89	1.71	288	0.197	8667	1.578	60	60
10	100	0	89	1.78	288	0.189	8667	1.578	64	60
10	100	0	89	1.85	288	0.180	8667	1.578	67	60
10	100	0	89	1.92	288	0.172	8667	1.578	71	60
10	100	0	89	1.99	288	0.163	8667	1.578	74	60
10	100	0	89	2.06	288	0.154	8667	1.578	77	60
10	100	0	89	2.13	288	0.145	8667	1.578	80	60
10	100	0	89	2.21	288	0.136	8667	1.578	83	60
10	100	0	89	2.28	288	0.126	8667	1.578	85	60
10	100	0	89	2.35	288	0.116	8667	1.578	89	60
10	100	0	90	1.71	288	0.198	8667	1.578	61	60
10	100	0	90	1.78	288	0.190	8667	1.578	65	60
10	100	0	90	1.85	288	0.181	8667	1.578	68	60
10	100	0	90	1.92	288	0.173	8667	1.578	72	60
10	100	0	90	1.99	288	0.164	8667	1.578	75	60
10	100	0	90	2.06	288	0.155	8667	1.578	78	60
10	100	0	90	2.13	288	0.146	8667	1.578	81	60
10	100	0	90	2.21	288	0.136	8667	1.578	84	60
10	100	0	90	2.28	288	0.127	8667	1.578	86	60
10	100	0	90	2.35	288	0.117	8667	1.578	88	60
10	100	0	91	1.71	288	0.199	8667	1.578	62	60
10	100	0	91	1.78	288	0.190	8667	1.578	66	60
10	100	0	91	1.85	288	0.182	8667	1.578	69	60
10	100	0	91	1.92	288	0.173	8667	1.578	73	60
10	100	0	91	1.99	288	0.164	8667	1.578	76	60
10	100	0	91	2.06	288	0.155	8667	1.578	79	60
10	100	0	91	2.13	288	0.146	8667	1.578	82	60
10	100	0	91	2.21	288	0.137	8667	1.578	85	60
10	100	0	91	2.28	288	0.127	8667	1.578	88	60
10	100	0	91	2.35	288	0.117	8667	1.578	90	60
10	100	0	92	1.71	288	0.200	8667	1.578	63	60
10	100	0	92	1.78	288	0.191	8667	1.578	66	60
10	100	0	92	1.85	288	0.183	8667	1.578	70	60
10	100	0	92	1.92	288	0.174	8667	1.578	74	60
10	100	0	92	1.99	288	0.165	8667	1.578	77	60
10	100	0	92	2.06	288	0.156	8667	1.578	80	60
10	100	0	92	2.13	288	0.147	8667	1.578	84	60
10	100	0	92	2.21	288	0.137	8667	1.578	87	60
10	100	0	92	2.28	288	0.128	8667	1.578	89	60

193

10	100	0	92	2.35	288	0.118	8667	1.578	91	60
10	100	0	93	1.71	288	0.201	8667	1.578	63	60
10	100	0	93	1.78	288	0.192	8667	1.578	67	60
10	100	0	93	1.85	288	0.184	8667	1.578	71	60
10	100	0	93	1.92	288	0.175	8667	1.578	75	60
10	100	0	93	1.99	288	0.166	8667	1.578	78	60
10	100	0	93	2.06	288	0.157	8667	1.578	82	60
10	100	0	93	2.13	288	0.147	8667	1.578	85	60
10	100	0	93	2.21	288	0.138	8667	1.578	88	60
10	100	0	93	2.28	288	0.128	8667	1.578	90	60
10	100	0	93	2.35	288	0.118	8667	1.578	93	60
10	100	0	94	1.64	288	0.210	8667	1.578	60	60
10	100	0	94	1.71	288	0.201	8667	1.578	64	60
10	100	0	94	1.78	288	0.193	8667	1.578	68	60
10	100	0	94	1.85	288	0.185	8667	1.578	72	60
10	100	0	94	1.92	288	0.176	8667	1.578	75	60
10	100	0	94	1.99	288	0.167	8667	1.578	79	60
10	100	0	94	2.06	288	0.157	8667	1.578	83	60
10	100	0	94	2.13	288	0.148	8667	1.578	86	60
10	100	0	94	2.21	288	0.138	8667	1.578	89	60
10	100	0	94	2.28	288	0.129	8667	1.578	92	60
10	100	0	94	2.35	288	0.119	8667	1.578	94	60
10	100	0	95	1.64	288	0.211	8667	1.578	61	60
10	100	0	95	1.71	288	0.202	8667	1.578	65	60
10	100	0	95	1.78	288	0.194	8667	1.578	69	60
10	100	0	95	1.85	288	0.185	8667	1.578	73	60
10	100	0	95	1.92	288	0.177	8667	1.578	76	60
10	100	0	95	1.99	288	0.168	8667	1.578	80	60
10	100	0	95	2.06	288	0.158	8667	1.578	84	60
10	100	0	95	2.13	288	0.149	8667	1.578	87	60
10	100	0	95	2.21	288	0.139	8667	1.578	90	60
10	100	0	95	2.28	288	0.129	8667	1.578	93	60
10	100	0	95	2.35	288	0.119	8667	1.578	96	60
10	100	0	96	1.64	288	0.212	8667	1.578	61	60
10	100	0	96	1.71	288	0.203	8667	1.578	65	60
10	100	0	96	1.78	288	0.195	8667	1.578	69	60
10	100	0	96	1.85	288	0.186	8667	1.578	73	60
10	100	0	96	1.92	288	0.177	8667	1.578	77	60
10	100	0	96	1.99	288	0.168	8667	1.578	81	60
10	100	0	96	2.06	288	0.159	8667	1.578	84	60
10	100	0	96	2.13	288	0.149	8667	1.578	88	60
10	100	0	96	2.21	288	0.140	8667	1.578	91	60
10	100	0	96	2.28	288	0.130	8667	1.578	94	60
10	100	0	96	2.35	288	0.120	8667	1.578	97	60
10	100	0	97	1.64	288	0.213	8667	1.578	62	60
10	100	0	97	1.71	288	0.204	8667	1.578	66	60
10	100	0	97	1.78	288	0.196	8667	1.578	70	60
10	100	0	97	1.85	288	0.187	8667	1.578	74	60
10	100	0	97	1.92	288	0.178	8667	1.578	78	60
10	100	0	97	1.99	288	0.169	8667	1.578	82	60
10	100	0	97	2.06	288	0.160	8667	1.578	85	60

194

10	100	0	97	2.13	288	0.150	8667	1.578	89	60
10	100	0	97	2.21	288	0.140	8667	1.578	92	60
10	100	0	97	2.28	288	0.130	8667	1.578	95	60
10	100	0	97	2.35	288	0.120	8667	1.578	98	60
10	100	0	98	1.64	288	0.214	8667	1.578	63	60
10	100	0	98	1.71	288	0.205	8667	1.578	67	60
10	100	0	98	1.78	288	0.197	8667	1.578	71	60
10	100	0	98	1.85	288	0.188	8667	1.578	75	60
10	100	0	98	1.92	288	0.179	8667	1.578	79	60
10	100	0	98	1.99	288	0.170	8667	1.578	83	60
10	100	0	98	2.06	288	0.160	8667	1.578	86	60
10	100	0	98	2.13	288	0.151	8667	1.578	90	60
10	100	0	98	2.21	288	0.141	8667	1.578	93	60
10	100	0	98	2.28	288	0.131	8667	1.578	96	60
10	100	0	98	2.35	288	0.121	8667	1.578	99	60
10	100	0	99	1.64	288	0.215	8667	1.578	63	60
10	100	0	99	1.71	288	0.206	8667	1.578	67	60
10	100	0	99	1.78	288	0.198	8667	1.578	72	60
10	100	0	99	1.85	288	0.189	8667	1.578	76	60
10	100	0	99	1.92	288	0.180	8667	1.578	80	60
10	100	0	99	1.99	288	0.171	8667	1.578	84	60
10	100	0	99	2.06	288	0.161	8667	1.578	87	60
10	100	0	99	2.13	288	0.152	8667	1.578	91	60
10	100	0	99	2.21	288	0.142	8667	1.578	94	60
10	100	0	99	2.28	288	0.132	8667	1.578	97	60
10	100	0	99	2.35	288	0.121	8667	1.578	100	60
10	100	0	100	1.64	288	0.216	8667	1.578	64	60
10	100	0	100	1.71	288	0.207	8667	1.578	68	60
10	100	0	100	1.78	288	0.199	8667	1.578	72	60
10	100	0	100	1.85	288	0.190	8667	1.578	76	60
10	100	0	100	1.92	288	0.181	8667	1.578	80	60
10	100	0	100	1.99	288	0.172	8667	1.578	84	60
10	100	0	100	2.06	288	0.162	8667	1.578	88	60
10	100	0	100	2.13	288	0.152	8667	1.578	92	60
10	100	0	100	2.21	288	0.142	8667	1.578	95	60
10	100	0	100	2.28	288	0.132	8667	1.578	98	60
10	100	0	100	2.35	288	0.122	8667	1.578	101	60
10	100	0	100	2.42	288	0.112	8667	1.578	104	60

Appendix F - Report of the Market Search of Electric Motors

F.1 Introduction

The market search reflected in this report was done in February 2015. The aim of the search was to find suitable electric motors for the actuator of the lower body joints of the exoskeleton in the sagittal plane. The average required power was originally estimated by the simulations to be between 140W and 250W. However, a larger range was chosen for the search, which is between 40W (30% of the lower bound) and 4,750W (1,900% of the upper bound).

F.2 Method

A number of search engines and websites were used for the search, as mentioned later. For each of these, a number of search keywords (mentioned below) were used. The first 10 pages of the results of each search were studied to find suitable products and identify their manufacturers. After that, the entire product range of the manufacturers were investigated, and the suitable ones (based on nominal power) were chosen.

F.2.1 The search Engines and Websites used

The first search engines used were google, eBay and Amazon. From the initial search results, the following websites were also found and used for further searches:

- http://www.directindustry.com/
- http://www.usinenouvelle.com/industry/
- http://www.thomasnet.com/
- http://www.globalmarket.com/
- http://www.seekpart.com/equipment-series/dc+motor+flat.html
- http://www.globalspec.com/

F.2.2 The search keywords

The keywords used were as follows:

- Electric motor
- DC motor
- Flat electric motor

- Pancake motor
- Robot motor
- Flat Motor

F.3 Extracting the specifications

Some of the manufacturers provide the numeric values of all required parameters, while others provide numeric values only for some of the parameters, and present graphs that contain information on other required parameters. These graphs are in the form of torque versus velocity curves for a given voltage, similar to the one shown in **Figure 4-13**. Wherever such graphs were presented instead of numeric values, the parameter values were extracted from the graphs using the linear regression method.

F.4 The search Results

The following table contains the motors found with all parameter values. The full list could be found in the DVD enclosed with this thesis.

nominal power	peak torque	rated torque	weight	operation voltage	Viscous damping, D	no load speed	winding resistance	dT/d(omega)(or: -Km^2)	KB (back emf constant)	Km	Kt	stall torque	Max current	A (or: -Kt^2*D/R)	B (or: Kt^2/R*DeltaTmax/TPR)	moment of inertia	model number
W	N.m	N.m	kg	V	N.m.s/rad	rad/s	Ohm	N.m.s/rad	V.s/Rad	SI units	N.m/A	N.m	A			kg.m^2	_
575	1.23	0.2952	0.425	240	4.11587E-05	3711.355984	1.44	-0.004356	0.07878402	0.066	0.097	16.16666667	13.8	-3.41329E-08	0.232371833	1.03E-05	KBM-10X01-C
785	2.48	0.4932	0.703	400	4.93713E-05	1944.20696	5.22	-0.0121	0.251153907	0.11	0.307	23.52490421	8.65	-1.93348E-07	0.787177538	1.49E-05	KBM-10X02-B
850	3.69	0.6244	0.99	240	5.82524E-05	1394.880412	2.34	-0.019044	0.211045679	0.138	0.259	26.56410256	15.5	-4.61421E-07	1.334756121	2.02E-05	KBM-10X03-D
910	4.91	0.9147	1.26	240	6.64651E-05	1047.117241	2.94	-0.026896	0.281712558	0.164	0.345	28.16326531	15.5	-9.44113E-07	1.93494334	2.55E-05	KBM-10X04-D
915	3.59	0.6472	1	400	1.79532E-05	3017.527818	1.29	-0.020449	0.16234283	0.143	0.199	61.70542636	19.4	-6.866E-07	1.426812298	3.36E-05	KBM-14X01-C
975	7.31	1.0462	1.68	240	2.69298E-05	961.7460577	1.69	-0.055225	0.304631545	0.235	0.374	53.11242604	21.8	-3.59669E-06	4.54093461	5.56E-05	KBM-14X02-D
1230	10.5	1.7797	3.08	400	3.59064E-05	12.33870182	1.96	-8.2369	0.406812032	2.87	0.498	101.6326531	24.5	-9.00949E-06	8.180188384	8.81E-05	KBM-14X03-C
855	6.35	0.9022	1.16	240	8.06939E-05	1014.703192	1.56	-0.053824	0.290307178	0.232	0.355	54.61538462	21.8	-3.6342E-06	4.056347086	8.62E-05	KMB-17X01-C
1290	12.8	2.1998	1.97	240	1.16505E-04	637.6565838	1.65	-0.128881	0.461244628	0.359	0.565	82.18181818	24.5	-1.89689E-05	12.38609676	1.28E-04	KMB-17X02-D
1275	19	1.9960	2.76	240	1.52793E-04	725.1358625	0.74	-0.221841	0.405857075	0.471	0.496	160.8648649	48	-4.37297E-05	23.39456069	1.75E-04	KMB-17X03-D
1550	24	2.9604	3.72	240	1.89082E-04	543.9693841	0.94	-0.310249	0.53955117	0.557	0.661	168.7659574	44	-9.0168E-05	35.52483265	2.40E-04	KMB-17X04-D
1025	15	2.3168	2.02	240	2.95082E-04	471.2526042	1.97	-0.198025	0.53955117	0.445	0.766	93.31979695	27.6	-7.37992E-05	21.3258245	4.34E-04	KBM-25X01-C
2545	29.7	6.0759	3.5	480	3.77208E-04	417.712688	3.7	-0.537289	0.53955117	0.733	1.73	224.4324324	22	-0.000176278	75.01101248	6.78E-04	KBM-25X02-B
2605	42.6	9.2136	4.9	240	4.95623E-04	300.4362827	1.06	-0.896809	0.53955117	0.947	1.19	269.4339623	47	-0.000401437	136.2655152	9.31E-04	KBM-25X03-D
1990	54.8	4.0433	6.35	480	5.48146E-04	501.2138774	1.08	-1.2769	0.53955117	1.13	1.44	640	48.5	-0.000743606	209.9444257	1.18E-03	KBM-25X04-D
3885	41.1	8.8334	5.17	480	3.59064E-04	468.9346742	1.75	-0.894916	0.53955117	0.946	1.53	419.6571429	34.7	-0.000306068	152.83247208257600	2.17E-03	KBM-35X01-C
4750	59.4	10.5490	7.21	480	5.72020E-04	441.9368421	1.14	-1.5625	0.53955117	1.25	1.64	690.5263158	49.5	-0.000293161	156.03494120539300	2.94E-03	KBM-35X01-D
259	7.26	1.389564	2.23	75	2.86E-05	218.461	1.69	-0.03996287	0.225370046	0.199907153	0.39	17.30769231	22	-0.000003346709	4.368698985	0.00005900000000000	AKM32H
nominal power	14.82637652	2.84	8.4	50	0.000488785470	134.67	0.94	-0.163174942	0.372434	0.40394918	0.4118	21.90658469	36	-0.00008819734	19.78808503965	6.28E-04	GM16H
W	6.505726209	1.26	3.6	64	0.000120974417	349.642	0.75	-0.04256846	0.176667	0.20632125	0.1807	15.42098064	36	-0.00000526767	3.24328610519	0.0001624	GM12H
236	10.22	1.956108	2.9	75	5.09E-05	162.027	1.96	-0.064158383	0.299856756	0.253295051	0.52	19.89795918	22.48	-0.000036986510	8.467245488		AKM33H

nominal power	peak torque	rated torque	weight	operation voltage	Viscous damping, D	no load speed	winding resistance	dT/d(omega)(or: -Km^2)	KB (back emf constant)	Km	Kt	stall torque	Max current	A (or: -Kt^2*D/R)	B (or: Kt^2/R*DeltaTmax/TPR)	moment of inertia	model number
W	N.m	N.m	kg	V	N.m.s/rad	rad/s	Ohm	N.m.s/rad	V.s/Rad	SI units	N.m/A	N.m	A			kg.m^2	_
208	6.36	1.217304	2.44	75	1.15E-04	230.087	1.56	-0.031980895	0.213910552	0.17883203	0.37	17.78846154	22.4	-0.000019382071	4.254323548	0.00008100000000000	AKM41H
280	7.416	0.9	4.6	24	0.0000006589507	331.7424	0.12	-0.043407174	0.07234529	0.208343883	0.072	14.4	103	-0.00000002846667	0.79901807129203	9.20E-04	GNM 8035/4
500	10.05	1.6	6.6	24	0.0000000000000	360.8237143	0.098	-0.045474182	0.066514475	0.213246763	0.067	16.40816327	150	-2.3635981E-21	2.55692892160000	1.55E-03	GNM 8070/4
495	2.531	1.011	1.63	90	9.04000000000E-05	685.8942	0.621	-0.02699409	0.127964348	0.164298781	0.131	18.98550725	19.32061069	-2.4981552E-06	3.25125418200949	0.00002118450000	BL3407-134
725	3.8	1.55	2.49	90	1.59200000000E-04	628.3000	0.25	-0.080308133	0.139423842	0.283386896	0.144	51.84	26.38888889	-1.3204685E-05	10.55104111949720	0.00004943050000	BL3415-146
880	4.94	1.976	3.31	90	2.24800000000E-04	586.4133	0.175	-0.131936973	0.149928378	0.363231294	0.154	79.2	32.07792208	-3.0464896E-05	17.40793624728160	0.00007061500000	BL3423-157
1040	6.84	2.736	3.63	90	2.50400000000E-04	523.5833	0.18	-0.163393283	0.169027535	0.404219351	0.174	87	39.31034483	-4.2117280E-05	21.46494552769670	0.00009179950000	BL3430-177
1000	7.98	2.96	3.97	24	2.77600000000E-04	534.0550	0.014	-0.149041632	0.045360497	0.386059104	0.046	78.85714286	173.4782609	-4.1957257E-05	19.62517256091740	0.00011298400000	BL3438-046
154	3.673191401	0.49	1.8	45	0.000044198262	586.706	0.85	-0.007840837	0.072577	0.08854850	0.0918	4.861576854	40	-0.00000043848	0.30646252966	0.000039	GN9
344	5.583855844	1.1	2.8	60	0.000120077474	442.771	0.75	-0.025062030	0.134649	0.15830992	0.1396	11.16771169	40	-0.00000311996	1.71542123183	0.0001624	GN12
800	13.12211747	2.55	5.3	60	0.000257602745	205.422	1	-0.093983015	0.286487	0.30656649	0.3281	19.6831762	40	-0.00002772288	11.15119080684	6.28E-04	GN16
420	6.192600322	1.33	5.1	60	0.000106904312	345.4	0.950	-0.027700885	0.169982	0.16643583	0.1548	9.778	40	-2.69710428E-06	1.42635282E+00	1.62400000E-04	GR12-no fan
420	6.192600322	1.33	5.1	60	0.000221915476	345.4	0.950	-0.027700885	0.169982	0.16643583	0.1548	9.778	40	-5.59873749E-06	5.19652466E+00	1.62400000E-04	GR12-with fan
1050	14.69035762	3.34	7.6	100	0.000220077145	278.0	0.950	-0.143978475	0.372434	0.37944496	0.3673	38.659	40	-3.12461196E-05	1.40421687E+01	6.28400000E-04	GR16-no fan
1050	14.69035762	3.34	7.6	100	0.000511071877	278.0	0.950	-0.143978475	0.372434	0.37944496	0.3673	38.659	40	-7.25609787E-05	6.75380995E+01	6.28400000E-04	GR16-with fan
553	8.254491444	1.7	3.2	72	0.000205308533	327.414	0.85	-0.058991382	0.218685	0.24288141	0.2293	19.422	36	-0.000012698830	4.30495644E+00	0.0006284	GPN16
324	3.32637009	1	3.2	48	0.000282883862	501.069	0.425	-0.020761720	0.095496	0.14408928	0.0924	10.436	36	-0.000005682708	1.724587295	0.0006284	GPN16LR
300	3.057844089	0.96	2.2	60	0.000180856940	533.405	0.85	-0.011260563	0.112685	0.10611580	0.0849	5.996	36	-0.000001535119	1.265035198	0.0006284	GPM16
221	2.90577204	0.73	2.2	36	0.000064826607	531.732	0.42	-0.011562041	0.060162	0.10752693	0.0807	6.918504857	36	-0.000001005593	0.751498978	0.0006284	GPM16LR
200	3.578927926	0.64	1.2	48	0.000104898512	495.519	1	-0.009588618	0.096451	0.09792149	0.0994	4.771903901	36	-0.000001036741	0.561815776	1.624E-04	GPN12
190	1.706734261	0.48	1.2	30	0.000073631460	626.21	0.45	-0.005030430	0.047748	0.07092552	0.0474	3.160619003	36	-0.00000036777	0.30441229434	1.624E-04	GPN12LR
110	3	0.35	0.8	23.5	0.000064405106	452.582	1	-2.5851999292E-03	0.050690195	0.05084486	0.051	1.1985	36	-0.00000016752	0.14899675237	1.62E-04	GPM12

nominal power	peak torque	rated torque	weight	operation voltage	Viscous damping, D	no load speed	winding resistance	dT/d(omega)(or: -Km^2)	KB (back emf constant)	Km	Kt	stall torque	Max current	A (or: -Kt^2*D/R)	B (or: Kt^2/R*DeltaTmax/TPR)	moment of inertia	model number
W	N.m	N.m	kg	V	N.m.s/rad	rad/s	Ohm	N.m.s/rad	V.s/Rad	SI units	N.m/A	N.m	A			kg.m^2	_
64	2	0.2	0.8	12	0.000063774365	494.516	0.45	-1.1105421619E-03	0.022715635	0.03332480	0.022	0.586666667	36	-0.00000006859	0.06772544544	1.62E-04	GPM12LR
94	3	0.3	0.65	22.5	0.000032428695	457.057	1.1	-2.1083524491E-03	0.04831641	0.04591680	0.048	0.981818182	36	-0.00000006792	0.10647103154	3.90E-05	GPN9
75	2.5	0.25	0.65	12	0.000032847277	483.509	0.42	-1.3732768272E-03	0.024032344	0.03705775	0.024	0.685714286	36	-0.00000004505	0.06913002109	3.90E-05	GPN9LR
41	1.3	0.131	0.7	14.5	0.000028105019	594.836	1.1	-4.7083670531E-04	0.023541835	0.02169877	0.022	0.29	36	-0.00000001237	0.01954842198	3.90E-05	GPM9
39	1	0.1	0.7	9	0.000029996049	731.628	0.42	-2.9061668120E-04	0.011624667	0.01704748	0.0105	0.225	36	-0.00000000787	0.01229339828	3.90E-05	GPM9LR
890	14.82637652	2.84	8.4	50	0.000488785470	134.67	0.94	-0.163174942	0.372434	0.40394918	0.4118	21.90658469	36	-0.00008819734	19.78808503965	6.28E-04	GM16H
396	6.505726209	1.26	3.6	64	0.000120974417	349.642	0.75	-0.04256846	0.176667	0.20632125	0.1807	15.42098064	36	-0.00000526767	3.24328610519	0.0001624	GM12H
197	3.0186774	0.57	2	48	0.000064977421	564.331	0.85	-0.008290145	0.084036	0.09105023	0.0839	4.735180236	36	-0.00000053749	0.64675520330	0.000039	GM9H
480	50.000	1.700	4.900	60	0.000861281177	314	0.741	-0.054114277	0.200500000	0.232625	0.200	16.194	250.000	-4.64913794140E-05	4.83704726021E+00	4.90000000000E-04	SL 140-2NFB, coil: 6/71
360	77.5	2	4.9	60	0.000733729182	209	1.503	-0.063025357	0.305586503	0.251049	0.310	12.375	250	-4.69E-05	5.690011534	0.00049	SL 140-2NFB, coil: 9/60
330	100	1.85	4.9	80	0.000926244908	210	2.653	-0.060478878	0.401082286	0.245925	0.400	12.063	250	-5.59E-05	5.4118583	0.00049	SL 140-2NFB, coil: 12/50
370	125	2.2	4.9	96	0.000828001648	202	3.786	-0.066845076	0.506127646	0.258544	0.500	12.679	250	-5.47E-05	5.403669477	0.00049	SL 140-2NFB, coil: 15/47.5
320	57.500	1.350	1.900	60	0.000507639	275	1.329	-0.039666	0.229189877	0.199164	0.230	10.384	250.000	-2.02073469460E-05	2.57086879162E+00	3.50000000000E-04	SL 120-2NFB, coil: 15/63
600.000	57.500	2.500	5.500	60.000	0	275.000	0.627	-0.084033810	0.22918988	0.28988586	0.230	21.999	250.000	-0.0000959372286	9.728804915466320	0.001130000	SL 160-2NFB, coil: 6/80
460	87.5	2.45	5.5	72	0.000959655	220	1.575	-0.076394373	0.343785	0.27639532	0.35	16.000	250	-7.46376030E-05	9.567193517363280	0.0011300000	SL 160-2NFB, coil: 9/63
570	115	3	5.5	96	0.001090229	221	2.263	-0.093166617	0.458380	0.30523207	0.46	19.512	250	-1.02E-04	11.5836444	0.0011300000	SL 160-2NFB, coil: 12/60
295	35	0.75	1.8	60	0.000386495	445.05	1.313	-0.015279325	0.143244	0.12360957	0.14	6.400	250	-5.77166200E-06	9.56677420E-01	3.50000000E-04	SL 120-1NFB, coil: 15/63
250	40	0.75	1.8	60	0.000379428	390	1.972	-0.013171832	0.162343	0.11476860	0.16	4.868	250	-4.92564338E-06	8.28423062E-01	3.50000000E-04	SL 120-1NFB, coil: 17/56
190	52.5	0.8	1.8	60	0.000360708	301.1	3.465	-0.012732771	0.210091	0.11283958	0.21	3.636	250	-4.59083358E-06	8.08477310E-01	3.50000000E-04	SL 120-1NFB, coil: 22/47.5

W	N.m	N.m	kg	V	N.m.s/rad	rad/s	Ohm	N.m.s/rad	V.s/Rad	SI units	N.m/A	N.m	A			kg.m^2	
190.3	3.6	0.6	3.3	39.4	2.86E-05	396.7150641	1	-0.009832246	0.099315614	0.099157681	0.099	3.9006	20	-9.22E-08	0.3419871	0.00015000000000000	MSS-2
397	7.58	1.26	4.5	67	8.59E-05	389.7787037	1.25	-0.023652395	0.171892408	0.153793353	0.172	9.2192	16	-3.24E-07	1.600878383	0.00037000000000000	MSS-4
575	11	1.83	5.8	67.8	1.72E-04	373.6731579	0.75	-0.043787999	0.181441986	0.209255823	0.181	16.3624	20	-1.46E-06	3.216272724	0.00040000000000000	MSS-6
805	15.38	2.56	8	89.7	2.01E-04	357.1515209	0.82	-0.076877598	0.251153907	0.277268099	0.251	27.45695122	20	8.25E-08	6.282477717	0.00082000000000000	MSS-8
1240	23.7	3.95	10	106.7	1.91E-04	362.180497	0.75	-0.115877765	0.294604488	0.340408233	0.295	41.96666667	30	-5.79E-06	15.11259952	0.00170000000000000	MSS-12
310	6	1	2.4	120	0.0002619671702	522.859	9.5	-0.017023349	0.286487347	0.130473556	0.5	6.315789474	12	-0.00000689387290	1.69595761187939	0.00008600000000	HV 10 S-300
630	12	2	3.2	140	0.0002697629981	472.737	4.7	-0.053712671	0.362883973	0.231759943	0.64	19.06382979	18.75	-0.00002350955830	6.50633949717611	0.00016400000000	HV 10 L-300
1250	24	4	6.6	150	0.0002343888924	469.045	1.55	-0.123903772	0.401082286	0.351999676	0.7	67.74193548	34.28571429	0.00007409713372	26.32373210707370	0.00065600000000	HV 13 S-300
2500	48	8	9.6	150	0.0004732004507	418.436	0.55	-0.55616108	0.401082286	0.74576208	0.7	190.9090909	68.57142857	0.00042157858335	105.46909793157800	0.00117500000000	HV 13 L-300
3750	60	12	13.1	165	0.0004017208616	418.147	0.4	-0.793411259	0.448830177	0.890736358	0.78	321.75	76.92307692	0.00061101743047	227.70384642020200	0.00324000000000	HV 16 S-300
5600	90	18	16.8	165	0.0003508882322	418.867	0.22	-1.081257162	0.448830177	1.039835161	0.78	585	115.3846154	0.00097036545657	423.25792897991700	0.00452000000000	HV 16 L-300
310	6	1	2.4	306	0.0003207197208	518.507	33.2	-0.017683432	0.503262773	0.132979068	0.87	8.018674699	6.896551724	-0.00000731183002	1.69304221692228	0.00008600000000	HV 10 S-600
630	12	2	3.2	318	0.0003140125840	473.219	14.3	-0.053273500	0.593983766	0.230810529	1.03	22.9048951	11.65048544	-0.00002329622031	6.83642314034846	0.00016400000000	HV 10 L-600
1250	24	4	6.6	318	0.0003675305574	473.469	5.4	-0.116313857	0.643641572	0.341048173	1.11	65.36666667	21.62162162	0.00008385822219	27.15157815194000	0.00056500000000	HV 13 S-600
2500	48	8	9.6	314	0.0004912792347	420.115	1.8	-0.53990245	0.675155181	0.734780547	1.17	204.1	41.02564103	0.00037361785800	102.26432589550100	0.00117500000000	HV 13 L-600
3750	60	12	13.1	314	0.0007396962199	417.304	1.3	-0.849767474	0.671335349	0.921828332	1.14	275.3538462	52.63157895	-0.00073946862107	229.35567763793200	0.00324000000000	HV 16 S-600
5600	90	18	16.8	308	0.0002834035532	420.129	0.7	-1.046039366	0.747731975	1.022760659	1.29	567.6	69.76744186	-0.00067373121838	426.16527830918900	0.00452000000000	HV 16 L-600
109	3.199	0.353	1.7	23	0.0000572974694	101.9896701	0.85	-0.002696351	0.047747891	0.051926405	0.048	0.275	72	-0.00000015531	0.27105882352941	3.95E-05	platinum U9D-A
133	3.849	0.424	1.7	26	0.0000572974694	88.2283845	0.85	-0.003842301	0.057297469	0.061986296	0.057	0.339	72	-0.00000021901	0.38223529411765	3.95E-05	platinum U9D-B
142	4.103	0.459	1.7	27	0.0000668470476	82.078125	0.85	-0.004386065	0.061117301	0.066227374	0.061	0.36	72	-0.00000029263	0.43776470588235	3.95E-05	platinum U9D-C
179	5.134	0.565	1.7	32	0.0000763966258	67.19606497	0.85	-0.006830757	0.076396626	0.082648395	0.076	0.459	72	-0.00000051914	0.67952941176471	3.95E-05	platinum U9D-D
W	N.m	N.m	kg	V	N.m.s/rad	rad/s	Ohm	N.m.s/rad	V.s/Rad	SI units	N.m/A	N.m	A			kg.m^2	
190.3	3.6	0.6	3.3	39.4	2.86E-05	396.7150641	1	-0.009832246	0.099315614	0.099157681	0.099	3.9006	20	-9.22E-08	0.3419871	0.00015000000000000	MSS-2

W	N.m	N.m	kg	V	N.m.s/rad	rad/s	Ohm	N.m.s/rad	V.s/Rad	SI units	N.m/A	N.m	A			kg.m^2	
190	5.459	0.6	1.7	33	0.0000859462040	62.95927984	0.85	-0.007735158	0.081171415	0.087949749	0.081	0.487	72	-0.00000066340	0.77188235294118	3.95E-05	platinum U9D-E
170	4.88	0.53	1.7	30	0.0000763966258	70.27039474	0.85	-0.006233066	0.072576795	0.078949768	0.073	0.438	72	-0.00000047896	0.62694117647059	3.95E-05	platinum U9D-F
94	2.909	0.318	1.7	22	0.0000763966258	105.5444664	0.85	-0.002273923	0.04392806	0.04768567	0.044	0.24	71	-0.00000017400	0.22776470588235	5.86E-05	platinum U9DT-A
123	3.728	0.388	1.7	25.1	0.0000763966258	93.26769149	0.85	-0.003334488	0.053477638	0.057745026	0.053	0.311	71	-0.00000025247	0.33047058823529	5.86E-05	platinum U9DT-B
128	3.863	0.428	1.7	25.7	0.0000763966258	90.68332027	0.85	-0.003583901	0.055387554	0.059865687	0.055	0.325	71	-0.00000027188	0.35588235294118	5.86E-05	platinum U9DT-C
165	4.936	0.53	1.7	30.1	0.0000763966258	71.83077021	0.85	-0.005902763	0.070666879	0.07682944	0.071	0.424	71	-0.00000045308	0.59305882352941	5.86E-05	platinum U9DT-D
187	5.614	0.6	1.7	32.9	0.0000763966258	64.50515501	0.85	-0.007549784	0.080216457	0.086889494	0.08	0.487	71	-0.00000057522	0.75294117647059	5.86E-05	platinum U9DT-E
160	4.802	0.508	1.7	29.6	0.0000763966258	73.4576456	0.85	-0.005581448	0.068756963	0.074709086	0.069	0.41	71	-0.00000042791	0.58252235294118	5.86E-05	platinum U9DT-F
275	9.074	0.918	3.1	43.3	0.0001241445170	45.82659768	0.75	-0.017871717	0.115549897	0.133685143	0.116	0.819	84	-0.00000222732	1.86589866666667	1.34E-04	U12D-A
298	9.907	0.953	3.1	46	0.0001527932516	42.35698503	0.75	-0.021177145	0.126054433	0.145523691	0.126	0.897	84	-0.00000323433	2.20147200000000	1.34E-04	U12D-B
325	10.882	1.059	3.1	49	0.0001718924081	38.81738506	0.75	-0.025478275	0.138468884	0.159619155	0.138	0.989	84	-0.00000436469	2.64076800000000	1.34E-04	U12D-C
362	12.315	1.13	3.1	55	0.0002100907210	34.25416052	0.75	-0.032784339	0.156613083	0.18106446	0.157	1.123	84	-0.00000690470	3.41799466666667	1.34E-04	U12D-D
387	13.368	1.236	3.1	59	0.0002387394557	31.71606907	0.75	-0.038529365	0.169982492	0.196288983	0.17	1.222	84	-0.00000919943	4.00746666666667	1.34E-04	U12D-E
380	13.664	1.236	3.1	59	0.0002578386121	30.65313566	0.75	-0.040322139	0.173802324	0.200803733	0.174	1.236	84	-0.00001040843	4.19827200000000	1.34E-04	U12D-F
250	8.319	0.812	3.1	40	0.0001145949387	49.46140362	0.75	-0.014981378	0.106000318	0.122398441	0.106	0.741	84	-0.00000171678	1.55805866666667	1.84E-04	U12DT-A
276	9.229	0.883	3.1	43	0.0001336940952	45.07815649	0.75	-0.018323731	0.117459812	0.135365175	0.117	0.826	84	-0.00000244018	1.89820800000000	1.84E-04	U12DT-B
301	10.133	0.953	3.1	47	0.0001527932516	41.08392908	0.75	-0.022174121	0.128919306	0.148909773	0.129	0.911	84	-0.00000339018	2.30755200000000	1.84E-04	U12DT-C
341	11.637	1.095	3.1	52	0.0001909915645	36.0163252	0.75	-0.029208977	0.148018463	0.170906339	0.148	1.052	84	-0.00000557797	3.03735466666667	1.84E-04	U12DT-D
373	12.916	1.165	3.1	57	0.0002291898774	32.63115074	0.75	-0.0359166	0.164252746	0.189516755	0.164	1.172	84	-0.00000821905	3.72957866666667	1.84E-04	U12DT-E
390	13.671	1.236	3.1	60	0.0002578386121	30.82673756	0.75	-0.040322139	0.173802324	0.200803733	0.174	1.243	84	-0.00001040843	4.19827200000000	1.84E-04	U12DT-F
85	0.95	0.2	0.6	21.3	0.0000105045360	186.3956667	1.2	-0.001072986	0.033423524	0.03275647	0.033	0.2	30	-0.00000000953	0.02949375	1.00E-05	DC-Pancake Servomotor U06FNC 24V80W
W	N.m	N.m	kg	V	N.m.s/rad	rad/s	Ohm	N.m.s/rad	V.s/Rad	SI units	N.m/A	N.m	A			kg.m^2	_
190.3	3.6	0.6	3.3	39.4	2.86E-05	396.7150641	1	-0.009832246	0.099315614	0.099157681	0.099	3.9006	20	-9.22E-08	0.3419871	0.00015000000000000	MSS-2

202

W	N.m	N.m	kg	V	N.m.s/rad	rad/s	Ohm	N.m.s/rad	V.s/Rad	SI units	N.m/A	N.m	A			kg.m^2	
41	1.2	0.131	0.54	14.5	0.0000372433551	205.6844767	0.905	-0.000782752	0.022918988	0.027977711	0.023	0.161	65	-0.00000002177	0.030154345	3.72E-05	DC-Pancake Servomotor U 09 FS
94	2	0.3	0.54	23	0.0000286487347	250.3984933	0.905	-0.000782752	0.047747891	0.027977711	0.048	0.196	65	-0.00000007294	0.13133386	3.88E-05	DC-Pancake Servomotor U 09 FN
110	3	0.35	1.2	24	0.0000410631864	117.4921	0.86	-0.001872466	0.050612765	0.043272004	0.051	0.22	70	-0.00000012419	0.393174419	1.34E-04	DC-Pancake Servomotor U 12 FS
220	6	0.7	1	38	0.0000410631864	329.8575	0.86	-0.002273709	0.113639981	0.047683426	0.114	0.75	70	-0.00000062053	1.964511628	1.34E-04	DC-Pancake Servomotor U 12 FN
300	7.6	0.96	2.3	43.3	0.0000945408244	158.3316	0.85	-0.005305321	0.112685023	0.072837636	0.112	0.84	65	-0.00000139520	1.918494118	6.28E-04	DC-Pancake Servomotor U 16 FS
534	13.6	1.7	2.3	76	0.0002387394557	170.8976	0.85	-0.007957982	0.218685341	0.089207521	0.219	1.36	65	-0.00001347080	7.335211765	6.28E-04	DC-Pancake Servomotor U 16 FN
43	1.44	0.137	0.6	17.3	0.0000105045360	114.633335	1.2	-0.001072986	0.030081171	0.03275647	0.03	0.123	45	-0.00000000788	0.046428571	6.00E-06	DC-Servomotor KN 06 M4
141	4.89	0.45	1.4	30	0.0000697119211	45.02816667	0.85	-0.009549578	0.072576795	0.097721943	0.073	0.43	79	-0.00000043705	0.388106443	3.96E-05	DC-Servomotor KN 09 M4
132	4.58	0.42	1.4	28	0.0000744867102	13.40373333	0.85	-0.029842432	0.067802005	0.172749622	0.068	0.4	79	-0.00000040521	0.3536	5.68E-05	DC-Servomotor KN 09 M4 T
426	14.38	1.36	2.8	46	0.0001814419863	57.652808	0.75	-0.021508059	0.1403788	0.146656262	0.14	1.24	92	-0.00000474168	2.123333333	1.34E-04	DC-Servomotor KN 12 M4 T
401	13.52	1.28	2.8	46	0.0001623428299	57.187866	0.75	-0.021508059	0.137513926	0.146656262	0.138	1.23	92	-0.00000412221	2.0631	1.84E-04	DC-Servomotor KN 12 M4 T
1000	35	3.2	7.9	128	0.0006207225848	22.12139583	0.94	-0.146916588	0.383893045	0.383296997	0.384	3.25	100	-0.00009737156	24.56970008	5.95E-04	DC-Servomotor KN 16 M4
910	32.8	2.9	6	115	0.0009358586662	50.7823475	0.94	-0.06006024	0.310361292	0.245071909	0.31	3.05	100	-0.00009567661	16.01256088	8.93E-04	DC-Servomotor KN 16 M4 T
104	3.1	0.33	2.1	24	0.0000515677224	81.710415	0.85	-0.003304352	0.046315454	0.057483496	0.0463	0.27	67	-0.00000013005	0.273215392	3.90E-05	U9M4
93	2.87	0.3	2.2	24	0.0000563425115	85.19748	0.85	-0.002816985	0.042973102	0.053075274	0.043	0.24	67	-0.00000012256	0.235656863	5.80E-05	U9M4T
258	8.7	0.82	3.7	44	0.0001222346013	39.87610667	0.75	-0.020062139	0.110775107	0.141640881	0.11	0.8	79	-0.00000197205	2.207719298	1.34E-04	U12M4
W	N.m	N.m	kg	V	N.m.s/rad	rad/s	Ohm	N.m.s/rad	V.s/Rad	SI units	N.m/A	N.m	A			kg.m^2	
190.3	3.6	0.6	3.3	39.4	2.86E-05	396.7150641	1	-0.009832246	0.099315614	0.099157681	0.099	3.9006	20	-9.22E-08	0.3419871	0.00015000000000000	MSS-2
235	7.9	0.75	3.9	44	0.0001336940952	43.113946	0.75	-0.016931876	0.101225529	0.130122543	0.101	0.73	79	-0.00000181842	1.861235088	1.84E-04	U12M4T

W	N.m	N.m	kg	V	N.m.s/rad	rad/s	Ohm	N.m.s/rad	V.s/Rad	SI units	N.m/A	N.m	A		kg.m^2	_
645	21	2.07	8.4	82	0.0004106318638	14.4980225	0.88	-0.134501102	0.222505173	0.366743919	0.223	1.95	95	-0.00002320490	10.49475649	5.90E-04	U16M4
620	19.4	1.98	8.7	82	0.0004392805984	15.45618	0.88	-0.116458271	0.205315932	0.341259829	0.205	1.8	95	-0.00002097814	8.868912338	7.90E-04	U16M4T
125	4	0.4	1.6	17	0.0000802164571	67.73074	0.34	-0.006201025	0.028648735	0.078746586	0.029	0.42	135	-0.00000019842	0.267965686	4.70E-05	DC-Servomotor KN 09 M4 LR
115	3.7	0.37	1.6	17	0.0000754416680	60.3168	0.34	-0.006631652	0.025974853	0.081434953	0.0266	0.4	125	-0.00000015700	0.225448039	6.80E-05	DC-Servomotor KN 09 M4 LR T
250	7.2	0.8	2.8	24	0.0001547031673	32.0433	0.31	-0.026526606	0.058252427	0.162869906	0.059	0.85	130	-0.00000173717	1.758764089	1.44E-04	DC-Servomotor KN 12 M4 LR
700	15.05	2.15	6	24	0.0005920738501	51.89758	0.05	-0.045474182	0.066847048	0.213246763	0.095	2.36	245	-0.00010686933	28.27108434	5.95E-04	DC-Servomotor KN 16 M4 LR
390	13.58	1.24	3.6	63	0.0001871717332	37.33149167	0.95	-0.030805091	0.169982492	0.175513792	0.17	1.15	80	-0.00000569396	3.954736842	1.20E-04	JR12M4CH
970	37.47	3.1	7.9	130	0.0006111730065	22.2575275	0.94	-0.146916588	0.372433551	0.383296997	0.372	3.27	100	-0.00008997507	27.34030395	5.90E-04	JR16M4CH
3000	97	9.58	23	140	0.0011459493872	15.380784	0.31	-0.530532124	0.415406653	0.728376361	0.411	8.16	238	-0.00062443521	177.0945968	3.25E-03	JR24M4CH
4250	134	13.53	32	155	0.0012223460131	11.50836167	0.22	-0.954957823	0.458379755	0.977219434	0.458	10.99	290	-0.00116547359	413.1715152	4.94E-03	JR25M8CH
171.5	0.82	0.204719083	0.32	340	0.0000256000000	16806.72269	0.7	-0.001156	0.032468566	0.034	0.04	19.42857143	28.8	-5.8514286E-08	0.08486562942008	1.11E-05	S-50-39
224.1	1.31	0.26750756	0.48	340	0.0000384000000	10577.77778	0.9	-0.0025	0.060162343	0.05	0.07	26.44444444	27.6	-2.0906667E-07	0.23603082851638	1.70E-05	S-50-52
353.2	2.26	0.421613879	0.9	340	0.0000320000000	5465.96755	1.4	-0.005776	0.12700939	0.076	0.13	31.57142857	25.2	-3.8628571E-07	0.67063492063492	3.40E-05	S-50-86
277.2	2.56	0.529428617	0.64	340	0.0000512000000	2223.076923	2.6	-0.01	0.185261818	0.1	0.17	22.23076923	16	-5.6910769E-07	0.45554854981085	1.06E-04	S-76-35
508.2	6.41	1.213273914	2.2	340	0.0001360000000	1697.824662	2.5	-0.032041	0.362883973	0.179	0.4	54.4	22.8	-8.7040000E-06	5.16129032258065	4.20E-04	S-76-85
342.8	11.43	2.182396944	4.3	340	0.0003040000000	537.755102	10	-0.0784	1.13162502	0.28	1.24	42.16	13.1	-4.6743040E-05	16.01666666666670	8.30E-04	S-76-149
986.9	9.42	2.356119688	1.87	340	0.0001096000000	1521.639628	1.4	-0.070225	0.358109184	0.265	0.44	106.8571429	30.4	-1.5156114E-05	14.40476190476190	1.60E-03	S-130-39
875.9	16.73	4.182237784	3.6	340	0.0002480000000	743.5299322	2	-0.198916	0.71048862	0.446	0.87	147.9	27.2	-9.3855600E-05	39.42187500000000	3.00E-03	S-130-60
924.9	23.55	5.888269935	5.3	340	0.0003840000000	514.8574823	2.5	-0.343396	1.063823014	0.586	1.3	176.8	25.6	-2.5958400E-04	70.41666666666670	4.70E-03	S-130-81
805.1	30.75	7.688365431	7	340	0.0005200000000	380.7488274	3.1	-0.5041	1.433391692	0.71	1.75	191.9354839	24.8	-5.1370968E-04	102.90658602150500	6.20E-03	S-130-102
W	**N.m**	**N.m**	**kg**	**V**	**N.m.s/rad**	**rad/s**	**Ohm**	**N.m.s/rad**	**V.s/Rad**	**SI units**	**N.m/A**	**N.m**	**A**		**kg.m^2**	**_**
190.3	3.6	0.6	3.3	39.4	2.86E-05	396.7150641	1	-0.009832246	0.099315614	0.099157681	0.099	3.9006	20	-9.22E-08	0.3419871	0.00015000000000	MSS-2
679.5	34.61	8.651917874	8.7	340	0.0006560000000	300.8523229	3.7	-0.665856	1.785771128	0.816	2.18	200.3243243	22.4	-8.4258768E-04	133.79504504504500	7.80E-03	S-130-123

627.7	23.98	5.994270253	4.24	340	0.0002992000000	422.9697452	3.2	-0.394384	1.283463314	0.628	1.57	166.8125	21.6	-2.3046815E-04	80.23763020833330	7.40E-03	S-180-44
1164.3	44.47	11.11857393	8.1	340	0.0006080000000	429.2894448	1.1	-1.108809	1.259589368	1.053	1.54	476	40.8	-1.3108480E-03	224.58333333333300	1.48E-02	S-180-69
96	1.07	0.229189877	0.6	340	0.0000080000000	4155.53093	5.8	-0.002116	0.123189559	0.046	0.15	8.793103448	9.8	-3.1034483E-08	0.14403379993172	1.96E-05	BMS35
112	1.31	0.26738819	1.1	340	0.0000480000000	3238.095238	8.4	-0.0025	0.181441986	0.05	0.2	8.095238095	9.2	-2.2857143E-07	0.17680339462518	1.96E-05	BMS60
133	2.26	0.423364635	1.5	340	0.0000800000000	1733.986128	12.9	-0.005776	0.381983129	0.076	0.38	10.01550388	8.4	-8.9550388E-07	0.41561132857472	3.71E-05	BMS100
381	6.41	1.212796435	3.6	340	0.0002480000000	1116.989909	5.7	-0.032041	0.544325959	0.179	0.6	35.78947368	15.2	-1.5663158E-05	2.34497133923919	4.66E-04	BMS280
457	11.43	2.182078625	5	340	0.0003600000000	808.2096475	4.4	-0.0784	0.75441668	0.28	0.82	63.36363636	19.6	-5.5014545E-05	5.67394239423942	9.28E-04	BMS465
129	1.84	0.205315932	1.2	72	0.0000560000000	1209.372638	0.9	-0.003969	0.060162343	0.063	0.06	4.8	30.66666667	-2.2400000E-07	0.14851485148515	3.80E-05	1035
146	2.52	0.23237307	1.6	72	0.0000880000000	1020.408163	0.7	-0.007056	0.06589209	0.084	0.07	7.2	36	-6.1600000E-07	0.25990099009901	5.70E-05	1050
200	5.22	0.381983129	3.7	104	0.0002560000000	644.3148688	1.4	-0.0196	0.173802324	0.14	0.17	12.62857143	30.70588235	-5.2845714E-06	0.76644271570014	3.50E-04	1135
220	7.1	0.700302403	4.1	137	0.0002880000000	658.4006151	1.8	-0.0289	0.247334076	0.17	0.25	19.02777778	28.4	-1.0000000E-05	1.28919141914191	9.20E-04	1210

Appendix G - The dynamic model of the exoskeleton

G.1 Exoskeleton Gait Model

Figure 7-6 shows a simplified CAD model of the exoskeleton, and **Figure 7-7** show the variables of the model.
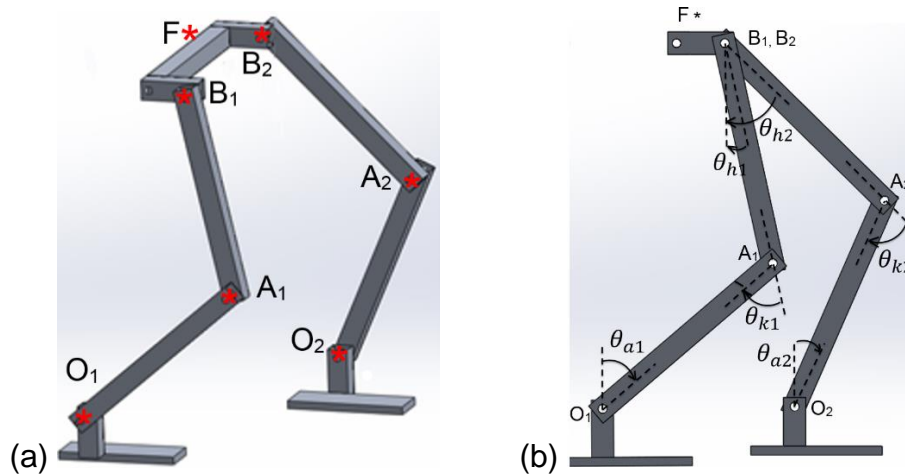
Figure 7-6. The simplified CAD model of the lower body exoskeleton. **The red points in the 3D view (a), designated by O, A and B (with subscripts 1 and 2 for the two legs) are located at the joints. The joint angles have been shown in the side view (b).**

The gait has been divided into three phases. The first stage, named the *single-limb stance* phase, begins with the "toe-off" of the swing leg, which is the leg on which all points are denoted by subscript "2" in **Figure 7-7**. The single-limb stance phase ends with the "heel-strike" of the swing leg, which is the leg on which all points are denoted by subscript "1" in **Figure 7-7**. Modelling of the motion in this phase of the gait cycle has been explained in section G.1.1. In the second phase, as in the previous, the stance foot is still fixed to the ground, while the heel of the swing foot is assumed to be pivoted to the ground. In the third stage, both feet are fixed to the ground. The second and third stages are both *double-limb support* phases, and are both explained in section G.1.2.
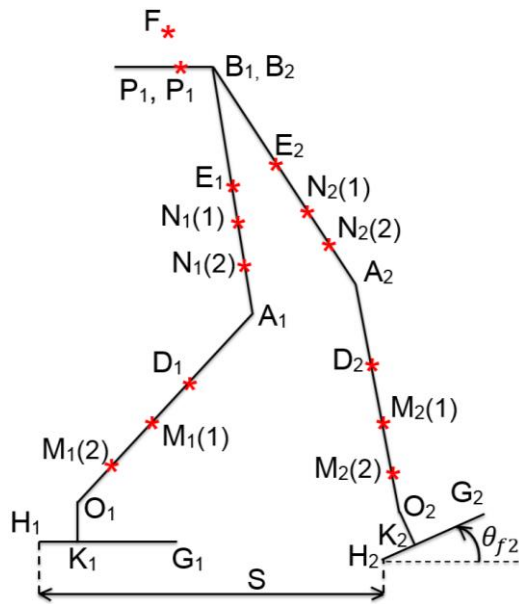
Figure 7-7. The location of the significant points in the exoskeleton model. The points designated by N, M and P (with subscripts 1 and 2 for the two legs) show the location of the mass points added to the model to factor in the mass of the motors, transmission mechanisms and other components of the actuators. S is the length of the stride.

The inputs of the simulation are the kinematic data obtained from motion capture experiments, as explained in the following: a human subject performed the intended motions, while a number of cameras were recording the location of markers placed on certain points on the subject's body. The markers were located on the lower back and the foot of the user, which are the points were there would be a connection between the user and the exoskeleton. Therefore, the motion of the exoskeleton and the user at these points would be identical. This means that the kinematic data of the motion of these points can be used as the input for the simulations.

In addition to the location of the marker points, their velocity and acceleration values are also required, and were obtained by numeric differentiations. Before performing differentiation, the high frequency noise was eliminated using a Butterworth low-pass filter. If the cut-off frequency of the filter is not high enough, then some noise would still be present in the filtered signals, and unrealistically large values would appear after differentiation. On the other hand, if the cut-off frequency of the filter is too low, then some of the frequency components of the human movements would be eliminated. Therefore, finding the right cut-off frequency is crucial. A survey on the literature on response requirements in tele-robotics has found the position bandwidth of human

movements to be no more than 10 Hz for reflexive actions, although it is around 5 Hz for "internally generated or learned trajectories" [90]. Since tele-robotic devices need to copy the movements of human operators, their response requirements are similar to those of robotic exoskeletons. Therefore, the cut-off frequency of the filter was decided to be 10 Hz.

G.1.1 The single-limb stance phase

Notice that this phase begins with the toe-off of the swing leg and ends by the "heel-strike" of the swing leg, which is the instance shown in the **Figure 7-7**.

G.1.1.1 Kinematics

The inputs to the kinematic problems are the values for the position, velocity and acceleration of the points O, A and B on each leg (with subscripts 1 and 2 for the stance and swing legs, respectively), in addition to the angle of the swing foot, θ_{f2} .

Because the stance foot remains horizontal, we can write:

$$\theta_{h1} = \theta_{k1} - \theta_{a1}$$

7-5

Also:

$$\theta_{k2} = \theta_{h2} - \theta_{a2} + \theta_{f2}$$

7-6

Notice that $X_{B1} = X_{B2}$, and $Y_{B1} = Y_{B2}$, and

$$Y_{B2} = Y_{A2} + \overline{A_2 B_2} \sin\left(\theta_{f2} + \frac{\pi}{2} - \theta_{a2} + \theta_{k2}\right)$$

7-7

Furthermore, the location of the points B_1 and B_2 is also dependent on the configuration of the rear leg:

$$X_{B2} = X_{O2} + \overline{O_2 A_2} \cos(\theta_{s2}) + \overline{A_2 B_2} \cos(\theta_{th2})$$

7-8

$$Y_{B2} = Y_{O2} + \overline{O_2 A_2} \sin(\theta_{s2}) + \overline{A_2 B_2} \sin(\theta_{th2})$$

7-9

where $\theta_{s2}(t)$ and $\theta_{th2}(t)$ are *defined* as follows:

$$\begin{cases} \theta_{s2} \overset{\text{def}}{=} \theta_{f2} + \frac{\pi}{2} - \theta_{a2} \\ \theta_{th2} \overset{\text{def}}{=} \theta_{s2} + \theta_{k2} \end{cases}$$

Now, the above equations need to be solved in order to obtain the joint angles of the exoskeleton (i.e. to solve the inverse kinematic problem). The inputs[1] are θ_{f2}, X_{B2} and Y_{B2}. To solve the equations, we adopt a geometric approach, as follows.

$$(\overline{O_2 B_2})^2 = (X_{B2} - X_{O2})^2 + (Y_{B2} - Y_{O2})^2 \qquad \text{7-10}$$

Notice that the variables on the right side of the above equation are all kinematic inputs of th eproblem.

Using the law of cosines, we can write:

$$(\overline{O_2 B_2})^2 = (\overline{O_2 A_2})^2 + (\overline{A_2 B_2})^2 - 2\overline{O_2 A_2}.\overline{A_2 B_2}.\cos(\pi - \theta_{k2}) \qquad \text{7-11}$$

Equation 7-11 results that:

$$\theta_{k2} = ArcCos\left(\frac{(\overline{O_2 B_2})^2 - (\overline{O_2 A_2})^2 - (\overline{A_2 B_2})^2}{2\overline{O_2 A_2}.\overline{A_2 B_2}}\right) \qquad \text{7-12}$$

The above equation gives the solution of the front knee anlgle. Now, equation 7-8 could be used to yield:

$$X_{B2} = X_{O2} + \overline{O_2 A_2}\cos(\theta_{s2}) + \overline{A_2 B_2}\cos(\theta_{s2} + \theta_{k2}) = X_{O2} + \overline{O_2 A_2}\cos(\theta_{s2}) + \overline{A_2 B_2}.\left(\cos\theta_{s2}.\cos\theta_{k2} - \sin\theta_{s2}.\sqrt{(1 - cos^2(\theta_{s2}))}\right)$$

The above equation can be reqritten as follows:

$$(\overline{O_2 A_2} + \overline{A_2 B_2}\cos(\theta_{k2})).\cos\theta_{s2} + (-X_{B2} + X_{O2}) \qquad \text{7-13}$$
$$= \overline{A_2 B_2}\cos(\theta_{k2})\sqrt{(1 - cos^2(\theta_{s2}))}$$

or:

$$A.\cos\theta_{s2} + B = C\sqrt{(1 - cos^2(\theta_{s2}))} \qquad \text{7-14}$$

where the definition of the intermediary variables A, B and C can be found form equation 7-13. Now, to solve equation 7-14, we can write:

$$(A^2 + C^2).cos^2(\theta_{s2}) + (2A.B)\cos\theta_{s2} + (B^2 - C^2) = 0$$

The solutions of the quadratic equation above are as follows:

---

[1] Obtain from Motion Capture data of human subject walking.

$$\cos \theta_{s2} = \frac{-2A.B \pm \sqrt{(4A^2B^2 - 4.(A^2 + C^2).(B^2 - C^2))}}{2(A^2 + C^2)} \qquad \text{7-15}$$

It was revealed by testing that the corect answer from equation 7-15 is the one with a "+" signe before the radical sign. Furthermore, while finding the values of θ_{s2} from $\cos \theta_{s2}$, it musty be noted that θ_{s2} will be in the first or the second quadrant.

Now the kinematic solution for the joint angles of the rear leg must be found, as follows. It must be noted that:

$$\begin{cases} X_{B1} = X_{B2} \\ X_{B1} = X_{B2} \end{cases}$$

Now:

$$\begin{cases} X_{A1} = X_{B1} + \overline{A_1 B_1} \sin\theta_{h1} \\ Y_{A1} = Y_{B1} - \overline{A_1 B_1} \cos\theta_{h1} \end{cases} \qquad \text{7-16}$$

$$\begin{cases} X_{O1} = X_{A1} + \overline{A_1 O_1} \sin(\theta_{h1} - \theta_{k1}) \\ Y_{O1} = Y_{A1} - \overline{A_1 O_1} \cos(\theta_{h1} - \theta_{k1}) \end{cases} \qquad \text{7-17}$$

Also:

$$\begin{cases} X_{O1} = -S + \overline{H_1 K_1} \\ Y_{O1} = \overline{O_1 K_1} \end{cases} \qquad \text{7-18}$$

Notice that the origin of the global coordinate system is at point H₂ in **Figure 7-7**.

Using the law of cosines, we have:

$$(\overline{O_1 B_1})^2 = (\overline{A_1 B_1})^2 + (\overline{A_1 O_1})^2 - 2\overline{A_1 B_1}.\overline{A_1 O_1}\cos(\pi - \theta_{k1})$$

or:

$$(\overline{O_1 B_1})^2 = (\overline{A_1 B_1})^2 + (\overline{A_1 O_1})^2 + 2\overline{A_1 B_1}.\overline{A_1 O_1}\cos(\theta_{k1})$$

Therefore:

$$\theta_{k1} = acos\left(\frac{(\overline{O_1 B_1})^2 - (\overline{A_1 B_1})^2 - (\overline{A_1 O_1})^2}{2\overline{A_1 B_1}.\overline{A_1 O_1}}\right) \qquad \text{7-19}$$

And the value of $\overline{O_1 B_1}$ can be obtained from:

$$(\overline{O_1 B_1})^2 = (X_{O1} - X_{B1})^2 + (Y_{O1} - Y_{B1})^2 \qquad \text{7-20}$$

Now, using the first equations from the equation sets 7-16 and 7-17, we have:

$$X_{O1} = X_{B1} + \overline{A_1 B_1} sin\theta_{h1} + \overline{A_1 O_1} sin(\theta_{h1} - \theta_{k1})$$

Also

$$sin(\theta_{h1} - \theta_{k1}) = sin\theta_{h1}.cos\theta_{k1} - cos\theta_{h1}.sin\theta_{k1}$$

Furhermore, becasue it is known that $\frac{-\pi}{2} \leq \theta_{h1} \leq \frac{\pi}{2}$, it could be said that:

$$cos\theta_{h1} = \sqrt{1 - sin^2(\theta_{h1})}$$

Therefore:

$$X_{O1} = X_{B1} + \overline{A_1 B_1}.sin\theta_{h1} + \overline{A_1 O_1}.sin\theta_{h1}.cos\theta_{k1} - \overline{A_1 O_1}.sin\theta_{k1}.\sqrt{1 - sin^2(\theta_{h1})}$$

or:

$$(\overline{A_1 O_1}.sin\theta_{k1})\sqrt{1 - sin^2(\theta_{h1})} = (X_{B1} - X_{O1}) + (\overline{A_1 B_1} + \overline{A_1 O_1}.cos\theta_{k1}).cos\theta_{h1} \qquad \text{7-21}$$

We can define the follwing intermediary variables for similplicity:

$$\begin{cases} D \stackrel{\text{def}}{=} (\overline{A_1 O_1}.sin\theta_{k1}) \\ E \stackrel{\text{def}}{=} (X_{B1} - X_{O1}) \\ F \stackrel{\text{def}}{=} (\overline{A_1 B_1} + \overline{A_1 O_1}.cos\theta_{k1}) \end{cases}$$

Then equation 7-21 can be rewritten as

$$D\sqrt{1 - sin^2(\theta_{h1})} = E + F.cos\theta_{h1} \qquad \text{7-22}$$

Equation 7-22 results:

$$D^2 - D^2.sin^2(\theta_{h1}) = E^2 + F^2.sin^2(\theta_{h1}) + 2E.F.sin\theta_{h1}$$

$$\Rightarrow (D^2 + F^2).sin^2(\theta_{h1}) + (2E.F)sin\theta_{h1} + (E^2 - D^2) \qquad \text{7-23}$$

The solutions of the quadratic equation above are as follows:

$$sin\,\theta_{h1} = \frac{-2E.F \pm \sqrt{(4E^2 F^2 - 4.(D^2 + F^2).(E^2 - D^2))}}{2(D^2 + F^2)} \qquad \text{7-24}$$

It was revealed after examination that the correct answer in equation 7-24 is the one with the "+" behind the radical sign. Furthermore, when obtaining the value of θ_{h1} from $sin\,\theta_{h1}$, it must be noted that $\frac{-\pi}{2} \leq \theta_{h1} \leq \frac{-\pi}{2}$. This means that:

$$\theta_{h1} = \mathrm{asin}\left(\frac{-2E.F \pm \sqrt{\left(4E^2F^2 - 4.(D^2+F^2).(E^2-D^2)\right)}}{2(D^2+F^2)}\right) \qquad \text{7-25}$$

The equations mentionned so far present the solution for the joint angles. Now, the velocity and acceleration solutions must be derived. It must be noted that the inputs here are the linear velocitys and accelerations obtained from the motion capture experiment.
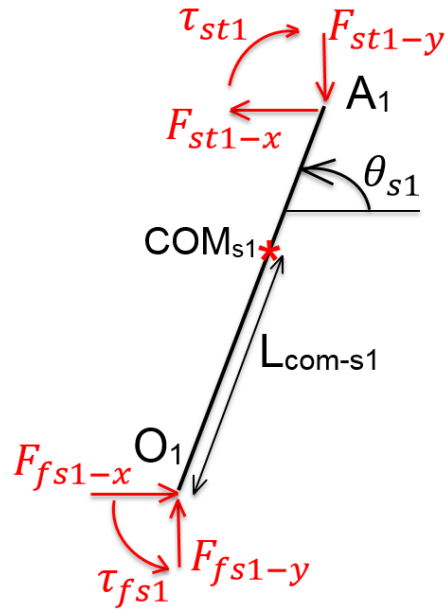
Figure 7-8. The free body diagram of the shin of the stance leg

Figure 7-8 shows the free body diagram of the shin of the stance leg. During this phase of gait, we have:

$$\boldsymbol{V}_{O1} = 0$$

where $\boldsymbol{V}$ denotes the velocity vector.

Now, using complex numbers for vectors, we have

$$\boldsymbol{V}_{A1} = \boldsymbol{V}_{O1} + \overline{A_1 O_1}.\omega_{s1}(-sin\theta_{s1} + cos\theta_{s1}.\hat{\boldsymbol{j}}) \qquad \text{7-26}$$

where

$$\theta_{s1} \stackrel{\text{def}}{=} \frac{\pi}{2} + \theta_{h1} - \theta_{k1}$$

and

$$\omega_{s1} \stackrel{\text{def}}{=} \frac{d(\theta_{s1})}{dt}$$

and $\hat{j} = \sqrt{-1}$

$$\Rightarrow V_{A1} = \overline{A_1O_1}.\omega_{s1}(-\cos(\theta_{h1} - \theta_{k1}) - \sin(\theta_{h1} - \theta_{k1}).\hat{j}) \qquad 7\text{-}27$$

Also, in this stage of the gait, we can write:

$$\theta_{h1} - \theta_{k1} = \theta_{a1}$$

$$\Rightarrow V_{A1} = \overline{A_1O_1}.\omega_{s1}(-\cos(\theta_{a1}) + \sin(\theta_{a1}).\hat{j}) \qquad 7\text{-}28$$

Also, only during this stage of gait, we have:

$$\omega_{s1} = -\dot{\theta}_{a1} \qquad 7\text{-}29$$

$$\omega_{s1} = \dot{\theta}_{s1} = \frac{d}{dt}\left(\frac{\pi}{2} + \theta_{h1} - \theta_{k1}\right) = \dot{\theta}_{h1} - \dot{\theta}_{k1} \qquad 7\text{-}30$$

$$a_{A1} = \overline{A_1O_1}.\omega_{s1}^2(-\sin(\theta_{a1}) - \cos(\theta_{a1}).\hat{j}) + \qquad 7\text{-}31$$
$$\overline{A_1O_1}.\alpha_{s1}.(-\cos(\theta_{a1}) + \sin(\theta_{a1}).\hat{j})$$

where a denotes the acceleration vector.

$$\alpha_{s1} = \frac{d^2}{dt^2}(-\theta_{a1}) = -\frac{d}{dt}(\dot{\theta}_{a1}) = -\ddot{\theta}_{a1} \qquad 7\text{-}32$$

$$\alpha_{s1} = \frac{d}{dt}(\dot{\theta}_{h1} - \dot{\theta}_{k1}) = \ddot{\theta}_{h1} - \ddot{\theta}_{k1} \qquad 7\text{-}33$$

$$a_{cms1-x} = L_{com-s_1}.\alpha_{s1}(-\sin(\theta_{s1}) + \cos(\theta_{s1}).\hat{j}) \qquad 7\text{-}34$$
$$+ L_{com-s_1}\omega_{s1}^2(-\cos(\theta_{s1}) - \sin(\theta_{s1}).\hat{j})$$

where a_{cms1-x} is the acceleration of the centre of mass of the stance leg's shank, and L_{com-s_1} denotes the distance of the centre of mass (after the addition of all mass particles) from the point O_1. Originally, before the addition of the mass of the motor and transmission mechanism, the centre of mass of the shank link is located at point D₁, as shown in figure **Figure 7-7**. The mass of any added components are model by adding mass particles at points M₁(1), M₂(2), etc. To find the location of the centre of mass of the shank link with the added mass of the actuator, we can write:

$$L_{D_1}.m_{s_1} + \sum_k L_{M_1(k)}m_{M_1(k)} = \left(m_{s_1} + \sum_k m_{M_1(k)}\right).L_{com-s_1}$$

$$\Rightarrow L_{com-s_1} = \frac{L_{D_1}.m_{s_1} + \sum_k L_{M_1(k)}m_{M_1(k)}}{m_{s_1} + \sum_k m_{M_1(k)}} \qquad 7\text{-}35$$

where m_{s_1} is the shank mass, and $m_{M_1(k)}$ and $L_{M_1(k)}$ are the mass of each added particle and its distance from point O_1, for k=1…number of added particles.

Equation 7-28 results:

$$\omega_{s1} = \frac{|\boldsymbol{V}_{A1}|}{\overline{A_1 O_1}} \qquad \text{7-36}$$

Equation 7-36 can be reqritten in the following form, so that the sign of ω_{s1} is also obtained:

$$\omega_{s1} = \frac{real(\boldsymbol{V}_{A1})}{\overline{A_1 O_1}.(-\cos(\theta_{a1}))} \qquad \text{7-37}$$

Similarly, we have:

$$real(\boldsymbol{a}_{A1}) = \overline{A_1 O_1}.\omega_{s1}^2(-\sin(\theta_{a1})) + \overline{A_1 O_1}.\alpha_{s1}(-\cos(\theta_{a1}))$$

$$\Rightarrow \alpha_{s1} = \frac{real(\boldsymbol{a}_{A1}) + \overline{A_1 O_1}.\omega_{s1}^2.\sin(\theta_{a1})}{\overline{A_1 O_1}.(\cos(\theta_{a1}))} \qquad \text{7-38}$$

Now, for the stance leg's thigh, depicted in Figure 7-9, we have:
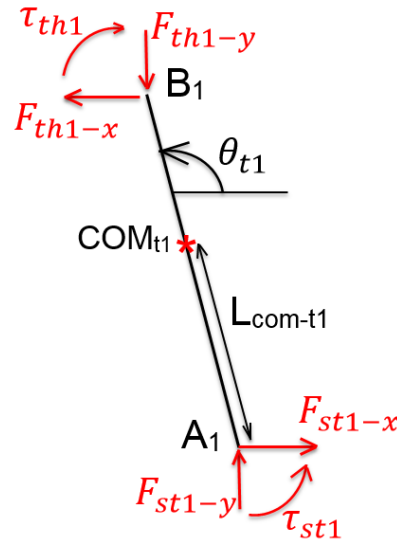
Figure 7-9. The Free body diagram of the thigh of the stance leg

$$\boldsymbol{V}_{A1} = \boldsymbol{V}_{B1} + \overline{A_1 B_1}.\omega_{t1}(\cos(\theta_{h1}) + \sin(\theta_{h1}).\hat{\jmath}) \qquad \text{7-39}$$

$$\omega_{t1} \overset{\text{def}}{=} \dot{\theta}_{h1} \qquad \text{7-40}$$

$$\omega_{t1} = \frac{real(\boldsymbol{V}_{A1} - \boldsymbol{V}_{B1})}{\overline{A_1 B_1}.\cos(\theta_{h1})} \qquad \text{7-41}$$

$$\boldsymbol{a}_{A1} = \boldsymbol{a}_{B1} + \overline{A_1 B_1}.\omega_{t1}^2(-\sin(\theta_{h1}) + \cos(\theta_{h1}).\hat{\jmath}) + \qquad \text{7-42}$$
$$\overline{A_1 B_1}.\alpha_{t1}(\cos(\theta_{h1}) + \sin(\theta_{h1}).\hat{\jmath})$$

$$\Rightarrow \alpha_{t1} = \ddot{\theta}_{h1} = \frac{real(\boldsymbol{a}_{A1} - \boldsymbol{a}_{B1}) + \overline{A_1 B_1}.\omega_{t1}^2 \sin(\theta_{h1})}{\overline{A_1 B_1}.\cos(\theta_{h1})} \qquad \text{7-43}$$

$$\boldsymbol{a}_{cmt1-x} = \boldsymbol{a}_{A1} + L_{com-t_1}.\alpha_{t1}(-\cos(\theta_{h1}) + \sin(\theta_{h1}).\hat{\jmath}) \qquad \text{7-44}$$
$$+ L_{com-t_1}\omega_{t1}^2(\sin(\theta_{h1}) - \cos(\theta_{h1}).\hat{\jmath})$$

Furthermore, the location of the centre of mass of the thigh could be found in a similar manner to that of the shank:

$$L_{com-t_1} = \frac{L_{E_1}.m_{t_1} + \sum_k L_{N_1(k)}m_{N_1(k)}}{m_{t_1} + \sum_k m_{N_1(k)}} \qquad \text{7-45}$$

Now the swing leg solution is found, as follows. For the front shin, shown in Figure 7-10, we have:
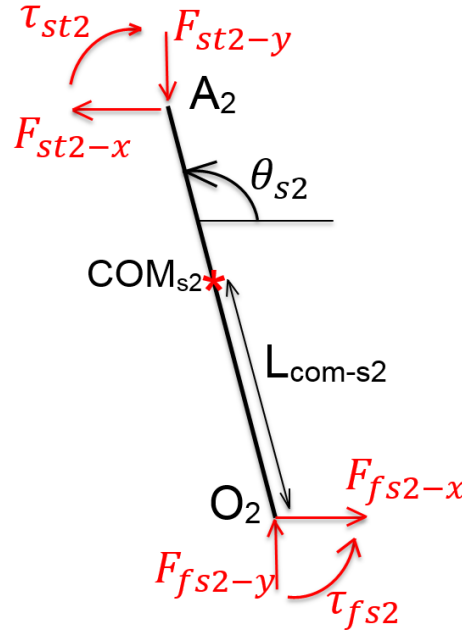
Figure 7-10. The free body diagram of the shin of the swing leg

$$\boldsymbol{V}_{A2} = \boldsymbol{V}_{O2} + \overline{A_2 O_2}.\dot{\theta}_{s2}(-\sin(\theta_{s2}) + \cos(\theta_{s2}).\hat{\jmath}) \qquad \text{7-46}$$

$$\Rightarrow \omega_{s2} \stackrel{\text{def}}{=} \dot{\theta}_{s2} = \frac{real(\boldsymbol{V}_{A2} - \boldsymbol{V}_{O2})}{-\overline{A_2 O_2}\sin(\theta_{s2})} \qquad \text{7-47}$$

$$\boldsymbol{a}_{A2} = \boldsymbol{a}_{O2} + \overline{A_2 O_2}.\dot{\theta}_{s2}^2(-\cos(\theta_{s2}) - \sin(\theta_{s2}).\hat{\jmath})$$
$$+ \overline{A_2 O_2}.\ddot{\theta}_{s2}(-\sin(\theta_{s2}) + \cos(\theta_{s2}).\hat{\jmath}) \qquad \text{7-48}$$

$$\Rightarrow \alpha_{s2} \stackrel{\text{def}}{=} \ddot{\theta}_{s2} = \frac{real(\boldsymbol{a}_{A2} - \boldsymbol{a}_{O2}) + \overline{A_2 O_2}.\dot{\theta}_{s2}^2 \sin(\theta_{s2})}{-\overline{A_2 O_2}.\sin(\theta_{s2})} \qquad \text{7-49}$$

For the swing thigh, the dimensions and forces are shown in Figure 7-11.
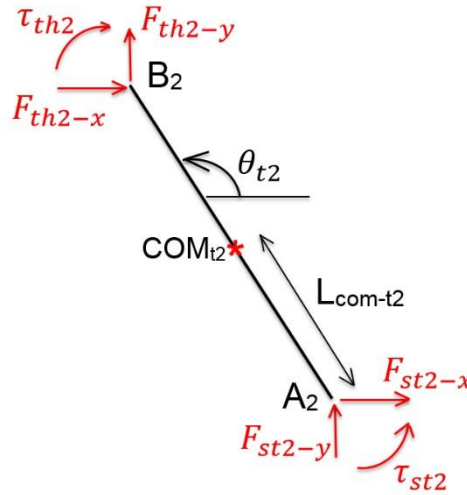
Figure 7-11. The free body diagram of the swing leg's thigh

$$\boldsymbol{V}_{A2} = \boldsymbol{V}_{B2} + \overline{A_2 B_2}.\dot{\theta}_{t2}(\sin(\theta_{t2}) - \cos(\theta_{t2}).\hat{\jmath}) \qquad \text{7-50}$$

$$\Rightarrow \omega_{t2} \stackrel{\text{def}}{=} \dot{\theta}_{t2} = \frac{real(\boldsymbol{V}_{A2} - \boldsymbol{V}_{B2})}{\overline{A_2 B_2}.\sin(\theta_{t2})} \qquad \text{7-51}$$

$$\boldsymbol{a}_{A2} = \boldsymbol{a}_{B2} + \overline{A_2 B_2}.\dot{\theta}_{t2}^2(\cos(\theta_{t2}) + \sin(\theta_{t2}).\hat{\jmath}) +$$
$$\overline{A_2 B_2}.\ddot{\theta}_{t2}(\sin(\theta_{t2}) - \cos(\theta_{t2}).\hat{\jmath}) \qquad \text{7-52}$$

$$\Rightarrow \alpha_{t2} \stackrel{\text{def}}{=} \ddot{\theta}_{t2} = \frac{real(\boldsymbol{a}_{A2} - \boldsymbol{a}_{B2}) + \overline{A_2 B_2}.\dot{\theta}_{t2}^2 \sin(\theta_{t2})}{\overline{A_2 B_2}.\sin(\theta_{t2})} \qquad \text{7-53}$$

$$\boldsymbol{a}_{com-t2} = \boldsymbol{a}_{B2} + (\overline{A_2 B_2} - L_{com-t2}).\dot{\theta}_{t2}^2(\cos(\theta_{t2}) + \qquad \text{7-54}$$
$$\sin(\theta_{t2}).\hat{\jmath}) + (\overline{A_2 B_2} - L_{com-t2}).\ddot{\theta}_{t2}(\sin(\theta_{t2}) - \cos(\theta_{t2}).\hat{\jmath})$$

Now, for the foot of the swing limb, shown in Figure 7-12, we have:
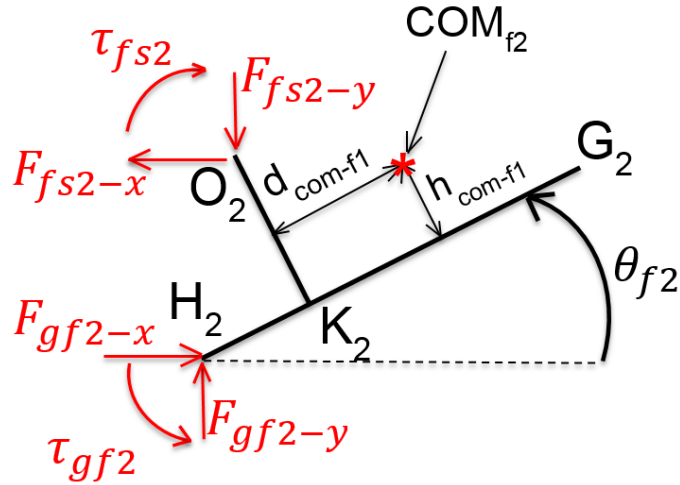
Figure 7-12. The free body diagram of the swing limb's foot

$$\boldsymbol{V}_{K2} = \boldsymbol{V}_{H2} + \overline{H_2 K_2}.\dot{\theta}_{f2}\big(-\sin(\theta_{f2}) + \cos(\theta_{f2}).\hat{\jmath}\big) \qquad \text{7-55}$$

$$\boldsymbol{V}_{O2} = \boldsymbol{V}_{K2} + \overline{K_2 O_2}.\dot{\theta}_{f2}\big(-\cos(\theta_{f2}) - \sin(\theta_{f2}).\hat{\jmath}\big) \qquad \text{7-56}$$

$$\boldsymbol{a}_{K2} = \boldsymbol{a}_{H2} + \overline{H_2 K_2}.\dot{\theta}_{f2}^2\big(-\cos(\theta_{f2}) + \sin(\theta_{f2}).\hat{\jmath}\big) \\ + \overline{H_2 K_2}.\ddot{\theta}_{f2}\big(-\sin(\theta_{f2}) + \cos(\theta_{f2}).\hat{\jmath}\big) \qquad \text{7-57}$$

$$\boldsymbol{a}_{O2} = \boldsymbol{a}_{K2} + \overline{K_2 O_2}.\dot{\theta}_{f2}^2\big(\sin(\theta_{f2}) - \cos(\theta_{f2}).\hat{\jmath}\big) \\ + \overline{K_2 O_2}.\ddot{\theta}_{f2}\big(-\cos(\theta_{f2}) - \sin(\theta_{f2}).\hat{\jmath}\big) \qquad \text{7-58}$$

$$\boldsymbol{a}_{com-f2} = \boldsymbol{a}_{K2} + d_{com-h}.\dot{\theta}_{f2}^2\big(-\cos(\theta_{f2}) + \sin(\theta_{f2}).\hat{\jmath}\big) + \\ h_{com-h}.\dot{\theta}_{f2}^2\big(\sin(\theta_{f2}) - \cos(\theta_{f2}).\hat{\jmath}\big) + \\ d_{com-h}.\ddot{\theta}_{f2}\big(-\sin(\theta_{f2}) + \cos(\theta_{f2}).\hat{\jmath}\big) + \\ h_{com-h}.\ddot{\theta}_{f2}\big(-\cos(\theta_{f2}) - \sin(\theta_{f2}).\hat{\jmath}\big) \qquad \text{7-59}$$

Finally, the kinematic equations of motion for the hip part must be developed, as follows. Figure 7-13 shows the free body diagram of the hip part. The kinematic relations for velocity and acceleration are as follows. The location of the centre of mass of the hip and upper body parts (COM$_h$) is shown in Figure 7-13, as well as the location of the load being carried (m$_l$). Furthermore, as shown in **Figure 7-7**, the mass of the hip joint actuators are located at points P$_1$ and P$_2$. The location of these points are assumed to be as follows:

$$l_{p1} \stackrel{\text{def}}{=} \overline{B_1 P_1} \qquad \text{7-60}$$
$$l_{p2} \stackrel{\text{def}}{=} \overline{B_2 P_2}$$

Now, the location of the centre of mass of the whole system (the hip and upper body, plus the actuators and the load), which we will call point G, is as follows:

$$x_G = \frac{-m_h \cdot l_{com-h} - m_{P1} \cdot l_{p1} - m_{P2} \cdot l_{p2} + m_l \cdot x_l}{m_h + m_{P1} + m_{P2} + m_l \cdot x_l} \qquad \text{7-61}$$

$$y_G = \frac{-m_h \cdot h_{com-h} - m_{P1} \cdot 0 - m_{P2} \cdot 0 + m_l \cdot y_l}{m_h + m_{P1} + m_{P2} + m_l \cdot x_l} \qquad \text{7-62}$$

where m_h is the mass of the hip part, and m_{P1} and m_{P2} are the mass of hip actuators. Notice that the origin of the local coordinate system (in which x_G and y_G are expressed) is on point B₁.
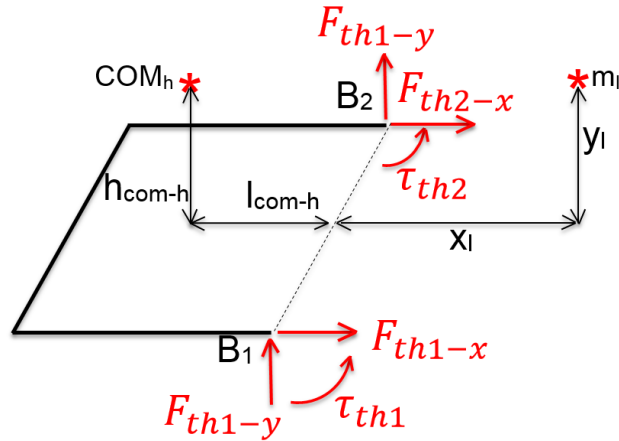
Figure 7-13. The Free body diagram of the hip part

Because the hip may tilt during the manoeuvres, we need to define a few more variables. Figure 7-14 shows the side view of the hip part, with point G being the centre of mass of the hip system (together with load and actuators). Let us define the absolute angle of the hip, θ_h^{abs}, as follows:

$$\theta_h^{abs} = \theta_a - \theta_k + \theta_h \qquad \text{7-63}$$

$$\dot{\theta}_h^{abs} = \dot{\theta}_a - \dot{\theta}_k + \dot{\theta}_h \qquad \text{7-64}$$

$$\ddot{\theta}_h^{abs} = \ddot{\theta}_a - \ddot{\theta}_k + \ddot{\theta}_h \qquad \text{7-65}$$

Now, θ_G, shown in Figure 7-14, can be calculated as follows:

$$\theta_G = \frac{\pi}{2} - \theta_h^{abs} - \tan^{-1}\left(\frac{x_G}{y_G}\right) \qquad \text{7-66}$$

The acceleration of point G can now be calculated as follows:

$$\boldsymbol{a}_G = \boldsymbol{a}_{B_1} + L_G \cdot \left(\dot{\theta}_h^{abs}\right)^2 \cdot (-\cos\theta_G - \sin\theta_G \cdot \hat{\jmath}) + \qquad \text{7-67}$$
$$L_G \cdot \ddot{\theta}_h^{abs} \cdot (\sin\theta_G - \cos\theta_G \cdot \hat{\jmath})$$

where is defined as:

$$L_G = \sqrt{(x_G^2 + y_G^2)} \qquad \text{7-68}$$
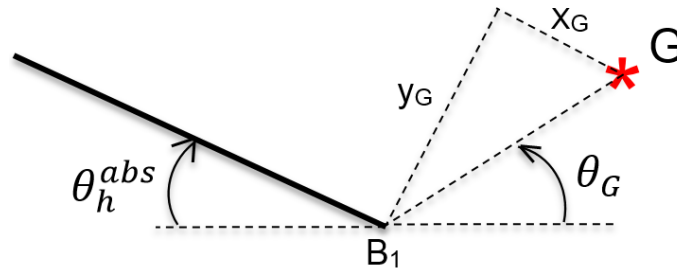
Figure 7-14. The side view of the hip part

G.1.1.2 Kinetics

For the stance leg, the following variables are defined here to represent the interaction forces between the foot, the shank and the hip part: F_{fs1-x} and F_{fs1-y} are the horizontal and vertical components of the force applied to the shank part by the foot part. Similarly, F_{st1-x} and F_{st1-y} are the horizontal and vertical components of the force applied to the thigh part by the shank part. The two component of the force applied to the hip part by the thigh are F_{th1-x} and F_{th1-y}. Finally, τ_{fs1}, τ_{st1} and τ_{th1} are the joint torque at the ankle, knee and hip, respectively. Similar nomenclature applies to the front leg, while the number 1 is replaced by 2 in the subscripts.

The laws of newton for the rear shank can be used to derive the equations.

$$\Sigma F_x = \left(m_{s_1} + \Sigma_k \; m_{M_1(k)}\right). \boldsymbol{a}_{cms1-x}$$

where $\boldsymbol{a}_{cms1}$ is the horizontal component of acceleration the centre of mass of the shank (with the added mass particles).

$$\Rightarrow F_{fs1-x} - F_{st1-x} = (m_{s_1} + \sum_k m_{M_1(k)}) \boldsymbol{a}_{cms1-x} \qquad \text{7-69}$$

$$\Sigma F_y = \left(m_{s_1} + \Sigma_k \; m_{M_1(k)}\right). \boldsymbol{a}_{cms1-y}$$

$$\Rightarrow F_{fs1-y} - F_{st1-y} = (m_{s_1} + \Sigma_k \; m_{M_1(k)})(\boldsymbol{a}_{cms1-x} + \boldsymbol{g}) \qquad \text{7-70}$$

where $\boldsymbol{a}_{cms1}$ is the horizontal component of acceleration the centre of mass, and **g** is the vector of the acceleration of gravity (almost equal to $9.81\hat{j}$).

The moment of inertia of the shank system (with the added mass points) can be calculated as follows:

$$I_{cms1} = I_{D1}^0 + \left(L_{D_1} - L_{com-s_1}\right)^2 . m_{s_1}$$
$$+ \sum_k \left(L_{M_1(k)} - L_{com-s_1}\right)^2 . m_{M_1(k)}$$

<div align="right">7-71</div>

In equation 7-71, I_{D1}^0 is the moment of inertia of the shank link (without the added mass-points) around point D₁.

$$\sum M_{cms1} = I_{cms1} . \alpha_{s1}$$
$$\Rightarrow \tau_{fs1} + F_{fs1-x} . L_{com-s_1} . \sin(\theta_{s1}) -$$
$$F_{fs1-y} . L_{com-s_1} . \cos(\theta_{s1}) - \tau_{st1} + F_{st1-x} . \left(L_{s_1} - L_{com-s_1}\right) . \sin(\theta_{s1}) - F_{st1-y} . \left(L_{s_1} - L_{com-s_1}\right) . \cos(\theta_{s1}) =$$
$$I_{cms1} . \alpha_{s1}$$

<div align="right">7-72</div>

Now, for the stance leg's thigh, we have:

$$\sum F_x = \left(m_{t_1} + \sum_k m_{N_1(k)}\right) . a_{cmt1-x}$$

Where $m_{N_1(k)}$ refers to the mass of each added mass-point $N_1(k)$ which represent the mass of the actuator.

$$\sum F_y = \left(m_{t_1} + \sum_k m_{N_1(k)}\right) . \left(a_{cmt1-y} + g\right)$$
$$\Rightarrow F_{st1-y} - F_{th1-y} = \left(m_{t_1} + \sum_k m_{N_1(k)}\right)\left(a_{cms1-x} + g\right)$$

<div align="right">7-73</div>

$$\sum M_{cmt1} = I_{cmt1} . \alpha_{t1}$$
$$\Rightarrow \tau_{st1} + F_{st1-x} . L_{com-t_1} . \cos(\theta_{h1}) + F_{st1-y} . L_{com-t_1} . \sin(\theta_{h1})$$
$$- \tau_{th1} + F_{th1-x} . \left(L_{t_1} - L_{com-t_1}\right) . \cos(\theta_{h1})$$
$$- F_{th1-y} . \left(L_{t_1} - L_{com-t_1}\right) . \sin(\theta_{h1}) = I_{cmt1} . \alpha_{t1}$$

<div align="right">7-74</div>

In equation 7-74, I_{cmt1} is the moment of inertia of the system around its centre of mass, which can be calculated as follows, similar to the case of the stance leg's shank:

$$I_{cmt1} = I_{E1}^0 + \left(L_{E_1} - L_{com-t_1}\right)^2 . m_{t_1}$$
$$+ \sum_k \left(L_{N_1(k)} - L_{com-t_1}\right)^2 . m_{N_1(k)}$$

<div align="right">7-75</div>

where , I_{E1}^0 is the moment of inertia of the shank link (without the added mass-points) around point E₁.

Now for the hip part, which is shown in Figure 7-13 and Figure 7-14, we have:

:

$$\Sigma(F_x)_{hip} = \left(m_h + \Sigma_k\, m_{p_1(k)} + \Sigma_k\, m_{p_2(k)}\right).\boldsymbol{a}_{G\_x}$$

$$\Rightarrow F_{th1-x} + F_{th2-x} = \left(m_h + \Sigma_k\, m_{p_1(k)} + \Sigma_k\, m_{p_2(k)}\right).\boldsymbol{a}_{G\_x} \qquad \text{7-76}$$

Similarly, for the vertical direction we have:

$$F_{th1-y} + F_{th2-y} = \left(m_h + \Sigma_k\, m_{p_1(k)} + \Sigma_k\, m_{p_2(k)}\right).\left(\boldsymbol{a}_{G\_y} + \qquad \text{7-77} \right.$$
$$\left. \boldsymbol{g}\right)$$

And for the moments of force:

$$-\left(F_{th1-y} + F_{th2-y}\right).\left(L_G.\cos\theta_G\right) + \left(F_{th1-x} + \qquad \text{7-78} \right.$$
$$F_{th2-x}).\left(L_G.\sin\theta_G\right) + \tau_{th1} + \tau_{th2} = I_G.\ddot{\theta}_h^{abs}$$

The hip moment of inertia around its centre of mass G is:

$$I_G = I_{com-h} + m_h.\left((l_{com-h} + x_G)^2 + (h_{com-h} - y_G)^2\right) + \qquad \text{7-79}$$
$$m_{P_1}.\left(\left(l_{p1} + x_G\right)^2 + (y_G)^2\right) + m_{P_2}.\left(\left(l_{p2} + x_G\right)^2 + (y_G)^2\right)$$

The aforementioned relations apply to the shin and thigh of the stance leg. The kinetic formulation of the swing leg is exactly similar, with the mere difference that the subscript 1 is replaced by 2. However, the foot of the swing leg also needs to be considered, as follows. Figure 7-12 shows the free body diagram of the swing leg's foot. The kinematic relations of the foot are as follows:

$$F_{gf2-x} - F_{fs2-x} = m_{f_1}.\boldsymbol{a}_{cmf2-x} \qquad \text{7-80}$$

$$F_{gf2-y} - F_{fs2-y} = m_{f_1}.\boldsymbol{a}_{cmf2-y} \qquad \text{7-81}$$

$$\Sigma M_{cmf2} = I_{cmf2}.\ddot{\theta}_{f2}$$

$$\Rightarrow -\tau_{fs2} + \tau_{gf2} + F_{fs2-x}.\left(\overline{K_2O_2} - h_{com-h} - \qquad \text{7-82} \right.$$
$$d_{com-h}.\tan\theta_{f2}\right) + F_{fs2-y}\cdot\left(\frac{d_{com-h}}{\cos(\theta_{f2})} + \left(\overline{K_2O_2} - d_{com-h} - \right.\right.$$
$$\left.\left. d_{com-h}.\tan\theta_{f2}\right)\sin(\theta_{f2})\right) + F_{gf2-x}.\left(\left(\overline{K_2H_2} + d_{com-h} - \right.\right.$$
$$\left. h_{com-h}.\tan\theta_{f2}\right).\sin(\theta_{f2}) + \frac{h_{com-h}}{\cos(\theta_{f2})}\right) - F_{gf2-y}.\left(\left(\overline{K_2H_2} + \right.\right.$$
$$\left.\left. d_{com-h} - h_{com-h}.\tan\theta_{f2}\right).\cos(\theta_{f2})\right) = I_{cmf2}.\ddot{\theta}_{f2}$$

Notice that h_{com-h} and d_{com-h}, shown in Figure 7-12, are fixed parameters.

Also, notice that the ground reaction forces and torques $(F_{gf2-x}, F_{gf2-y}, \text{and } \tau_{gf2})$ are zero in the single-limb stance phase, because the foot of the swinging limb is not in contact with the ground during this phase.

In order to solve the kinetic equations of motion, they have all been assembled into a matrix equation, in the form of:

$$A_k . X_k = B_k \qquad \text{7-83}$$

where X_k is the column vector of kinetic unknown variables (which includes the forces and torques), A_k is the coeffients matrix of the kinetic equation, and B_k is the right hand side column vector. The answer is then found by using:

$$X_k = A_k^{-1} . B_k \qquad \text{7-84}$$

To calculate the joint torques, the equation is used at each point of the discretised trajectory of the exoskeleton.

G.1.2 The "double-leg support" phase

Notice that this stage starts with the heel-strike of the swinging leg (the same instance shown in **Figure 7-7**), and consists of two stages itself, as follows.

G.1.2.1 From "heel-strike" to "foot-flat"

In this phase, the foot contact with the ground is simplified by a hinge joint at the heel of the swinging foot, which is point H_2 in **Figure 7-7** and Figure 7-12. During this stage, τ_{gf2} is zero, but the two components of the ground reaction force $(F_{gf2-x}$ and $F_{gf2-y})$ are unknown. This will cause redundancy in the problem, as the number of the unknown variables become more than the number of equations. To solve this issue, two extra equations are introduced, which are as follows:

$$F_{th1-x} = F_{th2-x} \qquad \text{7-85}$$

$$F_{th1-y} = F_{th2-y} \qquad \text{7-86}$$

$$\tau_{th1} = \tau_{th2} \qquad \text{7-87}$$

To understand the above equations, consider the free body diagram of the hip part, depicted in Figure 7-13. Now consider the second law of Newton in the x direction, stated in equation 7-76, which is repeated here:

$$\sum(F_x)_{hip} = \left(m_h + \sum_k m_{p_1(k)} + \sum_k m_{p_2(k)}\right).a_{G\_x}$$

Since the right hand side of the equation is comprised of the kinematic input of the problem (a_{G_x}) and the inertial terms, the sum of forces in the x direction $\sum(F_x)_{hip}$ is determined. However, we know that:

$$\sum(F_x)_{hip} = (F_{th1-x} + F_{th2-x})$$

and theoretically, any answer for the pair of forces $\begin{bmatrix} F_{th1-x} \\ F_{th1-y} \end{bmatrix}$ can be replaced by another answer in which equal but opposite values (which cancel out each other) have been added to F_{th1-x} and F_{th1-y}. As long as the sum of the two forces is equal to $\sum(F_x)_{hip}$, the answers are mathematically acceptable. However, during the double-leg support phase in efficient walking, there will not be equal but opposite forces which cancel out each other. Instead, actuation effort is equally divided between the two limb actuators. This means that, instead of one leg pushing the hip forward excessively hard and the other one providing little effort, both legs provide equal effort to push the hip forward. Therefore, equation 7-85 applies. A similar argument could be presented to supports equations 7-86 and 7-87.

For the phase of gait considered in this section, there are only two unknown variables, which are F_{gf2-x} and F_{gf2-y}. Therefore, only two extra equations are needed, which are equations 7-85 and 7-86. Using these equations, two of the variables are removed form the problem, namely F_{th2-x} which is replaced by F_{th1-x} and F_{th2-y} which is replaced by F_{th1-y}. This makes the number of equations equal to the number of unknowns, and the solution can be found from equation 7-84.

G.1.2.2   From to "foot-flat" to "opposite-toe-off"

During this stage, it is assumed that the two feet are both fixed on the ground. Therefore, in addition to F_{gf2-x} and F_{gf2-y}, now there is an unknown ground reaction torque τ_{gf2}.

In a similar way to what was explained in section G.1.2.1, we use equation 7-87, and therefore replace τ_{th2} by τ_{th1} in the equations. This makes the number of equations equal to the number of unknowns, and the solution can be found from equation 7-84.

G.2   The exoskeleton squat simulation

Due to the symmetrical nature of the squat manoeuvre, it could be simulated by considering only half of the exoskeleton model. In this method, the motion of one leg is studied, while half of the payload. Furthermore, the mass of the hip part (Figure 7-13) is assumed to be half of its actual mass.

The modelling of the leg motion in squat is identical to the modelling of the stance leg in the "single-limb stance phase", covered in section G.1.1. Therefore, the formulation will not be repeated here.

G.3   The nomenclature of the variables used

variable	Meaning
$\theta_{a1}, \theta_{k1}, \theta_{h1}$	Ankle, knee and hip angles of the stance leg
$\theta_{a2}, \theta_{k2}, \theta_{h2}$	Ankle, knee and hip angles of the swing leg
$\dot{\theta}_{a1}, \dot{\theta}_{k1}, \dot{\theta}_{h1}$	Ankle, knee and hip angular velocity of the stance leg
$\dot{\theta}_{a2}, \dot{\theta}_{k2}, \dot{\theta}_{h2}$	Ankle, knee and hip angular velocity of the swing leg
$\ddot{\theta}_{a1}, \ddot{\theta}_{k1}, \ddot{\theta}_{h1}$	Ankle, knee and hip angular acceleration of the stance leg
$\ddot{\theta}_{a2}, \ddot{\theta}_{k2}, \ddot{\theta}_{h2}$	Ankle, knee and hip angular acceleration of the swing leg
$\theta_{f2}, \dot{\theta}_{f2}, \ddot{\theta}_{f2}$	The angle between the sole of the swinging foot and the ground, and its first and second time-derivatives
$\begin{cases} \theta_{s2} \\ \theta_{th2} \end{cases}$	$\begin{cases} \stackrel{\text{def}}{=} \theta_{f2} + \dfrac{\pi}{2} - \theta_{a2} \\ \stackrel{\text{def}}{=} \theta_{s2} + \theta_{k2} \end{cases}$
$\boldsymbol{V}_{O1}, \boldsymbol{a}_{O1}$	The velocity and acceleration vectors of the point O_1; a similar nomenclature has been used for all points.

The nomenclature of the variables used (continued)

ω_{s1}, α_{s1}	**The angular velocity of the stance shank. A subscript of 2 denotes the swing shin.**
ω_{t1}, α_{t1}	The angular velocity of the stance thigh. A subscript of 2 denotes the swing shin.
m_h	The mass of the hip
$m_{s_1}, m_{t_1}, m_{f_1}$	The masses of the shin, thigh and foot of the stance leg. A subscript of 2 denotes the swing leg.
$I_{cmt1}, I_{cms1}, I_{cmf1}$	The moment of inertia of the shin, thigh and foot of the stance leg around their centre of mass. A subscript of 2 denotes the swing leg.
I_G	The moment of inertia of the hip around its centre of mass.
F_{th1-x}, F_{th1-y}	The x and y components of the interaction force between the thigh and hip section, on the stance leg side. A subscript of 2 denotes the swing leg.
F_{st1-x}, F_{st1-y}	The x and y components of the interaction force between the shin and thigh, on the stance leg side. A subscript of 2 denotes the swing leg.
F_{fs1-x}, F_{fs1-y}	The x and y components of the interaction force between the foot and shin, on the stance leg side. A subscript of 2 denotes the swing leg.
τ_{th1}	The joint torque of the hip joint on the stance leg side. A subscript of 2 denotes the swing leg.
τ_{st1}	The joint torque of the knee joint on the stance leg side. A subscript of 2 denotes the swing leg.
τ_{fs1}	The joint torque of the ankle joint on the stance leg side. A subscript of 2 denotes the swing leg.

Appendix H - The abridged decision table of the third iteration of the optimisation

Motor weight	Gear ratio	Total device weight	Maximum Load	Power consumption	Value function
3.03	81	73	60	54	4,366
2.235	105	72	60	59	4,358
2.895	97	73	60	56	4,350
2.445	105	72	60	60	4,331
4.14	81	76	60	53	4,308
3.315	97	74	60	57	4,308
3.63	89	75	60	56	4,301
2.805	73	73	60	64	4,260
3.195	89	74	60	63	4,253
1.89	129	71	60	71	4,239
5.58	73	78	60	53	4,216
5.25	34	78	60	56	4,207
3.3	97	74	60	68	4,181
1.5	153	70	60	80	4,152
3.195	97	74	60	71	4,151
1.635	129	71	60	80	4,151
5.4	58	78	60	60	4,145
4.995	81	77	60	62	4,142
1.905	121	71	60	81	4,120
3.6	113	75	60	72	4,113
6.6	73	81	60	57	4,107
1.485	160	70	60	85	4,103
7.35	50	82	60	53	4,102
5.295	89	78	60	65	4,098
6.6	65	81	60	60	4,076
6.36	42	80	60	61	4,072
7.755	34	83	60	56	4,051
4.905	89	77	60	74	4,014
4.905	89	77	60	76	3,987
5.505	81	78	60	74	3,977
7.95	42	83	60	61	3,977

7.605	81	83	60	64	3,965
4.905	97	77	60	78	3,964
2.805	145	73	60	90	3,960
5.505	81	78	60	76	3,952
7.605	81	83	60	65	3,951
9.525	42	86	60	55	3,945
5.505	81	78	60	77	3,942
8.4	81	84	60	64	3,917
9.6	50	87	60	57	3,915
5.805	105	79	60	78	3,909
9.6	50	87	60	58	3,908
10.815	34	89	60	58	3,838
7.995	89	83	60	74	3,826
5.1	113	78	60	90	3,818
10.5	42	88	60	63	3,792
5.1	153	78	60	95	3,756
4.5	145	76	60	102	3,711
3.6	113	75	60	71	3,941
10.005	73	87	60	75	3,686
12.15	26	92	60	65	3,668
13.095	42	94	60	62	3,643
13.095	42	94	60	64	3,619
13.05	34	93	60	66	3,599
16.8	34	101	60	67	3,358
16.8	34	101	60	67	3,354
3.195	129	74	60	116	3,246
4.905	65	77	48	80	3,323
4.095	153	76	60	115	2,868
1.8	176	71	60	154	2,506
1.35	184	70	60	140	2,563
6.45	42	80	38	78	2,779
6	65	79	37	62	2,897
1.05	137	69	55	94	2,728
1.8	160	71	60	151	2,116
3.705	160	75	60	118	2,244
1.995	168	71	60	164	1,960

2.4	81	72	28	97	2,284
2.205	121	72	58	190	1,635
1.2	160	70	60	153	1,706
1.8	121	71	54	132	1,825
0.96	145	69	60	128	1,627
2.205	113	72	53	126	1,535
3.975	81	75	12	58	1,839
4.605	81	77	33	86	1,526
3.195	42	74	12	104	1,340
1.8	121	71	60	132	917
3.3	121	74	46	140	803
6.6	50	81	8	123	719
1.5	81	70	18	161	395
1.605	113	71	46	172	283
0.72	81	73	60	54	4,366
1.2	105	71	60	60	4,372